uOttawa

L'Université canadienne
Canada's university

FACULTÉ DES ÉTUDES SUPÉRIEURES ET POSTOCTORALES

uOttawa

L'Université canadienne
Canada's university

FACULTY OF GRADUATE AND POSDOCTORAL STUDIES

Amir Jabri
AUTEUR DE LA THÈSE / AUTHOR OF THESIS

Ph.D. (Chemistry)
GRADE / DEGREE

Department of Chemistry
FACULTÉ, ÉCOLE, DÉPARTEMENT / FACULTY, SCHOOL, DEPARTMENT

Mechanism and Design of Homogeneous Heterobimetallic Early Metal-aluminum Alkyl Catalysts for Ethylene Trimerization and Polymerization

TITRE DE LA THÈSE / TITLE OF THESIS

Sandro Gambarotta
DIRECTEUR (DIRECTRICE) DE LA THÈSE / THESIS SUPERVISOR

CO-DIRECTEUR (CO-DIRECTRICE) DE LA THÈSE / THESIS CO-SUPERVISOR

EXAMINATEURS (EXAMINATRICES) DE LA THÈSE / THESIS EXAMINERS

Robert Crutchley

Georgii Nikonov (McGill University)

Darrin Richeson

Tom Woo

Gary W. Slater
Le Doyen de la Faculté des études supérieures et postdoctorales / Dean of the Faculty of Graduate and Postdoctoral Studies

Mechanism and Design of Homogeneous Heterobimetallic Early Metal-Aluminum Alkyl Catalysts for Ethylene Trimerization and Polymerization

Amir Jabri

September 2, 2009

Thesis submitted to the

Faculty of Graduate and Postdoctoral Studies

In partial fulfillment of the requirements

For the PhD degree in chemistry

Department of Chemistry

Faculty of Science

University of Ottawa

Your file Votre référence
ISBN: 978-0-494-61385-6
Our file Notre référence
ISBN: 978-0-494-61385-6

Abstract

This thesis describes an experimental study of the coordination chemistry of several early-metal based homogeneous catalysts for ethylene trimerization and polymerization. The first part of the thesis discusses a mechanistic study of chromium catalyzed ethylene trimerization and tetramerization based on the established $NCy(PPh_2)_2$ [PNP], $NH(CH_2CH_2SCy)_2$ [SNS], and pyrrole ligands. Through the isolation and characterization of catalytic resting states, many missing pieces to the mechanistic puzzle have been found, which aids the analysis of critical relationships between the chromium electronic state, geometry, nuclearity, and charge and the observed catalyst activity and selectivity. Some contributions include the first direct evidence for the involvement of Cr(I), Cr(II) and Cr(III) species in catalysis, 1-hexene selectivity enhancement via ligand-directed cocatalyst hemilability, and a well-defined single-component ethylene trimerization catalyst.

The second part of the thesis explores olefin polymerization catalysis with pyrrole complexes of vanadium and titanium. The pyrrole ligand was found to enhance alkyl transfer between the transition metal and aluminum centres via its hemilability, which enhances the activation of normally kinetically inert metal electronic configurations. In addition, the alkyl shuttling allows the isolation of well-defined thermally stable complexes which form highly active single-site single-component polymerization catalysts at high temperatures.

Contents

List of Figures

List of Tables

List of Abbreviations

atm	atmosphere (1 atm = 1 bar, 760 mm Hg, 101.3 kPa, 14.696 psi)
Å	angstrom
acac	acetylacetonato (ligand)
Ar	aryl
calcd	calculated
compd	compound
DFT	density functional theory
br	broad
c-	cis
$^{13}C\{^{1}H\}$	proton-decoupled carbon-13 (NMR)
Cy	cyclohexyl
d	doublet
SNS	$NH(CH_2CH_2SCy)_2$
PNP	$NCy(PPh_2)_2$
Pyr	Pyrrole
ESI	Electro Spray Ionization (mass spectrometry)
Hz	Hertz, cycles per second
IR	Infrared

J	coupling constant, in Hz
L	ligand
M	central metal atom in a complex
Mn	number-average molecular weight
m/z	mass to charge ratio
Mw	weight-average molecular weight
%	percent
NMR	Nuclear Magnetic Resonance
o	ortho
pyr	pyrrole
py	pyridine
q	quartet (NMR)
RT	room temperature
s	singlet (NMR)
t	triplet (NMR)
tert-,t	tertiary
t	trans
THF	tetrahydrofuran
XRD	X-Ray Diffraction
DMP	2,5-dimethylpyrrole

THC	2,3,4,5-tetrahydrocarbazole
TPP	2,3,4,5-tetraphenylpyrrole
TMP	2,3,4,5-tetramethylpyrrole
DMI	2,3-dimethylindole
TMA	trimethylaluminum
TEAL	triethylaluminum
TIBA	tri-isobutylaluminum
DEAC	diethylaluminumchloride
IBAO	diisobutylaluminumoxide
S.F.	Shultz-Flory distribution (random statistical distribution)

Articles based on this thesis work

1.) "Isolation of a Cationic Chromium(II) Species in a Catalytic System for Ethylene Tri- and Tetramerization."[1] I was responsible for the synthesis, characterization and initial catalytic screening, Robbert Duchateau and Patrick Crewdson reproduced my catalytic data. Ilia Korobkov was the crystallographer. Sandro supervised the project.

2.) "Role of the Metal Oxidation State in the [SNS]-Cr Catalyst for Ethylene Trimerization: Isolation of Di- and Trivalent Cationic Intermediates."[2] I was responsible for the synthesis, characterization and initial catalytic screening. Robbert Ducateau and Patrick Crewdson reproduced my catalytic data. Clair Temple reproduced my synthetic work. Ilia Korobkov was the crystallographer. Sandro supervised the project.

3.) "The Question of the Cr Oxidation State in the {Cr(SNS)} Catalyst for Selective Ethylene Trimerization : An Unanticipated Re-Oxidation Pathway."[3] I was responsible for the synthesis and characterization, and proposed the disproportionation mechanism. Clair Temple found the evidence for my proposed mechanism. Robbert Ducateau and Patrick Crewdson did the catalytic testing. Ilia Korobkov was the crystallographer. Sandro supervised the project.

4.) "Single-Site, Single-Component Catalysts for Very High Molecular Weight Polyethylene : A Robust "Ready-To-Go" Vanadium π-Bonded Complex Without a Preformed V-C Bond."[4] I was responsible for the synthesis, characterization and initial catalytic screening. Ilia Korobkov reproduced my synthesis of complex 1 in the article and was the crystallographer. Robbert Duchateau reproduced the catalytic testing. Sandro supervised the project.

5.) "Isolation of Single-Component Trimerization and Polymerization Chromium Catalysts: The Role of the Metal Oxidation State." [5] I was responsible for the synthesis, characterization and initial catalytic screening. Chris B. Mason and Yan Sim reproduced all the results. Robbert Ducateau reproduced the catalytic data. Terra Burchell was the crystallographer. Sandro supervised the project.

6.) "Chromium Oxidation State Dictates Catalytic Function."[6] C&E News citation of the above work.

Acknowledgements

Pursuing a career in science is very challenging, and achieving progress never occurs in a vacuum. I needed a great amount of support to reach this stage, but it does not take away from the pride and sense of achievement of completing it.

First of all I'd like to thank my supervisor Dr. Sandro Gambarotta, who I'm very lucky to have worked with because it is rare to find a supervisor who is always enthusiastic and ready to take on extremely tough research challenges. There is no need to mention how big of an impact he has had on the organometallic field. Secondly I'd like to thank Dr. Robbert Duchateau from TUE in Netherlands for providing his expertise in commercial polyolefins technology to our group, as well as for redoing all the catalytic experiments initiated here in Ottawa using the same rigorous methodology and advanced equipment used in the polyolefins industry. Third, I would like to thank Dr. Peter H. M. Budzelaar for his insights and helpful discussion into the mechanistic aspects of this chemistry. I also extend my thanks to the wonderful and exciting inorganic professors at this department and others who have been inspirational to me due to their dedication to education: Professors Deryn Fogg, Darrin Richeson, Eduardo dos Santos, Kazem Saidi, and Sean Barry. I'd also like to thank the undergraduates, graduate students, and post-docs that I've had the pleasure of working with the past years: Yan Sim, Chris B. Mason, Steven Horvath, Ilia Korobkov, Grigory Nikiforov, Jenn Scott, Pat Crewdson, and Indu Vidyaratne among many others.

Last I'd like to thank my loving and patient family: My father Radwan for inspiring me and pushing me to achieve great things. My mother Bahira for supporting me and comforting me. My brother Omar for being a true friend and providing me with invaluable advice. Finally, my wife Asma for making me feel truly special and giving me the confidence I needed to continue.

1 Introduction

1.1 Polyolefins

Polymers are large molecules composed of repeating structural units typically connected by covalent chemical bonds. Structured polymers are prevalent in nature, such as in plant cellulose (a polysaccharide) among many others that have evolved over billions of years. Our technological species has traditionally made innovative use of naturally-occurring polymers for thousands of years, but in the past century synthetic polyolefins have become more popular due to their durability, versatility, and low cost.

The world production of polyolefins in 2005 was estimated to be 110 million metric tons, a four-fold increase from 1985.[7] As an illustrative comparison, this would equal 50 of the great pyramid in Giza. This demand is expected to grow even more rapidly in the future, especially for specialized applications. Polyolefins can be readily tailored by modifying their underlying molecular structure. Variations in polymer branching, chain lengths, stereo-regularity, copolymer composition and block copolymer sequences can have a tremendous effect on the resulting polymer properties. For example, the block copolymer HIPS (high impact polystyrene-block-polyisoprene) is used in rubber tires because it exhibits domain phases between the two types of polymer blocks which imparts engineering strength beyond that of homopolymers or blends.

The types of high molecular weight ($> 50{,}000$) polyolefins that are currently in large-scale production globally (ordered by volume) are: LLDPE (linear low density polyethylene), HDPE (high density polyethylene), iPP (isotactic polypropylene), and LDPE (low density polyethylene). Low molecular weight (< 500) oligomers are also produced as synthetic lubricants for vehicles. Commercial polyethylenes are usually copolymerized with small amounts of α-olefins to make them more flexible than simple straight chain high density polyethylene. LLDPE is the most desired polymer commercially due to its greater strength when compared to the older LDPE polymer.

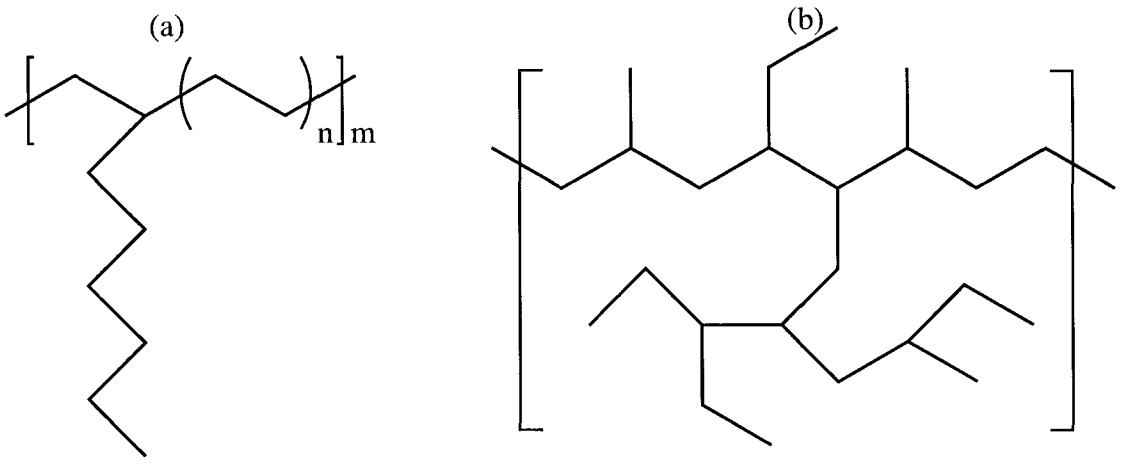

Figure 1: Molecular structure of (a) LLDPE and (b) LDPE

LLDPE is the linear copolymer of ethylene and 10-20% of 1-hexene or 1-octene (Figure 1a), while LDPE is a hyperbranched polyethylene produced from a free radical process. Both polymers form flexible and clear film materials. Because of the narrower molecular weight distribution and shorter chain branching of LLDPE, chains can "slide by" one another upon elongation, avoiding the undesirable hardening and failure of the hyperbranched LDPE chains. This allows LLDPE films to be very thin while maintaining high strength and toughness, with higher impact and puncture resistance, as well as higher tensile strength, making them more cost-effective.

The high demand for LLDPE film has raised interest in developing more efficient methods for producing both LLDPE and the 1-hexene and 1-octene comonomers used in its production. The recently discovered chromium-based selective ethylene trimerization/tetramerization catalysts[8] are an economical solution because virtually no waste byproducts are produced, in contrast to the traditionally used non-selective oligomerization catalysts which produce what is called a Shultz-Flory (S.F.) distribution. The mechanistic challenge in understanding ethylene trimerization catalysis has attracted the interest of the academic research community to the study of paramagnetic organochromium chemistry, resulting in its rapid development over the past few years. This thesis will report on our own mechanistic investigations of chromium catalyzed ethylene trimerization/tetramerization and early transition metal-pyrrolide based olefin polymerization catalysis. The following paragraphs provides a brief background of this field with an emphasis on mechanistic studies.

1.2 The birth of olefin polymerization and trimerization catalysis

Our modern olefin polymerization industry is built on the highly active heterogenous olefin polymerization catalyst discovered by Ziegler in the early 1950's,[9] which is based on the mixture of $TiCl_4$ and $AlCl_2Et$. This discovery sparked a great interest in developing more commercially valuable catalysts and new polymers, notably Natta's important discovery of stereoselective propene polymerization with Ziegler's catalyst. [10] The major fraction of polyolefins currently manufactured still uses supported versions of Ziegler-Natta catalysts on $MgCl_2$. However, most of the high molecular weight linear polyethylene is produced with chromium supported on silica. Although these heterogeneous catalysts are commercially successful for the production of a wide range of homopolymers, the diversity of active sites created in their preparation leads to broad polydispersities and poor comonomer incorporation. This limits their use in the production of high-quality copolymers such as LLDPE. Mechanistic studies to understand and rationally develop these valuable heterogeneous catalysts have been hampered until very recently by the difficulties encountered for their characterization (e.g. extreme sensitivity towards hydrolysis).

Simultaneously with the discovery of the Ziegler-Natta catalyst, the synthesis of the well-defined and diamagnetic titanocene complex, Cp_2TiCl_2, was reported by Wilkinson.[11] This complex was evaluated a few years later by Breslow[12, 13, 14] and Natta [15] for its olefin polymerization performance. Using the $AlClEt_2$ activator resulted in poor activity for ethylene polymerization, and no activity for propene polymerization. However, the well-defined nature of the complex made mechanistic studies simpler to carry out than in the other known catalysts at the time, which were poorly-defined systems. It was found that the low activity of the titanocene catalyst was partially due to its rapid deactivation by reduction to titanium(III).[14] Breslow identified the catalyst resting state that formed initially upon addition of the aluminum cocatalyst, by isolating a heterobimetallic aluminate complex containing a titanium-ethyl group. This titanium-ethyl functionality was proposed to insert into the ethylene substrate to generate a polymer chain (Figure 2a). Shilov [16] (Figure 2b) carried out kinetic studies which gave evidence for an 'intermittent' chain-growth, consistent with the rate-limiting dissociation of the aluminate anion to generate a cationic titanium centre, which was the first proposal of a cationic mechanism. Unfortunately, the

concentration of the active species was too low to be observed directly, and the idea of cationic catalyst intermediates did not find widespread acceptance for twenty years.

These mechanistic proposals anticipated several features of the well known Cossee-Arlman polymerization mechanism [17][18] which was proposed four years later as operating in the heterogeneous Ziegler-Natta catalyst (Figure 1c).

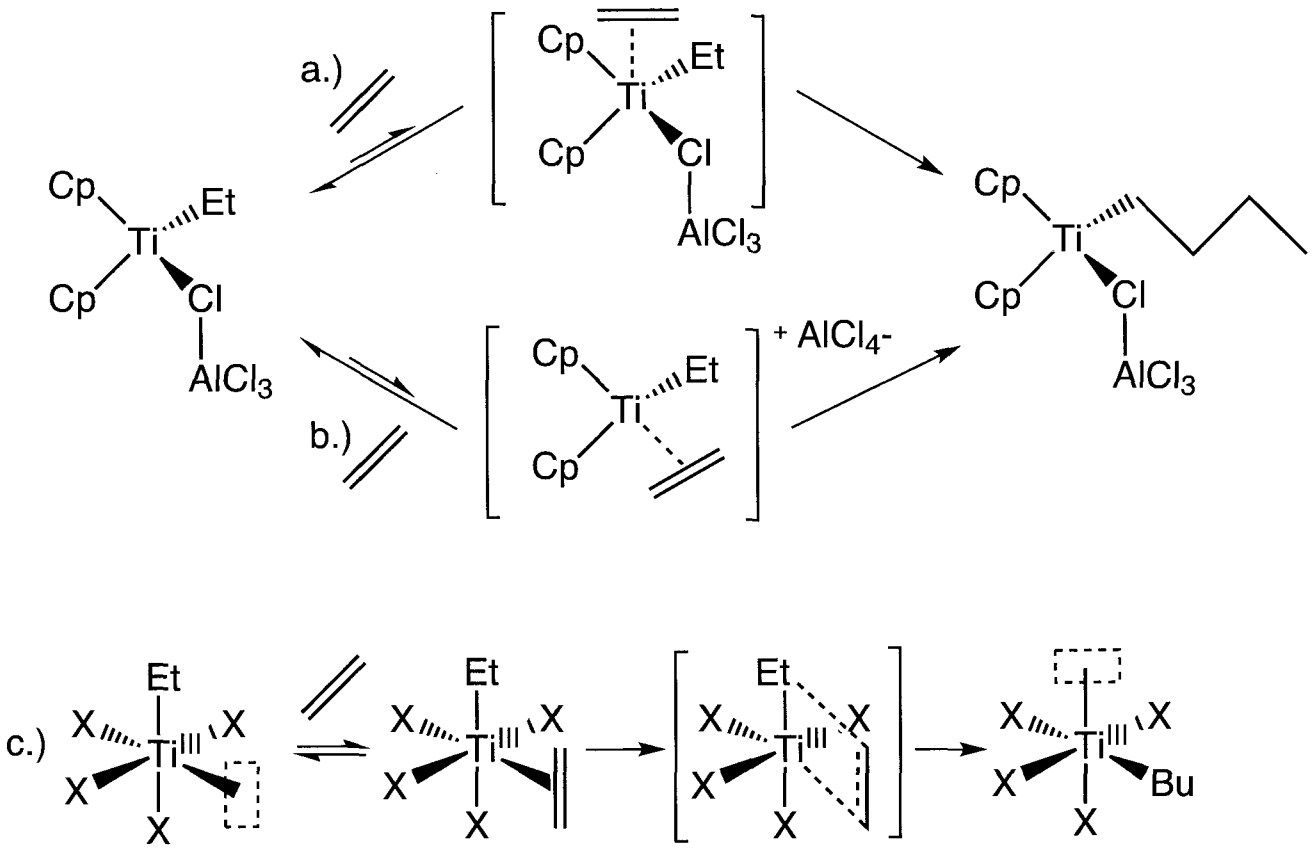

Figure 2: (a) Breslow (neutral), (b) Shilov (cationic), and (c) Cossee-Arlman mechanism

The research into discovering new olefin polymerization catalysts led to the unexpected discovery of selective ethylene trimerization to 1-hexene by Manyik in 1964. [19] In a patent related to olefin polymerization with a homogeneous chromium catalyst based on a mixture of $Cr(octanoate)_3$ and $(Al^iBu_2)_2O$, a small amount of 1-hexene and branched decene isomers were isolated along with the polymer. These isomers contained butyl branches consistent with trimerization of 1-hexene with the ethylene. The ethylene concentration dependence of the 1-hexene product was later reported to be second order,[20] while the polymer product was first order in ethylene concentration, indicative of different mechanisms for the formation of the two products. Based on this evidence,

the authors proposed that the 1-hexene product was produced by an unprecedented metallacycle mechanism (Figure 3). However, the highly paramagnetic nature of chromium limited any mechanistic analysis at the time, and no further progress in understanding ethylene trimerization catalysis was made for another 25 years. The field of homogeneous olefin polymerization catalysis continued to develop rapidly during this time, however.

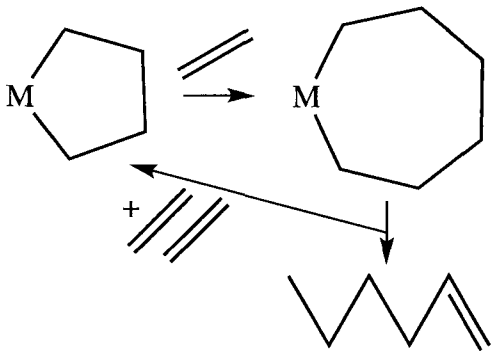

Figure 3: Manyik metallacycle mechanism

1.2.1 Modern olefin polymerization catalysis

An important breakthrough in olefin polymerization was made by Breslow in 1975, with the accidental discovery that traces of moisture can greatly increase the activity of the titanocene/$AlEt_2Cl$ catalyst system.[21] The authors suggested that the moisture reacted with the aluminum cocatalyst, forming aluminoxanes by partial hydrolysis. This was later confirmed experimentally by Sinn and Kaminsky [22] with the demonstration that the inactive $Cp_2ZrCl_2/AlMe_3$ system becomes highly active upon the addition of methylaluminoxane (MAO). Sinn et al. also found that the use of MAO even allows the polymerization of propene with zirconocenes. Methylaluminoxane is a poorly characterized polymeric glassy substance. After over 30 years of research, all that is known is that it is usually of molecular weight 900-1200 and the approximate composition $(MeAlO)_n$, which consists of linear, cyclic and cross-linked compounds, probably containing predominantly four coordinate Al centres and some OAlMe end groups.[23] The compound dissolves readily in toluene where, due to the facile ligand exchange in aluminium complexes, it establishes complex solution equilibria. Samples are usually rich in methyl groups, and even after drying in vacuo contain typically 34% free $AlMe_3$. Despite the high catalyst activity achieved with MAO, three main

drawbacks remain: (1) a poorly-defined structure (which prevents structural characterization of catalytic intermediates), (2) high cost, and (2) invariable need for a large excess to be used (which contaminates the polymer produced with aluminum residues).

Experimental evidence for the cationic mechanism proposed by Shilov was finally found in 1984, when Eisch reported that the insertion of the titanium methyl group of the titanocene catalyst into the hindered alkyne, $PhCCSiMe_3$, results in the formation of a cationic titanium vinyl complex.[24] At the same time Jordan characterized the cationic zirconium complex $\{Zr^{IV}Cp_2Me(THF)\}$ $\{BPh_4\}$,[25] which partially dissociates THF in dichloromethane to generate an empty coordination site for ethylene polymerization. This result afforded the first evidence that a well defined cationic metallocene complex is capable of polymerizing olefins in the absence of aluminium alkyl activators.[25] This mechanistic information has led to a new generation of commercially valuable well-defined polymerization catalysts based on weakly coordinating anions such as $B(C_6F_5)_4^-$.[23]

Other notable breakthroughs in olefin polymerization catalysis include (Figure 4): 1) the discovery of highly active "post-metallocene" ligands such as the well known "constrained geometry" ligands which support highly active titanium-based α-olefin polymerization catalysis;[26] 2) late metals which can form potent catalysts with lower oxophilicity allowing incorporation of polar comonomers for the first time;[27] 3) the very recent use of chain transfer agents to control molecular weight and create valuable block copolymer architectures (discussed in chapter 6).

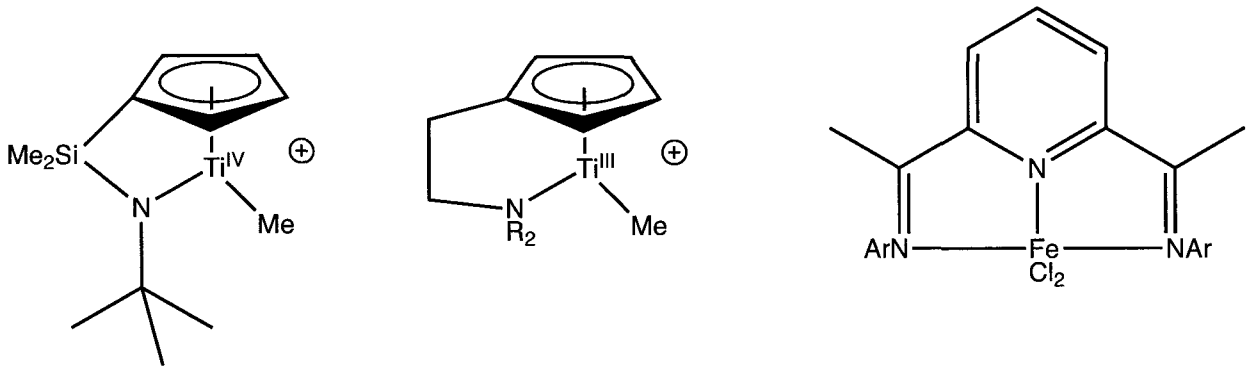

Figure 4: Recent breakthroughs in olefin polymerization catalysis

1.2.2 Modern ethylene trimerization catalysis

A major breakthrough in ethylene trimerization did not occur until 1991, with the discovery of the highly active and selective chromium/pyrrole/$AlEt_2Cl$ based trimerization catalyst by Reagan.[28] For the first time, 1-hexene selectivity was well over 90% and the activity, which is close to a ton of 1-hexene produced per gram of chromium catalyst, was high enough to be rapidly implemented in a viable commercial operation (>200,000 metric tons/year). Soon after the report, renewed interest led to many patents for chromium trimerization catalysts based on a large variety of ligands such as the pyrrole, [SNS] and $NCy(PPh_2)_2$ [PNP] (Figure 5).[29, 30, 31, 32, 33, 34] Trimerization catalysts based on the titanium and tantalum metals were also reported.[35, 36, 37] These systems are not as efficient as the best chromium catalysts, which account for over 90 % of the patent and scientific literature of ethylene trimerization. A significant factor to the commercial viability of a homogeneous ethylene oligomerization catalyst is the amount of reactor fouling (or HDPE byproduct) that the catalyst causes, which necessitates expensive cleaning operations. The commercial chromium pyrrole system is preferable to the titanium trimerization catalyst in this regard, because the polymer byproduct of the chromium system is a soluble low MW PE, while the titanium catalyst produces a significant quantity of insoluble HDPE.[38]

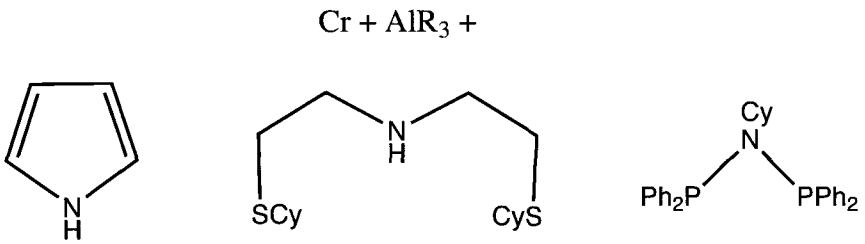

Figure 5: From left to right: Pyrrole, [SNS], and $NCy(PPh_2)_2$ [PNP] based trimerization catalysts

The first theoretical and experimental mechanistic studies of ethylene trimerization have appeared just in the last few years, supporting the original metallacycle mechanism proposed by Manyik half a century ago. Currently, the most cited report in ethylene trimerization (Science Citation Index) is the pioneering work by Jolly on the reactivity of model chromacyclopentane and chromacycloheptane complexes, and gives strong evidence for the existence of chromium metallacycle intermediates (Figure 6).[39] This allowed for experimental validation of the metallacyle

mechanism of Manyik which predicts that the thermolysis of the chromacyclopentane (at 100 °C) generates 1-butene, which is a much higher temperature than required to thermolyze the chromacyclononane (at 0 °C) to 1-hexene. These findings lend support to the proposal that the increased 1-hexene selectivity is due to the difference in kinetic stability between the chromacyclopentane and chromacycloheptane intermediates. Thus many of the basic catalytic steps were successfully modelled by Jolly with this one system, obviously chosen for it's enhanced stability and crystallinity. However, the major drawback of the choice of $CpCrPMe_3$ complexes to the mechanistic study of ethylene trimerization is that they are not catalytically selective for 1-hexene, but instead produce polyethylene with high activity. The study of the catalytic intermediates in selective trimerization catalysts are more important for specific mechanistic insights they can provide in the underlying dynamics important to the catalytic performance. As the isolation and characterization of stable organometallic intermediates from actual selective chromium trimerization catalyst mixtures had not been reported at the start of this thesis, this was chosen as the topic of study.[1, 2, 3]

Recently, isotopic labelling experiments of an ethylene trimerizaton catalyst was reported by Bercaw, which revealed that no isotopic scrambling is observed in the 1-hexene product as expected in the metallacycle mechanism.[40, 41] By contrast, catalysts operating via the Cossee mechanism result in isotopic scrambling due to β-H elimination. Finally, many theoretical DFT studies have supported the metallacycle mechanism.[42, 43, 44, 45, 46, 47, 48]

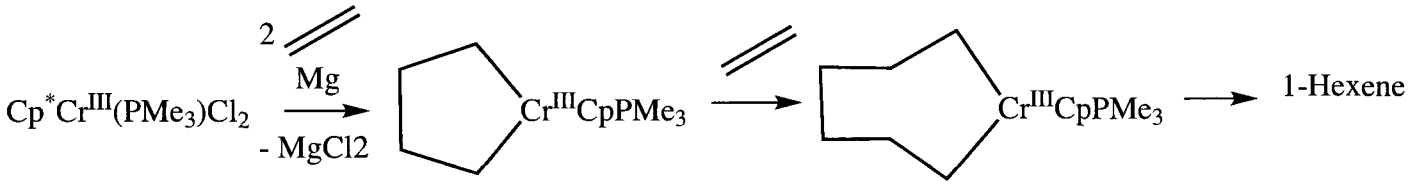

Figure 6: Model chromacycle reactivity reported by Jolly

Unexpectedly, in 2004 a research group at SASOL reported the discovery of a chromium-diphosphine catalyst that produces octene in 70% of the liquid fraction. Such high selectivity for 1-octene was previously thought to be impossible based on the original metallacycle mechanism.[49] An "extended" metallacyclononane mechanism was proposed in the same article to give rise to the 1-octene product (Figure 7). This extended metallacycle mechanism is supported by related

isotopic labelling studies of some non-selective chromium oligomerization catalysts.[50, 51] Mechanistically it is thought that that larger metallacycles can be formed in non-selective catalysts via a decreased rate of metallacycle elimination relative to metallacycle growth. Thus, the first major goal of this thesis was to explore the coordination chemistry of catalytic intermediates in established ethylene trimerization and tetramerization catalysts for mechanistic insights. Paramagnetic organochromium chemistry has seen a huge increase in interest in the past few years, leading to the discovery of some very interesting mechanistic features specific to organochromium species.

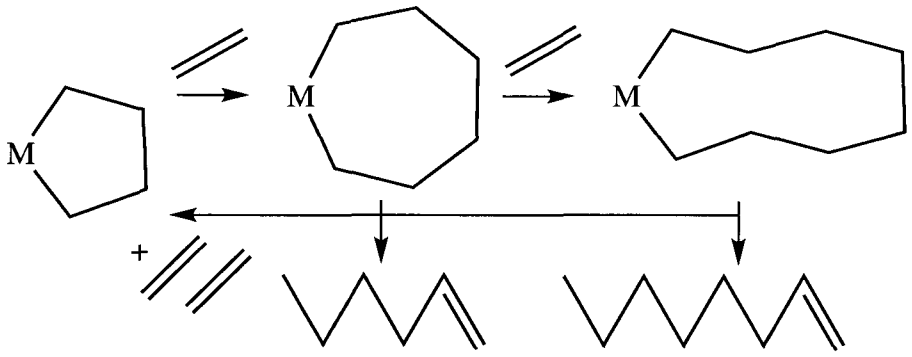

Figure 7: The "extended" metallacycle mechanism proposed for 1-octene formation

While there is agreement that ethylene trimerization involves a two-electron redox couple, the oxidation states of the actual catalyst remains unknown. The possibility that the oligomerization is performed by a Cr(II)/Cr(IV), Cr(I)/Cr(III) and Cr(III)/Cr(V) redox couple have been taken into consideration. In addition, there is no reason to eliminate the possibility that bimetallic intermediates are also be involved, as chromium has demonstrated rapid single-electron transfers. However, while Cr IV alkyls are poorly understood, the few reported examples are unusually kinetically stable [52], so it seems reasonable to assume that CrIV is not a catalytic intermediate, limiting the mechanistic possibilities to Cr (I, II, and III).

1.2.3 The pyrrole ligand in olefin polymerization catalysis.

The discovery of the commercial chromium-pyrrole catalyst was a great breakthrough not only because it raised interest in the development of organochromium chemistry, but also because it renewed interest in the coordination chemistry and catalytic properties of transition metal-pyrrole complexes. Recent years have also witnessed exciting discoveries in academia and in-

dustry using both simple and chelating pyrrole ligands for highly active and selective catalysis, including: olefin polymerization/copolymerization,[53] olefin hydroamination,[54] Heck and Suzuki coupling,[55] C-X direct arylation,[56] olefin and hydrocarbon oxidation and epoxidation,[57] and olefin metathesis.[58, 59]

Very little is known about the coordination properties of the pyrrole ligand during catalysis, and why it leads to a more active and selective chromium trimerization catalyst than the closely related Cp-chromium oligomerization catalyst. The analysis of the electronic structure of the pyrrolide anion reveals that the nitrogen lone pair retains the negative charge, and is thus equally competitive with the π system for binding to metal centres. Another important factor is the decreased aromaticity with respect to Cp. Thus, the hemilability of pyrrolide complexes is expected to be increased due to the relative ease of de-aromatization of the pyrrole ring. Therefore, the fine-tuning of the pyrrole ligand substituents is expected to play a large role in catalyst optimization, as it strongly affects the coordination properties of pyrrole and the resulting orbital hybridization of the metal centre. This information could assist substantially the rational development of these valuable catalyst systems in the future. From a structural standpoint, the evaluation of hundreds of metal pyrrolide structures in the Cambridge crystallographic database as well as several reported theoretical studies on the bonding properties of the pyrrole ligand reveals that, in fact, pyrrolide anions are readily capable of engaging in widely different coordination modes anywhere in a spectrum between the π-type η^5-NC_4R_4 and the σ-type η^1-NC_4R_4 (Figure 8, a).

In essence, the pyrrole ligand might be considered a useful and unique donor in catalysis not because it contains one single, extremely strong donation mode, like the well-known strongly σ-donating NHCs and phosphines, but because it provides a wide variety of different steric and electronic environments to the metal centre upon demand through facile ring slippage. This factor can be very useful in catalyst systems under circumstances where such continuous reorganization (hemilability) is required. Some established examples of the benefit of ligand hemilability are in the ethylene trimerization catalysis by titanium which is based on a hemilabile arene ligand.[60] In addition to its hemilability, pyrrole is also an ideal candidate to explore bimetallic chemistry (Figure 8, b) because it contains a soft π system which will form a stable bond with a low-valent

transition metal centre, and a hard nitrogen σ lone pair which forms a stable bond with a hard Lewis acid such as an aluminum (III) cocatalyst. As the chromium-pyrrole based trimerization catalyst makes use of the aluminum alkyl activators, it is possible that such bimetallic species play an important role in catalysis (Figure 8, b). These features make pyrrole an interesting ligand for early metal olefin polymerization catalysts in general, and the exploration of such complexes is the second topic of this thesis.

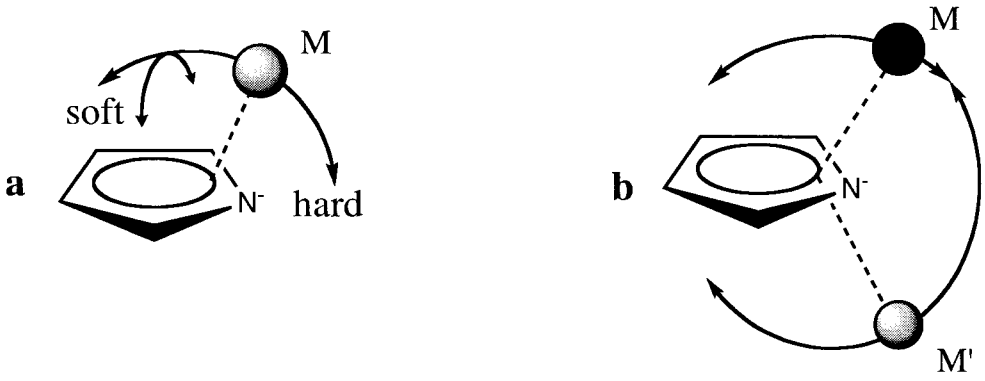

Figure 8: Pyrrole bonding modes

1.2.4 Terminology

The commonly used terms to describe the organometallic complexes which are observed and postulated in mechanistic studies of a catalyst are the catalyst resting state, catalytic intermediate, and transition state. While resting states are the most stable and most likely to be observed, they are not involved in productive catalytic steps, but are in equilibrium with less stable and very rarely observed catalytic intermediates. These intermediates are highly unstable species which have very short lifetimes, and are directly involved in the productive catalytic steps. Transition states are postulated as the energetic saddle point in the transition between two related catalytic intermediates (or saddle points on on the potential energy surface in the transition between two intermediates), and thus are impossible to observe directly experimentally.

1.3 Scope and layout of thesis

This thesis is organized as depicted in Figure 9, which shows the logical connections between the separate chapters. The first part of this thesis (chapters 2-4) discusses the mechanistic study of

ethylene trimerization with chromium catalysts ligated by the [SNS], [PNP], and Pyrrole ligands. The second part (chapters 5-6) detail the exploration of the pyrrole ligand on vanadium and titanium.

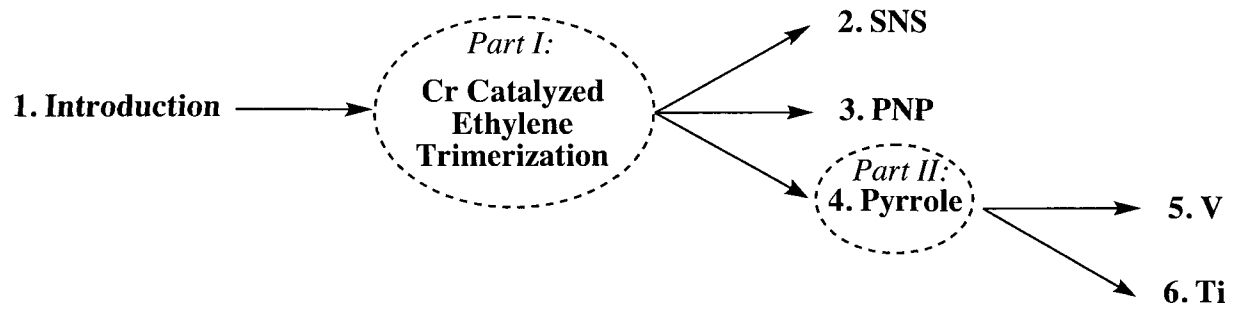

Figure 9: Pictorial summary of the scope and layout of the individual chapters of this thesis

Part I

Mechanistic Investigation of Chromium Catalyzed Ethylene Trimerization/Tetramerization

2 Mechanistic investigation of the chromium-[SNS] based ethylene trimerization catalysis

Abstract

This chapter describes the mechanistic investigation of the $NH(CH_2CH_2SCy)_2$ (SNS) chromium-based ethylene trimerization catalyst through the examination of the reaction of $\{(SNS)CrCl_3\}$ (**1**) with a wide range of aluminum alkyl reagents. The combination of **1** with excess Me_3Al affords the dicationic Cr(III) methyl dimer, $\{[(SNS)Cr^{III}Me(\mu\text{-}Cl)]_2\}$ $\{(AlMe_3)_2(\mu\text{-}Cl)\}_2$ (**2**). Although it was not possible to obtain crystalline samples of sufficient quality from the reaction of **1** with MAO (the best activator), the EPR spectrum of this green material **3**, is nearly identical to that of **2**, indicating a close structural similarity. Combination of **1** with excess $AlEt_2Cl$ affords the unusually thermally-stable dicationic Cr(III)-ethyl dimer, $\{[(SNS)Cr^{III}Et(\mu\text{-}Cl)]_2\}$ $\{AlCl_3Et\}_2$ (**4**). Addition of excess $AlEt_3$ to **4** results in significant decomposition, accompanied by a small amount of the reduced Cr(II) dimer, $\{[(SNS)Cr^{II}(\mu\text{-}Cl)]_2\}$ $\{AlCl_2Et_2\}_2$ (**5**). The reaction of **1** with the even more reducing Al^iBu_3 or $O(Al^iBu_2)_2$ promotes the quantitative reduction to $\{[(SNS)Cr^{II}(\mu\text{-}Cl)]_2\}$ $\{AlCl_2{}^iBu_2\}_2$ (**6**).

The reaction of the Cr(II) precursor, $\{(SNSCr^{II}Cl_2(THF)_2\}$ (**7**), with the same series of aluminum alkyls was also examined. The most reducing reagents, Al^iBu_3 or $O(Al^iBu_2)_2$, unsurprisingly result in the formation of complex **6**. The reaction of **7** with $AlEt_3$ results in decomposition, but its reaction with $AlEt_2Cl$ and $AlEtCl_2$ forms the neutral monomeric $\{(SNS)Cr^{II}(AlEt_2Cl_2)_2\}$ (**8**) and the cationic monomeric $\{(SNS)Cr^{II}(AlEtCl_3)\}$ $\{AlEtCl_3\}$ (**9**). Surprisingly, the reaction of **7** with the least reducing cocatalysts, $AlMe_3$ or MAO, results in its disproportionation to metallic chromium and **2** or **3** respectively. Based on these results it is concluded that the more reducing aluminum alkyls stabilize the chromium (II) oxidation state, while the less reducing aluminum alkyls stabilize the Cr(III) oxidation state, and that bimetallic mechanistic pathways exist for the redox change. As high catalytic activity requires the less-reducing MAO activator, it is concluded that the Cr(III) oxidation state is directly involved in the catalysis.

Treating **1** with increasing concentrations of $AlCl_3$, isolation of three different cationic trivalent complexes $\{(SNS)Cr^{III}Cl_2(THF)\}$ $\{AlCl_4\}$ (**10**), $\{[(SNS)Cr^{III}Cl(\mu\text{-}Cl)]_2\}$ $\{AlCl_4\}_2$

(**11**), and {(SNS)Cr^{III} (η^2-$AlCl_4$)} {Al_2Cl_7} (**12**). The increasing concentration of the aluminum cocatalyst affects geometry of both the chromium cation and the aluminate anion. In all these studies it was found that surprisingly none of the aluminum alkyl reagents is basic enough to deprotonate the acidic ligand N-H functionality. X-ray structural evidence reveals that in many cases this polarized N-H group is involved in a short-range and weak hydrogen-bonding to the aluminate anion. Based on this evidence, it is proposed that the role of the unusual N-H group is to direct the aluminate anion to coordinate loosely to a vacant site on chromium in the catalytic system, creating a MAO hemilability, which greatly enhances 1-hexene selectivity. Support for this hypothesis is found through the deliberate deprotonation of the acidic NH proton of the [SNS] ligand and complexation to chromium, resulting in {[(μ^2-SNS)$Cr^{II}Cl]_2$} (**13**). Complex **13** was found to be inert towards all aluminum alkyl reagents, suggesting that the deprotonation of the [SNS] ligand is actually a catalyst deactivation pathway.

The ethylene oligomerization catalysis by **1-13** was examined systematically under a range of conditions to gain more mechanistic insights into how the chromium precatalyst's oxidation state, nuclearity, coordination sphere and charge will affect the catalytic activity and selectivity. The use of a large excess MAO activator (>1000 eq.) results in lower selectivity, possibly due to the loss of the important NH-aluminate attraction. Chromium(II) precursors are more sensitive to MAO concentration than Cr(III), possibly due to lower solubility. Under identical conditions, an order of magnitude range of activity and a substantial difference in selectivity is observed for the different (SNS)Cr based precatalysts, leading to the unexpected conclusion that effective catalyst optimization can be carried out through preactivation with aluminum alkyls.

2.1 Introduction

The introduction to this thesis provided a background of chromium-catalyzed ethylene trimerization and the proposed metallacycle mechanism. The most important methodology for gaining mechanistic insight into a catalytic system is the isolation and characterization of well-defined resting states and stable intermediates. As currently the most active and selective chromium trimerization catalysts are based on the $NH(CH_2CH_2SCy)_2$ [SNS],[30] [PNP],[49] and pyrrole ligand,[61]

these systems are the most important systems to investigate mechanistically. Thus, the mechanistic study of the [SNS], [PNP], and pyrrole-based trimerization catalysts are described in Part I of this thesis (chapters 2-4 respectively). This chapter will discuss the results of study of the [SNS] chromium trimerization catalyst. The remainder of this introduction section will give a background of the scientific/patent literature relevant to the [SNS] system and some closely related systems for any mechanistic insights they may afford. Finally, to aid in the discussion of the experimental results obtained, a brief background of established organochromium(III) reactivity is presented as it is found to play a critical role in the chemistry of the [SNS] system. The background of established organochromium (II) and (I) chemistry is presented in chapters 3 and 4 respectively.

2.1.1 Background of [SNS]Cr-based ethylene trimerization catalysis

The analysis of the literature reveals that the majority of ligands found to provide high activity and selectivity for chromium catalyzed trimerization are tridentate ligands, of which the best performing examples are shown in Figure 10.[31, 62, 63, 34] Thus, the initial mechanistic study of a catalyst based on one of these tridentate ligands is expected to yield useful insights into the underlying organochromium chemistry. Of this group of ligands, the [SNS] ligand (Figure 10, complex d) is the most mechanistically interesting in that not only is it >99% selective for 1-hexene, but it is the only reported example which contains a meridionally-coordinating tridentate ligand as opposed to the facially-bound examples a-c in Figure 10. This is especially unusual, considering that all of the reported non-selective chromium oligomerization catalysts are also based on meridionally coordinating tridentate ligands. Thus the high selectivity of the [SNS] ligand is important to understand for key insights into the catalysis. The unusual acidic NH functionality of the [SNS] ligand would be expected to be highly susceptible to deprotonation in the highly basic catalytic environment containing a large excess of aluminum alkyl cocatalyst. This is an important question which is expected to be readily addressed by synthetic experimental studies.

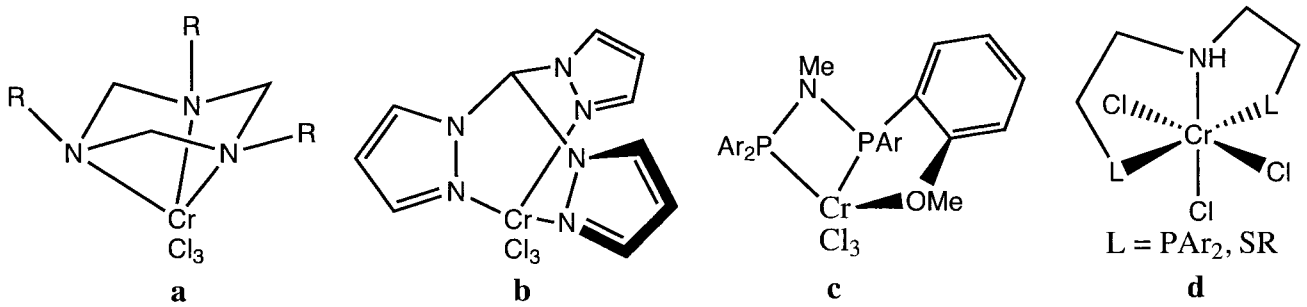

Figure 10: Reported complexes of tridentate ligands which afford highly active and selective chromium ethylene trimerization catalysts

2.1.2 Background of organochromium(III) chemistry

The introduction of this thesis also discussed the metallacycle mechanistic model proposed by Manyik for ethylene trimerization. Support for this mechanism was discussed as well, including the seminal work reported by Jolly on the synthesis, characterization and reactivity study of well-defined chromacyclopentane and chromacycloheptane complexes at the level of chromium (III) (Figure 6). Thus based on this report, the reactivity of the organochromium (III) intermediates are expected to play an important role in the trimerization catalyst mechanism. Many examples of the reactivity of organochromium (III) complexes have been reported in the literature. For instance the Cr(III)-R homolytic cleavage was established in aqueous environments almost a century ago.[64] Other reaction possibilities for chromium (III) alkyls have been established. For example, the preparation of chromium (I) arene complexes via reductive elimination of Cr(III) bis-aryl species was established half a century ago.[64] More recently the study of the reactivity of well-defined organochromium(III) species has revealed a wide variety of reactivity depending strongly on the ligand environment and the alkyl substituents (Figure 11).[65][66] Theopold established in 1988 that well-defined Cr(III) alkyls are capable of undergoing insertion of ethylene and generating polymer chains.[67] Thus, the influence of the coordination sphere of the metal centre on the reactivity is the driving force behind catalyst development.

Of relevance to the [SNS] ligand, the existence of the N-H proton in the presence of a chromium-alkyl bond is brought into question, although the chromium III alkyl bond may occasionally display exceptional kinetic stability against the thermodynamically favored hydrolysis, as in the case of $PhCrCl_2(THF)_3$ and $MeCrBr_2(THF)_3$. The circumstances where the different Cr-C bond

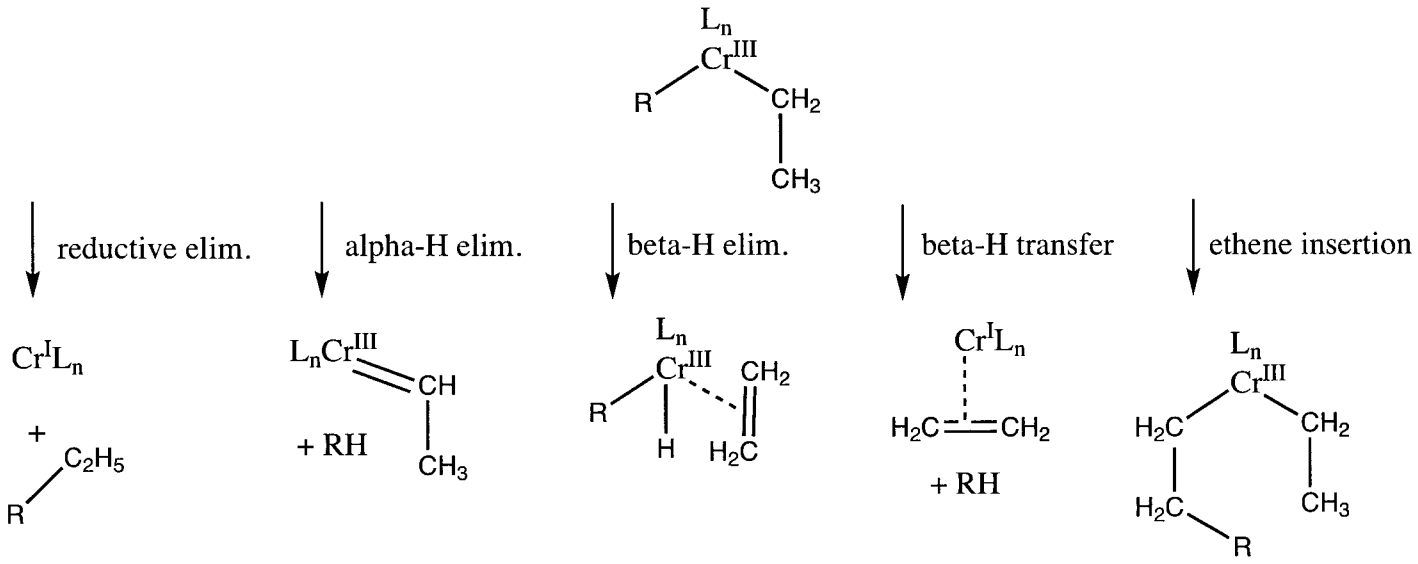

Figure 11: Potential reactions of organochromium(III) intermediates

breaking pathways (homolytic, heterolytic, and bimetallic pathways) can occur are important to document in the case of trimerization catalyst intermediates. Clarifying this would explain the effect of the ligand on the organochromium reactivity which leads to selective trimerization rather than polymerization etc. Only DFT calculations on a limited range of monometallic species have been attempted on actual chromium trimerization metallacycle thermolysis.[68] Little experimental support exhists for such a mechanism and alternative mechanisms have not been proposed or evaluated for comparison. Thus experimental studies are expected to shed more light on important mechanistic questions.

The experimental methodology chosen was to isolate organochromium intermediates containing the [SNS] ligand, to gain insights into the specific chromium reactivity pathways in the presence a ligand which promotes ethylene trimerization performance. Thus we chose to mimic the catalytic system as closely as possible while being able to still isolate and characterize intermediates. Thus not only MAO, but well defined aluminum alkyl reagents were employed, as they contained the required Lewis acidity making them close models for MAO. The chromium starting materials $CrCl_3(THF)_3$ and $CrCl_2(THF)_2$ were chosen for convenience.

2.2 Experimental

General

All reactions were carried out under a dry nitrogen atmosphere. Solvents were dried using an aluminum oxide solvent purification system. The catalytic reaction mixtures were analyzed using a CP 9000 gas chromatograph (GC) fitted with a 30 mm x 0.32 mm i.d. capillary CP volamine column and with an FID detector. Infrared spectra were recorded on an ABB Bomem FTIR instrument from Nujol mulls prepared in a drybox. Samples for magnetic susceptibility were preweighed inside a drybox equipped with an analytical balance and measured on a Johnson Matthey Magnetic Susceptibility balance. Elemental analysis was carried out with a Perkin-Elmer 2400 CHN analyzer. Data for X-ray crystal structure determination were obtained with a Bruker diffractometer equipped with a 1 K Smart CCD area detector. $CrCl_3(THF)_3$ and $CrCl_2(THF)_2$ were prepared according to standard procedures.[64] The complex (SNS)$CrCl_3$ (**1**) was prepared by a procedure reported in the literature.[30] Aluminum activators, $(Al^iBu_2)_2O$ (Aldrich), Al^iBu_3, Et_3Al, Et_2AlCl, $EtAlCl_2$, Me_3Al (Strem), and MAO (Chemtura) were used as received.

2.2.1 $\{[(SNS)Cr^{III}Me(\mu\text{-}Cl)]_2\}$ $\{(AlMe_3)_2(\mu\text{-}Cl)\}_2$ (2)

Method A: (from **1**) A mixture of **1** (460 mg, 1 mmol) and Me_3Al (720 mg, 10 mmol) in toluene (10mL) was stirred at 22°C resulting in a dark-green solution. After filtration, the resulting solution was stored at 22 °C for 24 h, resulting in the growth of large green crystals of analytically pure **2** (580 mg, 86%). IR (Nujol, cm^{-1}) N-H: 3181. Anal. Calcd (found) for $C_{30}H_{60}NS_2CrCl_2Al_2$: C 53.32 (53.21); H 8.95 (8.83); N 2.07 (2.01). μ_{eff}= 3.94 μ_B. E.P.R. (powder, - 78°C, figure 25).

Method B: (from **7**) A mixture of **7** (570 mg, 1 mmol) and Me_3Al (720 mg, 10 mmol) in toluene (10mL) was stirred at 22 °C for one minute resulting in a dark-green solution and extensive formation of metallic chromium. After filtration, the resulting green solution was stored at -35°C for 24 h, resulting in the growth of large green crystals of analytically pure **2** (120 mg, 17 %).

2.2.2 {[(SNS)Cr^{III}Me(μ-Cl)]$_2$} {MAO}$_2$ (3)

Method A: (from **1**) A mixture of **1** (460 mg, 1 mmol) and a 10% MAO solution (6.4 mL toluene, 10 mmol) in toluene (10 mL) was stirred at 22°C, affording a green solution initially followed by the gradual precipitation of a microcrystalline green solid (**3**) over the course of 10 minutes (600 mg). IR (Nujol, cm^{-1}) N-H: 3191. Anal. (found): C (50.91); H (7.63); N (2.31). E.P.R. (powder, - 78 C figure 25).

Method B: (from **7**) A mixture of **7** (570 mg, 1 mmol) and a 10% MAO solution (6.4 mL toluene, 10 mmol) in toluene (10 mL) was stirred at 22°C for one minute resulting in a dark-green solution and extensive formation of metallic chromium. After filtration, the resulting green solution was stored at 22°C for 24 h, resulting in the precipitation of green microcrystalline **3** (95 mg).

Degradation of 3 with pyridine; formation of $CrCl_3$(pyridine)$_3$

A suspension of **3** (0.250 g) in THF (10 mL) was treated with neat pyridine (2 mL). The insoluble solid partly dissolved, and after centrifugation the resulting solution was allowed to stand at room temperature for 3 days. Dark-green X-ray quality crystals of $CrCl_3$(pyridine)$_3$ separated (0.098 g). Anal. Calcd (found) for $C_{15}H_{15}N_3CrCl_3$: C 45.54(45.41); H 3.82 (3.79); N 10.62 (10.61). μ_{eff}= 3.87 μ_B. Crystallographic cell parameters were identical to those reported in the literature.

2.2.3 {[(SNS)Cr^{III}Et(μ-Cl)]$_2$} {$AlCl_3$Et}$_2$ (4)

A mixture of **1** (460 mg, 1 mmol) and Et_2AlCl (1.20 g, 10 mmol) in toluene (15 mL) was stirred at 22 °C for one minute to give a dark green solution. After filtration, the resulting green solution was stored at 22 °C for 24 h, resulting in the growth of large green crystals of analytically pure **4** (520 mg, 83 %). IR (nujol): NH = 3185 cm^{-1}. Elemental analysis (%) calcd for $C_{23.5}H_{45}AlCl_4CrNS_2$: C 45.05, H 7.24, N 2.24; found: C 45.41, H 7.63, N 2.01. μ_{eff}= 3.92 μ_B.

2.2.4 {[(SNS)Cr^{II}(μ-Cl)]$_2$} {($AlCl_2Et_2$}$_2$ (5)

A mixture of **4** (626 mg, 1 mmol) and Et_3Al (1.13 g, 10 mmol) in toluene (15 mL) was stirred for 1 minute resulting in the formation of significant quantities of metallic chromium, which was filtered

off leaving a pale blue solution. Layering the solution with hexanes and subsequent storage at -35 °C for one week resulted in the growth of blue crystals of **5** (61 mg, 9 %). IR (Nujol, cm^{-1}) N-H = 3167. Anal. Calcd (found) for $C_{20}H_{41}AlCl_3CrNS_2$: C 44.07 (44.01); H 7.59 (8.48); N 2.57 (2.58). μ_{eff}= 4.57 μ_B.

2.2.5 {[(SNS)Cr^{II}(μ-Cl)]$_2$} {$AlCl_2{}^iBu_2$}$_2$ (6)

Method A: A mixture of **1** (460 mg, 1 mmol) and a 10% IBAO solution (14 mL toluene, 4 mmol) was stirred at 22°C, forming a blue-green solution. After filtration, pale green-blue crystals of **6** (511 mg, 0.43 mmol, 86% based on chromium) deposited during storage at -35°C for 24 h IR (Nujol, cm^{-1}) N-H: 3169. Anal. Calcd (found) for $C_{24}H_{49}AlCl_3CrNS_2$: C 47.95 (47.91); H 8.22 (8.19); N 2.33 (2.28). μ_{eff}= 4.60 μ_B.

Method B: Same as method A, except IBAO was replaced with the equivalent amount of TIBA without any effect on product yield or purity. Method C: Same as method B, except **1** was replaced with the equivalent amount of **7** , without any effect on product yield or purity.

2.2.6 {(SNS$Cr^{II}Cl_2$(THF)$_2$} (7)

$CrCl_2(THF)_2$(1.06 g, 4 mmol) was dried under vacuum with stirring for 3 hours to remove excess THF. This sample was then combined with [SNS] (1.2 g, 4 mmol) in toluene (30 mL), and then stirred as the toluene/THF mixture was azeotropic distilled to remove excess THF. This procedure was repeated with 2 more aliquots of toluene (30 mL), resulting in a blue powder which was then redissolved in hot toluene (15 mL) and stored first at room temperature for 24 h for the first crop of crystals and then at -35°C for 24h for the second crop of crystals resulting in a high total yield of blue crystals of **1** (1.70 g, 95%). IR (Nujol, cm^{-1}) : 3173. Anal. Calcd (found) for $C_{20}H_{39}Cl_2CrNOS_2$: C 48.38 (48.31); H 7.92 (7.88); N 2.82 (2.79). μ_{eff}= 4.86 μ_B.

2.2.7 {(SNS)Cr^{II}(Cl_2AlEt_2)$_2$} (8)

A mixture of $CrCl_2(THF)_2$ (0.250 g, 0.93 mmol), [SNS] (0.285 g, 0.95 mmol) and Et_2AlCl (1.2 g, 9.5 mmol) in toluene (15 mL) was stirred at 22 °C to give a blue solution. Crystals of **8** as a

toluene solvate (394 mg, 82 %) formed over the course of three days at -35 °C. IR (nujol): NH = 3174 cm^{-1}. Elemental analysis (%) calcd for C22.32H44.59Al1.58Cl3.58CrNS2: C 41.57, H 7.14, N 2.20; found: C 41.03, H 7.22, N 2.11. μ_{eff}= 4.87 μ_B.

2.2.8 {(SNS)Cr^{II}(Cl_3AlEt)} {Cl_3AlEt} (9)

A mixture of $CrCl_2(THF)_2$ (0.250 g, 0.93 mmol), [SNS] (0.285 g, 0.95 mmol), and $EtAlCl_2$ (1.2 g, 9.5 mmol) in toluene (15 mL) was stirred at 22°C to give a blue solution. Crystals of **9** (405 mg, 93 %) formed over the course of three days at -35 °C. IR (nujol): NH = 3174 cm^{-1}. Elemental analysis (%) calcd for C20H41Al2Cl6CrNS2: C 35.41, H 6.09, N 2.06; found: C 35.61, H 6.33, N 2.01. μ_{eff}= 4.85 μ_B .

2.2.9 {(SNS)$Cr^{III}Cl_2$(THF)} {$AlCl_4$} (10)

A mixture of $CrCl_3(THF)_3$ (510 mg, 1.3 mmol), [SNS] (402 mg, 1.3 mmol) and anhydrous $AlCl_3$ (355 mg, 2.7 mmol) in toluene (15 mL) was refluxed for 5 min, forming a blue solution which was filtered. Blue-green crystals of analytically pure **10** (752 mg, 1.13 mmol, 87%) were grown during storage at -35°C for a few days. IR (Nujol, cm^{-1}) : 3178. Anal. Calcd (found) for C20H39Cl6CrNOS2Al: C 36.10 (36.09); H 5.91 (5.88); N 2.11 (2.06). μ_{eff}= 3.78 μ_B.

2.2.10 {[(SNS)Cr^{III}Cl(μ-Cl)]$_2$} {$AlCl_4$}$_2$ (11)

A mixture of **1** (460 mg, 1 mmol), and $AlCl_3$ (1.729 g, 13.0 mmol) in toluene (15 mL) was refluxed for 5 min, forming a dark-green solution, which was filtered. Dark-green crystals of analytically pure **11** (639 mg, 0.43 mmol, 66% based on chromium) were grown during storage at 22°C for 1 day, followed by storage at -35°C for 1 day. IR (Nujol, cm^{-1}) : 3188. Anal. Calcd (found) for C26.50H43NS2CrCl6Al: C 43.51 (43.49); H 5.93 (5.88); N, 1.91 (1.86). μ_{eff}= 3.94 μ_B.

2.2.11 {(SNS)Cr^{III}[η^2-(μ-Cl)$_2$$AlCl_2$]} {$Al_2Cl_7$} (12)

A mixture of $CrCl_3(THF)_3$ (503 mg, 1.3 mmol), [SNS] (402 mg, 1.3 mmol), and $AlCl_3$ (3.46 g, 26 mmol) in toluene (15 mL) was refluxed for 5 min, forming a red solution, which was filtered. Red

crystals of **12** mixed together with unknown blue-colored materials (726 mg total) were separated during storage at -35°C for a few days. Regrettably, the purification of **12** proved impossible and prevented meaningful analytical determination and catalytic activity testing.

2.2.12 {[(μ^2-SNS)CrCl]$_2$} (13)

To a stirring solution of [SNS] (500 mg, 1.6 mmol) in THF (15 mL), n-BuLi (0.67 mL of a 2.5 M solution, 1.7 mmol) was added dropwise at -35 C, and the resulting mixture was allowed to warm to room temperature. The addition of $CrCl_2(THF)_2$ (0.427 g, 1.6 mmol) to this solution afforded a light-blue solution, which was evaporated to dryness. The solid residue was recrystallized from hot toluene to yield blue crystals of **13** (560 mg, 87%) at room temperature. Anal. Calcd (found) for C16H30ClCrNS2: C 49.53 (49.49); H 7.79 (7.73); N 3.61 (3.57). μ_{eff}= 3.95 μ_B.

2.2.13 X-ray Characterization

Table 1: Crystal Data and Structure Analysis Results for Chromium [SNS]

Complex #	**2**	**4**	**5**	**6**	**7**
formula	C30H60Al2	C23.50H45	C26.25H48Al	C24H49Al	C20H39Cl2
	Cl2CrNS2	AlCl4CrNS2	Cl3CrNS2	Cl3CrNS2	CrNOS2
Mw	678.83	626.51	627.11	601.09	495.53
space group	P2(1)/c	C2/c	P2(1)/n	P	P2(1)/n
a (Å)	13.782(12)	27.329(4)	13.732(4)	10.987(4)	11.198(7)
b (Å)	12.776(11)	13.296(2)	18.050(5)	12.816(5)	20.051(15)
c (Å)	21.606(19)	21.528(3)	16.261(4)	13.475(5)	12.262(9)
α	90	90	90	67.230(6)	90
β	96.037(16)	124.302(2)	99.408(4)	83.158(6)	115.98(3)
γ	90	90	90	66.385(6)	90
V (Å^3)	3783(6)	6462.2(17)	3976.6(17)	1601.7(10)	2475(3)
Z	4	8	4	2	4
radiation	0.71073	0.71073	0.71073	0.71073	0.71073
T (K)	208(2)	208(2)	208(2)	208(2)	208(2)
D_{calcd} (g cm^{-3})	1.192	1.288	1.047	1.246	1.330
μ_{calcd} (mm^{-1})	0.630	0.855	0.630	0.778	0.857
F000	1457	2640	1330	640	1052
R, Rw_2	0.0734, 0.1659	0.0605, 0.1443	0.0521, 0.1329	0.0734, 0.1328	0.0642, 0.1173
GoF	1.042	1.034	1.017	1.033	1.012
8	**9**	**10**	**11**	**12**	**13**
C22.32H44.6S2	C23.50H45Al	C20H39Al	C26.50H43N	C16H30Al3	C16H30Cl
Al1.6Cl3.6CrN	Cl4CrNS2	Cl6CrNOS2	S2CrCl6Al	Cl12CrNS2	CrNS2
612.68	626.51	665.32	731.42	858.87	387.9(7)
P-1	C2/c	P2(1)/c	P2(1)/n	P	P
11.074(2)	27.329	7.4228(16)	10.8236(18)	9.467(5)	8.019(3)
12.746(3)	13.296	25.919(6)	29.167(5)	11.999(7)	8.794(4)
13.224(3)	21.528	16.281(3)	11.750(2)	17.895(10	14.224(6)
96.916(3)	90	90	90	83.573(10)	79.18(3)
99.913(4)	124.302	92.681(4)	104.261(3)	81.026(10)	78.75(6)
103.724(4)	90	90	90	67.885(9)	85.58(4)
1760.7(6)	6462.2(17)	3128.9(12)	3595.1(10)	1857.1(18)	965.5(7)
2	8	4	4	2	2
0.71073	0.71073	0.71073	0.71073	0.71073	0.71073
200(2)	200(2)	198(2)	198(2)	207(2)	209(2)
1.156	1.288	1.412	1.351	1.536	1.335
0.765	0.855	1.054	0.923	1.367	0.941
646	2640	1380	1520	864	412
0.0778, 0.2011	0.0605, 0.1443	0.0676, 0.1262	0.0684, 0.1643	0.0969, 0.2271	0.0397, 0.0671
1.060	1.034	1.040	1.027	1.069	1.012

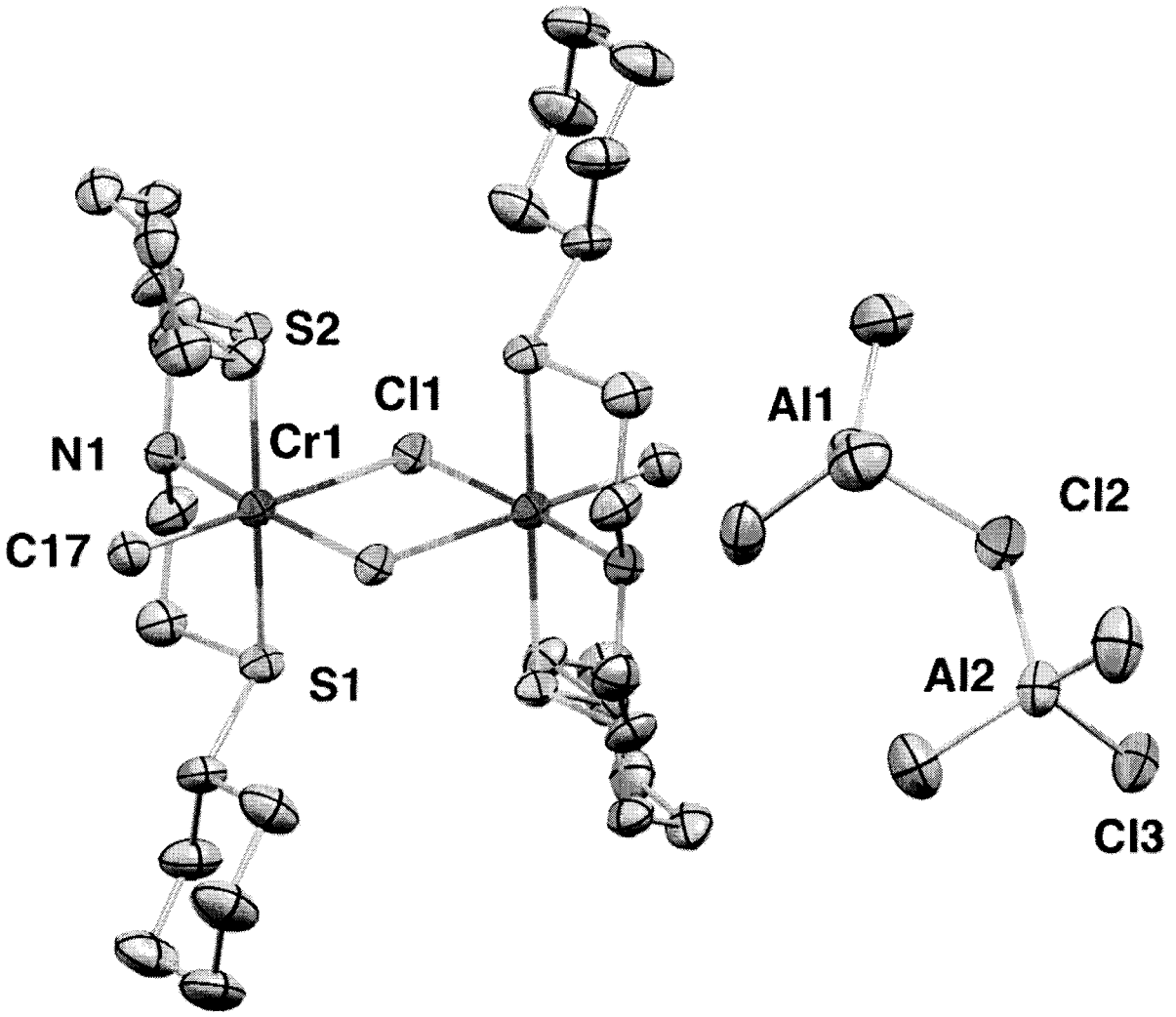

Figure 12: Partial thermal ellipsoid plot of $\{[(SNS)Cr^{III}Me(\mu\text{-}Cl)]_2\}$ $\{(AlMe_3)_2(\mu\text{-}Cl)\}_2$ (**2**) with ellipsoids drawn at 50% probability

Table 2: Selected Bond Distances (Å) and Angles (°) for $\{(SNS)Cr^{III}Me(\mu\text{-}Cl)_2\}$ $\{(AlMe_3)_2(\mu\text{-}Cl)\}_2$ (**2**)

Cr(1)–C(17)	2.049(5)	C(17)–Cr(1)–N(1)	91.8(2)
Cr(1)–N(1)	2.088(4)	C(17)–Cr(1)–Cl(1)	94.03(16)
Cr(1)–Cl(1)	2.339(2)	N(1)–Cr(1)–Cl(1)	174.09(12)
Cr(1)–S(1)	2.445(2)	C(17)–Cr(1)–S(1)	94.67(15)
Cr(1)–S(2)	2.446(2)	N(1)–Cr(1)–S(1)	83.63(13)
Cr(1)–Cl(1a)	2.519(2)	Cl(1)–Cr(1)–S(1)	95.09(7)
Al(1)–Cl(2)	2.412(3)	S(1)–Cr–S(2)	164.87(6)
		Al(1)–Cl(2)–Al(2)	114.28(9)

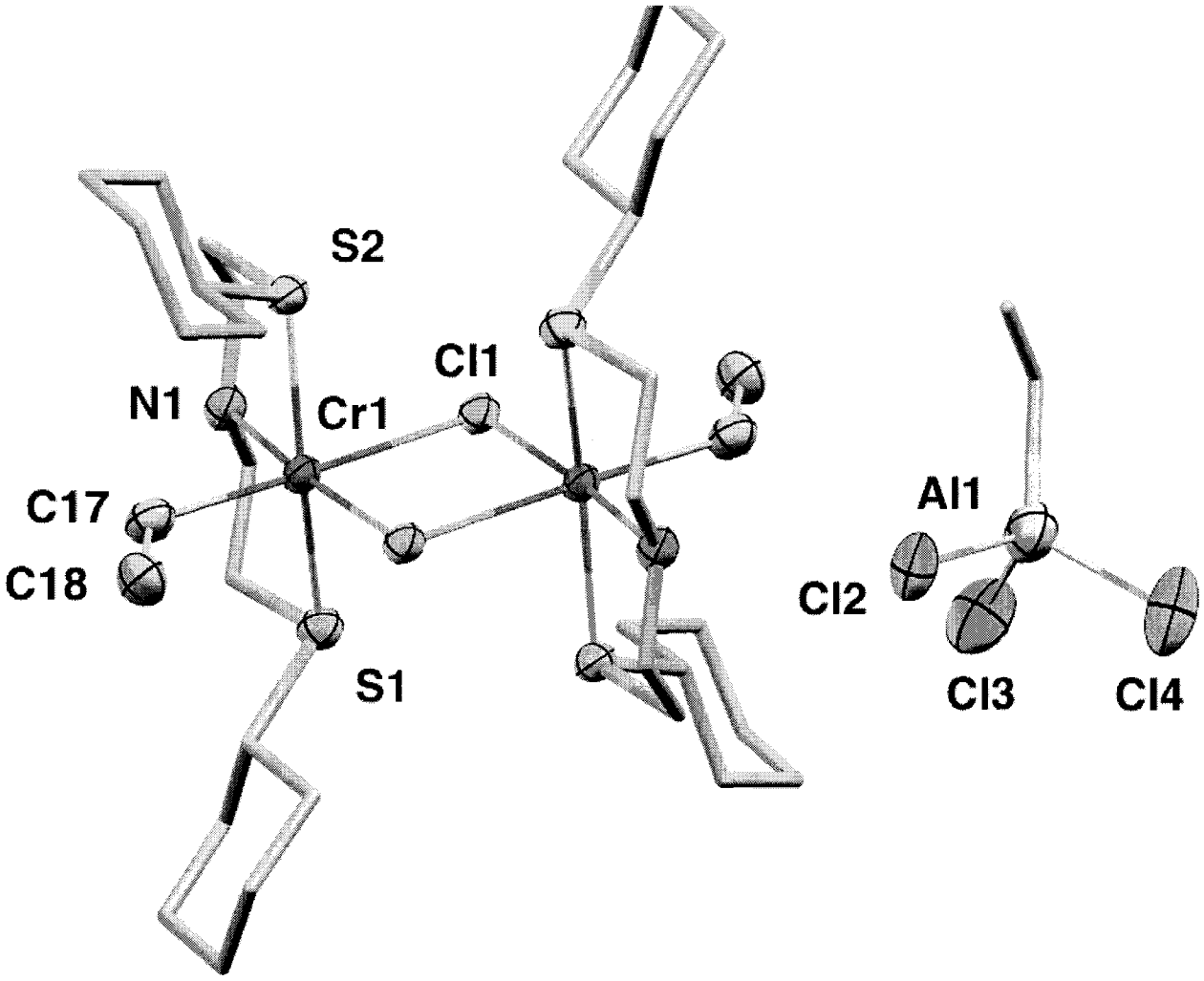

Figure 13: Partial thermal ellipsoid plot of $\{[(SNS)Cr^{III}Et(\mu\text{-}Cl)]_2\}$ $\{AlCl_3Et\}_2$ (**4**) with ellipsoids drawn at 50% probability

Table 3: Selected Bond Distances (Å) and Angles (°) for $\{[(SNS)Cr^{III}Et(\mu\text{-}Cl)]_2\}$ $\{AlCl_3Et\}_2$ (**4**)

Cr(1)-Cl(1)	2.5529(13)	C(17)–Cr(1)–N(1)	91.8(2)
Cr(1)-Cl(1A)	2.3574(13)	C(17)–Cr(1)–Cl(1)	94.03(16)
Cr(1)-C(17)	2.108(5)	N(1)–Cr(1)–Cl(1)	174.09(12)
Cr(1)-S(1)	2.4654(14)	C(17)–Cr(1)–S(1)	94.67(15)
Cr(1)-S(2)	2.4632(14)	N(1)–Cr(1)–S(1)	83.63(13)
Cr(1)-N(1)	2.090(4)	Cl(1)–Cr(1)–S(1)	95.09(7)
		S(1)–Cr–S(2)	164.87(6)

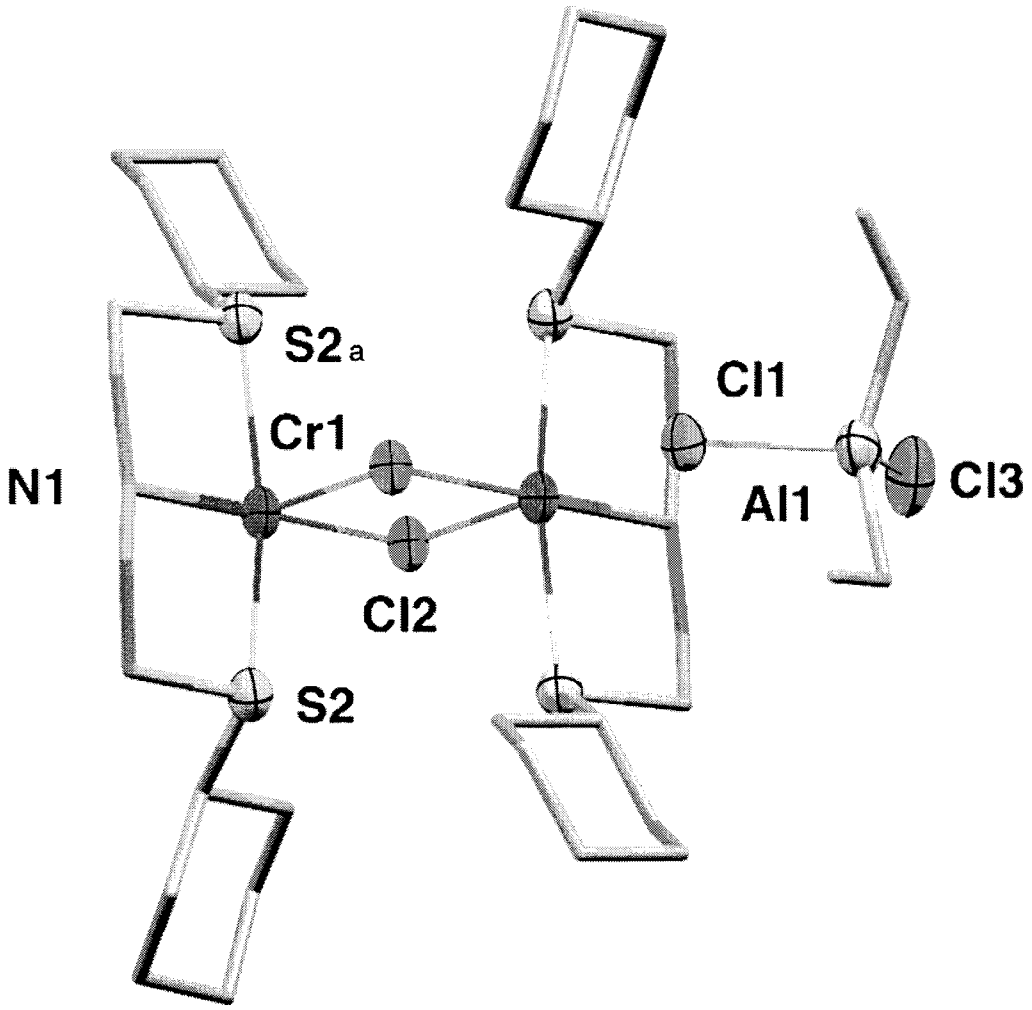

Figure 14: Partial thermal ellipsoid plot of $\{[(SNS)Cr^{II}(\mu\text{-}Cl)]_2\}$ $\{(AlCl_2Et_2\}_2$ (**5**) with ellipsoids drawn at 50% probability

Table 4: Selected Bond Distances (Å) and Angles (°) for $\{[(SNS)Cr^{II}(\mu\text{-}Cl)]_2\}$ $\{(AlCl_2Et_2\}_2$ (**5**)

Cr(1)–N(1)	2.134(5)	N(1)–Cr(1)–Cl(1)	178.79(16)
Cr(1)–Cl(1)	2.3486(19)	N(1)–Cr(1)–S(2)	82.45(17)
Cr(1)–S(2)	2.511(2)	Cl(1)–Cr(1)–S(2)	97.07(7)
Cr(1)–Cl(1a)	2.714(2)	N(1)–Cr(1)–Cl(1a)	187.57(16)
N(1)–C(2)	1.454(8)		

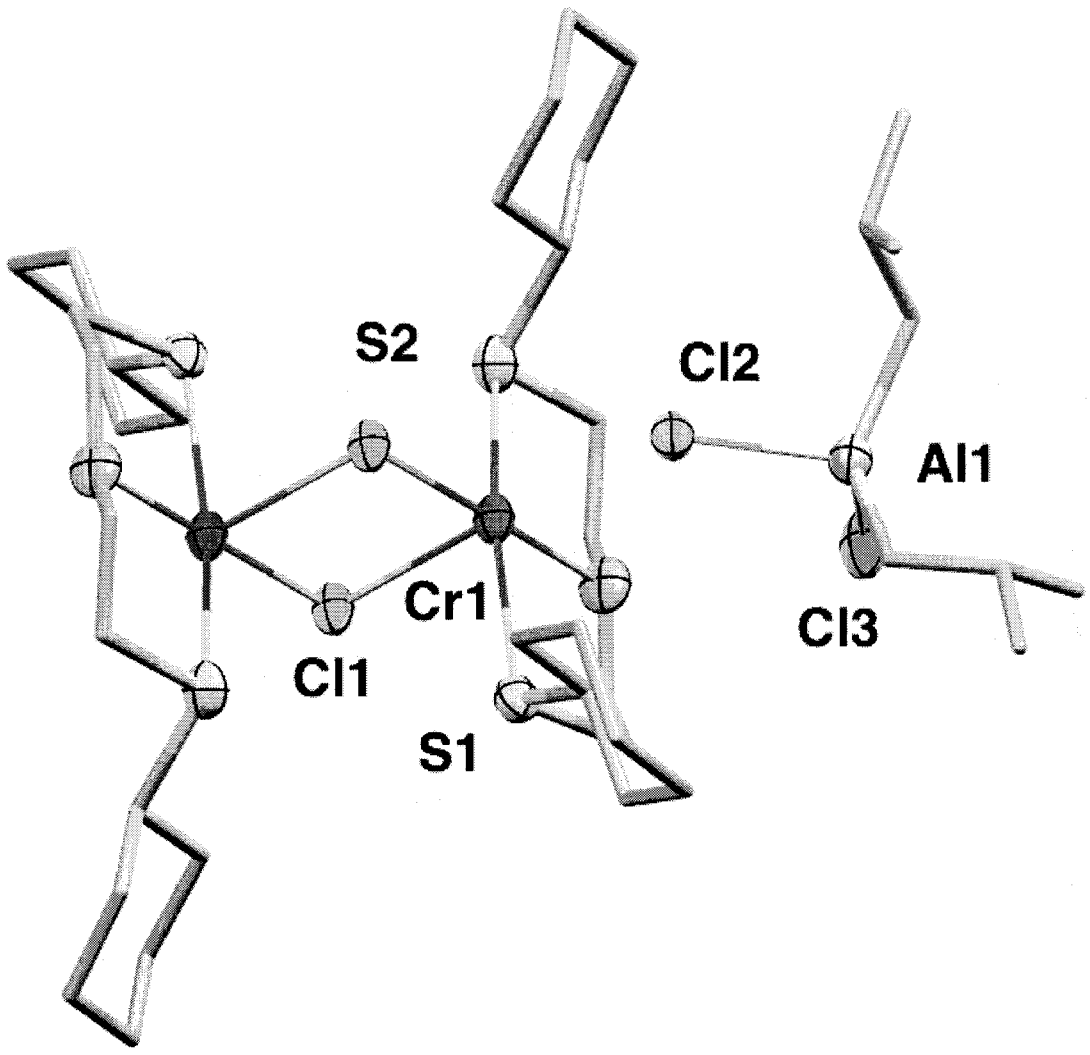

Figure 15: Partial thermal ellipsoid plot of $\{[(SNS)Cr^{II}(\mu\text{-}Cl)]_2\}$ $\{AlCl_2{}^iBu_2\}_2$ (**6**) with ellipsoids drawn at 50% probability

Table 5: Selected Bond Distances (Å) and Angles (°) for $\{[(SNS)Cr^{II}(\mu\text{-}Cl)]_2\}$ $\{AlCl_2{}^iBu_2\}_2$ (**6**)

Cr(1)–N(1)	2.134(5)	N(1)–Cr(1)–Cl(1)	178.79(16)
Cr(1)–Cl(1)	2.3486(19)	N(1)–Cr(1)–S(2)	82.45(17)
Cr(1)–S(2)	2.511(2)	Cl(1)–Cr(1)–S(2)	97.07(7)
Cr(1)–Cl(1a)	2.714(2)	N(1)–Cr(1)–Cl(1a)	87.57(16)
N(1)–C(2)	1.454(8)	Cr(1)-Cl(2)	2.714(2)

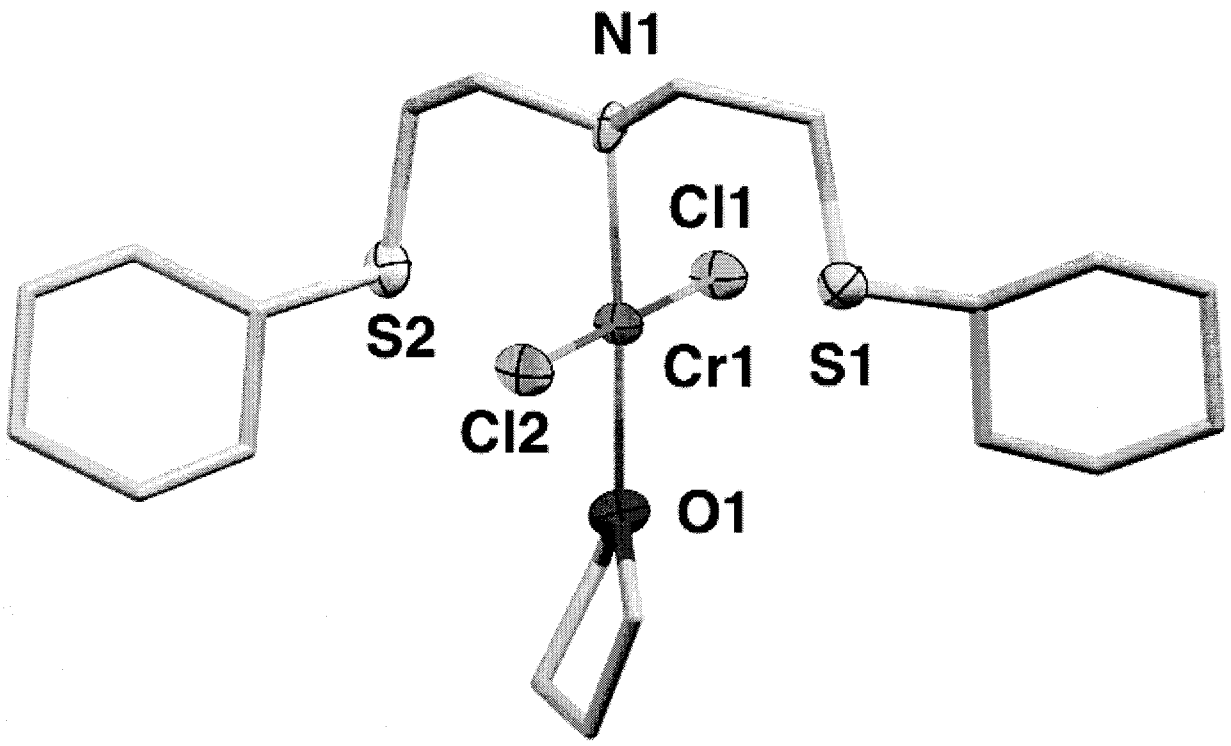

Figure 16: Partial thermal ellipsoid plot of {(SNS)$Cr^{II}Cl_2$(THF)} (**7**) with ellipsoids drawn at 50% probability

Table 6: Selected Bond Distances (Å) and Angles (°) for {(SNS$Cr^{II}Cl_2$(THF)$_2$} (**7**)

Cr(1)–O(1)	2.098(6)	O(1)–Cr(1)–N(1)	175.4(3)
Cr(1)–N(1)	2.142(7)	O(1)–Cr(1)–Cl(2)	90.49(18)
Cr(1)–Cl(2)	2.372(3)	N(1)–Cr(1)–Cl(2)	92.0(2)
Cr(1)–Cl(1)	2.405(3)	O(1)–Cr(1)–Cl(1)	90.00(18)
Cr (1)–S (1)	2.846(6)	N(1)–Cr(1)–Cl(1)	87.6(2)
Cr (1)–S (2)	2.840(6)		

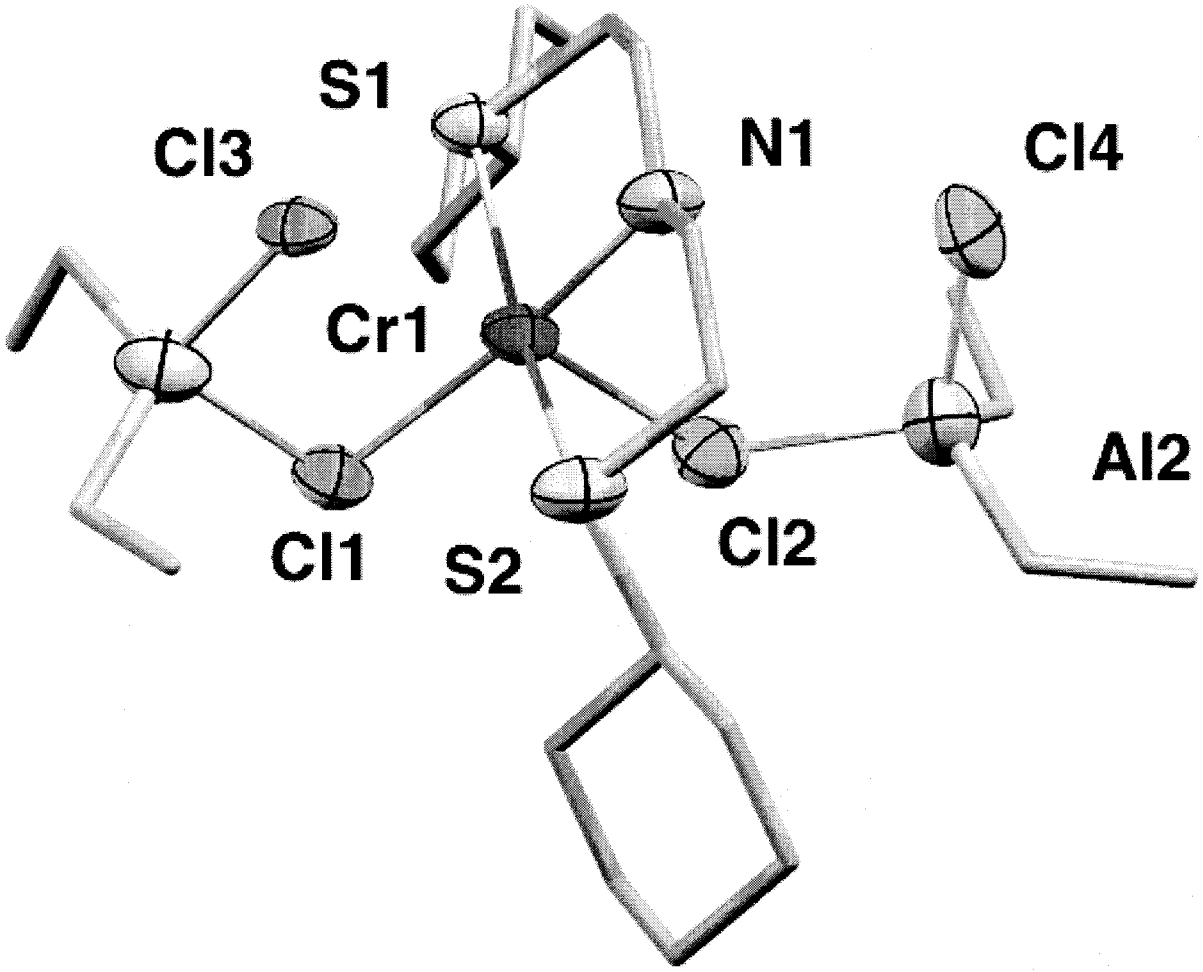

Figure 17: Partial thermal ellipsoid plot of $\{(SNS)Cr^{II}(Cl_2AlEt_2)_2\}$ (**8**) with ellipsoids drawn at 50% probability

Table 7: Selected Bond Distances (Å) and Angles (°) for $\{(SNS)Cr^{II}(Cl_2AlEt_2)_2\}$ (**8**)

Cr(1)-N(1)	2.044(6)	N(1)-Cr(1)-Cl(3)	171.8(2)
Cr(1)-Cl(3)	2.384(3)	N(1)-Cr(1)-S(2)	82.66(16)
Cr(1)-S(2)	2.485(2)	Cl(3)-Cr(1)-S(2)	97.35(9)
Cr(1)-S(1)	2.492(3)	N(1)-Cr(1)-S(1)	83.68(17)
Cr(1)-Cl(1)	2.709(3)	Cl(3)-Cr(1)-S(1)	94.79(9)

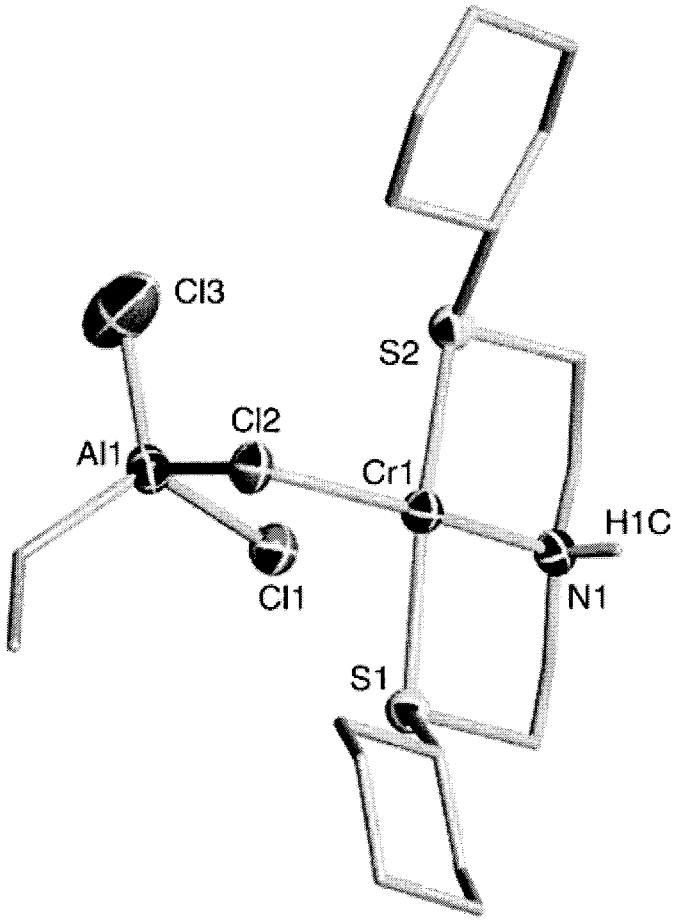

Figure 18: Partial thermal ellipsoid plot of {(SNS)Cr^{II}(Cl_3AlEt)} {Cl_3AlEt} (**9**) with ellipsoids drawn at 50% probability

Table 8: Selected Bond Distances (Å) and Angles (°) for {(SNS)Cr^{II}(Cl_3AlEt)} {Cl_3AlEt} (**9**)

Cr(1)-S(1)	2.4828(18)	N(1)–Cr(1)–Cl(1)	178.79(16)
Cr(1)-S(2)	2.4844(19)	N(1)–Cr(1)–S(2)	82.45(17)
Cr(1)-N(1)	2.092(4)	Cl(1)–Cr(1)–S(2)	97.07(7)
Cr(1)-Cl(2)	2.3974(17)	N(1)–Cr(1)–Cl(1a)	187.57(16)

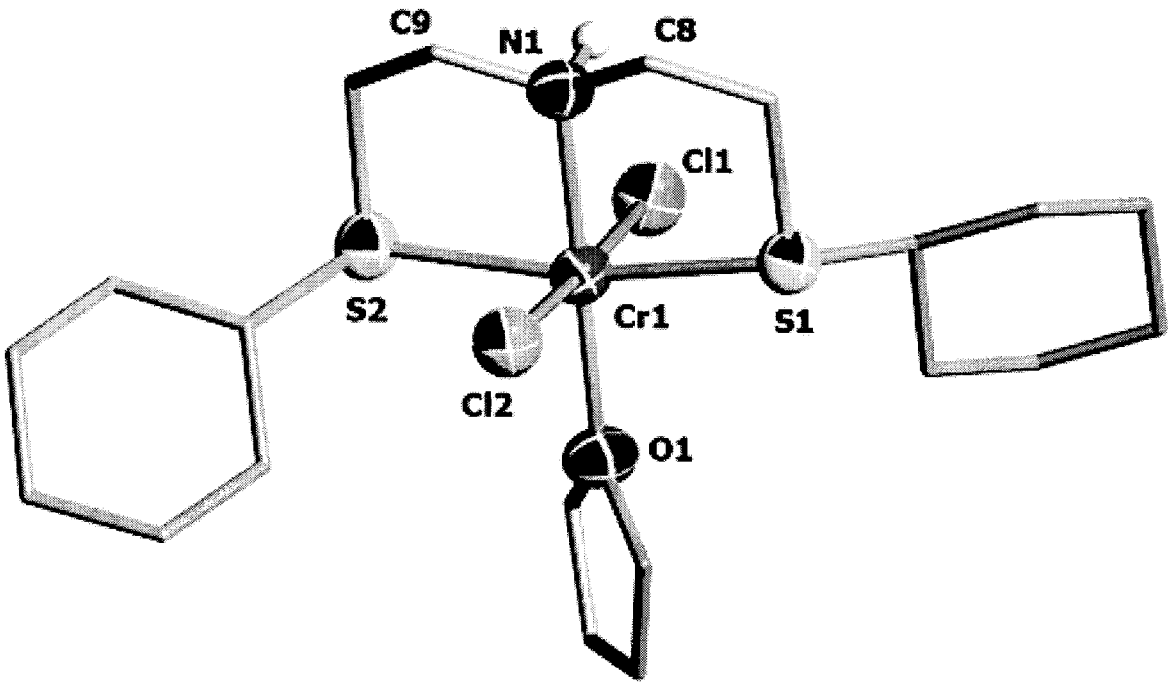

Figure 19: Partial thermal ellipsoid plot of {(SNS)$Cr^{III}Cl_2$(THF)} {$AlCl_4$} (**10**) with ellipsoids drawn at 50% probability

Table 9: Selected Bond Distances (Å) and Angles (°) for {(SNS)$Cr^{III}Cl_2$(THF)} {$AlCl_4$} (**10**)

Cr(1)–Cl(1)	2.295(2)	O(1)–Cr(1)–S(1)	95.50(15)
Cr(1)–Cl(2)	2.292(2)	O(1)–Cr(1)–S(2)	95.38(15)
Cr(1)–N(1)	2.068(6)	O(1)–Cr(1)–N(1)	179.0(2)
Cr(1)–S(1)	2.440(2)	N(1)–Cr(1)–Cl(1)	89.08(18)
Cr(1)–S(2)	2.443(2)	N(1)–Cr(1)–S(1)	84.31(17)
Cr(1)–O(1)	2.034(5)	Cl(1)–Cr(1)–Cl(2)	177.12(9)
O(1)–Cr(1)–Cl(1)	91.92(15)	S(1)–Cr(1)–S(2)	169.12(8)
O(1)–Cr(1)–Cl(2)	90.64(15)		

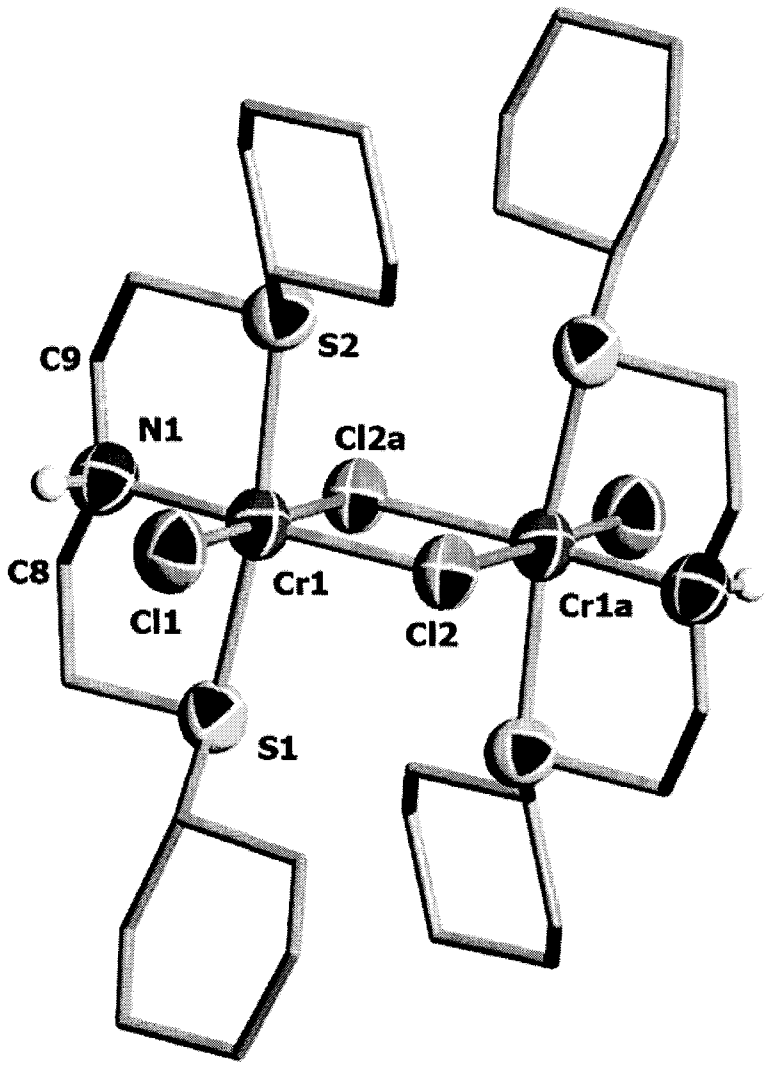

Figure 20: Partial thermal ellipsoid plot of $\{[(SNS)Cr^{III}Cl(\mu\text{-}Cl)]_2\}$ $\{AlCl_4\}_2$ (**11**) with ellipsoids drawn at 50% probability

Table 10: Selected Bond Distances (Å) and Angles (°) for $\{[(SNS)Cr^{III}Cl(\mu\text{-}Cl)]_2\}$ $\{AlCl_4\}_2$ (**11**)

Cr(1)–Cl(1)	2.233(3)	Cl(1)–Cr(1)–S(2)	93.45(10)
Cr(1)–N(1)	2.057(7)	Cl(1)–Cr(1)–Cl(2a)	179.10(11)
Cr(1)–Cl(2)	2.364(3)	S(1)–Cr(1)–S(2)	166.94(11)
Cr(1)–S(1)	2.436(3)	S(2)–Cr(1)–Cl(2)	166.94(11)
Cr(1)–S(2)	2.447(3)	S(1)–Cr(1)–Cl(2)	95.20(10)
		N(1)–Cr(1)–S(1)	84.4(2)
Cl(1)–Cr(1)–S(1)	93.41(11)	N(1)–Cr(1)–S(2)	84.3(2)
Cl(1)–Cr(1)–Cl(2)	94.34(10)	Cl(1)–Cr(1)–N(1)	91.7(2)

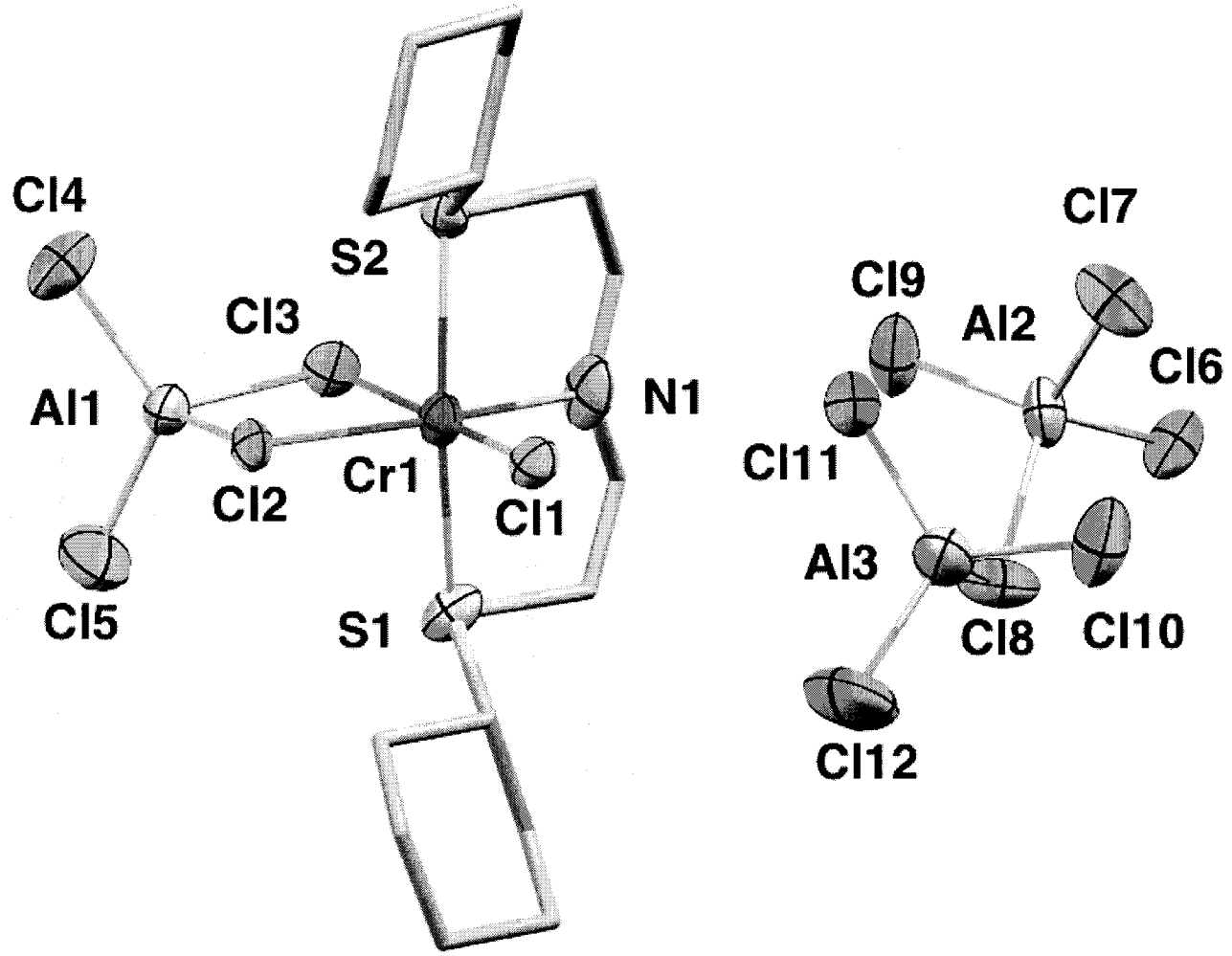

Figure 21: Partial thermal ellipsoid plot of $\{(SNS)Cr^{III}(\eta^2\text{-}AlCl_4)\}$ $\{Al_2Cl_7\}$ (**12**) with ellipsoids drawn at 50% probability

Table 11: Selected Bond Distances (Å) and Angles (°) for $\{(SNS)Cr^{III}(\eta^2\text{-}AlCl_4)\}$ $\{Al_2Cl_7\}$ (**12**)

Cr(1)–Cl(1)	2.498(4)	Al(1)–Cl(2)	2.247(5)
Cr(1)–Cl(2)	2.409(3)	N(1)–Cr(1)–Cl(2)	170.6(4)
Cr(1)–Cl(3)	2.229(3)	Cl(1)–Cr(1)–Cl(3)	178.20(13)
Cr(1)–N(1)	2.058(10)	S(1)–Cr(1)–S(2)	166.16(12)
Cr(1)–S(1)	2.447(4)	Cr(1)–Cl(1)–Al(1)	90.91(14)
Cr(1)–S(2)	2.464(4)	Cl(1)–Cr(1)–Cl(2)	82.89(11)
Al(1)–Cl(1)	2.218(5)	Cl(1)–Al(1)–Cl(2)	93.36(16)

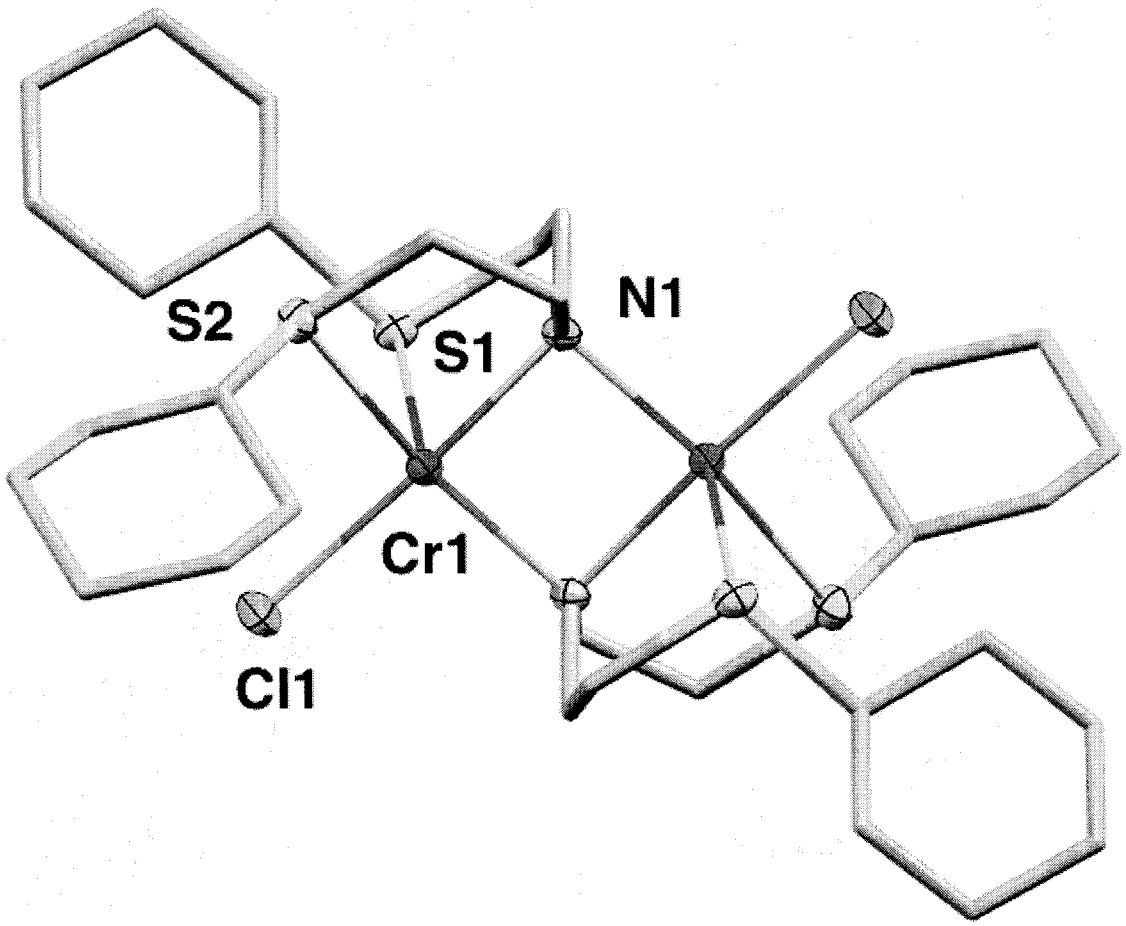

Figure 22: Partial thermal ellipsoid plot of $\{[(\mu^2\text{-SNS})Cr^{II}Cl]_2\}$ (**13**) with ellipsoids drawn at 50% probability

Table 12: Selected Bond Distances (Å) and Angles (°) for $\{[(\mu^2\text{-SNS})Cr^{II}Cl]_2\}$ (**13**)

Cr(1)–N(1)	2.071(3)	N(1)–Cr(1)–N(1a)	88.61(11)
Cr(1)–N(1a)	2.093(3)	N(1)–Cr(1)–Cl(1)	176.29(8)
Cr(1)–Cl(1)	2.3581(16)	N(1a)–Cr(1)–Cl(1)	94.68(8)
Cr(1)–S(2)	2.5359(17)	N(1)–Cr(1)–S(2)	80.26(8)
Cr(1)–S(1)	2.6948(17)	N(1a)–Cr(1)–S(2)	154.52(8)
Cr(1)–Cr(1)	2.9796(18)		

2.2.14 Catalytic Evaluation of 1-13

General Oligomerization Procedure: A 250-mL steel Büchi reactor was dried in an oven at 120 °C for 3 h prior to each run and then placed under vacuum for 30 min and purged with three cycles of Ar/vacuum. The reactor was then preheated, charged with toluene and the desired amount of

MAO, pressurized with 35 bar of ethylene, and stirred at 50 °C. After 15 min, the pressure was momentarily released to allow injecting the catalyst solution into the reactor under a stream of ethylene, and then the reactor was immediately repressurized. The reaction was allowed to run for 45 min, after which the temperature was rapidly reduced, the reactor was depressurized, and a mixture of EtOH/HCl was injected to quench the reaction. The organic and aqueous phases were then separated from the polymer. Precautions were taken to maintain the temperature as low as possible during the workup to minimize loss of volatiles. Polymeric materials were sonicated with an aqueous solution of HCl and dried at 60 °C for 18 h under reduced pressure before the final mass was weighed. Ratios (or selectivity) of oligomers were obtained by GC by using calibrated standard solutions. The overall catalytic activity was determined by integrating the intensity of the olefinic NMR resonances versus the Me group of the toluene solvent. Results are summarized in Table 13.

Table 13: Catalytic Data for Cr [SNS] complexes **1-13**

Cat.	MAO	Alkenes	PE	activity	activity	C_6	C_8	C_{10}	C_{12}	C_{14}
#	(eq.)	(mL)[a]	(g)	(g/mol/h)	(g/gCr/h)	(%)	(%)	(%)	(%)	(%)
1	1000	13.5	0.08	302850	5824	>98	-	-	-	-
2	2000	3.5	4.26	78516	1510	32	28	18	11	6
	1000	16.0	0.8	358933	6903	>98	-	-	-	-
	500	18.5	0.4	415016	8024	>98	-	-	-	-
3	2000	4.5	3.2	100950	1941	96.69	0.74	0.74	0.74	0.64
	1000	5.1	2.3	114410	2200	>98	-	-	-	-
4	1000	21.0	0.8	487916	9383	>98	-	-	-	-
5	1000	7.3	0.89	163784	3149	68.38	10.11	9.56	6.12	3.87
6	2000	3.8	1.47	85247	1639	53.37	17.90	12.26	8.37	5.04
	1000	6.0	0.86	134600	2588	70.79	9.23	8.61	5.66	3.47
	500	8.2	0.78	185075	3559	96.53	0.99	0.87	0.72	0.49
	300	10.5	0.70	235550	4530	98	0.36	0.39	0.29	0.19
	150	12.3	0.50	276628	5320	>98	-	-	-	-
7	1000	6.7	2.6	151425	2912	>98	-	-	-	-
8	1000	7.2	1.76	162725	3129	>98	-	-	-	-
9	1000	9.5	1.54	214707	4128	>98	-	-	-	-
10	1000	32.2	1.01	723475	13913	>98	-	-	-	-
11	1000	10.5	0.18	235550	4530	>98	-	-	-	-
12	1000	0	0.12	0	0	0	0	0	0	0
d	1000	0	0.08	0	0	0	0	0	0	0
e	1000	0	0.42	-	-	-	-	0	0	0

T = 50 °C, V = 150 mL, P = 35 bar, catalyst = 30 µmole, time = 1 h. [a] By integration of the NMR olefinic resonances with respect to the Me of the toluene solvent. [b] By G.C.: values of C4 are not given due to volatility. [d]blank. [e]$CrCl_2(THF)_2$. (-) = traces of oligomers detected.

2.3 Results

2.3.1 Reaction of (SNS)$CrCl_3$ (1) with aluminum cocatalysts

The reaction of $CrCl_3(THF)_3$ with the $NH(CH_2CH_2SCy)_2$ [SNS] ligand in toluene resulted in the quantitative formation of a standard ethylene trimerization catalyst precursor {(SNS)$CrCl_3$} (**1**). The structure of the related phenyl-substituted [SNS] and a related diphenylphosphine- substituted derivative have been reported. Their structural analysis revealed that these ligands are invariably bound in a meridional fashion.[30, 31] This section describes the reactions of **1** and related [SNS] chromium precursors with an excess of the following aluminum alkyls (arranged from the predicted strongest Lewis acidity and least-reducing to the predicted least Lewis acidic and most-reducing):

$(AlMeO)_n$, Me_3Al, Et_2AlCl, Et_3Al, $(Al^iBu_2)_2O$, Al^iBu_3 (Figure 23).

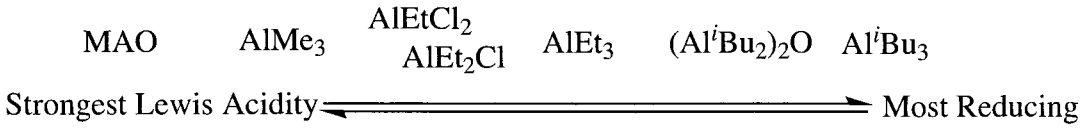

Figure 23: The range of properties of aluminum cocatalysts

The reaction of **1** with excess Me_3Al (10 eq.) afforded a high yield of $\{[(SNS)Cr^{III}Me(\mu\text{-}Cl)]_2\}$ $\{(AlMe_3)_2(\mu\text{-}Cl)\}_2$ (**2**), which was isolated as large dark-green X-ray quality crystals (Figure 24). The structure of **2** (Figure 12) consists of a symmetry generated dicationic dimer with an edge-sharing bi-octahedral structure, counterbalanced by two $\{(AlMe_3)_2(\mu\text{-}Cl)\}$ anions. The two slightly distorted octahedral chromium atoms in the cationic unit are connected by two bridging chlorine atoms [Cr(1)-Cl(1) = 2.339(2) Å; Cr(1)-Cl(1a) = 2.519(2) Å] forming a Cr_2Cl_2 planar core [Cl(1)-Cr(1)-Cl(1a) = 85.54(6)°; Cr(1)-Cl(1)-Cr(1a) = 94.46(6)°]. The equatorial plane [Cl(1)-Cr(1)-N(1) = 174.09(12)°; Cl(1)-Cr(1)-C(17) = 94.03(16)°; N(1)-Cr(1)-C(17) = 91.8(2)°] around each chromium atom is defined by the two bridging chlorides, the terminally bonded Me group [Cr(1)-C(17) = 2.049(5) Å], and the protonated nitrogen atom of the ligand [Cr(1)-N(1) = 2.088(4) Å]. The sulfur atoms of each ligand are placed on the two axial positions [Cr(1)-S(1) = 2.445(2) Å; Cr(1)-S(2) = 2.446(2) Å], showing substantial deviation from linearity [S(1)-Cr(1)-S(2) = 164.87(6)°]. The presence of the hydrogen on the ligand nitrogen atom is clearly indicated by the deviation of the nitrogen coordination geometry from planarity [C(2)-N(1)-Cr(1) = 113.0(3)°; C(3)-N(1)-Cr(1) = 112.4(3)°; C(2)-N(1)-C(3) = 111.7(4)°] as well as the I.R. signal characteristic for the N-H stretch at 3181 cm^{-1}. The two $\{(AlMe_3)_2(\mu\text{-}Cl)\}$ anions are not connected to the dicationic chromium unit, and two molecules of interstitial toluene complete the structure. The room-temperature magnetic moment of **2** of 3.94 μ_B per chromium atom is consistent with three unpaired electrons expected for the d^3 configuration of chromium(III).

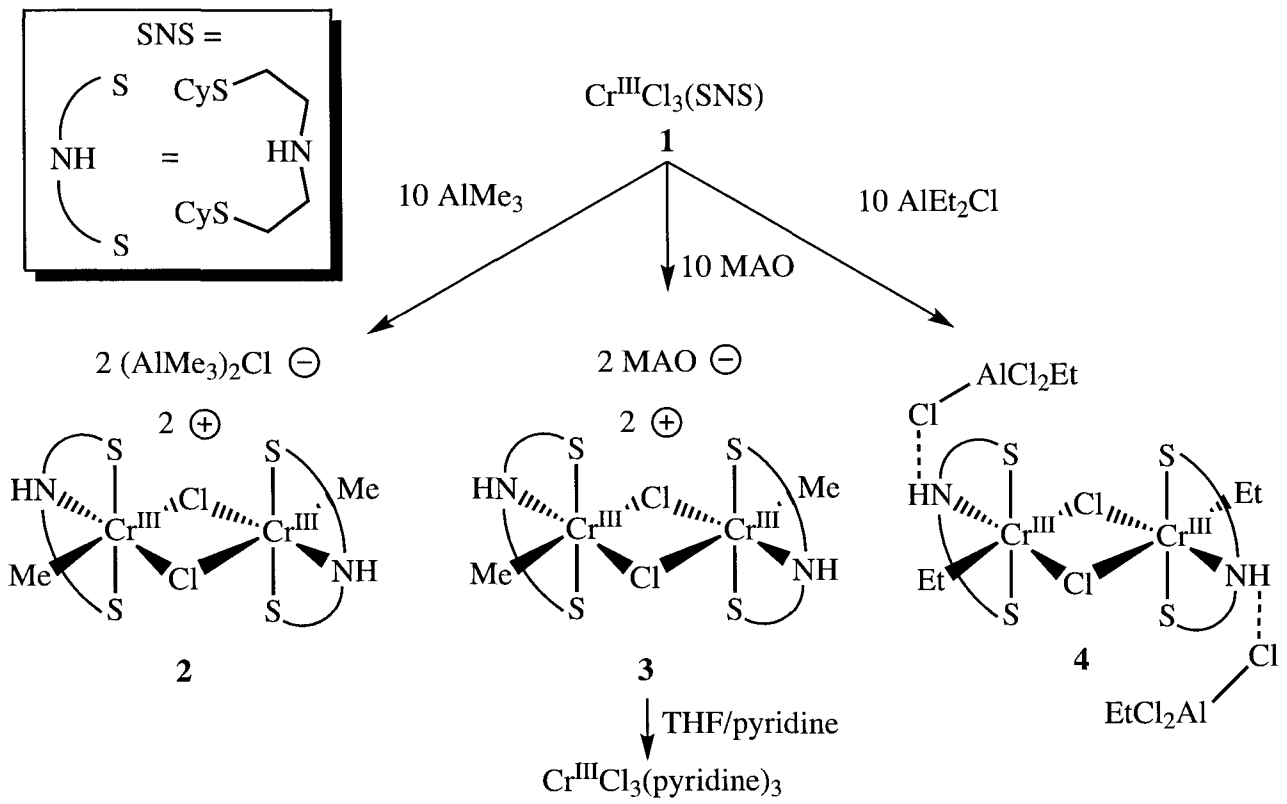

Figure 24: Reaction of 1 with excess Me_3Al, MAO, and Et_2AlCl

The relatively acidic N-H functionality remains intact even in close proximity to the reactive chromium alkyl, which is consistent with the established hydrolytic stability of chromium alkyls. This is obviously due more to kinetic stability of the electronic and geometric configuration of **2**. Furthermore, complex **2** is surprisingly thermally robust for a chromium alkyl and showed signs of partial decomposition only after 1 h of reflux in toluene. However, the rate of the decomposition was greatly accelerated by the presence of a large excess of MAO or Me_3Al. Complete decomposition occurred at room temperature within 1 h upon treatment with 100 eq. of either alkyl aluminum reagent.

The reaction of **1** with an excess of the best catalyst activator, MAO (10 eq.), also afforded a homogeneous dark-green microcrystalline material which regrettably was of insufficient quality for X-ray structural determination. However, the very close similarity of the colors of the well-defined **2** and this new material formed with MAO suggested that the two species might both possess trivalent chromium with similar coordination environments. To substantiate this point, we have recorded the EPR spectra of both complexes (Figure 25), and found that the binuclear d^3 Cr(III)

configuration furnishes an extremely strong fingerprint pattern due to magnetic coupling between the two chromium centres, while the high spin d^4 Cr (II) electronic configuration is generally EPR silent. As it can be observed, the spectra of **2** and the MAO complex **3** display only minor differences. The complexity of the spectra would require an in-depth magnetic study to enable simulation of the spectral features from the structure of **2** and **3** that are beyond the scope of this study. A recent EPR study of related mononuclear and binuclear Cr (III) complexes reveals that diagnostic features consistent with these are observed in general for dichromium (III) complexes.[69] However, for the purpose of this thesis, it will suffice to observe the close spectral similarity, or fingerprint, which substantiates the conclusion that even in the case of **3**, two trivalent chromium species are part of a binuclear species with an overall integer spin configuration. The room-temperature magnetic moment of **3** (3.93 μ_B per chromium atom), is as expected for the high-spin d^3 electronic configuration of an octahedral Cr(III). This is of course assuming the same formulation of **2** with the only difference consisting of the replacement of the Me_3AlCl counteranion of **2** with the heterogeneous $1/n(MeClAl)_2O_n$ counteranion for **3**. We suspect that the heterogeneous nature of the MAO counteranion is most likely responsible for the poor crystallinity.

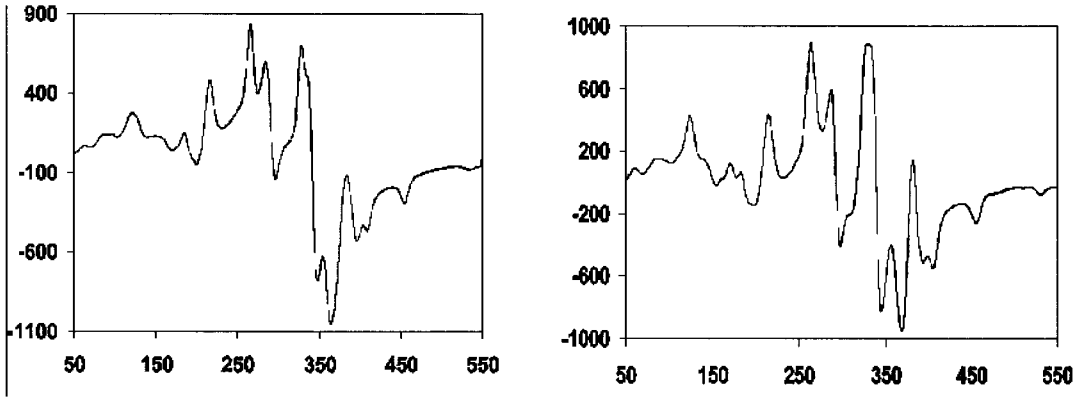

Figure 25: Powder EPR spectrum of **2** (left) and **3** (right) at -160 °C. Frequency 9118.995 and 9119.687 MHz, respectively. X axis in mT

The IR spectrum of **3** indicated that, even in this case, the ligand was not deprotonated at the nitrogen atom [νN-H = 3191 cm^{-1}]. More support for the assignment of the Cr(III) oxidation state was found by degradation of **2** in THF with an excess of pyridine, which afforded a small quantity of the well-defined crystalline $CrCl_3(pyridine)_3$ (Figure 24). Although other ill-defined

byproducts were also formed during this degradation, this experiment qualitatively confirms that **3** contains trivalent chromium. The only significant spectral difference between **2** and **3** consists of the presence of a large and intense absorption at 580 cm^{-1} in the spectrum of **3**, attributable to the Al-O-Al groups.

After completing the initial investigation of the less-reducing aluminum alkyls, it was of interest to examine the reaction of **1** with more reducing aluminum alkyls for comparison. Thus the reaction of **1** with an excess of Et_2AlCl (10 eq.) surprisingly still afforded a high yield (83%) of dark green crystals of the dicationic chromium (III) dimer $\{[(SNS)Cr^{III}Et(\mu\text{-}Cl)]_2\}$ $\{AlCl_3Et\}_2$ (**4**), containing a terminal ethyl group on each of the two symmetrical chromium centres (Figure 24). This is the first example of a stable dicationic chromium (III) ethyl dimer complex in the literature, attesting to the high kinetic inertness of the bimetallic Cr(III) [SNS] complexes. The crystal structure of **4** (Figure 13) is very similar to **2** except for substitution of chromium methyl with chromium ethyl. The other minor difference observed in the X-ray structure of **4** is the close contact between the NH group of the [SNS] ligand and one chloride of the aluminate counterion. This is tentatively attributed to a short range attractive hydrogen-bonding type of interaction although crystal packing forces cannot be discounted. Complex **4** also displays a remarkable thermal stability in both solid state and boiling toluene. A slow degradation to metallic chromium is observed only after one hour under reflux. This is possibly due to the kinetic inertness of the dicationic edge-sharing bioctahedral chromium (III) core, where the two alkyl groups are not in close proximity.

The addition of excess Et_3Al (10 eq.) to **4** also triggered its rapid degradation to metallic chromium even at room temperature, similar to the reaction of **2** with excess Me_3Al. However, after removal of the insoluble metallic chromium product, a faint blue solution remained, from which a few light blue crystals of the new Cr (II) complex, $\{[(SNS)Cr^{II}(\mu\text{-}Cl)]_2\}$ $\{(AlCl_2Et_2\}_2$ (**5**) could be isolated. This product was obviously formed via reduction of **4** (Figure 26). To gain further insights into this interesting development of the reduction of chromium, the reaction of **1** with the much more reducing Al^iBu_3 and $(Al^iBu_2)_2O$ were investigated.

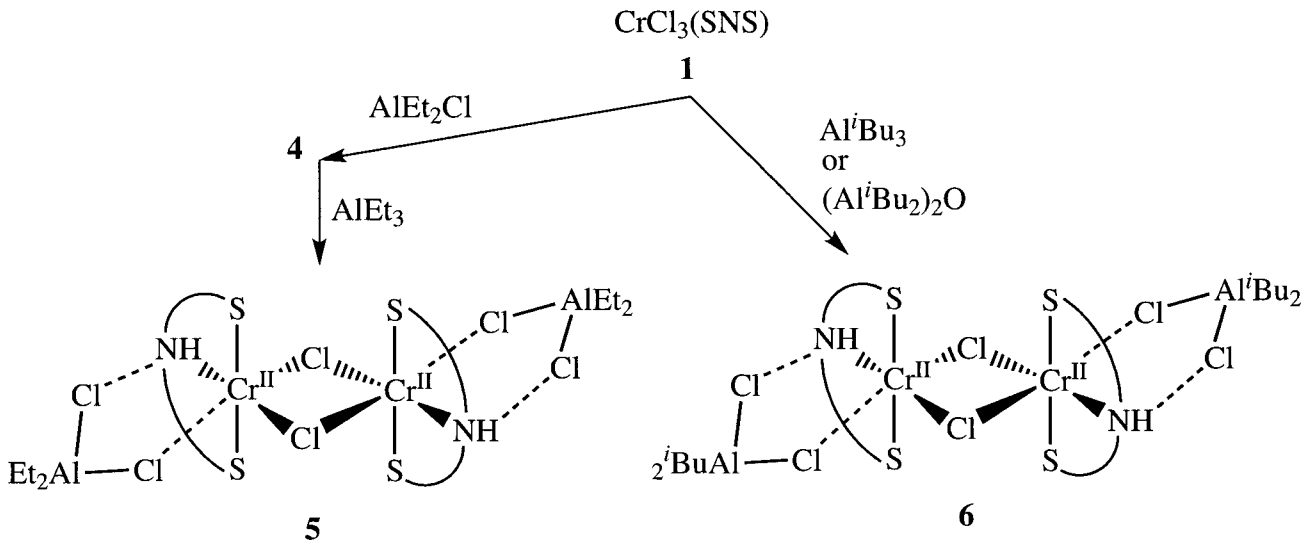

Figure 26: Reaction of **4** with Et_3Al and **1** with Al^iBu_3

Thus the reaction of **1** with either TIBA or TIBAO resulted in the near quantitative formation of the dicationic dimer $\{[(SNS)Cr^{II}(\mu\text{-}Cl)]_2\}$ $\{AlCl_2{}^iBu_2\}_2$ (**6**), which is structurally very similar to the X-ray crystal structure of **5** (Figure 14). The X-ray crystal structure of **6** (Figure 15) reveals the coordination geometry around each of the two metal centres as square pyramidal [Cl(1)–Cr(1)–S(1) = 97.66(7)°; Cl(1)–Cr(1)–S(2) = 97.07(7)°; N(1)–Cr(1)–S(1) = 82.74(17)°; N(1)–Cr(1)–S(2) = 82.45(17)°] with the basal plane defined by one of the two bridging chlorides [Cr(1)–Cl(1) = 2.3486(19) Å], the ligand nitrogen [Cr(1)–N(1) = 2.134(5) Å], and the two sulfur atoms [Cr(1)–S(1) = 2.519(2) Å, Cr(1)–S(2) = 2.511(2) Å]. The second bridging chlorine is located on the axial position [Cr(1)–Cl(1a) = 2.714(2) Å; Cl(1a)–Cr(1)–N(1) = 87.57(16)°; Cl(1a)–Cr(1)–S(1) = 87.05(7)°; Cl(1a)–Cr(1)–S(2) = 88.74(7)°; Cl(1a)–Cr(1)–Cl(1) = 91.30(6)°]. The chromium atom shows little deviation from the basal plane [Cl(1)–Cr(1)–N(1) = 178.79(16)°; S(1)–Cr(1)–S(2) = 164.76(7)°]. Even in this case, the presence of the proton on the nitrogen atom is indicated by the deviation from the planarity of the N atom [C(2)–N(1)–C(3) = 114.8(6)°; C(2)–N(1)–Cr(1) = 112.8(4)°; C(3)–N(1)–Cr(1) = 111.7(4)°]. Two $\{^iBu_3AlCl_2\}$ anions complete the structure. One of the two chlorine atoms of the aluminate unit is loosely coordinated to the chromium atom [Cr(1)–Cl(2) = 2.794(2) Å] occupying the sixth position of an ideal octahedron centreed on chromium.

The major structural difference observed between the chromium(II) complexes **5** and **6** with

the chromium (III) complexes is mainly due to the additional vacant site on chromium which may be attacked by aluminate anion. In summary so far, the reaction of **1** with a series of aluminum alkyl reagents revealed that Cr (III) is stable in the presence of Me_3Al, MAO, and DEAC, while the highly reducing IBAO and TIBA affords a clean reduction to chromium (II).

2.3.2 Reaction of {(SNS)$Cr^{II}Cl_2$(THF)} (7) with aluminum cocatalysts

Upon completing the above series of reactions of aluminum alkyls with the Cr (III) precursor **1**, it was highly desirable to mechanistically compare the reactivity of a well-defined Cr (II) [SNS] precursor under similar conditions. Reactivity differences between the two chromium oxidation states would allow further discrimination of their role in catalysis. To generate a well-defined precursor, the simple reaction of $CrCl_2(THF)_2$ with the neutral [SNS] ligand in toluene was attempted, giving an equilibrium mixture of the precursor $CrCl_2(THF)_2$ and the desired product {(SNS$Cr^{II}Cl_2(THF)_2$} (**7**) (Figure 27). However, it was discovered that the excess of THF in the solution limits the conversion. This problem could be solved by drying the chromium precursor in vacuo, then by drying the THF/toluene mixture several times with aliquots of fresh toluene. X-ray structural analysis of **7** reveals its monomeric nature (Figure 16) with the chromium atom in the centre of a regular square plane [N(1)-Cr(1)-Cl(1) = 87.6(2)°; N(1)-Cr(1)-Cl(2) = 92.0(2)°; O(1)-Cr(1)-Cl(1) = 90.00(18)°; O(1)-Cr(1)-Cl(2) = 90.49(18)°] defined by the nitrogen atom of the ligand [Cr-N(1)) 2.142(7) Å], two chlorides in trans to each other [Cr-Cl(1) = 2.405(3) Å; Cr-Cl(2) = 2.372(3) Å; Cl(1)-Cr(1)-Cl(2) = 178.49(11)°], and one coordinated molecule of THF [Cr(1)-O(1) = 2.098(6) Å]. The two sulfur atoms are located on the axis of the ideal octahedron centreed on chromium. However, the two Cr-S distances [Cr(1)-S(1) = 2.846(6) Å, Cr(1)-S(2) = 2.840(6) Å] are beyond the normal bonding range. The nitrogen atom of the ligand appears also to carry the proton, as indicated by its pyramidal arrangement [C(8)-N(1)-C(9) = 110.5(6)°; C(8)-N(1)-Cr(1) = 114.3(5)°; C(9)-N(1)-Cr(1) = 112.2(5)°]. The distorted octahedral coordination environment was obtained for the d^4 electronic configuration (μ_{eff} = 4.86 μ_B), **7** shows a curious positioning of the two sulfur donor atoms, which are placed on the axial positions of the ideal octahedral geometry centreed on chromium. Conversely, in the divalent **5** and **6** , the [SNS] ligand

appears to be fully coordinated as a probable result of the absence of the THF and chloride ligands, as well as the greater electrophilicity inherent to a cationic metal centre. As a confirmation of this hypothesis, the reaction of **7** with either TIBA or TIBAO, produced **6** quantitatively by the simple THF and Chloride extraction (Figure 27). The reaction of **7** with excess Et_3Al also resulted in extensive decomposition to metallic chromium, possibly due to extensive alkylation of the chromium centre. However, the reaction of **7** with the Et_2AlCl and $EtAlCl_2$ reagents resulted in the quantitative formation of the neutral and cationic derivatives $\{(SNS)Cr^{II}[(\mu\text{-}Cl)_2AlEt_2]_2\}$ (**8**) and $\{(SNS)Cr^{II}[(\mu\text{-}Cl)_2AlEtCl)\}$ $\{Cl_3AlEt\}$ (**9**), respectively. The analysis of the X-ray structures of **8** (Figure 17) and **9** (Figure 18) also revealed close contacts between the aluminate chloride and NH group of the [SNS] ligand.

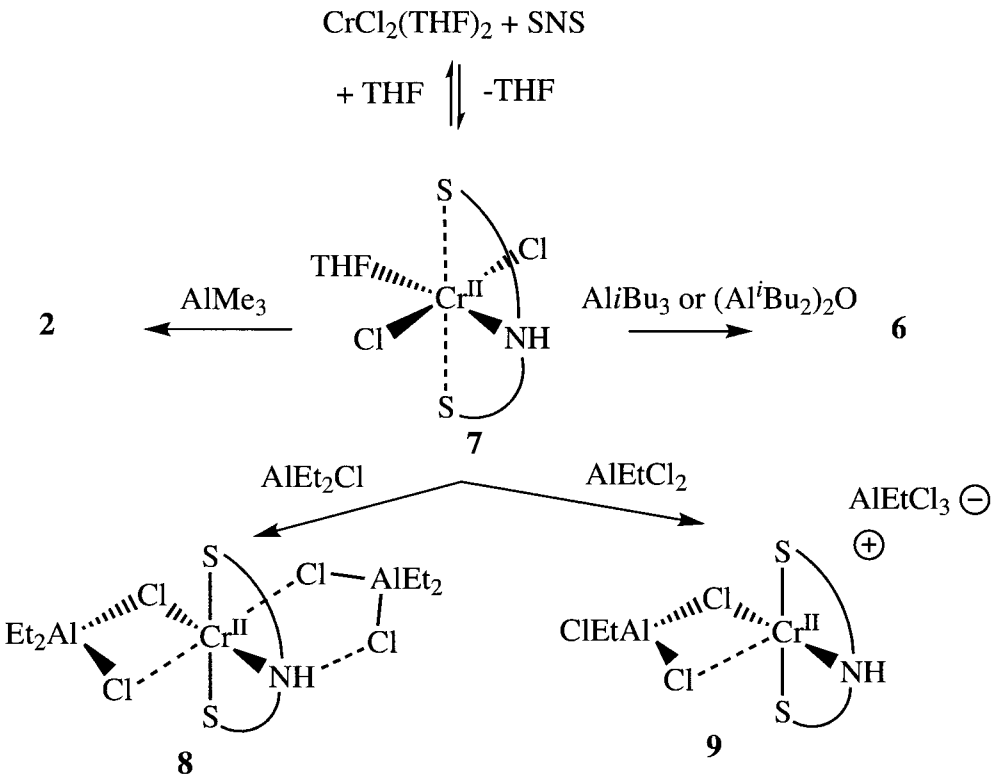

Figure 27: Reactions of **7** with Al^iBu_3, Et_2AlCl, and $EtAlCl_2$ to generate **7**, **8** and **9** respectively

Finally, the reaction of **7** with an excess of the powerful Lewis acids Me_3Al and MAO resulted in its extensive decomposition to metallic chromium, but a dark green solution also formed immediately. When the same reaction was carried out with Me_3Al, the cationic Cr (III) complex **2** was formed and subsequently isolated in 17 % yield. A substantial amount of metallic

chromium was invariably present in these reaction mixtures as a black, pyrophoric, and insoluble material. The X-ray fluorescence spectrum of this material confirmed the presence of Cr as the only heavy element while both the IR spectrum and combustion analysis showed the absence of organic functions. Furthermore, the EPR spectrum of the crude reaction mixture with metallic residue was found to be identical to that of an analytically pure sample of **2**, thereby conclusively proving that **2** is the only EPR-active species formed during this unusual reaction. In a brief summary so far, the chromium (II) based [SNS] precursor was reacted with a series of aluminum alkyl reagents. It was found that the more reducing $Al^{i}Bu_3$, $Al^{i}Bu_2)_2O$, Et_2AlCl, and $EtAlCl_2$ led to the formation of the expected cationic products **5**, **6**, **8**, and **9** respectively. Surprisingly, the strongly Lewis-acidic Me_3Al and MAO resulted in disproportionation to metallic chromium and the previously-characterized chromium (III) complexes **2** and **3**, respectively.

2.3.3 Reaction of (SNS)$CrCl_3$ with three different $AlCl_3$ concentrations

So far, the examination of the chromium reactivity with aluminum reagents was limited to relatively small quantities due to unstable organochromium redox behavior at high concentrations leading to catalyst decomposition. However, the fact that actual catalyst runs require upwards of 100 equivalents of the aluminum cocatalyst MAO suggests that further molecular rearrangement takes place at those high cocatalyst loadings to generate the active species. The answer to the challenging but important question of the effect of the high aluminum cocatalyst concentration on the chromium geometry was partly addressed by avoiding the redox-induced decomposition. This was achieved by treating **1** with three different concentrations of the alkyl-free $AlCl_3$ reagent. This procedure resulted in the formation of three different trivalent complexes: monomeric $\{(SNS)Cr^{III}Cl_2(THF)\}$ $\{AlCl_4\}$ (**10**), dimeric $\{[(SNS)Cr^{III}Cl(\mu\text{-}Cl)]_2\}$ $\{AlCl_4\}_2$ (**11**) and monomeric $\{(SNS)Cr^{III}(\eta^2\text{-}AlCl_4)\}$ $\{Al_2Cl_7\}$ (**12**) (Figure 28).

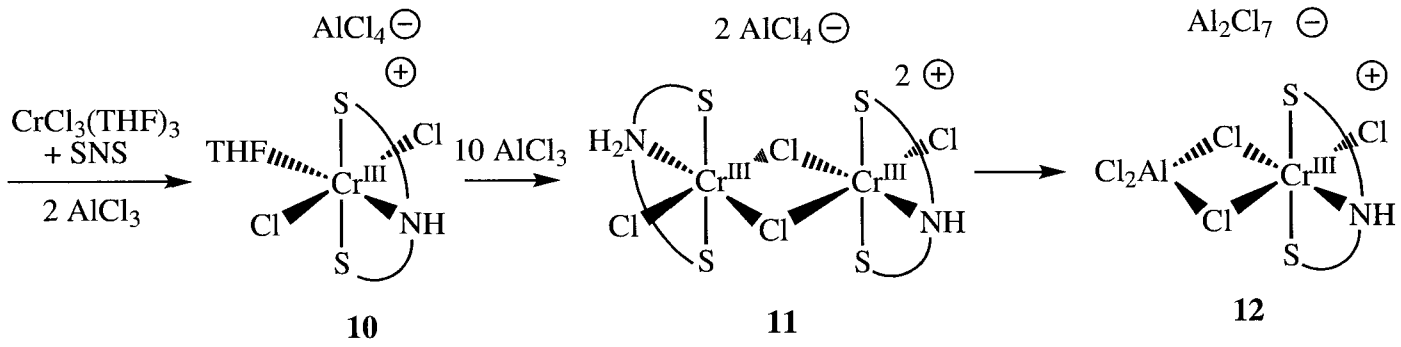

Figure 28: Effect of increasing $AlCl_3$ equivalents on chromium and anion geometry

The structure of **10** (Figure 19) is ionic with the cationic moiety consisting of an octahedral chromium atom counterbalanced by one $\{AlCl_4\}$ tetrahedral anion. The cationic unit has the octahedral coordination geometry of the chromium atom defined by the ligand meridionally arranged [S(1)-Cr(1)-N(1) = 84.31(17)°; S(1)- Cr(1)-S(2) = 169.12(8)°; N(1)-Cr(1)-S(2) = 84.81(17)°]. The three residual coordination sites are occupied by the two trans-located chlorine atoms [Cr(1)-Cl(1) = 2.295(2) Å; Cr(1)-Cl(2)) 2.292(2) Å; Cl(1)-Cr(1)-Cl(2)) 177.12(9)°] and the oxygen atom of one THF molecule [Cr(1)-O(1) = 2.034(5) Å]. Despite the close similarity with the structure of **7**, the Cr-S distances [Cr(1)-S(1) = 2.440(2) Å; Cr(1)-S(2) = 2.443(2)Å] are substantially shorter in the bonding range as a result of the higher oxidation state in combination with the cationic charge for **3** compared to **7**. The nitrogen donor atom of the ligand [Cr(1)-N(1) = 2.068(6) Å] is sp^3 hybridized, as indicated by the out-of-plane arrangement with respect to the two neighboring carbon and chromium atoms [C(8)-N(1)-Cr(1) = 113.8(7)°, C(9)-N(1)-Cr(1) = 111.6(6)°; C(8)-N(1)-C(9) = 115.6(9)°].

Complex **11** (Figure 20) has the same structure as **2** except for the replacement of the Me groups by chlorine in both the cationic and anionic moieties consisting of a symmetry-generated ionic dimer very similar to **2** and **4**. The dicationic unit is formed by two slightly distorted octahedral chromium atoms connected by two bridging chlorine atoms [Cr(1)-Cl(2) = 2.364(3) Å; Cr(1)-Cl(2a) = 2.391(3) Å] forming a planar Cr_2Cl_2 core [Cl(2)-Cr(1)-Cl(2a) = 84.81(9)°; Cr(1)-Cl(2)-Cr(1a) = 95.19(9)°]. The equatorial plane [Cl(2)-Cr(1)-N(1) = 173.9(2)°; Cl(2)-Cr(1)-Cl(1) = 94.34(10)°; N(1)-Cr(1)-Cl(1) = 91.7(2)°] around each chromium atom is defined by three chlorine atoms (two bridging and one terminally bonded) [Cr(1)-Cl(1) = 2.233(3) Å] and the ligand nitrogen

atom [Cr(1)-N(1) = 2.057(7) Å]. The sulfur atoms of each ligand are placed on the two axial positions [Cr(1)-S(1) = 2.436(3) Å; Cr(1)-S(2) = 2.447(3) Å], and the protonation of the ligand nitrogen atom is emphasized by its pyramidal geometry [C(9)-N(1)-C(8) = 113.8(8)°; Cr(1)-N(1)-C(8) = 113.5(6)°; Cr(1)-N(1)-C(9) = 114.5(6)°]. Two tetrahedral $\{AlCl_4\}$ anions unconnected to the dicationic unit complete the structure.

The structure of **12** (Figure 21) shows a heterobimetallic cationic complex formed by one chromium atom in a regular octahedral coordination environment bridged by two chlorine atoms to a tetrahedral $AlCl_3$ residue. A heavily disordered $\{Al_2Cl_7\}$- anion completes the structure. The coordination environment of the chromium atom [Cl(3)-Cr(1)-Cl(1) = 178.20(13)°; Cl(2)-Cr(1)-N(1) = 170.6(4)°; Cl(2)-Cr(1)-Cl(3) = 95.41(12)°; N(1)-Cr(1)-Cl(1) = 87.7(4)°] is defined by the chlorine atom bridging the aluminum centre [Cr(1)-Cl(1) = 2.218(5) Å; Cr(1)-Cl(2) = 2.247(5) Å], one terminal chlorine atom [Cr(1)-Cl(3) = 2.229(3) Å], and the N atom of the ligand system [Cr(1)-N(1) = 2.058(10) Å]. The two sulfur atoms are located on the axial positions [Cr(1)-S(1) = 2.447(4) Å; Cr(1)-S(2) = 2.464(4) Å; S(1)-Cr(1)-S(2) = 166.16(12)°; S(1)-Cr(1)-N(1) = 85.0(3)°; S(1)-Cr(1)-Cl(1) = 85.00(11)°]. The aluminum moiety displays the typical tetrahedral coordination geometry [Cl(1)-Al-Cl(2) = 93.36(16)°); Cl(4)-Al-Cl(5) = 118.7(2)°] with two terminally bonded chlorine atoms [Al(1)-Cl(4) = 2.088(5) Å; Al(1)-Cl(5) = 2.080(5) Å] and the other two bridging the chromium centre [Al(1)-Cl(1) = 2.218(5) Å; Al(1)-Cl(2) = 2.247(5) Å]. The $Cr(N\text{-}Al\text{-}Cl)_2$ core is coplanar with the N atom and terminally bonded chlorine atom bonded to chromium [the torsion angles are: Al(1)-Cl(2)-Cr(1)-Cl(1) = -3.80(14)°; A(1)-Cl(2)-Cr(1)-N(1) = 2(2)°]. The protonation of the nitrogen atom is evident from the pyramidal geometry of the nitrogen atom [Cr(1)-N(1)-C(1) = 114.8(9)°; Cr(1)-N(1)-C(3) = 116.1(11)°; C(1)-N(1)-C(3) = 122.0(13)°].

In summary, the treatment of **1** with increasing concentrations of the alkyl-free $AlCl_3$ resulted in the formation of three different complexes. This confirmed the observation from catalytic testing that higher concentrations of aluminum cocatalyst are potentially needed to break up the dimeric and inactive catalytic intermediates in to more reactive monomeric species.

2.3.4 Deprotonation of the [SNS] ligand

The final important parameter to be examined in this remarkable catalytic system is obviously whether the possible deprotonation of the acidic N-H functionality of the ligand may play any part in the catalytically active species. As clearly indicated by the crystal structures and the IR spectra of all the complexes reported so far, the N-H function of the [SNS] ligand remains unreacted in the presence of aluminum alkylating agents. This suggests that the Al-R and Cr-R functional groups do not have sufficient basicity to deprotonate the [SNS] ligand. Final confirmation of this hypothesis was given by the deliberate deprotonation of the acidic NH proton of the [SNS] ligand with BuLi and then complexation to chromium. The reaction resulted in the formation of the $\{[(\mu^2\text{-SNS})Cr^{II}Cl]_2\}$ (**13**) dimer, which was found to be unreactive with aluminum alkyl reagents (Figure 29). This suggests that the deprotonation of the [SNS] ligand is actually a route to catalyst deactivation by formation of highly stable dimer similar to **13**.

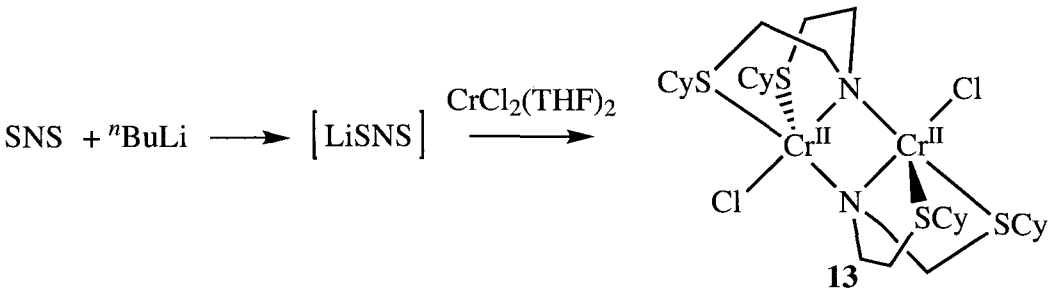

Figure 29: Deprotonation of [SNS] and reaction with $CrCl_2(THF)_2$ to generate **13**

The X-ray structure of **13** (Figure 22) revealed a symmetry-generated dimer, where the bridging interaction is realized through the deprotonated nitrogen atoms of two ligands forming a planar Cr_2N_2 core [Cr(1)-N(1) = 2.071(3) Å; Cr(1a)-N(1) = 2.093(3) Å; N(1)-Cr(1)-N(1a) = 88.61(11)°; Cr(1)-N(1)-Cr(1a) = 91.39(11)°]. The coordination geometry of each of the two identical chromium atoms is regular trigonal bipyramidal. The equatorial plane is defined by the two sulfur atoms [Cr(1)-S(1) = 2.6948(17) Å; Cr(1)- S(2) = 2.5359(17) Å] of the same ligand and the bridging nitrogen atom [Cr(1)-N(1a) = 2.093(3) Å] of the second ligand attached to the other chromium atom [S(1)-Cr(1)-N(1a) = 104.93(8)°; S(1)-Cr(1)-S(2) = 96.20(5)°; S(2)-Cr(1)-N(1a) = 154.52(8)°]. The terminally bonded chlorine [Cr(1)-Cl(1) = 2.3581(16) Å] and the nitrogen atoms [Cr(1)-N(1)

= 2.071(3) Å] of the ligand coordinated to the chromium atoms are located on the axial positions [N(1)-Cr(1)-Cl(1) = 176.29(8)°].

The binuclear structure of **13**, which contains two high-spin coordinatively saturated Cr (II) centres in a trigonal bipyramidal coordination environment bridged by two amide donors is extremely robust against the attack by an aluminum alkyl cocatalyst. This is a sharp deviation from the behavior of the more reactive chloride-bridged cores discussed previously, which is possibly due to the lack of free lone pairs on the nitrogen atoms in **13** preventing bonding to aluminum as in the chloride-bridged complexes which contain lone pairs.

2.3.5 Catalytic oligomerization by 1-13

A comparison of the ethylene oligomerization performances of **1-13** while in combination with the MAO activator was undertaken to gain mechanistic insights into the effect of the precursor composition on catalytic performance (Table 13). First, the most obvious trend from the catalytic results is that a large excess of MAO activator (>1000 equivalents) results in much lower selectivity and activity regardless of the catalyst precursor used. The higher concentrations of MAO also generally led to higher quantities of undesirable polyethylene byproduct, possibly via an increased stability of an undesirable chromium species that polymerizes ethylene. On closer examination, it is observed that these effects of increasing MAO concentration are more pronounced in some precursors than others.

Another interesting observation is that one order of magnitude fluctuation in activity is observed when comparing the precatalysts **1-12** at the standard 1000 eq. MAO activation, between the least active precursor **6** (3 mL of 1-hexene) and the most active precursor **10**. However, the large fluctuation in activity for both Cr (III) and Cr(II) precursors seems to rule out any trend based purely on oxidation state of the precursor. Within a group of bimetallic dicationic chromium (III) precursors, the increase in activity with no change in selectivity is observed for complexes **11**, **2**, and **4** following the order of substitution on chromium of Cl < Me < Et, possibly reflecting the increased solubility of the alkyl substituted complexes. This may also explain the poor activity of **12**, which contains no alkyl substituents on aluminum. When considering bimetallic vs.

monometallic precursors, the results show that monometallic chromium (III) precursors generally produce less polymer than bimetallic precursors. It was also noticeable that a reverse of this trend is seen for chromium (II) precursors. Significantly more polymer is produced by the monometallic Cr(II) precursors **7**, **8**, and **9** than by the bimetallic chromium (II) precursors **5** and **6**, suggesting that polymer formation results from a monometallic chromium (II) species. Decreasing the amount of MAO cocatalyst from 1000 eq. to 150 eq. the bimetallic Cr (II) precursor **6** increased both selectivity and activity, suggesting that a large excess of MAO probably deactivates a large percentage of the precatalyst. In this event, only a minute amount of the catalyst relative to a large quantity of MAO would remain present, resulting in the observed loss of selectivity at 1000 eq. rather than the usual 2000 eq. of MAO for other precursors.

It was interesting that the most active precursor, the THF-bound complex **10**, was three times as active as the precatalyst **1**. This result suggests that monomeric, cationic chromium (III) [SNS] precursors are the most ideal precursors to evaluate catalytic performance. Thus any future exploration of the effect of ligand modifications on the catalytic performance of chromium [SNS] in ethylene trimerization should use the same convenient synthesis method which gave rise to the precatalyst **10**. Finally, it is clear that the deprotonated [SNS]-based complex **13** is completely inactive for oligomerization and polymerization, suggesting that the NH proton is critically important to catalytic performance.

2.4 Discussion

In a brief summary, the important mechanistic questions raised in the introduction about the nature of the intermediates in the selective chromium [SNS] trimerization catalyst resulted in the evaluation of the reaction of chromium (III) [SNS] and chromium (II) [SNS] precursors with a range of aluminum cocatalysts and concentrations. The analysis of the results from these experiments reveals trends in structural and reactivity of these well-defined catalytic intermediates, from which mechanistic insights may be found. This section will discuss these insights, divided into the following three categories: the effect of the aluminum alkyl substitution on the chromium (III) [SNS] precursor **1** and chromium (II) [SNS] precursor **7**, the effect of the $AlCl_3$ concentration on

1, and finally the N-H effect of the [SNS] ligand on ion pairing. This discussion leads to the logical proposal of a mechanistic model which can account for some of the selectivity trends observed for the Cr [SNS] system in different environments.

2.4.1 Reaction of {(SNS)$CrCl_3$} (1) and {(SNS)$CrCl_2$(THF)} (7) with aluminum cocatalysts

The treatment of the (SNS)$CrCl_3$ precursor **1**, with the least reducing of the aluminum alkyls (Me_3Al, MAO, and Et_2AlCl respectively) resulted in the formation of dicationic dimeric chromium (III) alkyl complexes **2**, **3**, and **4**. This result indicates that the [SNS] ligand system has an unanticipated ability to stabilize organochromium (III). However treatment of **1** with the more reducing aluminum alkyls IBAO and TIBA resulted in a clean reduction to the dicationic dimeric **6**. The use of a large excess of Me_3Al or MAO did not result in a reduction to a similar dimeric chromium (II) complex, suggesting that more reducing alkyl groups with β-hydrogens are required (Figure 30, path b). This conclusion also implies that C-C reductive elimination of ethane from **2** is not possible (Figure 30, path a). Assuming the same behavior in the actual catalytic chromacycle intermediates suggests that the metallacyclopentane intermediate, which does not contain accessible β-hydrogens, does not undergo either β-H elimination readily (path b) or C-C coupling (path a). Only after ethylene insertion and ring expansion, the greater accessibility of the β-hydrogens of the metallacycloheptane intermediate to the chromium centre allows a kinetically rapid reductive elimination of the olefin. On the other hand, the identical reaction of **7** with either methylaluminoxane (MAO) or Me_3Al did not lead to the expected Cr(II)derivatives, but instead gave a thermally robust cationic organochromium (III) species **2** and **3**. The Cr(II) precursors of this ligand system display the same selectivity as the Cr(III) precursors and that oxidation of Cr(II) to the trivalent state cannot normally be foreseen in the presence of reducing alkyl aluminum activators. A database search for precedents of the disproportionation of organochromium (II) to (III) and (I) revealed only one well-characterized example (Figure 31).[70] Thus it is proposed that chromium (II) [SNS] intermediates in solution undergo disproportionation as shown in Figure 32. This unexpected pathway suggests that mechanistically, chromium (II) intermediates cannot be

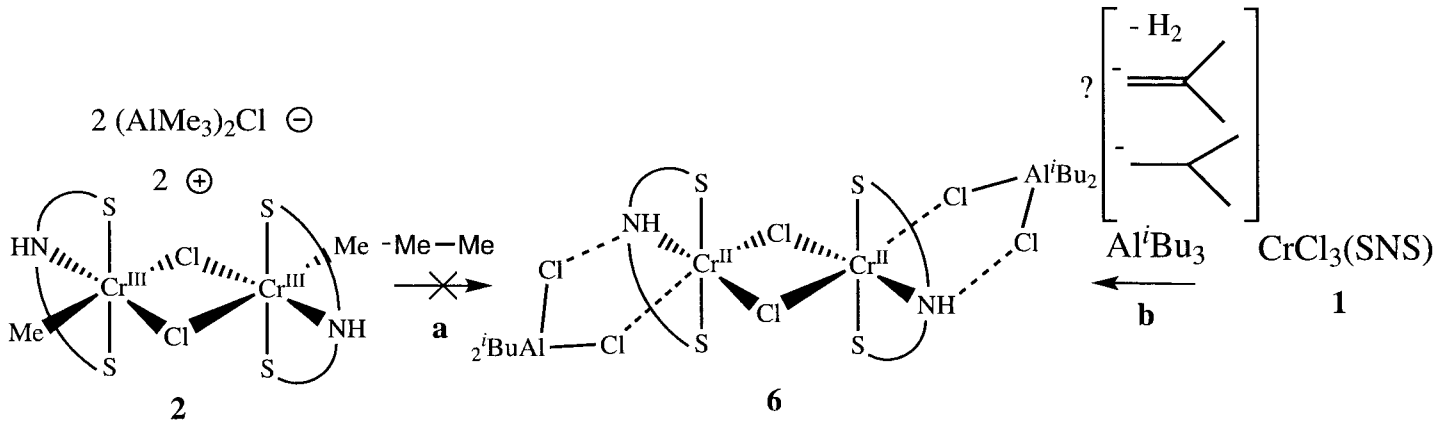

Figure 30: Forbidden (a) and allowed (b) Reduction Paths in [SNS]Cr (III) intermediates

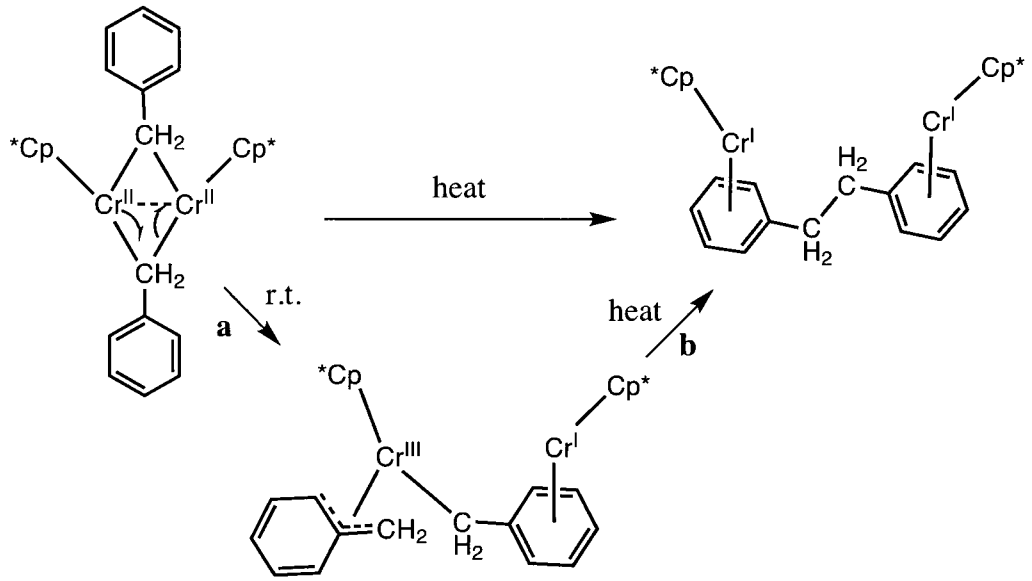

Figure 31: The only well-defined example of disproportionation of a bimetallic Cr(II) alkyl to Cr(I) and Cr(III) (a), followed by reductive elimination to two Cr(I) centres (b) by Theopold (see text).

ignored in future mechanistic studies, and their role in the catalytic selectivity remains a mystery.

The increase in the polymer formation observed for the [SNS]Cr(II) monomeric precursor **7** could suggest that the monomeric chromium (II) species is responsible for olefin polymerization. On the other hand, it is also possibly converted to chromium (I) and (III) via disproportionation (Figure 32). Experimental evidence for comproportionation and disproportionation of chromium (II) and (III) ions in aqueous solution have also been reported.[71]

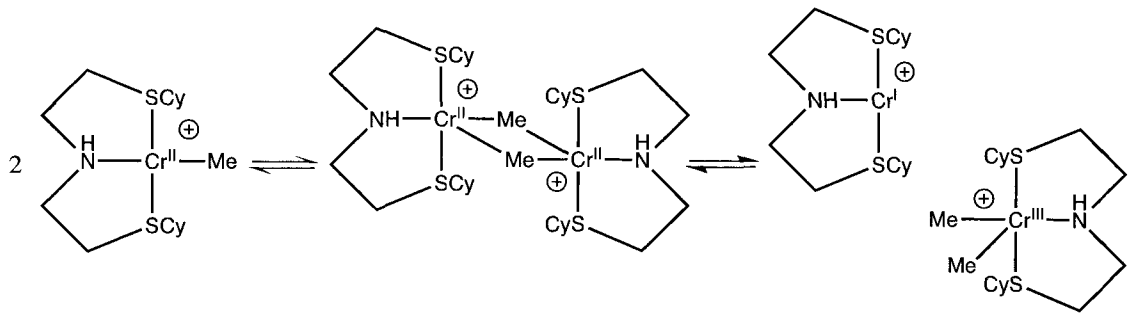

Figure 32: Proposed disproportionation mechanism of [SNS]Cr (II) intermediates

2.4.2 The aluminum cocatalyst concentration effect on the chromium and anion geometry

Treatment of **1** with an increasing concentration of the Lewis acid $AlCl_3$ resulted in the formation of **10**, **11**, and **12**. Thus the increasing concentration of aluminum cocatalyst can be concluded to modify the geometry around the chromium centre. The counter anion also becomes more weakly coordinating with a higher concentration of the $AlCl_3$ Lewis acid, switching from the $AlCl_4$ anion to the more weakly coordinating Al_2Cl_7 anion. The coordinating properties of the anion are expected to play an important role in the catalytic selectivity and activity which is discussed in the following paragraph.

2.4.3 The [SNS] N-H effect on anion coordination to chromium

The deliberate deprotonation of the [SNS] ligand and the formation of its chromium derivative **13**, allowed for the unambiguous catalytic evaluation of a chromium [SNS] precursor which did not contain the N-H proton. The fact that **13** is inactive, and that all previous reactions of aluminum alkyl reagents with chromium [SNS] precursors did not result in deprotonation of the ligand suggested that the N-H group plays an important role in the trimerization catalysis. This is an important mechanistic insight, but it does not provide any information regarding the exact role that this polar functionality plays. However, the analysis of the X-ray structures of the aluminate complexes reported above revealed that in many circumstances a very close contact exists between the N-H group of the [SNS] ligand and the chloride atom of the aluminate anion. As this type of hydrogen bonding attraction is a pervasive interaction in influencing selectivity in

natural enzyme catalysis such as hydrogenase, it may have an influence on the selectivity of the CrSNS ethylene trimerization catalyst. More information about the catalytic role of the [SNS] N-H group is obtained from the effect of increasing the aluminum cocatalyst concentration on the geometry of both the chromium cation and aluminate anion. These geometric parameters play a strong role on the observed hydrogen-bonding interaction between the [SNS] NH group and the aluminate anion. Thus it is observed that increasing the concentration of the aluminum cocatalyst results in an overall weaker hydrogen bond to the aluminate anion, disrupting the ion pairing. If it is justifiable to assume that the MAO cocatalyst behaves in a similar fashion as established for Me_3Al and $AlCl_3$, then it can be concluded that increasing the concentration of MAO also results in a loss of the hydrogen bonding interaction of the MAO anion with the N-H group. The fact that higher concentrations of MAO also result in loss of selectivity can be linked to this proposed loss of H-bonding interaction between the anion and the [SNS] ligand. In effect, at low MAO concentrations, the tethered MAO anion is proposed to act as a hemilabile ligand. This "tethered" hemilabile MAO anion could then loosely coordinate to the remaining vacant site on chromium in the proposed metallacycloheptane catalytic intermediate (Figure 33, a). As mentioned in the introduction to this thesis, the metallacycle mechanism has been established to be able to switch between selective trimerization and non-selective oligomerization depending on the relative rate of ring expansion to the rate of metallacycle collapse to the oligomer depending on the coordination sphere of the chromium metal centre. Thus in the case of low MAO concentrations, the tethered MAO anion loosely coordinates to the vacant site on chromium which slows down the rate of ring expansion relative to metallacycle collapse. At high MAO concentrations, instead the non-tethered MAO anion does not compete with ethylene for the vacant site on chromium metallacycle intermediates, allowing for a faster rate of metallacycle ring expansion relative to metallacycle collapse. In turn, this produces a nonselective distribution of oligomer products. This theory is supported by catalytic studies of related [SNS] ligands in which the N-H group has been exchanged with alkyl or other non-hydrogen bonding functionalities, resulting in the complete loss of selectivity in favor of the S.F. distribution.[31]

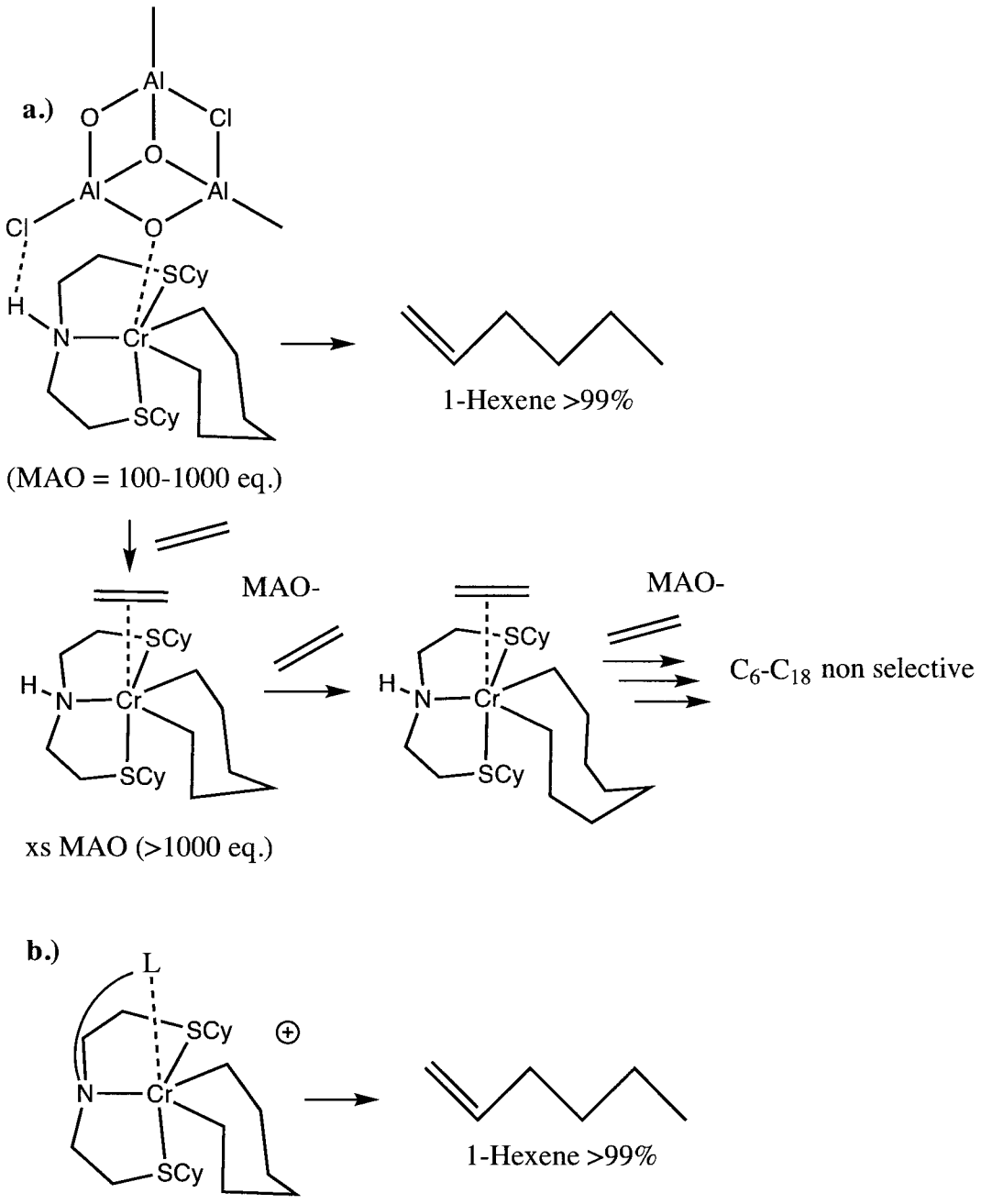

Figure 33: a.) Proposed effect of N-H-tethered MAO anion (truncated model) on catalytic selectivity, and b.) design of a novel hemilabile ligand for ethylene trimerization.

Future experiments could elaborate on the importance of the N-H group. For instance, substitution of the protic hydrogen with deuterium could result in an enhanced selectivity (but lower activity) due to stronger hydrogen bonding. Other ways to elaborate on the hemilability include the substitution of the N-H group with a hemilable donor which can compete with ethylene for the

sixth coordination site in the proposed metallacycle intermediates, which could effectively increase selectivity (Figure 33, b).

2.5 Conclusion

In conclusion, the examination of the reaction of a range aluminum alkyls with chromium [SNS] precursors has illustrated the close relationship between the Cr(III) and Cr(II) oxidation states via reduction and disproportionation pathways in catalytically relevant conditions. The high kinetic stability of the Cr(III) [SNS] dimers suggests that these species could be the catalyst resting state (and thus may be an observable species under catalytic conditions), although further experimentation is necessary to confirm this proposal. Obviously Cr(II) and Cr(I) species may be present in appreciable concentrations during catalysis, which must be explored in further detail. This methodology has also led to evidence for the importance of the non-bonding attraction between the [SNS] N-H group and the aluminum cocatalyst anion in the catalytic selectivity. Rational catalyst design and optimization in the future may make use of these missing pieces to the mechanistic puzzle. The following chapter on the CrPNP ethylene tetramerization catalyst serves as an important comparison with the CrSNS trimerization catalyst for understanding mechanistic differences in the underlying organochromium chemistry which relate to the 1-hexene/1-octene catalytic selectivity.

3 Mechanistic investigation of chromium-diphosphine based ethylene tetramerization catalysis

Abstract

This chapter discusses the mechanistic study of the chromium-diphosphine based ethylene tetramerization catalysis by the examination of the reaction of the diphosphine-Cr precursor, $\{[(PNP)Cr^{III}Cl_3]_2\}$ (**14**), with aluminum cocatalysts. The addition of 3 equivalents of Me_2AlCl to **14** results in alkylation and cationization to form the thermally stable cationic Cr(III) dimer, $\{(PNP)MeCr^{III}(\mu\text{-}Cl)_3Cr^{III}Me(PNP)\}$ $\{Me_2AlCl_2\}$ (**15**). The addition of more Me_2AlCl to **15** resulted in its quantitative reduction to the chloride- and Me_2AlCl_2-bridged cationic Cr(II) dimer, $\{(PNP)Cr^{II}(\mu\text{-}Cl)_2(\mu^2,\eta^2\text{-}Me_2AlCl_2)Cr^{II}(PNP)\}$ $\{Me_2AlCl_2\}$ (**16**), which is accompanied by the formation of ethane. The treatment of either **14**, **15** or **16** with excess Me_3Al afforded the divalent, monomeric bis-PNP Cr(II) cation, $\{(PNP)_2Cr^{II}(\mu\text{-}Cl)AlMe_3\}$ $\{Me_3AlCl\}$ (**17**), which is a candidate as the EPR-silent resting state identified in a previously published study. Surprisingly, no reaction occurred between the [PNP] ligand and $CrCl_2(THF)_2$ in toluene until the addition of excess Me_2AlCl, Me_3Al, or $AlCl_3$, resulting in the formation of **15**, **17**, or the neutral monomer $\{(PNP)Cr^{II}[(\mu\text{-}Cl)AlCl_3]_2\}$ (**18**) respectively. Complexes **15-18** retain the catalytic performance of the original precursor **14** when activated with excess MAO, suggesting that they all form the same catalyst resting state. Based on the C-C coupling reactivity observed in the conversion of **15** to **16**, a bimetallic mechanism is proposed to give rise to 1-octene via a similar reductive C-C coupling of bimetallic metallacyclopentane intermediates. Unlike the controvertial "extended" metallacycle model, this bimetallic metallacycle model is consistent with experimentally established kinetics, ligand bite angle effects, and isotopic effects. In addition, it furnishes a rational mechanistic explanation for several established experimental parameters which strongly affect product selectivity simply through their effect on the catalyst monomer/dimer equilibria.

3.1 Introduction

The previous chapter explored the reaction of various chromium-SNS ethylene trimerization catalyst precursors with a range of aluminum alkyl activators to gain mechanistic insight into the

organometallic chemistry underlying catalytically relevant conditions. This chapter discusses a similar mechanistic investigation of the organochromium [PNP] system. Such a study is important on its own for the mechanistic insights it may provide into the valuable chromium-diphosphine based tetramerization catalysis. The comparison with the [SNS] system may also afford important insight into ligand effects. This introduction section will first provide a brief background of the chromium diphosphine tetramerization catalysis with an emphasis on the mechanistically important experimental observations. This will be followed by a brief background of some relevant established organochromium (II) chemistry in well-defined model systems which will aid in clarifying the discussion of the results.

3.1.1 Background of chromium-diphosphine based ethylene tetramerization catalysis

In 2003, Wass reported on the discovery that a tridentate diphosphine-based ligand, $NMe(PAr_2)_2$ (Ar = ortho-methoxyphenyl), gave a highly active and selective chromium ethylene trimerization catalyst. This methoxy-substituted diphosphine ligand was also established to bind in a tridentate fashion facially to the chromium centre (Figure 10). However, soon after the original report, Bollmann discovered that the use of the simpler unsubstituted diphosphine, $NCy(PPh_2)_2$ [PNP], provided high activity and selectivity for 1-octene rather than 1-hexene. Dozens of experimental reports have since appeared on the effect of various parameters on the catalytic performance by diphosphine-chromium tetramerization catalysts due to the high commercial value of the 1-octene product as a comonomer for LLDPE.[49, 72, 73, 74, 75, 76] These reports have established the influence of several important experimental parameters on the activity and product distribution (Figure 34). These parameters are discussed below for their mechanistic significance, and are divided into the following categories: ligand effects, anion/cocatalyst effects, solvent effects, and finally kinetic effects.

The analysis of these experimental reports reveals mechanistically interesting trends related to the effect of ligand stereo-electronic factors on the catalyst performance that have not been discussed previously in the open literature. In general, the best overall activity and selectivity for $1\text{-}C_8$ is achieved through the use of a small-bite angle ligand, such as the [PNP] ligand containing

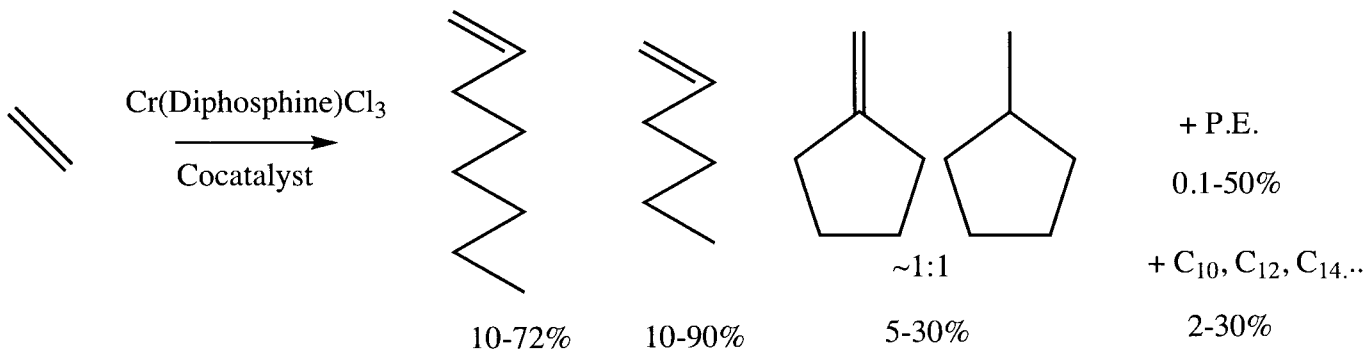

Figure 34: Experimentally established product distribution in the diphosphine-chromium tetramerization catalyst systems

an alkylamine bridging group between the two diaryl-phosphine donors (which furnishes an approximate bite angle of 65°). In general, the selectivity of 1-C_8 ranged between 10% and 70% of total product depending on the bite angle, with the other products being 1-C_6, cyclic C_6 isomers, higher oligomers and polymer. Any changes from this bridging group to a wider bite angle, such as with the ethyl-bridged bis-diphenylphosphinoethane (DPPE) (85°), is accompanied by a dramatic loss in both activity and 1-C_8 selectivity, with a large increase of polymer formation (40%).

Bite angle effects are usually rationalized as both a steric effect, related to ligand-ligand and ligand-substrate repulsion, and an electronic effect related to the bite angle of the donor orbitals to the metal centre, which can affect the metal hybridization and consequently the metal orbital energies and catalytic reactivity. The analysis of many diverse catalytic systems has established that the bite angle of the diphosphine correlates directly with catalyst activity and selectivity, such as in rhodium catalyzed hydroformylation and nickel catalyzed hydrocyanation.[77] It is found experimentally that in these late metal catalysts a wide bite angle (>110°) increases their activity and selectivity by enhancing the rate-limiting reductive-elimination product-forming step to a low-valent metal intermediate. In contrast, the diphosphine-chromium tetramerization catalyst shows the opposite trend, where a smaller bite angle (65°) is required to enhance the activity and selectivity. This indicates that the small bite angle diphosphine may stabilize chromium in a higher oxidation state, which logically should enhance the rate of the oxidative coupling of two ethylenes by a low valent intermediate to generate a high-valent metallacycle intermediate (Figure 35).

Thus in summary, it is experimentally-established that the small bite angle diphosphine ligand

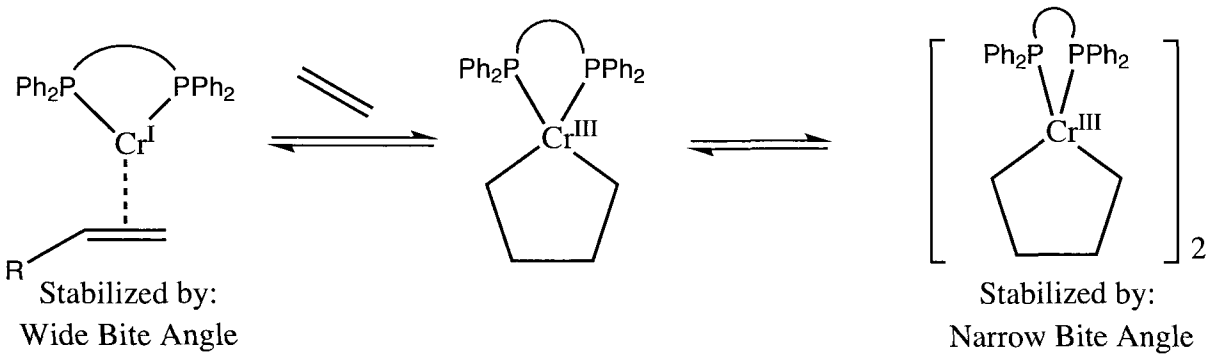

Figure 35: Predicted bite angle effect on the stability of diphosphine chromium tetramerization catalyst intermediates

improves the rate of 1-octene formation, and that the role of the small bite angle diphosphines is to increase the rate of oxidative coupling of two ethylenes to form a high-valent metallacycle. Then the rate limiting step in the formation of 1-octene is logically expected to be this step (which is in fact already established experimentally which is discussed later). In addition to the bite-angle effect on the preferred oxidation state of the chromium centre, the lower steric impact of the phosphine substituents found in smaller bite angle ligands could also stabilize bimetallic intermediates more than wide-bite angle diphosphines phosphines (which is also established experimentally and discussed in more detail later) (Figure 35).

Small modifications of the alkyl substituent on nitrogen atom of the [PNP] ligand also result in a wide range of activity and selectivity. Generally, an increased steric bulk results in lower selectivity for the undesirable cyclic C_6 byproducts and a higher overall selectivity for the desirable 1-C_8 + 1-C_6 fraction of over 90%.[74] The effect of the ligand modification on selectivity is again attributed to a further decrease of the bite angle through increased steric pressure. The percentage of undesirable cyclic C_6 byproduct in the total C_6 fraction was very sensitive to the experimental parameters and ranged between 75% to 10%, and generally the two cyclic C_6 byproducts form in a 1:1 ratio, suggesting a strong mechanistic link in their formation. By contrast, the percentage of 1-C_8 product in the C_8 fraction rarely dropped below 95%. This is unusual, considering the metallacycloheptane and metallacyclononane intermediates are both expected to exhibit the same reactivity via the "extended" metallacycle mechanism, and should both exhibit the same percentage of cyclic byproducts.

Once it was determined that the the small-bite angle [PNP] framework was optimal, the effects of the substituents on the phosphine donors was examined. While increasing the steric impact of the aryl substituents of the phosphine donors did not affect the activity of the catalyst, the selectivity changed dramatically. For instance, when all the phenyl groups were replaced by bulkier o-tolyl groups, the selectivity shifted from the normal fraction of 1-hexene of 10% to an incredible 90%. The use of [PNP] ligands containing only three or two o-tolyl substituents instead of the phenyl substituents gave further insight into the remarkable sensitivity of this catalyst to ligand steric effects. For example, the $(o\text{-tolyl})_3$ substituted [PNP] ligand afforded 40% C_6 (of which 80% is 1-C_6), and 40% 1-C_8. While, the symmetrically substituted bis o-tolyl [PNP] derivative produced only 17% C_6 (with 50% being cyclic C_6 isomers) and 66% 1-C_8. Surprisingly, the unsymmetrically substituted bis o-tolyl [PNP] gave 30% C_6 products where a large component (75%) is the cyclic C_6 byproducts. The 1-C_8 fraction amounted to 50%. In summary, the steric effect of the diphosphine attached to chromium dramatically influences product selectivity. An important requisite of any mechanistic model which explains the 1-C_8 product formation must be the ability to rationalize also the greatly sensitive selectivity for the other byproducts as well.

The second major experimental parameter which has a strong influence on the tetramerization performance is the cocatalyst effect.[78, 79, 80, 81, 48] The analysis of these results reveals a general trend, with the strongest Lewis acids (which are also by definition the weakest coordinating anions as they easily extract an alkyl group from chromium) providing the highest activity as well as the highest 1-C_8 selectivity overall. The use of weaker Lewis acids (which are more likely weakly associated to chromium) resulted in both lower activity but also a much higher 1-hexene selectivity of 90%. Thus, based on these observations it is reasonable to conclude that weak Lewis acids do not efficiently cationize chromium, creating a more coordinatively saturated catalyst which produces 1-hexene. However very strong Lewis acids completely cationize the chromium centre, generating a coordinatively unsaturated species which produces 1-octene.

The third major parameter which strongly influences tetramerization performance is the solvent. The analysis of several experimental reports evaluating the effect of solvent polarity on the catalytic performance reveals a trend in which the least polar aliphatic hydrocarbon solvents pro-

vide the highest activity and selectivity for 1-C_8. The more polar toluene gave similar selectivity but also a large loss in activity.[82, 72] However, use of the highly polar chlorobenzene solvent results in much higher oligomerization activity than toluene, but at a complete loss of selectivity for 1-C_8 and 1-C_6. However, it was discovered that catalytic quantities of such polar halogenated co-solvents can significantly enhance the 1-octene selectivity. For example, simply adding just 0.5 equivalents of 1,2-dichloroethane per chromium centre results in a substantial (5%) increase in 1-octene selectivity without any loss in activity, while further increases in the 1,2-dichloroethane amounts resulted in decreased selectivity. While the use of aliphatic hydrocarbon solvents are found to lead to the best activity, the actual solubility of the catalyst in these solvents is found experimentally to be very poor.[83, 84] Thus the actual catalyst solution is probably not homogeneous, actually being a fine dispersion of oily droplets of the highly polar ionic catalyst/cocatalyst mixture in the hydrocarbon solvent. In such a scenario, the actual environment around the chromium catalyst in the least polar hydrocarbon solvent is likely locally much more polar than even chlorobenzene due to its complete insolubility and formation of a highly polar heterogeneous suspension. This idea is the basis of a patent for a highly active and selective chromium trimerization catalyst in a highly polar ionic liquid solvent.[68]

The last category of important experimental parameters which can strongly affect the catalyst selectivity and activity are the temperature and the pressure of the ethylene substrate. Experimental studies have revealed that the overall 1-C_8 selectivity increases with higher ethylene concentration and lower temperatures.[85, 86] However, these factors are actually important mechanistically from a kinetic perspective, as any change in the temperature or ethylene pressure also directly changes the concentration of dissolved ethylene in the solvent. In fact, consistent with the observed ligand-bite angle effects, the rate of formation of the 1-C_8 product is established to be exactly second order in the ethylene concentration, whereas the 1-C_6 product in the same reactor is actually first order in ethylene concentration. Thus at higher concentrations of ethylene (i.e. higher pressure), the rate of 1-C_8 formation increases with the square of the ethylene concentration, while the rate of C_6 formation increases only linearly with ethylene concentration, resulting in a higher selectivity for 1-C_8 at higher pressures of ethylene. However, the different ethylene

concentration dependence of C_6 and C_8 products is a direct evidence that is inconsistent with the kinetics proposed in the "extended" metallacycle mechanism, which predicts that all oligomer product will have the same concentration dependence (as they are proposed to form via similar steps involving the insertion of a single molecule of ethylene into a metallacycle intermediate).

In addition to this unexpected difference in ethylene concentration dependence between the C_6 and C_8 products of the diphosphine-chromium tetramerization catalyst, there is also a significant difference in their kinetic isotope effects (KIE). The KIE, or ratio of standard ethylene to deuterated ethylene incorporated in the product (X) differs for the C_6 and C_8 fractions. Whereas X was determined to be the same within experimental error for 1-hexene and methylcyclopentane/methylcyclopentene products (X = 2.5), the value of X for 1-octene was significantly lower (X= 1.9).[49] Thus based on the experimentally determined KIE and the experimentally determined ethylene concentration dependence for the 1-C_8 product, it is possible that the rate-limiting step in the appearance of the 1-octene product is the oxidative coupling of two ethylene molecules to form a metallacyclopentane intermediate (which was also concluded based on bite-angle effects). This is consistent with a transition state involving two molecules of ethylene. In addition, it would also be logical by the same experimentally-determined kinetics to conclude that the rate limiting step for the formation of the 1-C_6 product is the insertion of one ethylene molecule into the metallacyclopentane intermediate. As mentioned, the major failure of the "extended" metallacycle mechanism is that it does not accurately model these kinetics.

A more accurate mechanistic model should be able to predict the ethylene concentration dependence, as well as to predict why the experimentally-determined kinetic isotope effect for the 1-C_8 and C_6 products are different. Hints as to the actual mechanism are found in the isotopic labelling, which reveals that while the observed isotopomer distribution of the 1-C_6 and 1-C_8 products correlates well with the predicted distribution from the metallacycle mechanism (no scrambling), the cyclic C_6 products contain a random distribution consistent with a disproportionation pathway, providing strong evidence for the involvement of bimetallic intermediates for their simultaneous formation. Thus the kinetics study of the diphosphine chromium tetramerization catalyst and the previously-reported DFT studies have largely raised doubt on the validity of the "extended"

metallacycle mechanism.

The physical basis for the high 1-C_8 selectivity via the "extended" metallacycle mechanism is that the metallacycloheptane intermediate (which gives rise to 1-C_6) is more kinetically stable than the metallacyclononane intermediate (which gives rise to 1-C_8). However, this physical basis has been directly contradicted by DFT calculations reported by Budzelaar and Ziegler on the stability of larger metallacycles,[68, 43, 87, 45, 46, 47, 88] which conclude that the larger metallacycles are all equally stable kinetically due to their conformational flexibility. The "extended" metallacycle mechanism is the basis for some non-selective oligomerization catalysts. Thus the "extended" metallacycle mechanism, while originally conceived to explain the selective formation of 1-octene, has proven highly accurate in explaining the behavior of non-selective chromium oligomerization catalysts.[50]

Thus the actual mechanism underlying the high selectivity for 1-C_8 is now by no means certain. However, some of the puzzling features that can be observed with kinetics is that the rate of the formation of 1-octene is actually the ethylene oxidative coupling step. It, therefore logically, bypasses the formation of a metallacycloheptane intermediate which is slower (explaining the lower 1-C_6 selectivity) and is rate-limited by the insertion of ethylene into the metallacyclopentane intermediate. Envisioning how the 1-C_8 can form without going through a metallacycloheptane intermediate is a bizarre possibility, but however this conclusion is well-supported by experimental kinetics, ligand bite angle effects, and DFT studies of the stability of larger metallacycles. However, no further progress can be made in mechanistically defining a model to fit these experimental results without the further isolation and study of actual organometallic models, where the effect of the experimental parameters on the underlying organochromium coordination chemistry can be analyzed directly. This critical information would allow tetramerization catalyst development from a rational perspective for the first time. Thus, the the experimental methodology which was successfully developed in chapter 2 is employed again in this chapter. However, to aid in the rationalization of the underlying organochromium [PNP] chemistry which will be discussed, a brief background is first provided of some established organochromium (II) reactivity. The focus is particularly on the reactivity of bimetallic species which have already been implicated

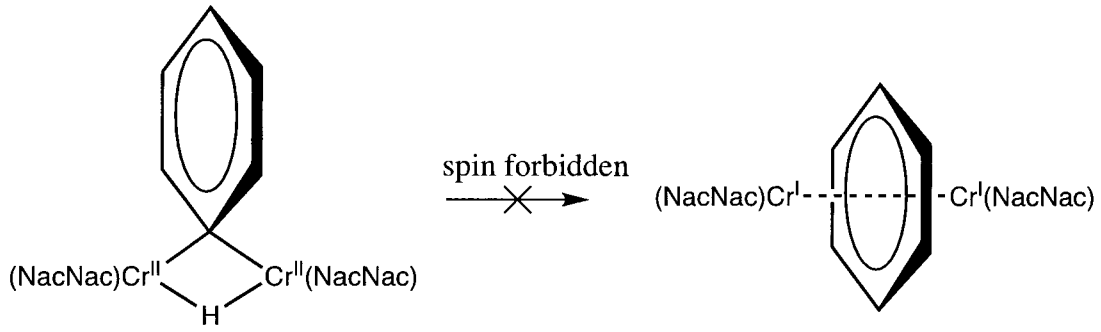

Figure 36: Spin-forbidden reductive elimination of bimetallic organochromium (II) complexes

in the formation of the two cyclic C_6 byproducts by the chromium diphosphine tetramerization catalyst.[89, 90]

3.1.2 Background of bimetallic organochromium (II) chemistry

Theopold et al have recently reported that bimetallic organochromium (II) complexes cannot undergo direct reductive elimination, as it was found experimentally and through DFT studies that the energy barrier to the spin flip required for the transformation is too high, making it a spin forbidden process (as opposed to disproportionation described in the previous chapter which is allowed) (Figure 36).[90][91] The formation of high-spin Cr(I) is not favorable due to a high energy, however the spin crossover from high-spin to intermediate or low-spin also occurs at a high energy, thus making the direct formation of Cr(I) from Cr(II) via bimetallic reductive elimination unlikely in a catalytic process due to the high barrier.

The unusual reactivity of such bimetallic organochromium (II) intermediates may be the key to the observed cyclic C_6 byproducts, as it was proposed that, based on this reactivity, the cyclic C_6 products forming in a 1:1 ratio must form via bimetallic intermediates. It is thought that bimetallic reductive elimination from chromium (III) dimers gives rise to the methylcyclopentane product.[90][91] The resulting Cr (II) dimers cannot undergo further reductive elimination of another molecule of methylcyclohexane to give chromium (I), as it is already established to be a spin forbidden process. Instead only β-hydrogen elimination from the Cr(II) dimer is possible, resulting in the methylenecyclopentane product (Figure 37).

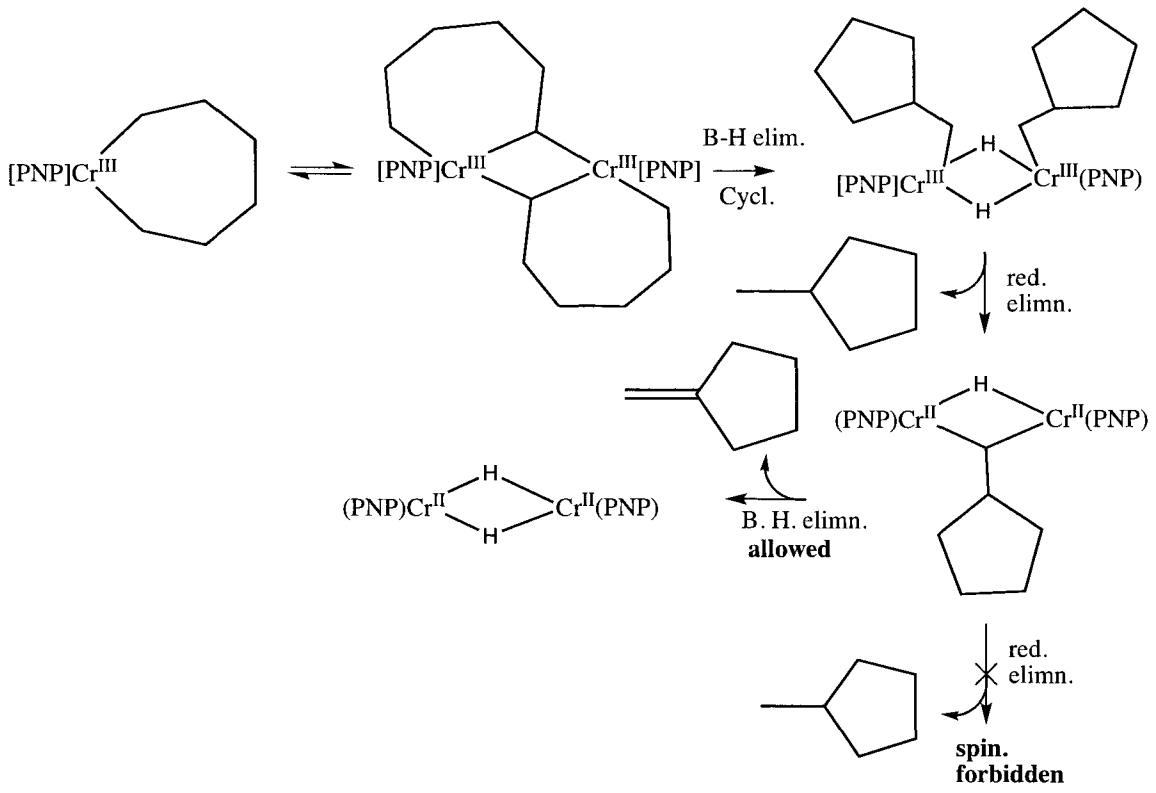

Figure 37: Previously proposed influence of spin control in the catalytic formation of the two cyclic C_6 byproducts in a 1:1 ratio

However, the formation of these intermediates requires that the tetramerization catalyst forms stable dimers and that these dimers can react in a bimetallic fashion to form the observed products. There is, however, such evidence that, in fact, bimetallic catalytic intermediates exhibit a different reactivity than the analogous monometallic derivatives, as is reported in a seminal work by Jolly (some of which was alluded to in the introduction, see Figure 6).[42, 92, 93, 94, 95, 96, 97, 98, 99, 100, 101, 39] The analysis of these reports reveals that coordinatively saturated Cp-phosphine-based chromium complexes were found to be monomeric in solution and promote selective ethylene trimerization via two-electron redox steps (Figure 38). By contrast, the analogous coordinatively unsaturated donor-free Cp-chromium derivatives were found to form stable bimetallic complexes which catalyze C-C coupling via 1 electron redox steps (Figure 38). For example, several bimetallic CpCr (II) -arene and -alkyne intermediates have also been isolated and shown to catalyze alkyne trimerization, while the analogous monometallic CpCr (I) arene complex is catalytically inactive.

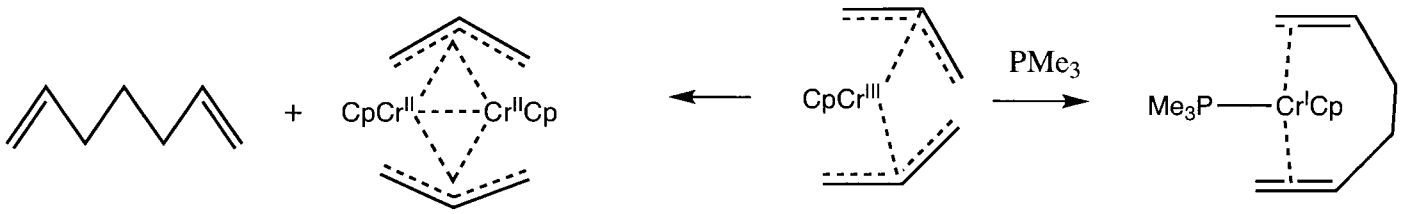

Figure 38: Divergent reactivity of related monometallic and bimetallic organochromium species

Thus, at least one relevant example of olefin trimerization in the literature shows a difference in reactivity between monometallic and bimetallic chromium complexes based on the coordinative unsaturation dictated by the ligand set. This suggests that similar mechanistic differences may exist in the comparison of some established chromium trimerization catalysts containing tridentate ligands which should favor monometallic reactivity. Instead, diphosphine-chromium based tetramerization catalysts should favor bimetallic reactivity. These different donor sets to chromium can be organized according to their relative steric impact and tendency to form dimer complexes (Figure 39). Thus our experimental work will aim at finding this information. Later on in this chapter ligand effects on the chemical reactivity of these bimetallic intermediates will be discussed in light of the experimental findings.

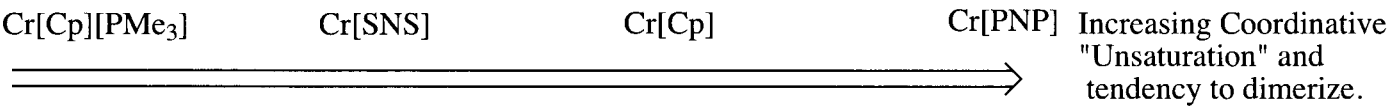

Figure 39: Direct relation between coordinative unsaturation of chromium and its tendency to dimerize

3.2 Experimental

General

All manipulations were carried out using standard Schlenk line or drybox techniques under an atmosphere of dry dinitrogen. Samples for magnetic susceptibility were preweighed inside a drybox equipped with an analytical balance and measured on a Johnson Matthey Magnetic Susceptibility balance. Catalytic reaction mixtures were analyzed using a CP 9000 gas chromatograph (GC) fitted with a 30 m x 0.32 mm i.d. capillary CP volamine column and with an FID detector.

Elemental analysis was carried out with a Perkin-Elmer 2400 CHN analyzer. Infrared spectra were recorded on an ABB Bomem FTIR instrument from Nujol mulls prepared in a drybox. Data for X-ray crystal structure determination were obtained with a Bruker diffractometer equipped with a 1 K Smart CCD area detector. The $CyN(PPh_2)_2$ [PNP] ligand was prepared using a slightly modified literature procedure.[49] The purple complex $\{[(PNP)Cr^{III}Cl_3]_2\}$ (**14**) was prepared by adapting the procedure reported in the literature.[49] Aluminum activators, $(Al^iBu_2)_2O$ (Aldrich), Al^iBu_3, Me_3Al (Strem), and MAO (Chemtura) were used as received.

General Oligomerization Procedure: A 45 mL Parr reactor was dried in an oven at 120 °C for 3 h prior to each run and then placed under vacuum for 30 min while cooling. The reactor was then charged with toluene, catalyst, and cocatalyst, and 40 bar of ethylene and heated to 115 °C with stirring. The reaction was allowed to run for 1 h, after which the temperature was rapidly reduced to 5 °C, the reactor was depressurized, and a mixture of MeOH/HCl was injected to quench the reaction. The organic and aqueous phases were then separated from the polymer. Precautions were taken to maintain the temperature as low as possible during the workup to minimize loss of volatiles. Polymeric materials were sonicated with an aqueous solution of HCl and dried at 60 °C for 18 h under reduced pressure before the final mass was weighed. Yields of oligomers were obtained by GC by using calibrated standard solutions. The overall catalytic activity was determined by integrating the intensity of the olefinic NMR resonances versus the Me group of the toluene solvent.

3.2.1 $\{(PNP)MeCr^{III}(\mu\text{-}Cl)_3Cr^{III}Me(PNP)\}$ $\{Me_2AlCl_2\}$ (15)

A mixture of **14** (625 mg, 0.5 mmol) and Me_2AlCl (161 mg, 1.5 mmol) in chlorobenzene (15 mL) at 22°C turned dark green upon mixing, which was then filtered and layered with hexanes (10 mL) yielding green plates of **15** (581 mg, 93 %) upon standing for one week at 22°C. μ_{eff}= 3.72 μ_B per Cr atom. Anal. Calcd (found) for C64H74AlCl5Cr2N2P4: C, 61.40 (61.32); H, 5.96 (6.04); N, 2.24 (2.20). E.P.R. (powder, - 78°C, in text).

3.2.2 {(PNP)Cr^{II}(μ-Cl)$_2$(μ^2,η^2-Me_2AlCl_2)Cr^{II}(PNP)} {Me_2AlCl_2} (16)

Method A: (from **15**) To a green solution of **15** (651 mg, 0.5 mmol) in chlorobenzene (10 mL) was added Me_2AlCl (92 mg, 1 mmol) at 22°C resulting in the instant color change to a deep blue solution. NMR analysis of the gas evolved, by passing through a cooled C_7D_8 solution (-78°C) and then sealing the tube, allowed the detection of a significant quantity of dissolved ethane gas. After filtering and layering with hexanes, blue X-ray quality crystals of **16** (566 mg, 83 %) grew. μ_{eff}= 4.68 μ_B. Anal. Calcd (found) for C64H74Al2Cl6Cr2N2P4: C, 56.26 (55.87); H, 5.46 (5.41); N, 2.05 (2.11).

Method B: (from **14**) To a purple solution of **14** (625 mg, 1 mmol) in chlorobenzene (10 mL) was added Me_2AlCl (536 mg, 5 mmol) while stirring for 1 min, resulting initially in a green solution which rapidly turned blue. Centrifugation and layering with hexanes (10 mL) resulted in X-ray-quality crystals of **15** (505 mg, 74 %). Similar yields could also be obtained from $CrCl_2(THF)_2$ as a starting material.

3.2.3 {$(PNP)_2Cr^{II}$(μ-Cl)$AlMe_3$} {$Me_3Al(Cl_{0.34}/Me_{0.66})$} (17)

Method A: A suspension of $CrCl_2(THF)_2$ (56 mg, 0.21 mmol) and [PNP] (200 mg, 0.42 mmol) in toluene (15 mL) did not afford any color change, even upon refluxing the mixture. The addition of Me_3Al (144 mg, 2.0 mmol) in toluene and stirring for 1 h at 22°C resulted in a color change, initially to brownish red and finally to light blue. The resulting solution was filtered, then allowed to stand at room temperature for several hours, upon which crystals of analytically pure **17** (230 mg, 0.19 mmol, 90%) deposited. Anal. Calcd (found) for C69.16H89.73Al2Cl1.34CrN2P4: C, 67.73 (67.38); H, 7.37 (7.31); N, 2.28 (2.14). μ_{eff}= 4.80 μ_B.

Method B: (from **14**) a bluish-purple suspension of **14** (1.70 g, 2.72 mmol) in toluene (15 mL) was added Me_2AlCl (1.96 g, 27.20 mmol) in toluene (15 mL). The color immediately changed initially to green and then gradually to light blue over 1 min. After centrifugation of the solution and layering with hexanes (10 mL), crystals of analytically pure **17** (1.68 g, 45%) were grown upon allowing the mixture to stand at -35°C over 2 days. The same procedure using **15** or **16** also produced similar yields.

3.2.4 {(PNP)Cr^{II}[(μ-Cl)$AlCl_3$]$_2$} (18)

A mixture of $CrCl_2(THF)_2$ (250 mg, 0.93 mmol), [PNP] (467 mg, 1 mmol) and $AlCl_3$ (665 mg, 5 mmol) in toluene (15 mL) was stirred for 2 h at 22°C, resulting in a deep blue solution. After centrifugation and layering with hexanes (10 mL) at 22°C for three days, blue crystals of analytically pure **18** (594 mg, 73 %) formed. Anal. Calcd (found) for C30H31Al2Cl8CrNP2: C, 42.05 (41.87); H, 3.62 (3.56); N, 1.64 (1.63). μ_{eff}= 4.78 μ_B.

3.2.5 X-ray Characterization

Table 14: Crystal Data and Structure Analysis Results for Chromium [PNP]

Complex #	**15**	**16**	**17**	**18**
formula	C64H74Al	C65.50H76.50N2	C69.16H89.73Al2	C44H47NP2
	Cl5Cr2N2P4	Al2Cl9Cr2P4	Cl1.34CrN2P4	Cl8Al2Cr
Mw	1302.25	1492.68	1226.51	1041.39
space group	P	P-1	P-1	P-1
a (Å)	13.244(9)	13.541(1)	12.366(2)	11.756(2)
b (Å)	18.083(10)	14.5513(1)	16.214(3)	12.503(2)
c (Å)	14.782(9)	20.0854(2)	21.347(4)	12.911(2)
α	90	77.910(1)	96.191(3)	110.01(2)
β	90.252(2)	76.880(2)	106.453(3)	111.30(2)
γ	90	87.023(2)	91.839(3)	94.16(2)
V (Å^3)	3540(6)	3768.8(6)	4072.0(12)	1619(4)
Z	2	2	2	1
radiation	0.71073	0.71073	0.71073	0.71073
T (K)	208(2)	208(2)	208(2)	208(2)
D_{calcd} (g cm^{-3})	1.192	1.315	0.997	1.068
μ_{calcd} (mm^{-1})	0.630	0.754	0.318	0.608
F000	1457	1541	1294	534
R, Rw_2	-	0.0786, 0.1879	0.0781, 0.2015	0.0547, 0.1308
GoF	-	1.068	1.035	1.015

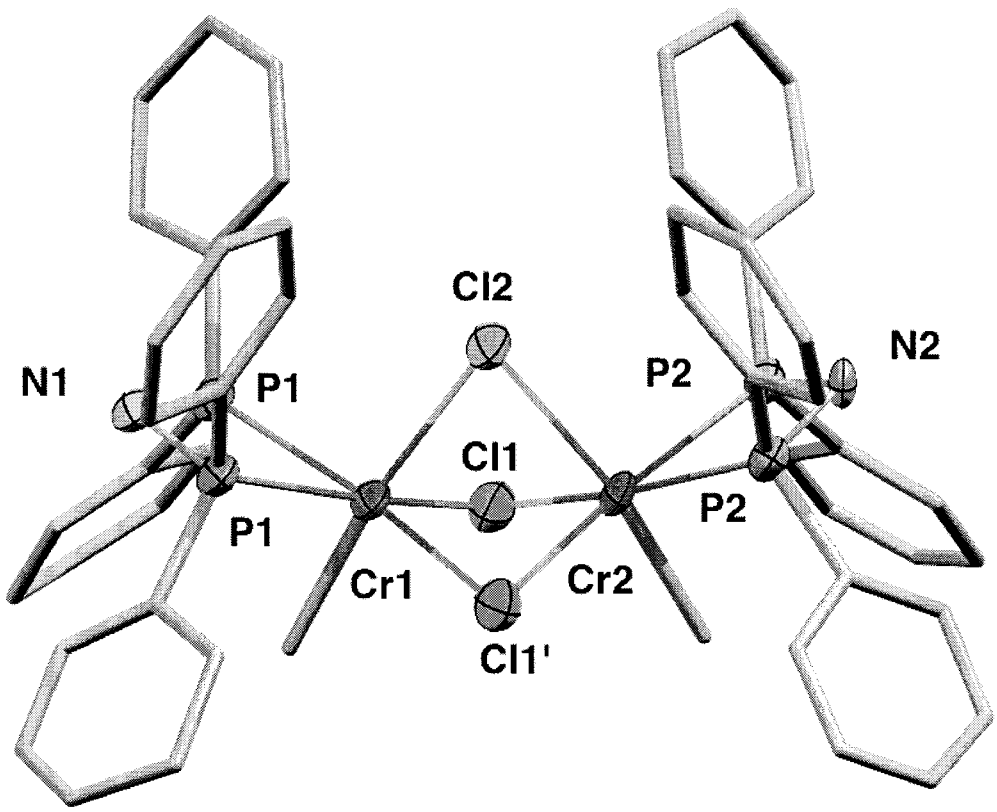

Figure 40: Partial thermal ellipsoid plot (50% probability) of {(PNP)MeCr^{III}(μ-Cl)$_3$Cr^{III}Me(PNP)} {Me_2AlCl_2} (**15**) , the {Me_2AlCl_2}- anion and highly disordered cyclohexyl groups are omitted for clarity

Table 15: Selected Bond Distances (Å) and Angles (°) for {(PNP)MeCr^{III}(μ-Cl)$_3$Cr^{III}Me(PNP)} {Me_2AlCl_2} (**15**)

Cr(1)-Cl(1/1a)	2.397	Cr(2)-Cl(1/1a)	2.384
Cr(1)-Cl(2)	2.466	Cr(1)-Cl(2)	2.431
Cr(1)-C(19)	2.117	Cr(2)-C(38)	2.139
Cr(1)-P(1/1a)	2.433	Cr(2)-P(2/2a)	2.446
P(1)-Cr(1)-P(1a)	66.96	P(2)-Cr(2)-P(2a)	67.46
Cl(1)-Cr(1)-Cl(2)	82.43	Cl(1)-Cr(2)-Cl(2)	83.24
Cl(1)-Cr(1)-Cl(1a)	90.91	Cl(1)-Cr(2)-Cl(1a)	91.57
Cr(1)-Cl(1/1a)-Cr(2)	76.89	Cr(1)-Cl(2)-Cr(2)	74.76

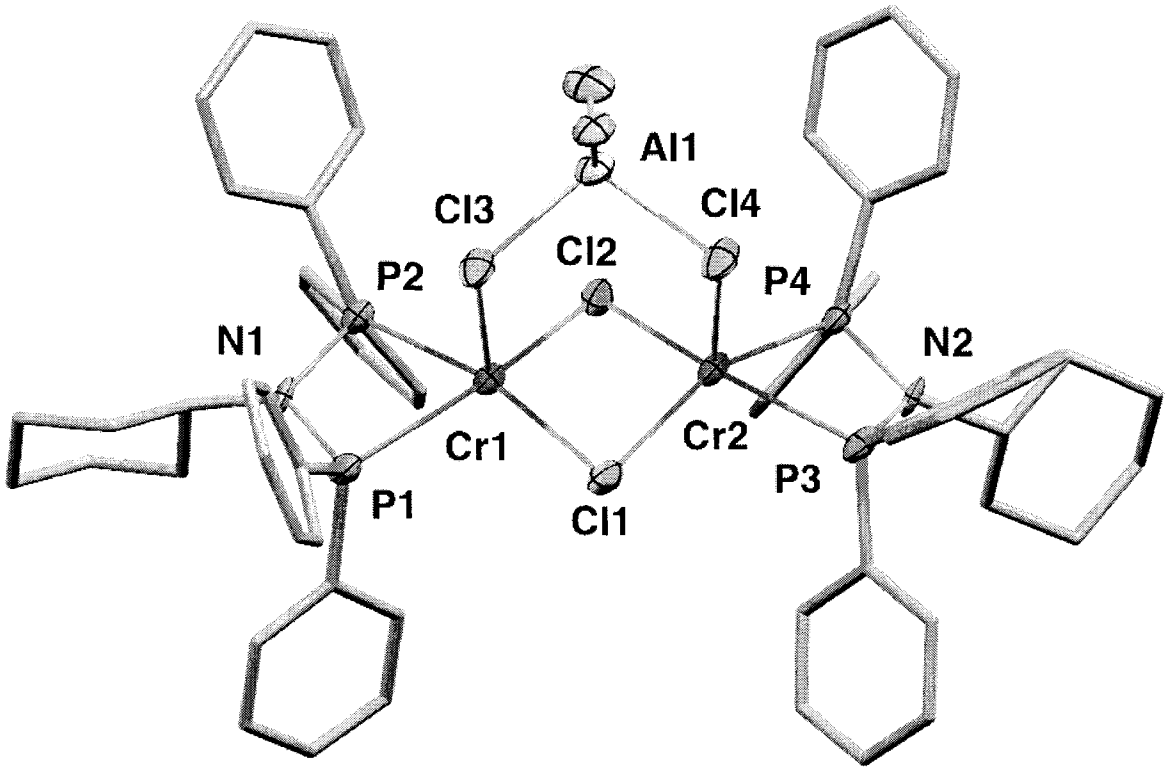

Figure 41: Partial thermal ellipsoid plot (50% probability) of $\{(PNP)Cr^{II}(\mu\text{-}Cl)_2(\mu^2,\eta^2\text{-}Me_2AlCl_2)Cr^{II}(PNP)\}$ $\{Me_2AlCl_2\}$ (**16**)

Table 16: Selected Bond Distances (Å) and Angles (°) for $\{(PNP)Cr^{II}(\mu\text{-}Cl)_2(\mu^2,\eta^2\text{-}Me_2AlCl_2)Cr^{II}(PNP)\}$ $\{Me_2AlCl_2\}$ (**16**)

Cr(1)-Cl(1)	2.366(3)	Cr(2)-Cl(1)	2.401(4)
Cr(1)-Cl(2)	2.372(3)	Cr(2)-Cl(2)	2.349(3)
Cr(1)-Cl(3)	2.578(4)	Cr(2)-Cl(4)	2.549(4)
Cr(1)-P(1)	2.485(4)	Cr(2)-P(3)	2.454(4)
Cr(1)-P(2)	2.428(4)	Cr(2)-P(4)	2.453(4)
P(1)-Cr(1)-P(2)	67.12(11)	P(3)-Cr(2)-P(4)	66.90(12)
Cl(1)-Cr(1)-Cl(2)	92.37(12)	Cl(1)-Cr(2)-Cl(2)	92.07(12)
Cl(1)-Cr(1)-Cl(3)	98.38(12)	Cl(1)-Cr(2)-Cl(4)	98.08(13)
Cr(1)-Cl(1)-Cr(2)	86.70(11)	Cr(1)-Cl(2)-Cr(2)	86.70(11)

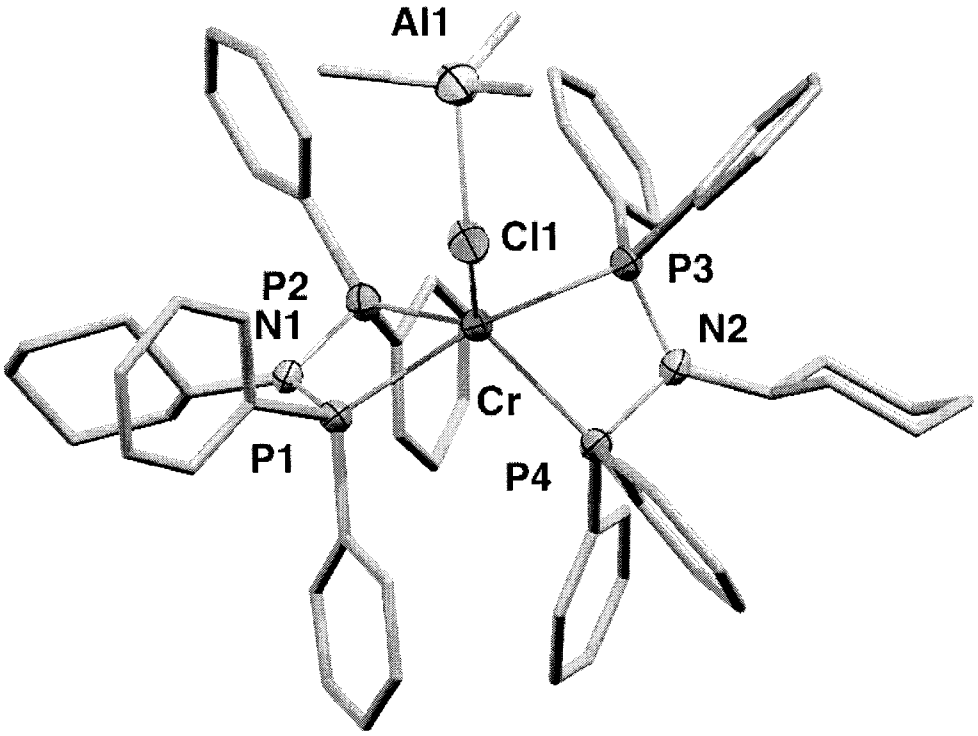

Figure 42: Partial thermal ellipsoid plot (50% probability) of $\{(PNP)_2Cr^{II}(\mu\text{-}Cl)AlMe_3\}$ $\{Me_3Al(Cl/Me)\}$ (**17**), the $\{Me_3Al(Cl/Me)\}$ anion omitted for clarity

Table 17: Selected Bond Distances (Å) and Angles (°) for $\{(PNP)_2Cr^{II}(\mu\text{-}Cl)AlMe_3\}$ $\{Me_3Al(Cl/Me)\}$ (**17**)

Cr(1)-Cl(1)	2.368(2)	Cl(1)-Al(1)	2.428(3)
Cr(1)-P(1)	2.528(2)	Al(1)-C(61)	1.971(9)
Cr(1)-P(2)	2.488(2)	Al(2)-Cl(2)	2.237(10)
Cr(1)-P(3)	2.477(2)	Al(2)-C(75)	1.949(16)
Cr(1)-P(4)	2.500(2)	P(2)-Cr(1)-P(4)	102.07(6)
Cr(1)-Cl(1)-Al(1)	137.60(11)	P(3)-Cr(1)-P(4)	66.57(5)
P(1)-Cr(1)-P(2)	66.39(6)	Cl(1)-Cr(1)-P(1)	122.01(7)
P(1)-Cr(1)-P(3)	107.39(6)	Cl(1)-Cr(1)-P(2)	98.60(6)
P(1)-Cr(1)-P(4)	114.66(6)	Cl(1)-Cr(1)-P(3)	96.87(6)
P(2)-Cr(1)-P(3)	164.26(7)		

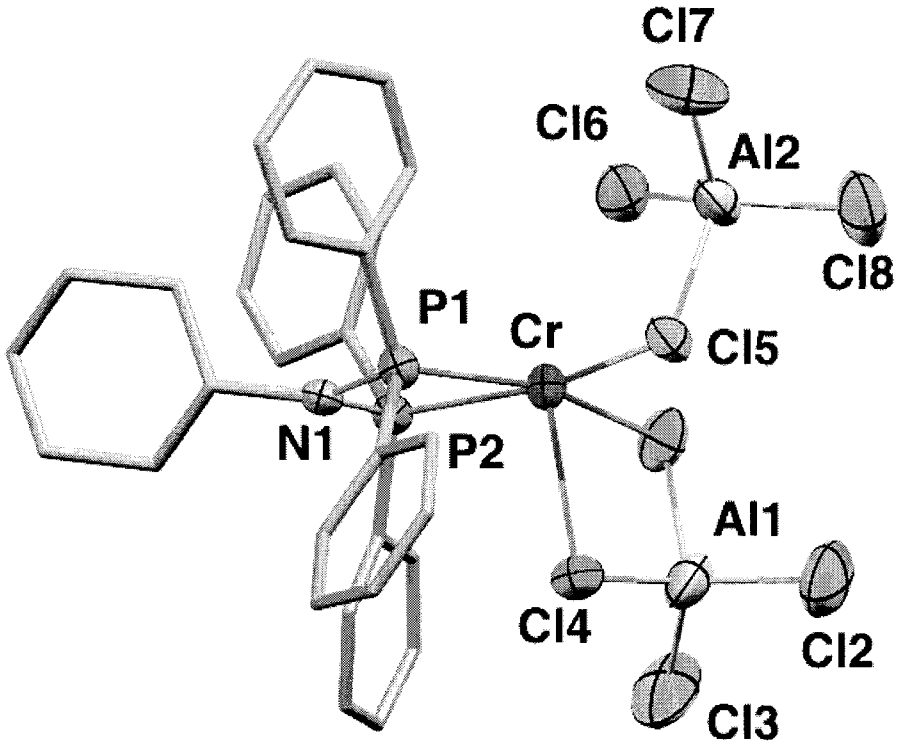

Figure 43: Partial thermal ellipsoid plot (50% probability) of $\{(PNP)Cr^{II}[(\mu\text{-}Cl)AlCl_3]_2\}$ (**18**)

Table 18: Selected Bond Distances (Å) and Angles (°) for $\{(PNP)Cr^{II}[(\mu\text{-}Cl)AlCl_3]_2\}$ (**18**)

Cr(1)-Cl(1)	2.464(3)	P(1)-Cr(1)-P(2)	67.42(3)
Cr(1)-Cl(5)	2.435(4)	Cl(1)-Cr(1)-P(1)	165.29(6)
Cr(1)-P(1)	2.478(3)	Cl(1)-Cr(1)-P(2)	98.62(5)
Cr(1)-P(2)	2.466(3)	Cl(1)-Cr(1)-Cl(5)	95.23(3)
Cr(1)-Cl(6)	3.036(5)	Cl(4)-Cr(1)-Cl(6)	150.81(4)
Cr(1)-Cl(4)	2.789(4)		

3.2.6 Catalytic Data

Table 19: Catalytic Data for Cr [PNP] complexes **14-18**

Cat	MAO	PE	activity	activity	C_6	C_8
#	(eq.)	(g)	(g/mol/h)	(g/gCr/h)	(mol%)	(mol%)
14	1000	0.5	416000	8000	32.1	59.4
15	1000	0.8	436000	7800	25.3	67.6
16	1000	0.7	421000	8100	22.8	69.7
17	1000	0.9	437000	8400	18.4	73.4
18	1000	0.3	354000	6800	35.3	62.0

Conditions: T = °C, V = 150 mL, P = 35 bar, catalyst = 30 µmole, time = 1 h. Activity calculated by integration of the NMR olefinic resonances with respect to the Me of the toluene solvent. Values of 1-C_4 are not given due to volatility.

3.3 Results

3.3.1 Reaction of CrPNP chloride precursors with aluminum cocatalysts

The reaction of $CrCl_3(THF)_3$ with the cyclohexyl-substituted diphosphine ligand $PPh_2NCyPPh_2$ [PNP] resulted in the quantitative formation of the purple ethylene tetramerization catalyst precursor $\{[(PNP)Cr^{III}Cl_3]_2\}$ (**14**). The structure of the closely related isopropyl-substituted $\{[(PNP)Cr^{III}Cl_3]_2\}$ derivative has been reported, revealing that the [PNP] ligand is bound in a bidentate fashion and that the complex is binuclear, being composed geometrically of an edge-bridging chloride bi-octahedra configuration.[49] The reaction of **14** with various amounts of Me_2AlCl, Me_3Al and MAO was explored to gain mechanistic insights into the role of the [PNP] ligand in influencing catalytic selectivity towards the valuable ethylene tetramerization product (Figure 44).

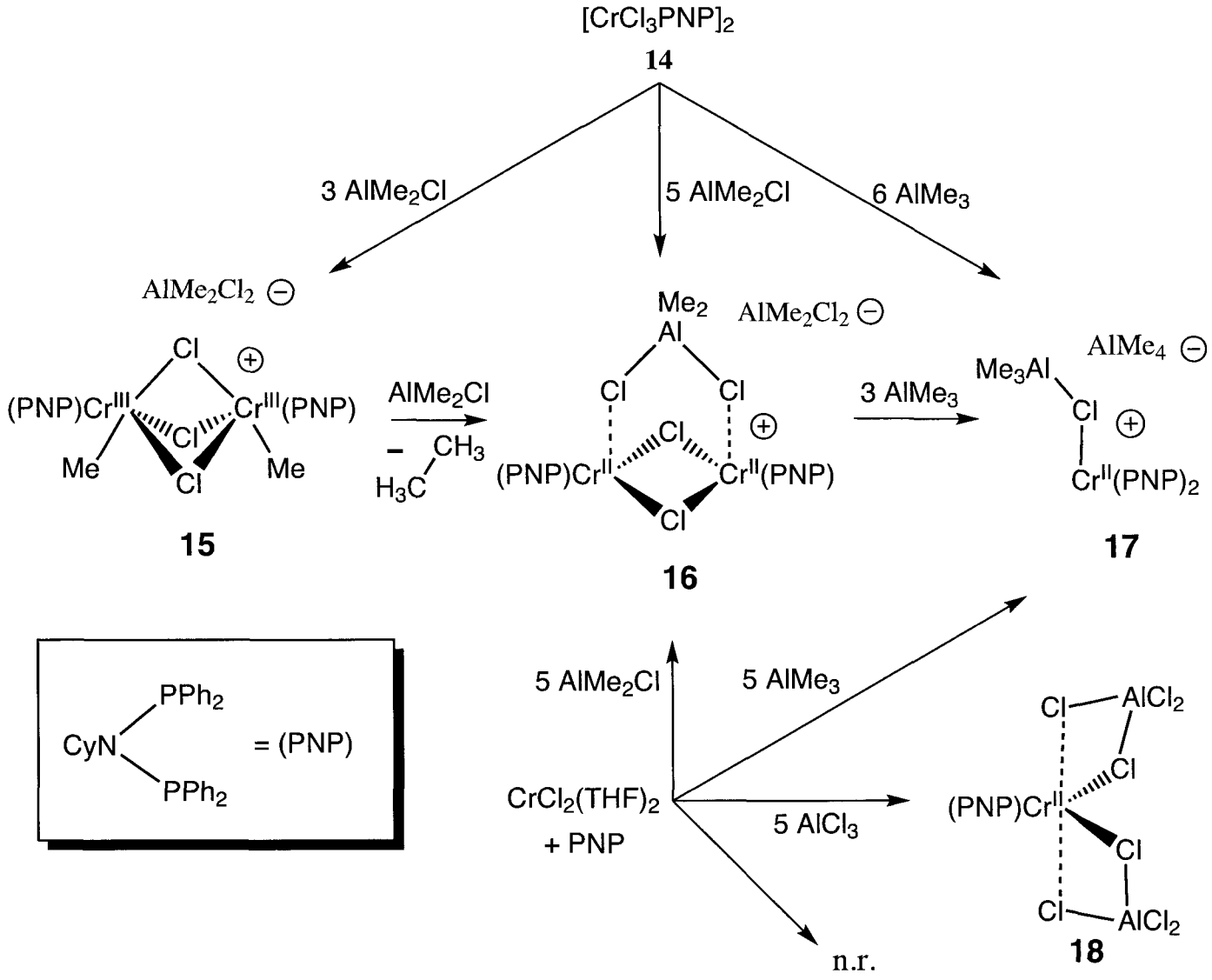

Figure 44: Summary of the reaction of chromium chloride precursors with the [PNP] ligand and aluminum cocatalysts

The reaction of **14** with Me_2AlCl (3 eq.) afforded a high yield of the cationic trivalent methyl dimer, $\{(PNP)MeCr^{III}(\mu\text{-}Cl)_3Cr^{III}Me(PNP)\}$ $\{Me_2AlCl_2\}$ (**15**), which was isolated as small dark-green plates (Figure 44). The structure of **15** (Figure 40) consists of a symmetry generated cationic Cr(III) dimer with a face-sharing bi-octahedral structure, counterbalanced by an aluminate $\{Me_2AlCl_2\}$ anion. The two slightly distorted octahedral chromium atoms in the cationic unit are symmetrically connected by three face-bridging chlorine atoms [Cr(1)-Cl(1/1a) = 2.397 Å; Cr(1)-Cl(2) = 2.466 Å] forming a Cr_2Cl_3 trigonal bipyramidal core [Cl(1)-Cr(1)-Cl(1a) = 91.57°; Cl(1)-Cr(1)-Cl(2) = 83.44°; Cr(1)-Cl(1/1a)-Cr(2) = 76.89°; Cr(1)-Cl(2)-Cr(2) = 74.76°]. The remaining

coordination sites of chromium filled by the P atoms of the [PNP] ligand [Cr(1)-P(1/1a) = 2.433 Å; P(1)-Cr(1)-P(2) = 66.96°] and the carbon of the terminally bonded Me group [Cr(1)-C(17) = 2.117 Å]. The [Me_2AlCl_2] counter anion is unconnected to the cationic chromium unit. The room-temperature magnetic moment of **15** is 3.72 μ_B per chromium atom, with the expected high spin d^3 configuration of chromium (III). The elemental analysis was also consistent with the structural assignment. Finally, the low-temperature powder spectrum of **15** is the first such example, and is found to be consistent with the characteristic spectra observed in magnetically-coupled Cr (III) dimers (Figure 45).[2, 102] Contrasting this result is the in-situ EPR study of the MAO activated Cr [PNP] system, which has already been reported in the literature.[103] In that case it was found that reaction with excess MAO results in a rapid reduction to a blue colored EPR-silent species. Complex **15** was found to be thermally stable, as no decomposition or color change was observed even upon heating a chlorobenzene solution at 60°C for 10 minutes.

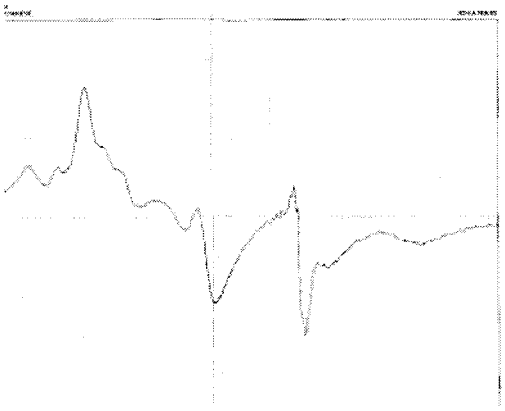

Figure 45: Powder EPR spectrum of **15** at -160 °C. Frequency 9121.042 MHz. X axis in mT

To gain further insights into the possible organochromium reduction pathways, the reaction of **15** with additional aluminum alkyl reagents was explored. A green-colored solution of **15** in chlorobenzene turned blue almost instantly upon addition of Me_2AlCl (1 eq.) and, upon layering with hexanes afforded high yield of the bimetallic cationic Cr(II) derivative, {(PNP)Cr^{II}(μ-Cl)$_2$(μ^2,η^2-Me_2AlCl_2)Cr^{II}(PNP)} {Me_2AlCl_2} (**16**), which is the product of a reduction (Figure 41). Complex **16** could also be generated directly from **14** by using an excess of Me_2AlCl. The X-ray crystal structure of **16** (Figure 41) consists of a cationic dimer with an edge-sharing distorted square pyramidal structure containing a bridging Me_2AlCl_2 anion in the two apical sites,

the dichromium cation is counterbalanced by a non-coordinating aluminate $\{Me_2AlCl_2\}$ anion. The $\{Me_2AlCl_2\}$ anion is unconnected to the cationic dichromium unit. The room-temperature magnetic moment of **16**, of 4.68 μ_B per chromium atom is consistent with four unpaired electrons expected for the high spin d^4 electron configuration of chromium (II). The elemental analysis was also consistent with the structural assignment. The analysis of the gas formed in the reaction revealed that the reduction of **15** to **16** was also accompanied by the formation ethane as detected by NMR, implicating the reductive elimination of the Cr-Me groups.

The examination of further transformation of **16** in the presence of a large excess of aluminum cocatalyst was of interest due to the typical use of a large excess of MAO in catalysis. Thus the treatment of **16** with the stronger acid Me_3Al (3eq.) resulted in its conversion to bis-PNP $\{(PNP)_2Cr^{II}(\mu\text{-}Cl)AlMe_3\}$ $\{Me_3Al(Cl/Me)\}$ (**17**) in moderate yield (Figure 44). The X-ray crystal structure of **17** (Figure 41) reveals that this time the cation is monomeric, and consists of a Cr atom placed in the centre of a distorted trigonal bipyramid with two P atoms from two ligands occupying the axial positions. The three equatorial positions are defined by the remaining two P atoms and the chlorine atom, which in turn bridges a Me_3Al unit. One $ClAlMe_3$ counteranion, not connected with the Cr-containing cation, was present in the lattice. The Me_3Al was equally disordered over two positions, while the chlorine atom was partially disordered with another methyl group. Both the connectivity and the magnetic moment (4.80 μ_B) clearly indicate a Cr(II) oxidation state. Complex **17** is the product of ligand disproportionation and is obviously accompanied by the production of an unidentified chromium byproduct which is postulated to be a volatile species such as $\{Cr(Me_2AlCl_2)_2\}$, since no byproduct remained in the solvent upon taking the solution to dryness after isolating **17**. Carrying out the reaction in the presence of excess [PNP] ligand however did not increase substantially the yield of **17**, suggesting that the byproduct is also relatively inert.

Surprisingly, the combination of the chromium (II) precursor, $CrCl_2(THF)_2$, with the [PNP] ligand resulted in no reaction. The treatment of this mixture with Me_3Al, Me_2AlCl, and $AlCl_3$ allowed isolation of **17**, **16**, and the neutral $\{(PNP)Cr^{II}[(\mu\text{-}Cl)AlCl_3]_2\}$ (**18**), respectively (Figure 44). Complex **18** (Figure 43) contains a distorted square pyramidal geometric arrangement, with the apical site occupied by a chloride donor, while the equatorial sites are occupied by the two

phosphines of the [PNP] ligand and the chlorides of the two $AlCl_4$ ligands. Both the connectivity and the magnetic moment (4.78 μ_B) is consistent with the high spin d^4 electronic configuration typical of Cr(II).

The catalytic testing of **15-18** revealed they were all competent precursors for ethylene tetramerization, producing a similar performance as the precursor **14**. However, chromium (II) [PNP] precursors were not as sensitive to the MAO cocatalyst as the previously discussed [SNS] Cr system. More detailed catalytic testing must be carried out before any conclusions can be made however.

3.4 Discussion

The introduction to this chapter discussed the mechanistically interesting chromium-diphosphine based ethylene tetramerization catalyst, which led to the experimental work to furnish a key piece to the mechanistic puzzle. Thus the analysis of these experimental results and their comparison with other well-defined organochromium model systems in the literature leads to mechanistic insights into the unique reactivity of the chromium complexes of small-bite angle diphosphine ligands which may underlie the high 1-octene selectivity. These differences are discussed in the following three categories: 1) ligand effects on monomer/dimer equilibria of well-defined Cr(III) alkyl species, 2) ligand effects on bimetallic reactivity of well-defined chromium (III) alkyl species, and 3) a speculative section on ligand effects on proposed bimetallic intermediates in ethylene trimerization/tetramerization catalysis.

3.4.1 Ligand effects on the monomer/dimer equilibria of well-defined [PNP] Cr intermediates

The products of the reaction of the [PNP] chromium precursor **14** with aluminum alkyl reagents were the bimetallic Cr(III) complex **15** and Cr(II) complex **16**, as well as the monometallic bis-PNP complex **17** formed in excess Me_3Al. Thus the question of the monomer-dimer equilibria exhibited by chromium complexes of the small-bite angle [PNP] ligand is addressed by the observation of stable bimetallic intermediates when only one [PNP] ligand is bound to the complex in both the chromium (III) and chromium (II) oxidation states. However in the presence of excess Me_3Al,

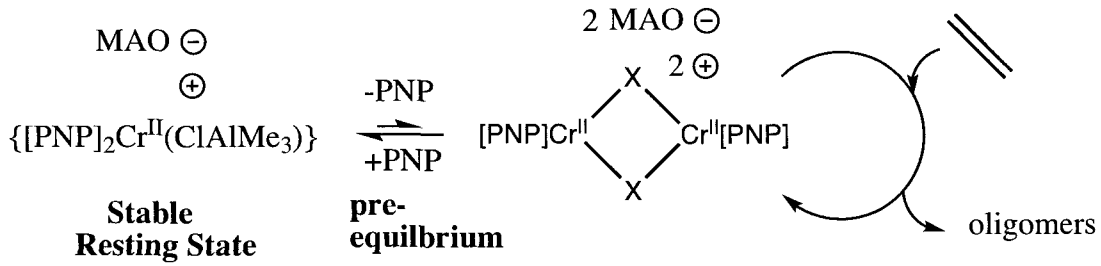

Figure 46: Proposed catalyst generation from a possible cationic bis-[PNP]Cr(II) resting state

the most stable complex is **17**. Thus, it is possible that this highly stable EPR-silent bis-PNP Cr (II) species is the catalyst resting state (which was also established to be EPR silent in the [PNP]$CrCl_3$ + MAO system). The active catalyst can form via [PNP] ligand dissociation from the bis PNP complex to a mono-PNP species possibly structurally related to **16** (Figure 46), which could disproportionate to the catalytically active Cr(I) and Cr(III) oxidation states.

As the catalytically important intermediates in ethylene oligomerization are thought to be based on the Cr(III) and Cr(I) oxidation states, the analysis of the behavior of these species is more likely to afford more direct insight into the 1-octene formation mechanism. However, only the bimetallic form of the Cr(III) [PNP] species, complex **15**, was formed quantitatively under catalytically relevant conditions, suggesting that the bimetallic configuration is the most stable form of the Cr(III) intermediates in solution.

Analysis of a series of similar organochromium (III) methyl intermediates with different ligands suggests that the monomer/dimer equilibrium is strongly affected by the stereoelectronic effect of the various donors on chromium (Figure 47). Thus the more strongly donating Cp and [SNS] ligands result in a greater stability of monomeric species than the bidentate [PNP] ligand, as the Cp and [SNS] Cr(III) systems have been experimentally observed as capable of existing in monomeric form.[102]

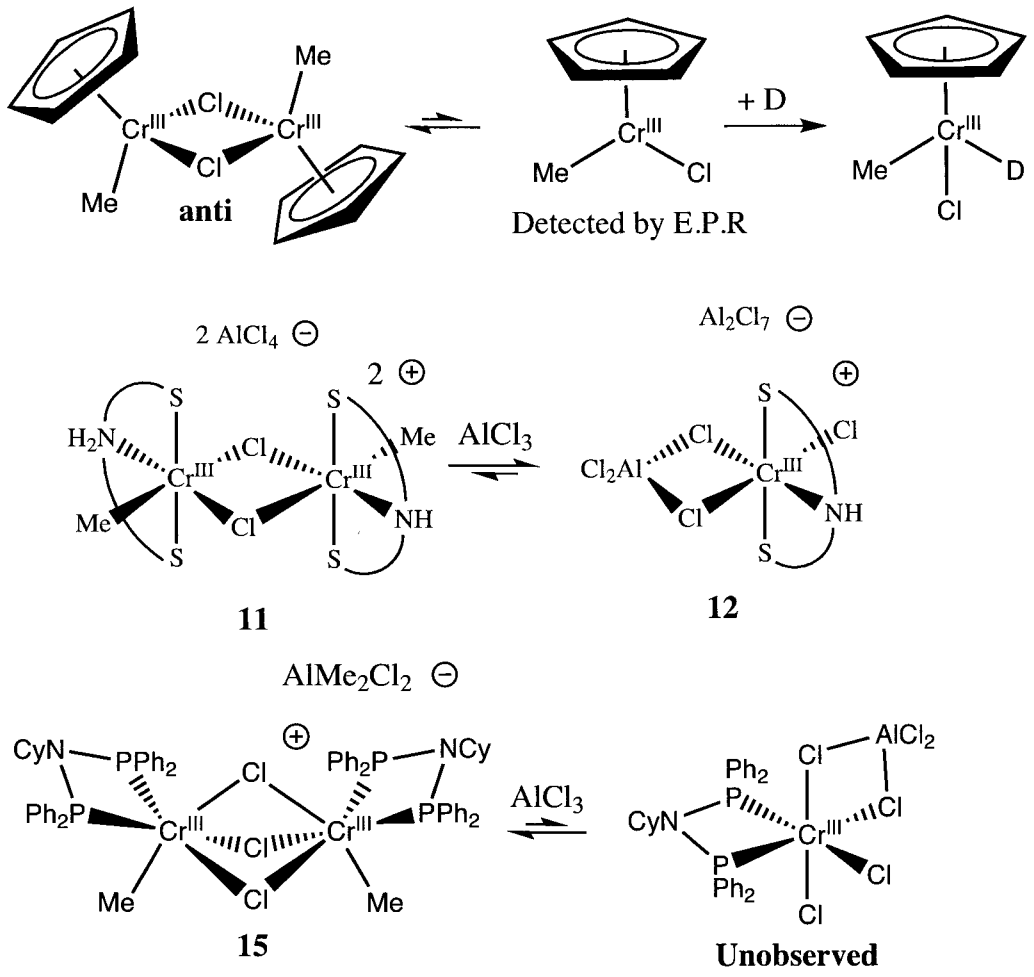

Figure 47: Ligand effects on organochromium (III) monomer/dimer equilibria

3.4.2 Ligand effects on bimetallic reactivity of well-defined chromium (III) alkyl species

The unusual reduction of **15** to **16** was accompanied by the formation of ethane, suggesting that one possibility for the reduction mechanism is a bimetallic reductive elimination of the two Cr-Me groups. However the rationalization of this reaction is difficult, as the two Cr-Me groups in **15** are too far away to reasonably imagine a low barrier for this transformation. On the other hand, additional Me_2AlCl is needed to trigger the transformation, raising the possibility that a molecular reorganization occurs by the coordination of Me_2AlCl to one of the bridging chlorides of **15**. One mechanistic possibility for this proposed transformation is that the coordination of Me_2AlCl generates the intermediate I-1-Syn (Figure 48). This intermediate is proposed to be

relatively thermodynamically stable, but since the two Cr-Methyl groups are now in close proximity, a kinetically rapid pathway exists for their irreversible oxidative coupling to ethane resulting in the quantitative formation of complex **16**. The analogous I-1-anti is predicted to be much less stable than I-1-Syn due mainly to an obvious dicationic charge and resulting greater electrophilicity of the chromium centres.

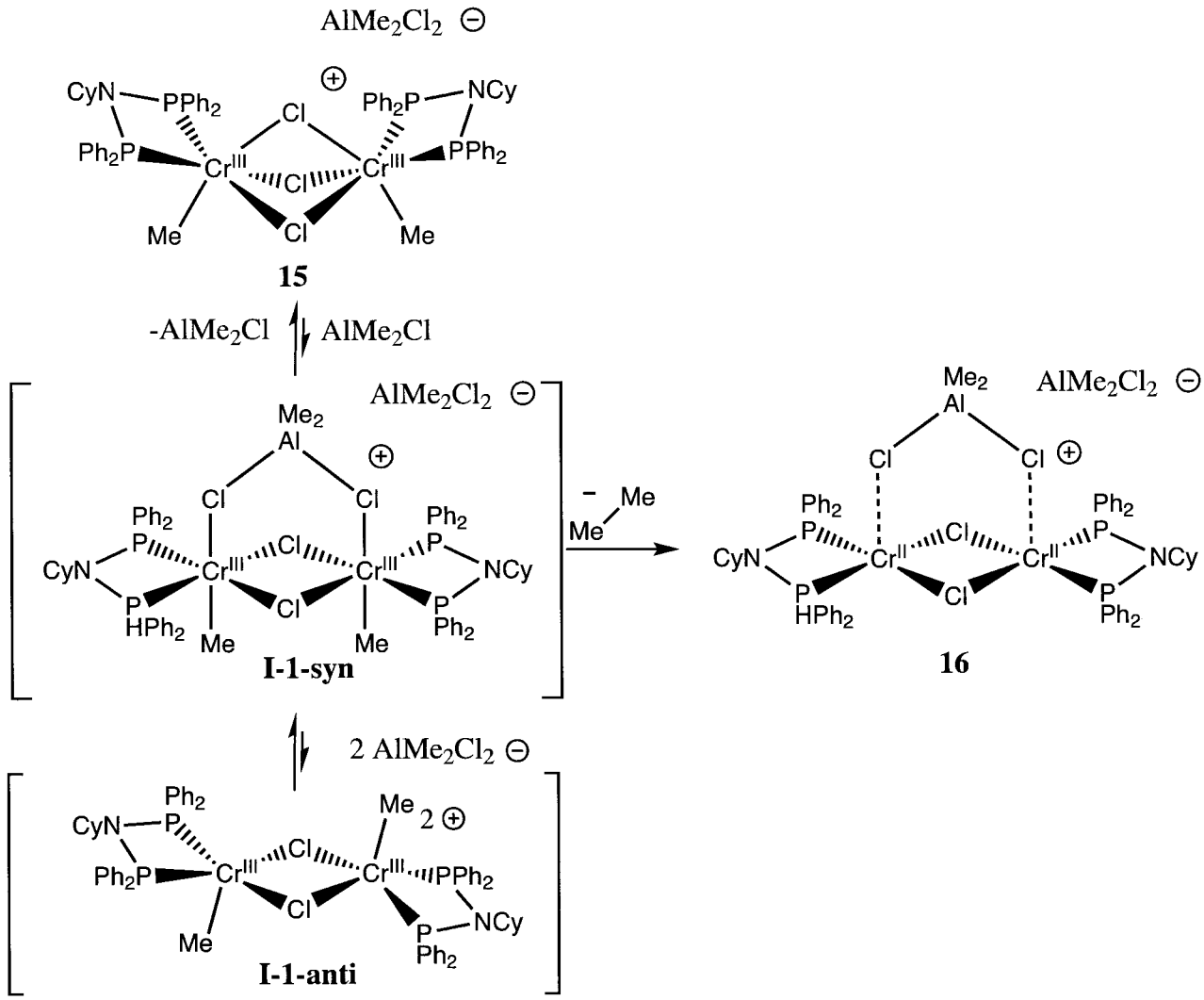

Figure 48: Proposed [PNP] Cr (III) cation bimetallic equilibria

The fact that this reduction pathway does not exist in the analogous [SNS] chromium methyl chloride dimer **2** suggests that the meridional [SNS] ligand coordination somehow blocks the formation of any possible bimetallic intermediates which contain the two Cr-Methyl groups in close proximity (Figure 49), not even in a proposed *syn* isomer. As complex **2** is already dicationic, it is doubtful that Me_3Al is strong enough of a Lewis acid to extract a bridging chloride from **2** to

generate a tri-cationic species.

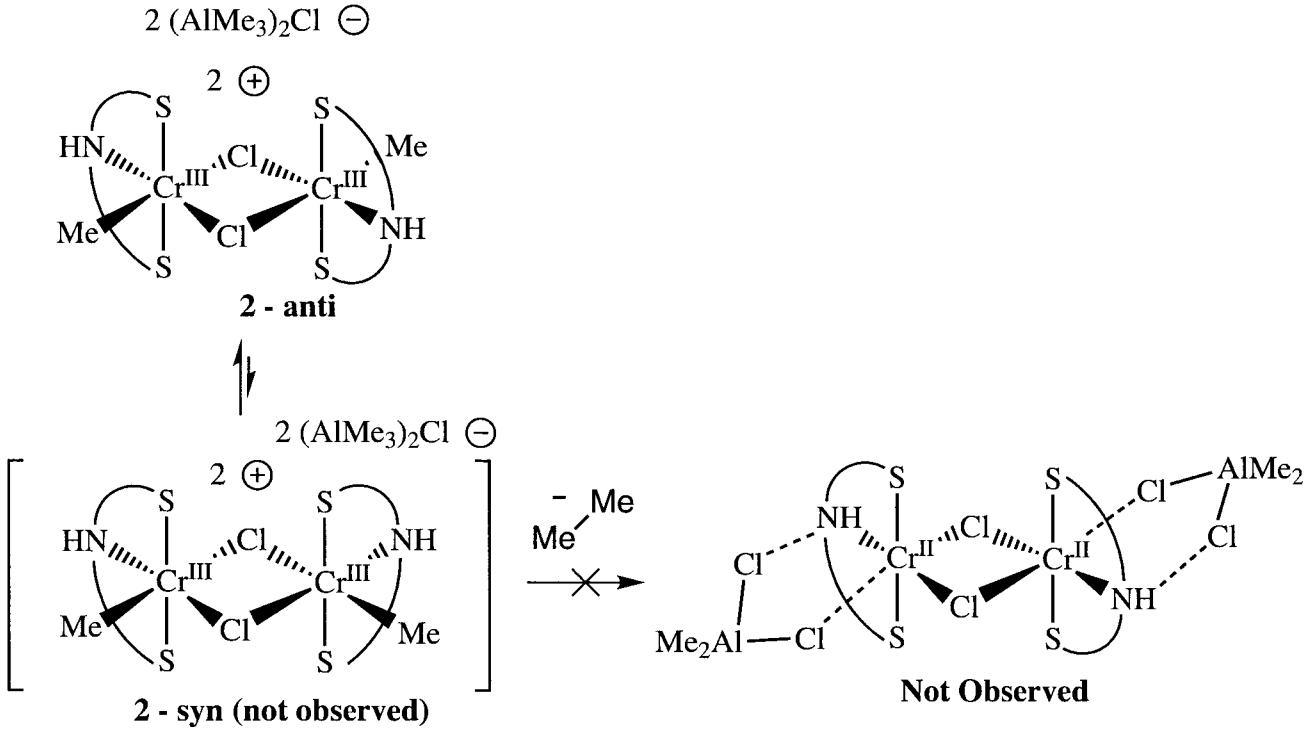

Figure 49: The analysis of possible [SNS] Cr (III) bimetallic equilibria reveals that a *syn* conformation does not offer low-energy C-C coupling pathway

Finally, the most well-established organochromium (III) chemistry in the literature is based on the Cp ligand. The CpCr(III)MeCl dimer complexes were first reported by Richeson and Theopold in 1986.[65] These complexes were isolated as the *anti* isomer, and NMR studies revealed that only the *anti* isomer was observable in solution (Figure 50). However, thermolysis of these complexes led to products from α-hydrogen elimination. This result suggests that they can isomerize at higher temperatures to a spectroscopically unobservable amount of *syn* isomer, but that these proposed *syn* isomers rapidly form the α-hydrogen elimination product. However, this means that the proposed *syn* isomer does not have a kinetically rapid pathway to reductive elimination of ethane. This cannot be due to the instability of the proposed Cr(II) dimeric product, which has been synthesized by a different route and is found to be stable.[65] This suggests that the reductive elimination pathway is just kinetically unavailable even despite being thermodynamically feasible. The high kinetic barrier to reductive elimination is possibly due to the unstable geometry generated by the proposed direct reductive elimination of ethane from the required *syn* isomer, which would

then need further reorganization to the established stable Cr (II) geometry. Recall again that the proposed transformation of **15** to **16** above does not require major geometric reorganization after the oxidative coupling. The preference for α-H elimination in the Cp system is possibly due to the kinetic stability of the Cr (III) oxidation state and the close proximity of the methyl groups in the *syn* isomer which allows α-hydrogen elimination to occur through proton tunneling across the bimetallic system.

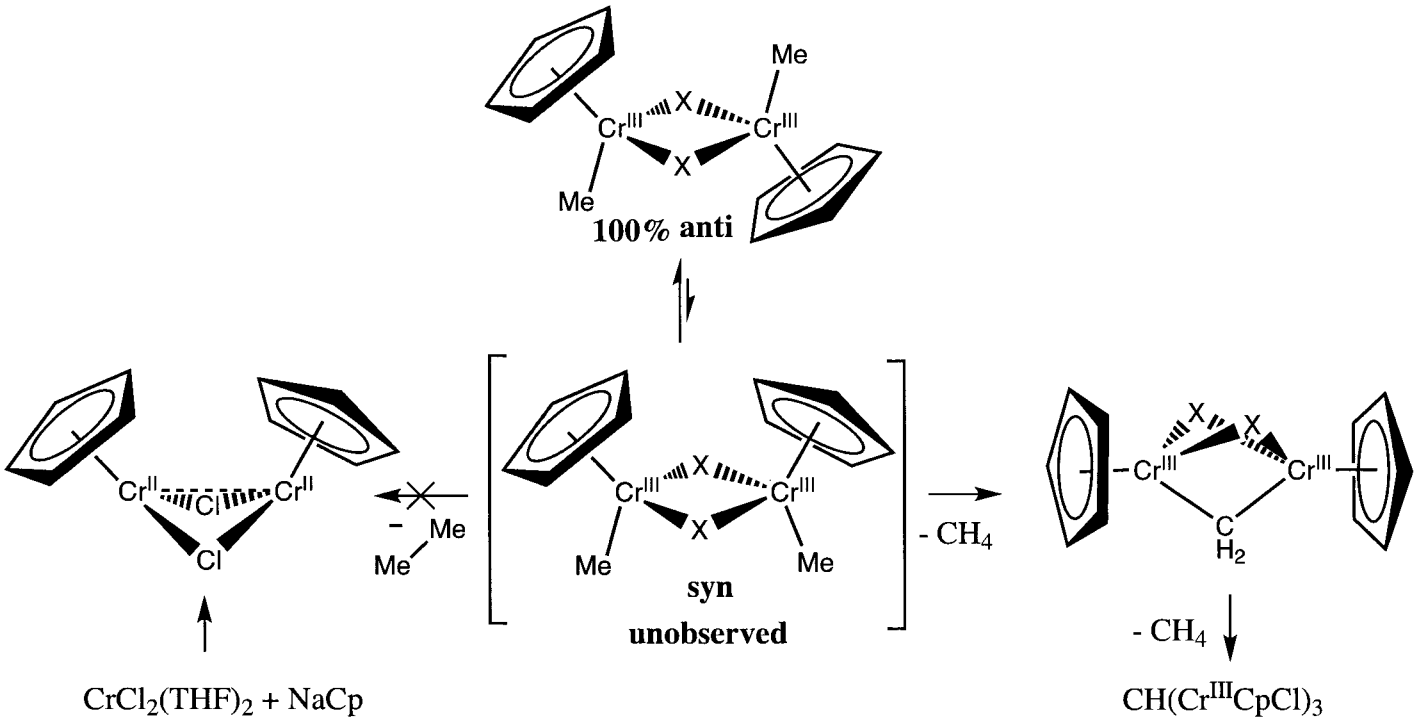

Figure 50: Experimentally established $[CpCr(III)Me(X)]_2$ (X = Me, Cl) geometrically forbidden and allowed bimetallic reactivity

This proposal assumes that the unobserved *syn* isomer actually forms. Evidence for this isomer is found indirectly by the $[CrCp^*(CH_2SiMe_3)Cl]_2$ analog, which was observed to exist as both the *syn* and *anti* isomers in a solution equilibrium which are separated by a significant thermodynamic barrier to isomerization (Figure 51). Again, these species only underwent α-hydrogen elimination under forcing conditions, possibly for the same geometric reason as the methyl derivative.

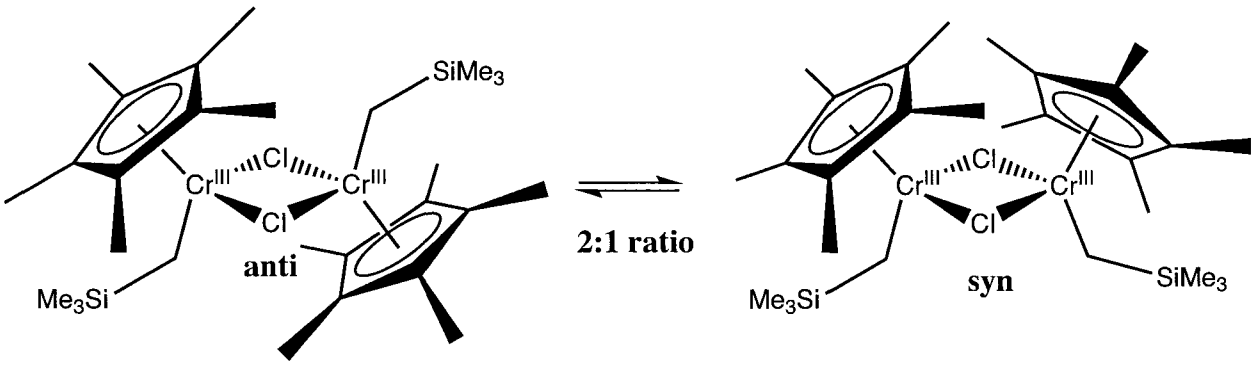

Figure 51: Experimentally established $[CrCp^*(CH_2SiMe_3)Cl]_2$syn/anti equilibria

A structurally stable analogue of **15**, based on a chelating small-bite angle bis-N-heterocyclic-carbene ligand, was recently reported by Theopold to readily reduce to a chromium (II) species in the presence of alkylating agents. However, the chromium (II) product was not characterized structurally.[104][105] Finally, Theopold also reported the synthesis of the well-defined monomeric chromium (III) dialkyl (Figure 52 b) from the bidentate (nacnac)Cr(III)Cl_2 precursor (Figure 53 a),[106] which does not contain β-hydrogens and was also established to undergo reductive elimination to a bimetallic chromium (II) alkyl hydride species (Figure 53 c) upon hydrogenolysis of one of the alkyl groups of (b). The intermediate proposed to give rise to the bimetallic chromium (II) product is a bimetallic Cr(III) bridging hydride (f) which can undergo bimetallic reductive elimination, while steric repulsion makes the possible intermediate (e) unstable. Although no experimental evidence for such intermediate species was provided, this hypothesis seems reasonable based on the reactivity of the well-defined model systems discussed above. However, attempts to form a similar diethyl Cr(III) derivative resulted in direct formation of a bimetallic Cr(II) dihydride (d), which may have formed through the β-H elimination to a mono-hydride mono alkyl and reductive elimination from a bimetallic Cr (III) bridging hydride intermediate. An alternative pathway could be monochromium reductive elimination of tetramethylsilane accompanied by Cr(I), which could then comproportionate with the Cr(III) precursor to form the same product. However reductive elimination from Cr(III) to form Cr(I) can be high in energy when there is no pi-accepting ligands in the vicinity of the transition state to stabilize the electron-rich Cr(I) product. Thus possibly revisiting this reaction with DFT calculations in the future may shed light mechanistically on whether a bimetallic or monometallic reductive elimination is favored, providing insight into

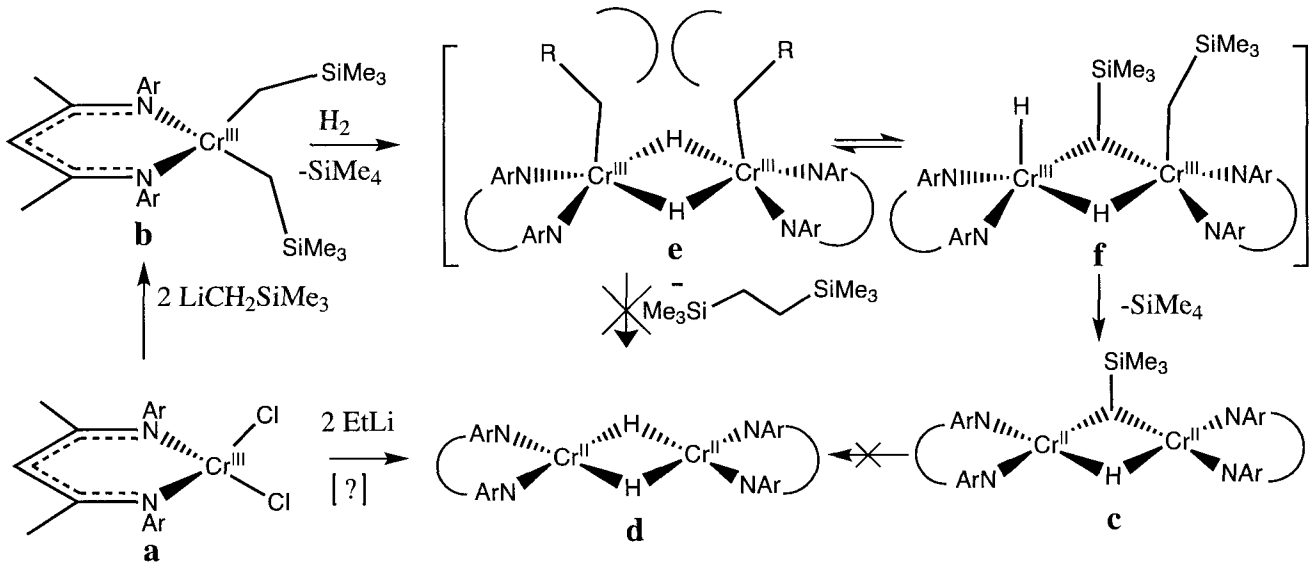

Figure 52: Example of bimetallic reductive elimination by some bidentate-chromium (III) complexes

the factors which favor these individual pathways.

Thus, in summary the analysis of ligand effects in a series of related bimetallic organochromium (III) species led to the conclusion that the steric effect of the ligand controls the relative equilibrium between the *syn* and *anti* isomers (Figure 53). Small bite-angle bidentate ligands such as the [PNP] ligand is proposed to be unique in that it is sterically small enough to allow complex **15** to proceed through a reactive bimetallic *syn* methyl isomer upon reaction with Me_2AlCl (I-1-syn), which then produces the observed oxidative coupling of the methyl groups and formation of **16**. This type of reactivity is also suggested to play a role in the reduction of some well-defined organochromium (III) complexes of bidentate ligands in the literature as discussed above.

There are many reports of bimetallic systems, including many natural metalloenzymes, which readily undergo this proposed bimetallic reductive elimination. These species are also implicated in highly selective catalytic processes such as in hydroformylation, where the diphosphine ligand was established also to control the bimetallic equilibria and, through this, the catalytic performance.[107] Thus, we have discovered direct evidence for an unusual bimetallic reductive C-C coupling pathway in the CrPNP tetramerization system, which does not exist in the tridentate CrSNS trimerization system or even in well-defined Cp chromium analogues. A steric model has been proposed for this transformation (Figure 53), which can partially explain the high barrier

preventing the C-C coupling in the related Cp and [SNS] systems based on the relative stability of the *syn* and *anti* isomers.

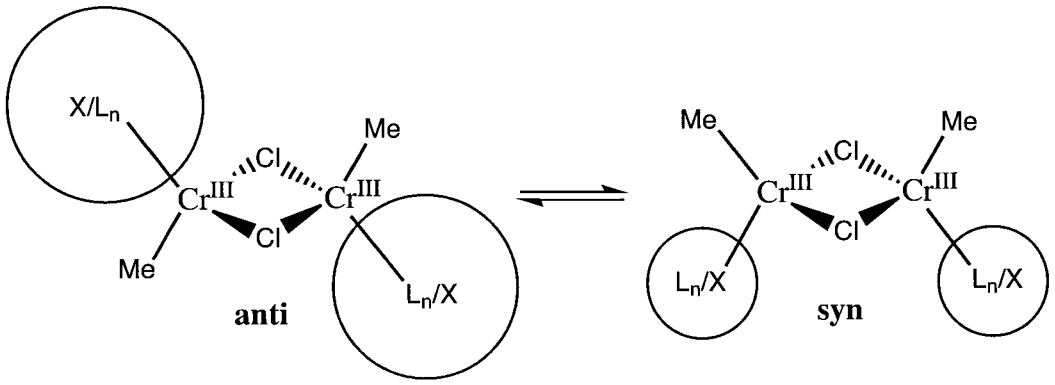

Figure 53: Proposed Steric model for equilibrium binuclear organochromium (III) geometry

3.4.3 Proposed ligand steric effects on bimetallic intermediates in ethylene tetramerization catalysis

The experimental details of the [PNP]-chromium tetramerization catalyst discussed up to this point suggest that the formation of the bimetallic [PNP] Cr(III) alkyl **15** is highly energetically favorable, as well as the bimetallic reductive elimination to the bimetallic chromium (II) complex **16** and ethane gas. Please also recall from the introduction that the established kinetics studies for the [PNP] catalyst strongly suggest that the 1-octene product does not form via a single ethylene insertion into a metallacycloheptane intermediate. Thus the evidence for a stable bimetallic Cr(III) [PNP] intermediate in **15** and its facile C-C coupling raises the possibility that analogous metallacycle [PNP] Cr(III) intermediates in the catalytic system may undergo similar reactivity. One possibility is that these proposed metallacyclopentane intermediates are in dimer/monomer equilibrium in the catalytic solution. Thus in these circumstances, it is possible that a metallacyclononane forming step is actually a oxidative coupling of the two Cr-alkyl groups in bimetallic intermediates as is established in the transformation of **15** to **16** (Figure 54). This proposed mechanism has the benefit over the previously proposed "extended" metallacycle mechanism in that it is consistent with the experimentally-determined kinetics for the 1-C_8 product formation, where the rate of formation of 1-octene depends on the rate limiting step which is the formation of the metallacyclopentane intermediate via the oxidative coupling of two ethylene molecules. The

1-octene product is favored by small bite angle diphosphines which were also previously established to increase the rate of the oxidative coupling of ethylene. Thus, this bimetallic mechanism is consistent with the kinetics, as it bypasses the requirement for the relatively kinetically slow insertion of ethylene into the metallacycle intermediates for ring expansion.

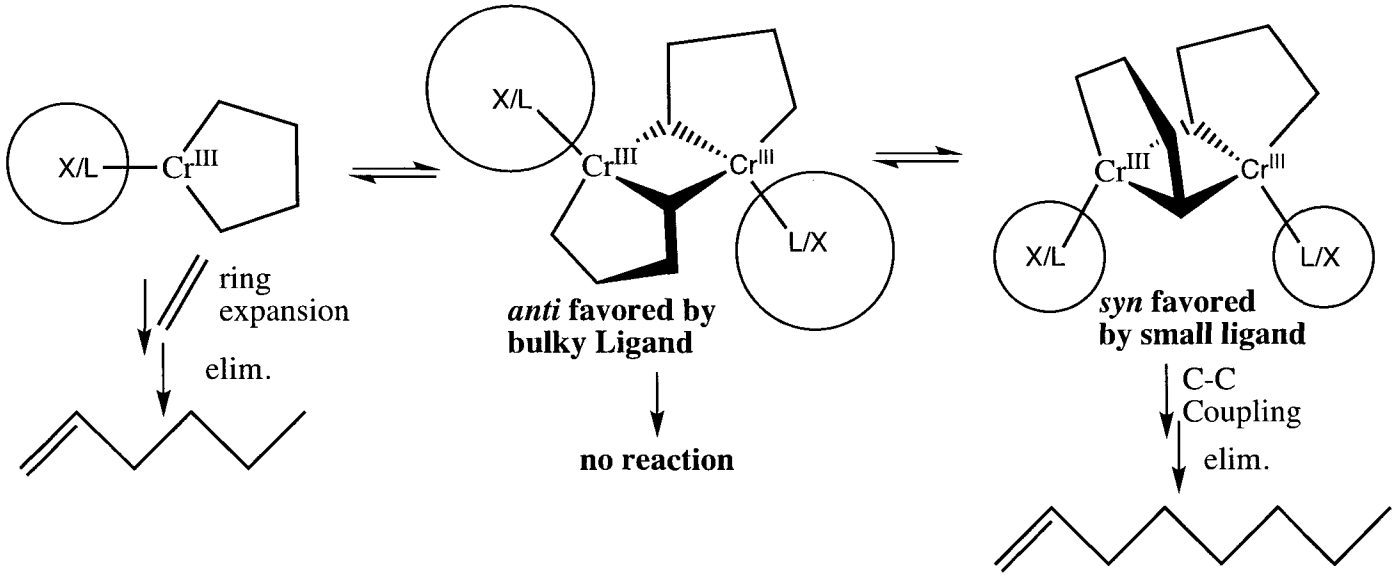

Figure 54: Proposed bimetallic mechanism for formation of 1-octene by the diphosphine chromium tetramerization catalyst.

Assuming this new model is the correct mechanistic option in the production of 1-octene, the effects of established experimental parameters on catalyst selectivity that were discussed in the introduction can be readily rationalized. For example, the diphosphine bite angle effects on 1-octene selectivity are consistent with the increase in the rate of the rate-limiting step which is the oxidative coupling of ethylene to generate a metallacyclopentane intermediate. However, the small-bite angle also favors the formation of bimetallic intermediates due to the decreased steric impact of the phosphine donors as they are brought closer together by the -NR bridge. Additionally, the established cocatalyst influence on the product selectivity for either 1-hexene or 1-octene is also easily rationalized with the possibility that strongly coordinating anions and solvents will prevent the formation of the necessary bimetallic metallacyclopentane intermediates for the formation of 1-octene. Instead, neutral and solvated chromium monomers, which will then insert ethylene into the metallacyclopentane ring to generate 1-C_6 products, will be formed exclusively. The rate of formation of cyclic C_6 byproducts could also derive from the extent of the analogous dimerization

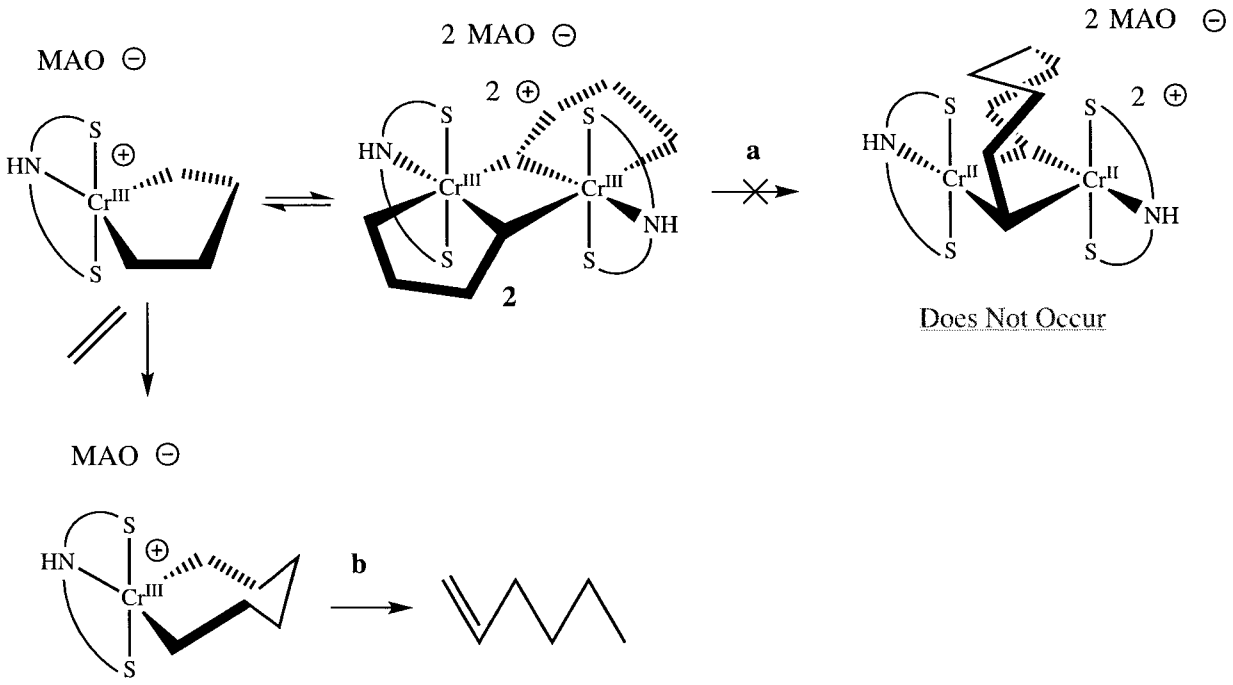

Figure 55: Bimetallic metallacycle dynamics in the [SNS]Cr trimerization catalyst

of metallacycloheptane intermediates as already proposed in the literature (Figure 37), which rationally explains why the 1-C_8 product is always accompanied by the formation of cyclic C_6 products, as they both form under conditions that favor bimetallic catalytic intermediates. Also recall evidence that has been reported in the literature that the cyclic C_6 byproducts also form via bimetallic intermediates. This was supported by the 1:1 stoichiometric ratio of the two products formed and which is consistent with the established spin-forbidden transitions of chromium and the isotopic distribution of the C_6 byproducts. Finally, the effect of increased solvent polarity such as chlorobenzene on decreasing the selectivity for 1-octene can be rationalized as the shift in the dimer/monomer equilibrium to more polar solvated cationic monomers, resulting both in higher activity and loss of selectivity. However oxidation of chromium by the chlorinated solvent cannot be discounted. Most likely the highly polar conditions favor the "extended" metallacycle mechanism, which is predicted to provide a non-selective distribution of oligomer products.

3.5 Conclusion

In conclusion, the treatment of the chromium-diphosphine ethylene tetramerization catalyst precursor **14** with Me_2AlCl resulted in the formation of the bimetallic trivalent monocation **15**. Further treatment of **15** with Me_2AlCl resulted in its reduction to the bimetallic trivalent **16** via a proposed bimetallic reductive C-C coupling. When this reactivity is analyzed in comparison with similar organochromium (III) bimetallic complexes of other ligands, some mechanistically interesting questions emerged relating to bimetallic reactivity in the formation of 1-octene. Based on the difference in reactivity discovered in the diphosphine system and the previously reported kinetics results, a new bimetallic mechanism for ethylene tetramerization is proposed. This new proposed mechanism allows for the rationalization of the selectivity effects of various experimental parameters previously established, although much more investigation is needed to prove or disprove this possibility. However, the rational design of improved dinucleating ligands could follow directly from this working hypothesis to determine if there is some effect on catalytic 1-octene selectivity by controlling the metal-metal interaction.

4 Mechanistic investigation of chromium-pyrrole based ethylene trimerization catalysis

Abstract

This chapter discusses the mechanistic study of the commercial chromium-pyrrole based ethylene trimerization catalyst through the isolation and characterization of stable complexes from the catalytic mixtures. The deprotonation of 2,5-dimethylpyrrole (DMP), 2,3,4,5-tetraphenylpyrrole (TPP), and 2,3,4,5-tetrahydrocarbazole (THC), followed by complexation with $CrCl_2(THF)_2$ allowed the isolation of the monomeric square-planar bis-pyrrolyl complex $\{(DMP)_2Cr^{II}(THF)_2\}$ (**19**), and the dimeric trigonal-bipyramidal mono-indolyl complex, $\{[(THC)Cr^{II}(THF)_2(\mu\text{-}Cl)]_2\}$ (**21**). Treatment of these precursors with a variety of aluminum alkyl reagents led to either insoluble microcrystalline materials or highly soluble oils, which could not be characterized structurally. However, the reaction of **19** with excess $AlCl_3$ resulted in complete ligand extraction and the formation of a Cr(II) bis-tetrachloroaluminate, $\{Cr^{II}[(\mu\text{-}Cl)_2AlCl_2]_2\}$ (**22**).

The highly-active trimerization catalyst mixture of $CrCl_3(THF)_3$, DMP and Et_3Al/Et_2AlCl results in the precipitation of a brown powder, which possibly contains a low-spin Cr(I) species, based on its E.P.R. spectrum. A similar mixture using either the THC or 2,3-dimethylindole (DMI) ligand results in the formation of monomeric square-planar chromium (II) bis-indolyls, $\{[\eta^2\text{-}(THC\text{-}AlEt_2Cl)]_2Cr^{II}\}$ (**23**) and $\{[\eta^2\text{-}(DMI\text{-}AlEt_2Cl)]_2Cr^{II}\}$ (**24**), which are which are single-component ethylene polymerization precatalysts. By contrast, a mixture of the non-chlorinated Cr(octanoate)$_3$, Et_3Al/Et_2AlCl, and either THC or DMI produced the monomeric Cr(I) bis-indolyl sandwich complexes, $\{[(\eta^6\text{-}THC\text{-}AlEt_2)_2(\mu\text{-}Cl)]Cr^{I}\}$ (**25**) and $\{[(\eta^6\text{-}DMI\text{-}AlEt_2)_2(\mu\text{-}Cl)]Cr^{I}\}$ (**26**). **25**/**26** can also be synthesized by one-electron reduction of **23**/**24**. Complexes **25** and **26** are the first examples of single-component ethylene trimerization catalyst precursors. The reaction of the brown microcrystalline material formed from $CrCl_3(THF)_3$, pyrrole and Et_3Al/Et_2AlCl with the alkyne $C_2(SiMe_3)_2$ resulted in the formation of the dimeric chromium (I) alkyne complexes, $\{[(\eta^5\text{-}C_4H_4N\text{-}AlEt_3)Cr(\mu\text{-}C_2(SiMe_3)_2]_2\}$ (**27**) or $\{[(\eta^5\text{-}C_4H_4N\text{-}AlEt_2Cl)Cr(\mu\text{-}C_2(SiMe_3)_2]_2\}$ (**28**), depending on the chloride concentration in the mixture. Chromium alkyne complexes **27** and **28** were also found to be single-

component oligomerization catalysts, confirming that stable Cr(I)-olefin complexes can carry out ethylene trimerization.

4.1 Introduction

The previous two chapters described the reactions of [SNS] and [PNP] chromium (II) and (III) precursors with aluminum cocatalysts, providing some key pieces to the chromium-catalyzed ethylene trimerization/tetramerization mechanistic puzzle. However, these two experimental studies afforded no structural information about the actual catalytic resting states and intermediates, which only form in the presence of a large excess of the poorly-defined MAO activator. Thus the studies discussed above are limited in their significance to the actual catalytic system, as the effect of only a small excess of aluminum alkyls on the organochromium chemistry was possible to evaluate. However, the commercial chromium-pyrrole trimerization system is an ideal fit for this methodology, as only a small excess of simple alkylaluminum reagents are needed for catalyst activation. The introduction to this chapter will first provide a background to the chromium-pyrrole trimerization catalyst, focusing on mechanistically important information. In addition, a brief background is then given of established organochromium (I) chemistry, which will aid in the mechanistic discussion of the experimental results.

4.1.1 Background of chromium-pyrrole based ethylene trimerization catalysis

The introduction to this thesis (Chapter 1) briefly discussed the chromium-pyrrole based ethylene trimerization catalysis which was discovered in 1991 by Reagan.[28] This catalyst is currently operating in a large-scale commercial plant (>200,000 metric tons/year) due to many desirable features, which include: inexpensive and convenient catalyst preparation, very high activity (1 ton of 1-hexene per gram of chromium) and selectivity for 1-hexene (> 90%), and only a low quantity (< 1 %) of low molecular weight (Mw < 10,000) polymer byproduct. The initial exploration of chromium pyrrolide complexes was encouraged by the close structural similarity of pyrrole with the popular Cp ligand, which is extensively used in industrial olefin polymerization catalysis. The first well-defined chromium pyrrolide complexes were introduced in 1990, and consisted of σ-bound

neutral and anionic chromium (II) and (III) pyrrolide species (Figure 56).[108]

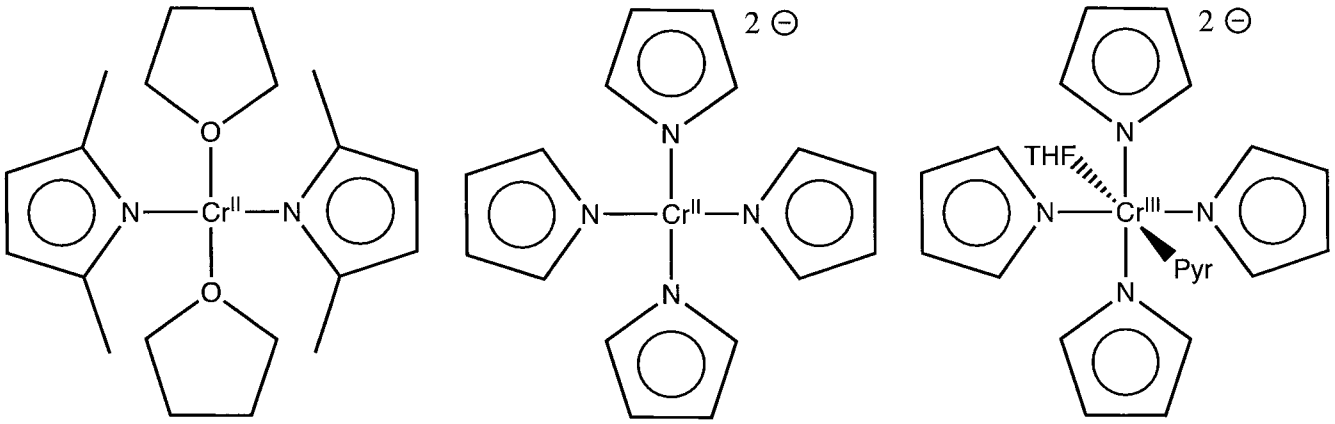

Figure 56: Well-defined chromium pyrrolide-based trimerization catalyst precursors

When these closely related species are treated with aluminum alkyl activators,[28] highly active catalysts for ethylene trimerization are formed. Additionally, a few years later it was also reported that active trimerization catalysts could be conveniently prepared by simply combining the highly soluble Cr^{III}(octanoate)$_3$ precursor with pyrrole and a mixture of Et_3Al and Et_2AlCl in an aliphatic hydrocarbon solvent. While the actual nature of the trimerization catalyst formed was not explored mechanistically, significant progress in the catalyst optimization was made by purely empirical methods for 20 years. The analysis of these reports furnishes some important mechanistic insights into the effects of various experimental parameters on catalytic selectivity and activity, and which can be separated into the following categories: ligand effects, cocatalyst effects, and solvent effects.

The 2,5-dimethylpyrrole [DMP] ligand selected for the commercial plant arrived after much screening. However, much of this early work in pyrrole ligand optimization was not disclosed in the open literature. Thus, the exact effects of the pyrrole ligand substituents on the catalytic performance is still unknown.[68] While the simple pyrrole ligand is inexpensive, it does not provide very high activity in trimerization, and is very sensitive to acid and light. However, the DMP ligand is relatively inexpensive, but leads to excellent activity and can be stored conveniently for prolonged periods without decomposition. By contrast, the closely related 2,3,4,5-tetramethylpyrrole is difficult and costly to prepare, as well as being air sensitive.

The cocatalyst effects on performance have been reported extensively both in the patent and academic literature, allowing for the analysis of cocatalyst effects for mechanistically important

trends.[109, 110, 61] Early on, researchers discovered that the presence of a halogen donor, such as diethyl aluminium chloride (DEAC) or 1-bromobutane during the catalyst preparation led to marked improvements in both the catalyst activity and selectivity towards formation of 1-hexene. For example, catalyst activities exceeding 156,666 g/g Cr per hour could be achieved at a reaction temperature of 115 °C and a reaction pressure of 100 bar. This catalyst was prepared by combining Cr(III)(octanoate)$_3$, 2,5-dimethylpyrrole, Et_2AlCl and Et_3Al in molar ratios of 1:3.3:7.8:10.8 at room temperature using a nitrogen purge to stir the reagents. The trimerization reaction produced 99.85% liquid oligomers containing 93.83% hexenes of which 99.2% was 1-hexene (93% overall 1-hexene). The main side products were a mixture of linear and branched dodecenes (5.38%) formed by the re-incorporation of 1-hexene into another trimer. Catalysts prepared with additional weakly coordinating Lewis acids such as $B(C_6F_5)_3$ exhibited significantly higher activities. In general, there seemed to be a trend where, as the number of chlorine atoms in the organochloro component increased, the 1-hexene selectivity and ethylene conversion rate also increased. Currently the most active catalyst mixture is chromium (III) 2-ethylhexanoate, 2,5-dimethylpyrrole, hexachloroethane and triethylaluminium in molar ratios of 1:6:4:40, and by carefully controlling the molar ratio of 1-hexene to ethylene inside the reactor (at less than 0.5:1), it is possible to achieve catalyst activities of up to 3,780,000 g/g Cr per hour at 105 °C and 50 bar. The reaction mixture contains 99.96% liquid oligomers including 95.9% hexenes of which 99.5% is 1-hexene (or 95.4% overall 1-hexene). Thus, it is obvious that fine-tuning the exact balance of the components will result in activities which vary by 2 or 3 orders of magnitude. Therefore, the effect of these parameters on the underlying coordination chemistry of chromium is of high mechanistic interest.

The third experimental parameter which was found to strongly affect catalytic performance was the solvent. While catalyst preparation has been reported in toluene, the presence of an excess quantity of an aromatic hydrocarbon solvent during catalysis had a detrimental effect on the catalyst activity. However, this effect isn't due to the increased polarity of toluene relative to the aliphatic hydrocarbons, as much more polar imidazolium ionic liquids containing based on {1-ethyl-2,3,-dimethylimidazolium} {Et_3AlCl} as the solvent resulted in highly active ethylene trimerisation reactions. Fore example, at 115°C and 50 bar the ionic liquid solvent yielded 65.3%

1-C_6 in catalyst activities exceeding 25,000 g/g Cr per hour. Ionic liquids offer the process benefits of high catalyst solubility and easy separation the 1-hexene product from the catalyst solution which facilitates the recycling of the catalyst.

While all these experimental parameters are established to play a strong role in catalyst activity and selectivity, their effect on the underlying organochromium chemistry is a complete mystery, as no catalytic resting states or intermediates have been isolated for the chromium pyrrole system. Thus the isolation of such catalytic intermediates is highly valuable as it will provide a key missing piece to the mechanistic puzzle. Finally, a brief background of organochromium (I) chemistry is presented as it will aid in the discussion of the experimental work described in this chapter.

4.1.2 Background of organochromium (I) chemistry

While chromium (I) intermediates have been postulated to be important in trimerization catalysis, no direct experimental evidence exists for organochromium (I)-based catalytic intermediates. However, the analysis of established organochromium (I) chemistry affords important mechanistic insights into the properties of the proposed Cr (I) catalytic intermediates. The strong tendency of Cr(I) to form stable π complexes with arenes is well documented (Figure 57). Arguably, the first reported organometallic sandwich complex was the bis-arene Cr(I) which was first reported by Hein in 1919, however structural characterization of this species would have to wait almost half a century until the development of X-ray crystallography.[100]

Arene substitution rates for chromium arene complexes were established to be greatly accelerated by arene ligands which have haptotropic lability, such as naphthalene, which is postulated to enhance the rate of slippage to η^4 bound intermediates containing a vacant site on the chromium centre.[111] In addition to the use of X-ray crystallography, EPRwas in some cases found to be diagnostic of low-spin Cr(I) arene complexes. [2, 103, 112]

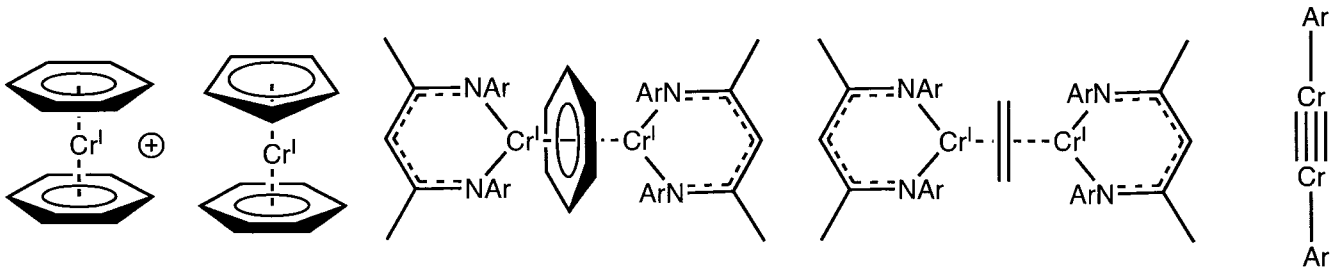

Figure 57: Summary of established stable organochromium (I) complexes.

Very recently, Cr (I) chemistry has achieved a high-profile status thanks to exciting reports on a stable Cr (I) ethylene complex by Theopold,[89, 91] not to mention the report of a multiply-bonded Cr (I)-dimer which was also found to form stable arene complexes when exposed to aromatic solvents.[113] As pyrrole is an aromatic ligand, it is possible that π-pyrrolide donation would stabilize organochromium (I).

In summary, the introduction has raised some mechanistically interesting questions related to the pyrrole-chromium trimerization catalyst. These questions lead directly to the experimental work described below.

4.2 Experimental Procedures

All reactions were carried out under the atmosphere of dry nitrogen. Solvents were dried, using an aluminum oxide solvent-purification system. Samples for magnetic susceptibility analysis were preweighed inside a drybox equipped with an analytical balance, and measured on a Johnson–Matthey magnetic susceptibility balance. Deutero solvents were predried over activated 4 Å molecular sieves and were refluxed over the appropriate drying agent, distilled, and stored under dinitrogen. NMR samples were prepared under dinitrogen in 5 mm Wilmad 507-PP tubes flame sealed under dinitrogen using standard Schlenk apparatus. ^{1}H and $^{13}C\{^{1}H\}$ NMR spectra were recorded on a Bruker Avance 300 MHz multinuclear NMR instrument. ^{1}H and ^{13}C assignments were confirmed when necessary with the use of DEPT-135, DEPT-90, and two-dimensional ^{1}H-^{1}H and ^{13}C-^{1}H NMR experiments. ^{1}H and ^{13}C spectra were referenced internally to residual protio solvent (^{1}H) or solvent (^{13}C) resonances and are reported relative to tetramethylsilane (δ) 0 ppm). Chemical shifts are quoted in δ (ppm), and coupling constants in hertz. $CrCl_2(THF)_2$,

$CrCl_3(THF)_3$, and $\{Cr^I(\eta^5\text{-}C_6H_6)_2\}I$ (via the Fischer-Hafner procedure[64]) were prepared according to standard procedures. Cr(2-ethylhexanoate)$_3$ was used as received (Strem). Pyrrole and 2,5-dimethylpyrrole (Aldrich) were purified by distillation before use. 2,3-Dimethylindole and 2,3,4,5-tetrahydrocarbazole (Aldrich) were recrystallized before use. The alkylaluminum reagents Et_2AlCl (Aldrich), Et_3Al (Aldrich), and MAO (Chemtura) were used as received. Mass spectra were recorded on a Micromass Quattro-LC Electrospray- Triple Quadrupole Mass Spectrometer. Experiments were carried out in the negative mode.

4.2.1 $\{(DMP)_2Cr^{II}(THF)_2\}$ (19)

DMP (2 g, 20 mmol) and NaH (480 mg, 20 mmol) were suspended in 30 mL of THF and refluxed for 3 hours until gas evolution ceased, yielding a clear colorless solution. To this solution was added $CrCl_2(THF)_2$ (2.7 g, 10 mmol) and stirred for 1 hour to give a purple solution and white precipitate, which was filtered off. The filtrate was layered with hexanes for one week to yield purple crystals of **24** (2.4 g, 61 %). E.A. was previously reported.[108] μ_{eff}= 4.90 μ_B.

4.2.2 $\{[(THC)Cr^{II}(THF)_2(\mu\text{-}Cl)]_2\}$ (21)

THC (169 mg, 1mmol) and KH (40 mg, 1mmol) were dissolved in 15 mL of THF and stirred for 1 hour until gas evolution ceased, yielding a clear colorless solution. To this solution was added $CrCl_2(THF)_2$ (267 mg, 1mmol) and stirred for 1 h to give a blue solution and white precipitate, which was filtered off. The filtrate was layered with hexanes for one week to yield blue crystals of **21** (323 mg, 81 %). μ_{eff}= 4.74 μ_B. Anal. Calcd (found) for C20H28ClCrNO2: C, 60.08 (59.84); H, 7.01 (6.89); N, 3.50 (3.46).

4.2.3 $\{Cr^{II}[(\mu\text{-}Cl)_2AlCl_2]_2\}$ (22)

A mixture of **21** (400 mg, 1 mmol) and $AlCl_3$ (532 mg, 4 mmol) in dichloromethane (10 mL) was stirred for 1 h resulting in a clear, colorless solution, which was filtered and stored at -35^o C for one week to yield colorless blocks of **22** (241 mg, 62 %). Anal. Calcd (found) for Al2Cl8Cr: C, 0 (0); H, 0 (0); N, 0 (0). μ_{eff} = 4.92 μ_B.

4.2.4 Reaction of $\{Cr^{I}(\eta^5\text{-}C_6H_6)_2\}I$ with Li-DMP

^{n}BuLi (0.40 mL of a 2.5 M solution, 1.0 mmol) was added dropwise to a stirring solution of 2,5-dimethylpyrrole (95 mg, 1 mmol) in THF at -35C, resulting in a clear solution. To this solution was added $\{Cr^{I}(\eta^6\text{-}C_6H_6)_2\}$ {I}, resulting in a gradual color change from yellow to black within minutes. The solution was taken to dryness to desolvate the lithium iodide salt byproduct. The residue was redissolved in toluene (10 mL), then the solution was filtered and layered with hexanes and stored at -35°C, resulting in black crystals of $Cr^{0}(\eta^6\text{-}C_6H_6)_2$ (129 mg, 62 %).

4.2.5 In-situ Cr-DMP trimerization catalyst

A mixture of $Cr^{III}Cl_3(THF)_3$, DMP and Et_3Al then finally Et_2AlCl in chlorobenzene (10 mL) resulted in a brown solution, which was filtered and layered with hexanes (10 mL) for 3 days resulting in the formation of a homogeneous brown microcrystalline solid. E.P.R. (powder, r.t. in text).

4.2.6 $\{[\eta^2\text{-}(THC\text{-}AlEt_2Cl)]_2Cr^{II}\}$ (23)

Method A: $CrCl_3(THF)_3$ (374 mg, 1 mmol) was added to a colorless solution of THC (340 mg, 2 mmol) and Et_3Al (684 mg, 6 mmol) in pentane (10 mL), resulting in a deep green solution. Centrifugation and storage for 1 week at -35°C resulted in the growth of blue crystals of **23** (270 mg, 45 %) from a dark red supernatant. μ_{eff}= 4.9 μ_B. Anal. Calcd (found) for C32H44Al2Cl2CrN2 : C 60.60 (60.00), H 7.00 (6.98), N 4.42 (4.38).

Method B: $CrCl_2(THF)_2$ (267 mg, 1 mmol) was added to a colorless solution of THC (340 mg, 2 mmol) and Et_3Al (684 mg, 6 mmol) in pentane (10 mL), resulting in a blue solution. Centrifugation and storage for 1 week at -35°C resulted in the growth of blue crystals of **23** (530 mg, 84 %).

4.2.7 $\{[\eta^2\text{-}(DMI\text{-}AlEt_2Cl)]_2Cr^{II}\}$ (24)

Method A: $CrCl_3(THF)_3$ (374 mg, 1 mmol) was added to a colorless solution of 2,3-dimethylindole (290 mg, 2 mmol) and Et_3Al (684 mg, 6mmol) in hexanes (10 mL), resulting in an green solution. Centrifugation and freezing resulted in the growth of aqua-marine crystals of **24** (238 mg, 41 %)

from a dark red supernatant. μ_{eff}= 4.9 μ_B. ESI-MS – molecular ion (Toluene/NEt3 0.2%, rel. int.) m/z = 580.0 ([M]-, 100). Anal. Calcd (found) for C28H40Al2Cl2CrN2: C, 57.83 (57.48); H, 6.88 (6.78); N, 4.82 (4.73).

Method B: $CrCl_2(THF)_2$ (267 mg, 1 mmol) was added a colorless solution of 2,3-dimethylindole (290 mg, 2 mmol) and Et_3Al (684 mg, 6 mmol) in hexanes (10 mL), resulting in a aquamarine solution. The solution was stirred for a period of 10 minutes, centrifuged, and stored at -35 °C for 3 days to yield 487 mg (85 %) of **24** as aqua-marine crystals.

4.2.8 {[(η^6-THC-$AlEt_2$)$_2$(μ-Cl)]Cr^I} (25)

Method A: To a solution of Et_3Al (570 mg, 6 mmol) and 2,3,4,5-tetrahydrocarbazole (340 mg, 2 mmol) in 10 mL of toluene was added a green solution of Cr(2-ethylhexanoate)$_3$ (481 mg, 1 mmol) in 10 mL of toluene and stirred for 10 minutes resulting in a brown solution. This was followed by the addition of Et_2AlCl (170 mg, 1 mmol) and filtration. Then layering with hexanes for one week at -35 °C results in the growth of brown crystals of **25** (97 mg, 15 %) accompanied by an oily material.

Method B: To a blue solution of **23** (632 mg, 1mmol) in toluene was added finely divided potassium (40 mg, 1mmol). The mixture was stirred for 24 h gradually turning to a dark brown solution over 2 h. The solution was then filtered, layered with hexanes and stored at -35°C for one week to yield highly pure brown crystals of **25** (540 mg, 90 %). Anal. Calcd (found) for C32H44Al2ClCrN2: C 64.26 (64.23), H 7.42 (7.41), N 4.68 (4.67). μ_{eff}= 1.87 μ_B.

4.2.9 {[(η^6-DMI-$AlEt_2$)$_2$(μ-Cl)]Cr^I} (26)

Method A: To a solution of Et_3Al (570 mg, 6 mmol) and 2,3-dimethylindole (290 mg, 2 mmol) in 5 mL of chlorobenzene was added to a green solution of Cr(2-ethylhexanoate)$_3$ (481 mg, 1 mmol) in 10 mL of chlorobenzene and stirred for 10 minutes, resulting in a brown solution. This was followed by the addition of Et_2AlCl (170 mg, 1 mmol) and filtration and then layering with hexanes for one week at -35°C, resulting in brown crystals of **26** (130 mg, 26 %) accompanied by an oily material.

Method B: To a blue solution of **24** (580 mg, 1 mmol) in toluene (20 mL) was added finely

divided potassium and stirred for 4 h., gradually turning to a dark brown solution. The solution was filtered, layered with hexanes (10 mL) and stored at -35°C for one week to yield pure brown crystals of **26** (530 mg, 99%) co-crystallized with toluene. μ_{eff}= 1.90 μ_B. Anal. Calcd (found) for C31.50H44Al2ClCrN2: C, 67.73 (67.38); H, 7.37 (7.31); N, 2.28 (2.14).

4.2.10 {[η^5-(C_4H_4N-$AlEt_3$)Cr(μ-$C_2(SiMe_3)_2$]$_2$} (27)

A purple suspension of $CrCl_3(THF)_3$ (374 mg, 1 mmol) and pyrrole (134 mg, 2 mmol) in 5 mL hexanes was combined with a colorless solution of Et_3Al (798 mg, 7 mmol) and $C_2(SiMe_3)_2$ (170 mg, 1 mmol) in 5 mL of hexanes, resulting in a dark green solution. The solution was stirred for a period of 1 h, centrifuged, and stored at -35°C for 3 days to yield 140 mg (35 %) of dark green crystals of **27**. A second crop of crystals could be isolated by concentrating the solution to half the volume and storing for one week at -35°C , giving an additional yield of 80 mg (10 %, 45% overall). ^{1}H NMR (C_7D_8): δ = 3.34 (m, 4H; Pyr), 1.43 (br m, 12H; $SiCH_3$), 1.20 (br m, 12H; $SiCH_3$), 1.01 (m, 4H; Pyr), 0.86 (br m, 12H; $SiCH_3$), 0.12 (br s, $AlCH_2CH_3$), -0.12 (br s, 18H; $AlCH_2CH_3$). $^{13}C\{^1H\}$ NMR: 70.8 (s, Pyr), 32.1 (s, $SiMe_3$), 25.0 (s, Pyr), 23.1 (s, $AlCH_2CH_3$), 14.4 (s, $SiMe_3$), 10.4 (s, $SiMe_3$), 9.5 (s, $C_2(SiMe_3)_2$), -5.8 ($AlCH_2CH_3$). ESI-MS (Toluene/NEt3 0.2%, rel. int.) m/z = 803.1 ([M-H]-, 75), 732.1 ([M-SiMe3]-, 100). Anal. Calcd (found) for C36H74Al2Cr2N2Si4: C 53.69 (53.67), H 9.26 (9.21), N 3.48 (3.47).

4.2.11 {[η^5-(C_4H_4N-$AlEt_2Cl$)Cr(μ-$C_2(SiMe_3)_2$]$_2$} (28)

A green solution of Cr(2-Ethylhexanoate)$_3$ (500 mg, 1 mmol) and pyrrole (134 mg, 2 mmol) in 5 mL chlorobenzene was combined with a colorless solution of Et_3Al (798 mg, 7 mmol) and $C_2(SiMe_3)_2$ (170 mg, 1 mmol) in 5 mL of chlorobenzene, resulting in a dark brown solution. The solution was stirred for a period of 1 h, followed by the addition of $AlCl_3$ (1.04 g, 8 mmol) and stirred for an additional hour, then centrifuged, and stored at -35 °C for one week to yield 90 mg (17 %) of reddish brown crystals of **28**, which were highly insoluble. Anal. Calcd (found) for C42H70Al2Cl4Cr2N2Si4: C, 49.65 (49.33); H, 6.90 (6.85); N, 2.76 (2.71).

4.2.12 X-ray Characterization

Table 20: Crystal data and structure analysis results for chromium pyrrole complexes (**19-28**)

Complex #	**19**	**21**	**22**	**23**	**24**
formula	C20H32	C20H24Cl	Al2Cl8Cr	C32H44Al2	C28H40Al2
	CrN2O2	CrNO2		Cl2CrN2	Cl2CrN2
Mw	384.48	397.85	389.56	633.55	581.48
space group	P-1	P-1	Pnma	P2(1)/n	P-1
a (Å)	8.5086(13)	7.971(3)	12.940(2)	10.053(5)	8.224(3)
b (Å)	11.5596(17)	11.558(4)	6.0378(10)	9.809(5)	9.663(3)
c (Å)	11.6634(18)	11.626(4)	7.5228(13)	16.313(8)	10.182(3)
α	89.580(2)	76.996(5)	90	90	83.337(5)
β	71.824(2)	81.008(5)	90	92.743(9)	71.021(4)
γ	76.395(2)	73.632(5)	90	90	80.184(5)
V (Å^3)	3783(6)	996.4(6)	587.74(17)	1606.9(13)	752.3(4)
Z	2	2	2	2	1
radiation	0.71073	0.71073	0.71073	0.71073	0.71073
T (K)	203(2)	203(2)	203(2)	203(2)	203(2)
D_{calcd} (g cm^{-3})	1.208	1.326	2.201	1.309	1.284
μ_{calcd} (mm^{-1})	0.555	0.720	2.880	0.601	0.635
F000	412	416	372	668	306
R, Rw_2	0.0438, 1214	0.0781, 0.1852	0.0295, 0.0784	0.0376, 0.0914	0.0419, 0.0976
GoF	1.032	1.024	1.025	1.068	1.043
Complex #	**25**	**26**	**27**	**28**	
formula	C32H44Cl	C31.50H44	C36H74Al2	C42H70Al2	
	Al2CrN2	Al2ClCrN2	Cr2N2Si4	Cl4Cr2N2Si4	
Mw	598.10	592.10	805.29	1015.12	
space group	P2(1)	P2(1)/c	P 21/n	P-1	
a (Å)	10.543(7)	13.899(7)	11.4912(16)	10.0293(18)	
b (Å)	28.920(19)	10.898(6)	12.3763(18)	11.741(2)	
c (Å)	10.762(7)	21.681(11)	16.618(2)	12.250(2)	
α	90	90	90	80.905(2)	
β	110.679(9)	107.459(6)	99.366(2)	72.512(2)	
γ	90	90	90	74.475(2)	
V (Å^3)	3070(3)	3133(3)	2331.9(5)	1320.9(4)	
Z	4	4	2	1	
radiation	0.71073	0.71073	0.71073	0.71073	
T (K)	203(2)	203(2)	203(2)	203(2)	
D_{calcd} (g cm^{-3})	1.294	1.255	1.147	1.276	
μ_{calcd} (mm^{-1})	0.541	0.529	0.631	0.767	
F000	1268	1256	868.0	534	
R, Rw_{2a}	0.0552, 0.1262	0.0461, 0.1296	0.0613, 0.1609	0.0595, 0.1672	
GoF	0.997	1.084	1.045	1.064	

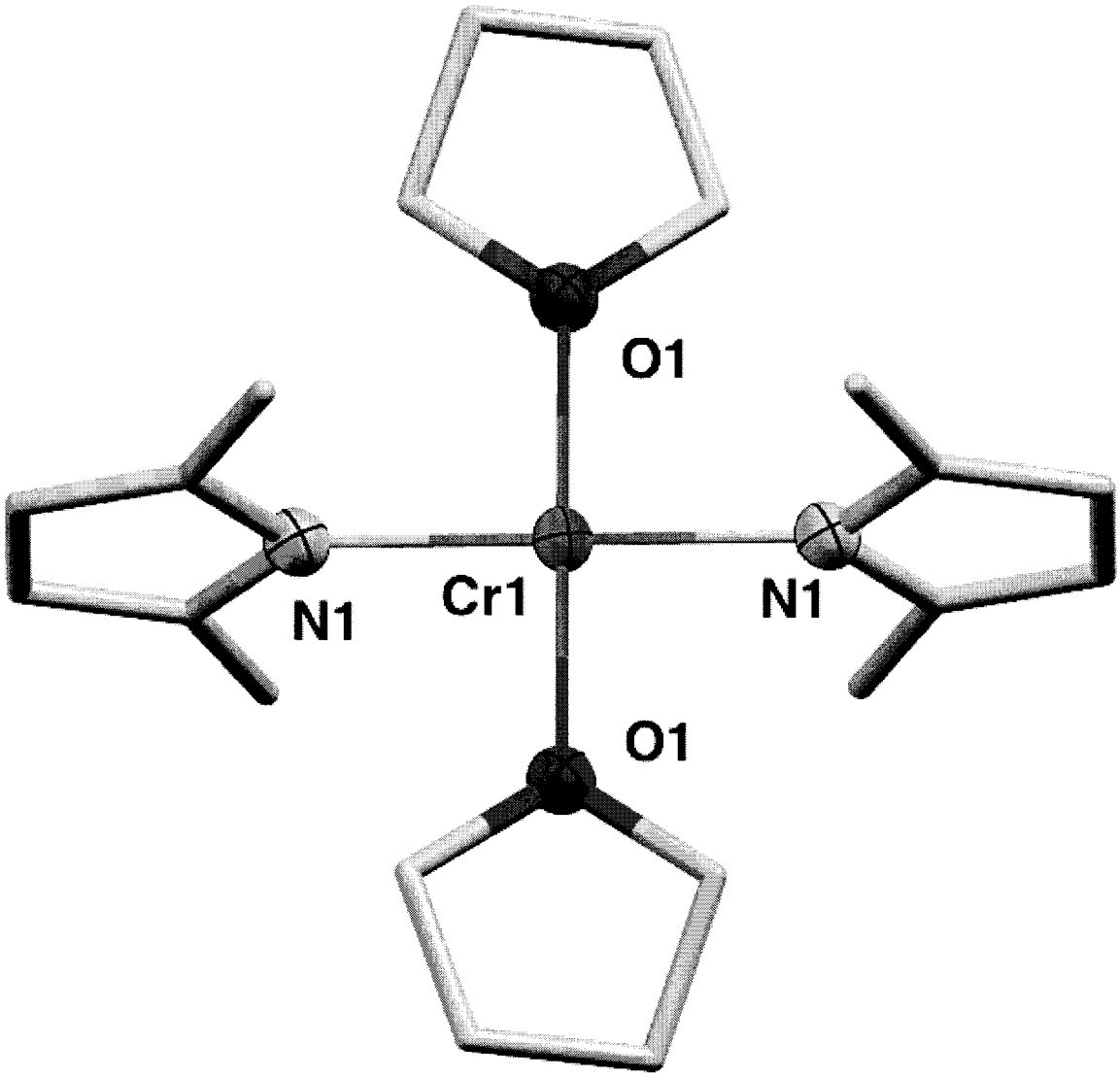

Figure 58: Partial thermal ellipsoid plot of $\{(DMP)_2Cr^{II}(THF)_2\}$ (**19**) with ellipsoids drawn at 50% probability

Table 21: Selected Bond Distances (Å) and Angles (°) for $\{(DMP)_2Cr^{II}(THF)_2\}$ (**19**)

Cr(1)-N(1)	2.036(2)	C(3)-C(4)	1.395(5)
Cr(1)-O(1)	2.0510(18)	C(4)-C(5)	1.366(4)
N(1)-C(2)	1.373(4)	N(1a)-Cr(1)-N(1)	180.00(1)
N(1)-C(5)	1.381(4)	N(1a)-Cr(1)-O(1)	90.30(8)
C(1)-C(2)	1.486(5)	N(1)-Cr(1)-O(1)	89.70(8)
C(2)-C(3)	1.365(4)	O(1)-Cr(1)-O(1)	180.00(1)

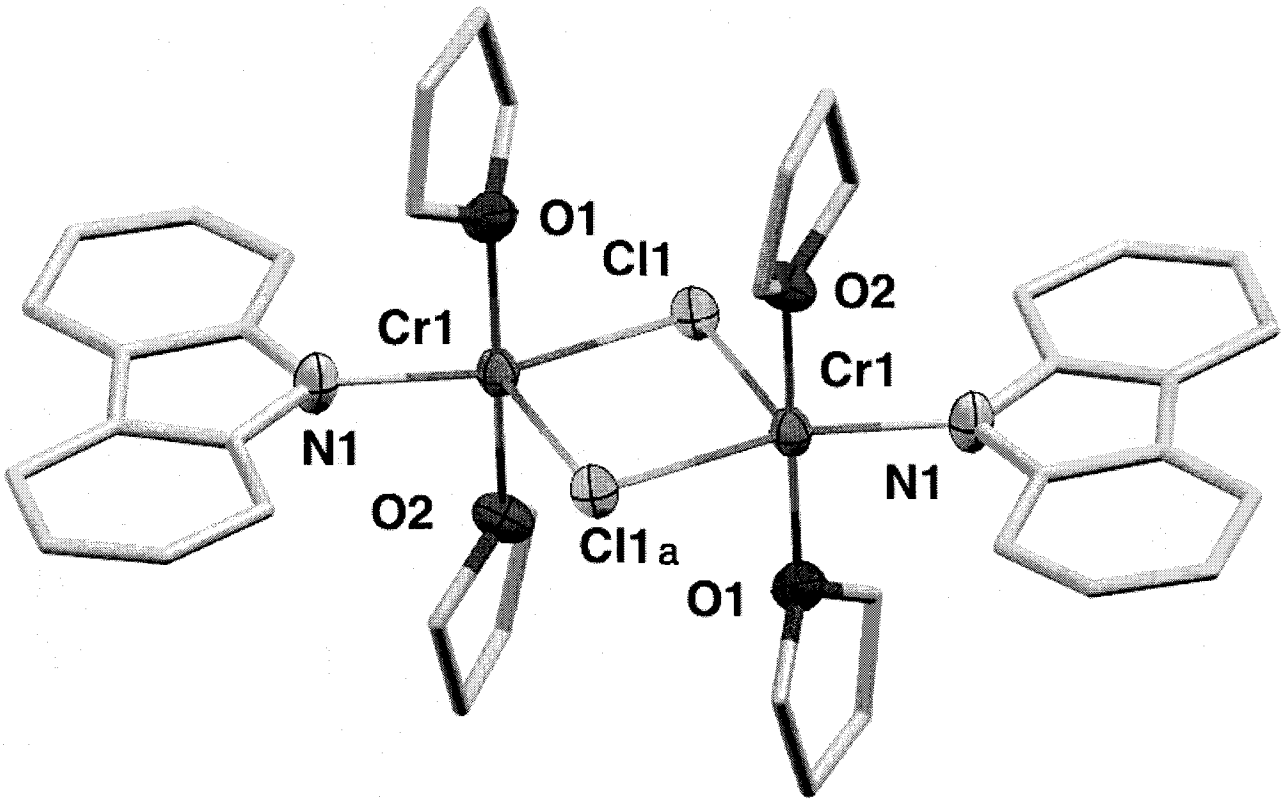

Figure 59: Partial thermal ellipsoid plot of $\{[(THC)Cr^{II}(THF)_2(\mu\text{-}Cl)]_2\}$ (**21**) with ellipsoids drawn at 50% probability

Table 22: Selected Bond Distances (Å) and Angles (°) for $\{[(THC)Cr^{II}(THF)_2(\mu\text{-}Cl)]_2\}$ (**21**)

Cr(1)-N(1)	2.028(8)	N(1)-Cr(1)-O(2)	89.8(3)
Cr(1)-O(2)	2.068(6)	O(2)-Cr(1)-O(1)	174.5(3)
Cr(1)-O(1)	2.066(7)	N(1)-Cr(1)-Cl(1)	157.8(2)
Cr(1)-Cl(1)	2.412(3)	O(1)-Cr(1)-Cl(1)	88.6(2)
Cr(1)-Cl(1a)	2.640(3)	C(6)-C(7)	1.428(13)
N(1)-C(1)	1.405(12)	C(7)-C(12)	1.410(13)
C(1)-C(6)	1.390(13)		

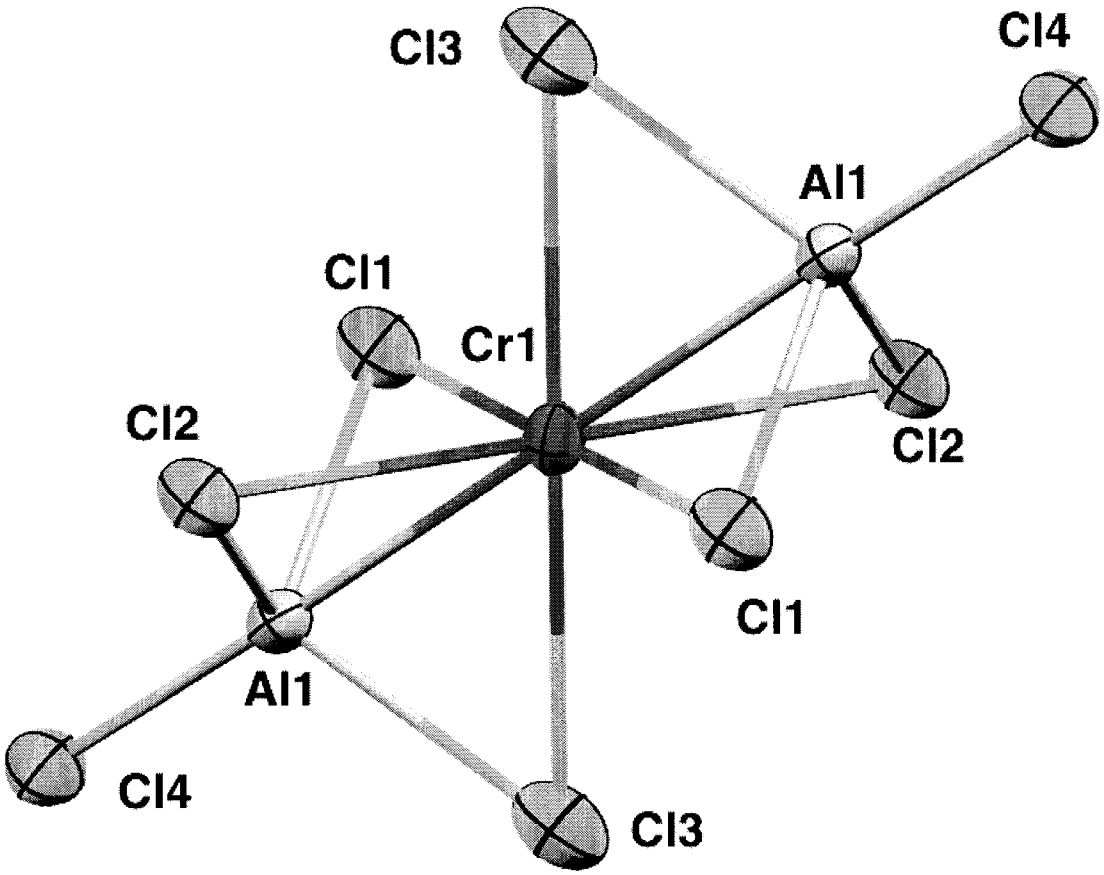

Figure 60: Partial thermal ellipsoid plot of $\{Cr^{II}[(\mu\text{-}Cl)_2AlCl_2]_2\}$ (**22**) with ellipsoids drawn at 50% probability

Table 23: Selected Bond Distances (Å) and Angles (°) for $\{Cr^{II}[(\mu\text{-}Cl)_2AlCl_2]_2\}$ (**22**)

Cr(1)-Al(1)	2.4742(19)	Cl(2)-Cr(1)-Cl(2a)	180.0
Cr(1)-Cl(2)	2.4742(19)	Cl(2)-Cr(1)-Cl(1a)	98.33(3)
Cr(1)-Cl(1)	2.4937(10)	Cl(2)-Cr(1)-Cl(1)	81.67(3)
Cr(1)-Cl(3)	2.7234(11)	Cl(2a)-Cr(1)-Cl(1)	98.33(3)
Al(1)-Cl(4)	2.070(2)	Cl(2)-Cr(1)-Cl(3a)	92.21(3)
Al(1)-Cl(1)	2.154(2)	Al(1)-Cl(3)	2.3075(19)
Al(1)-Cl(2)	2.151(2)		

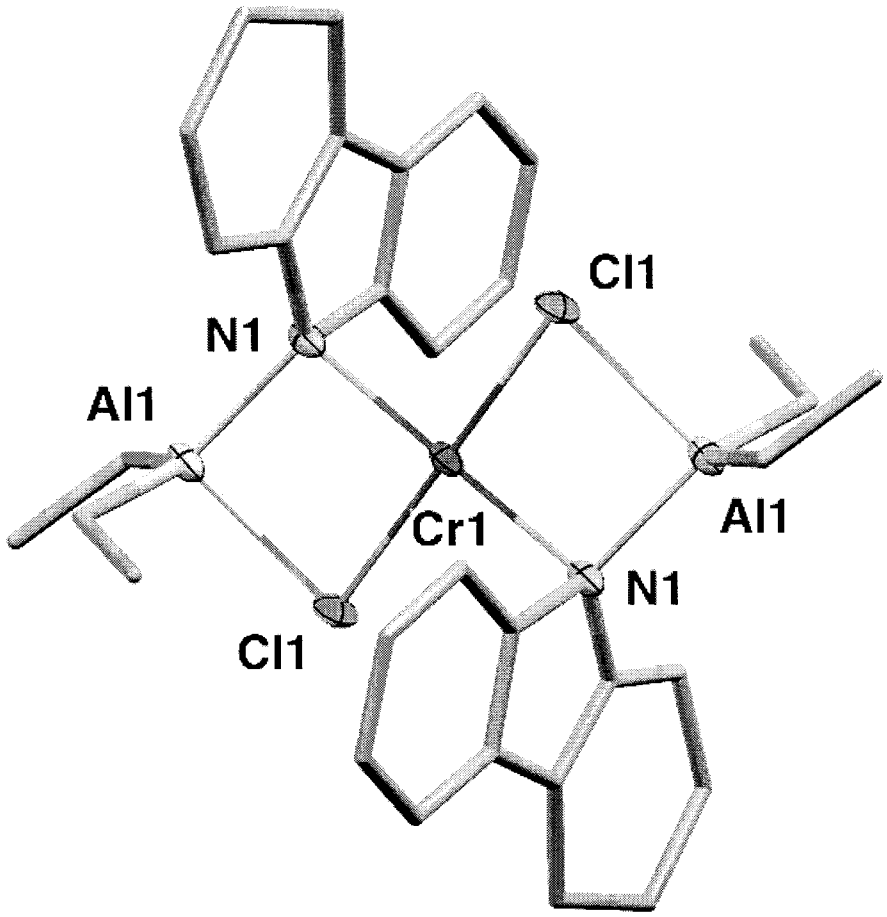

Figure 61: Partial thermal ellipsoid plot of $\{[\eta^2\text{-}(THC\text{-}AlEt_2Cl)]_2Cr^{II}\}$ (**23**) with ellipsoids drawn at 50% probability

Table 24: Selected Bond Distances (Å) and Angles (°) for $\{[\eta^2\text{-}(THC\text{-}AlEt_2Cl)]_2Cr^{II}\}$ (**23**)

Cr(1)-N(1)	2.1477(17)	N(1)-Cr(1)-Cl(1)	84.21(5)
Cr(1)-Cl(1)	2.3589(9)	N(1a)-Cr(1)-Cl(1)	95.79(5)
Al(1)-N(1)	1.9510(15)	N(1)-Cr(1)-N(1a)	180.00(1)
Al(1)-Cl(1)	2.3139(10)	C(6)-C(7)	1.434(2)
N(1)-C(1)	1.436(2)	C(7)-C(12)	1.353(2)
C(1)-C(2)	1.399(2)	N(1)-C(12)	1.436(2)
C(1)-C(6)	1.401(2)		

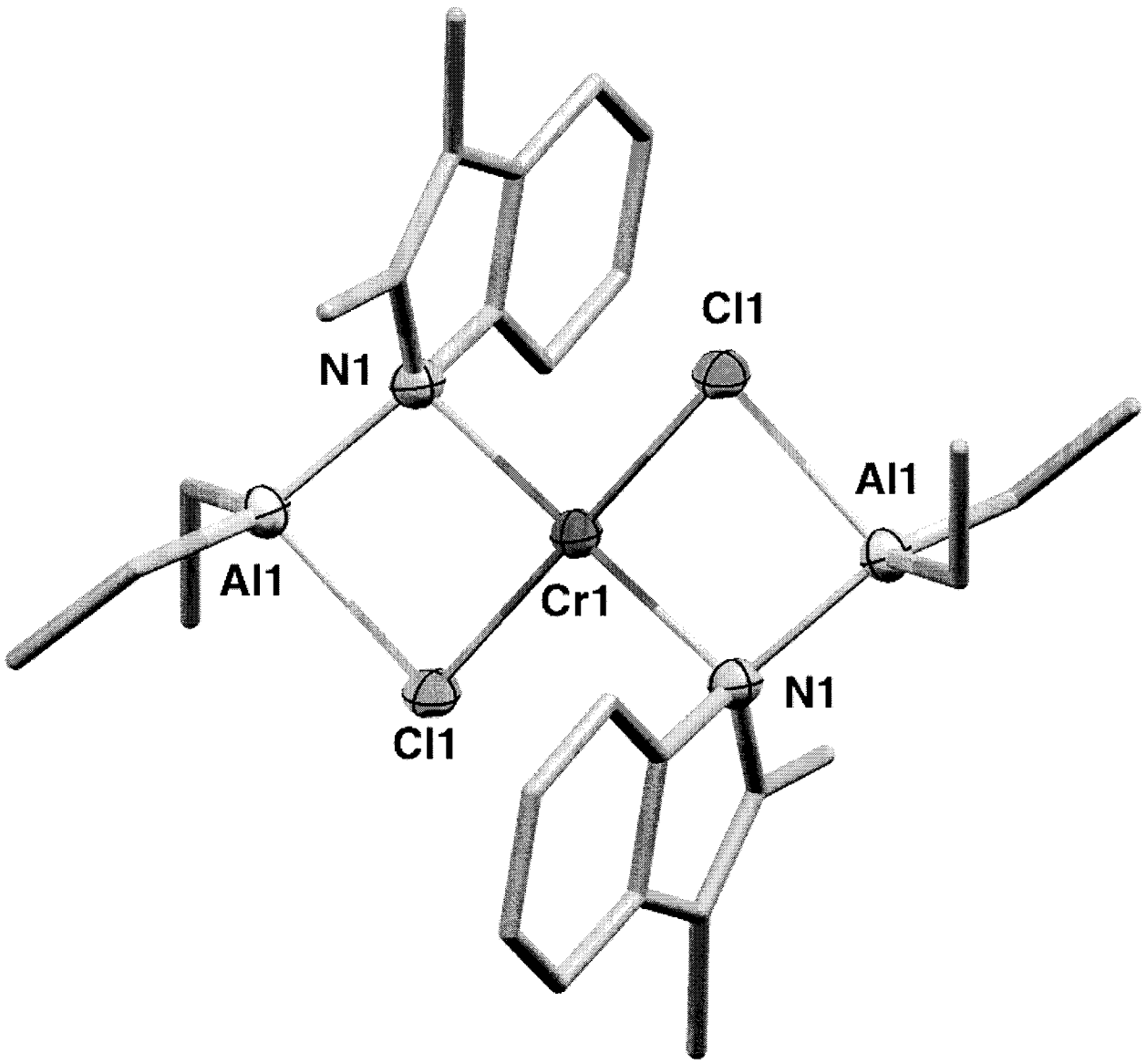

Figure 62: Partial thermal ellipsoid plot of $\{[\eta^2\text{-}(DMI\text{-}AlEt_2Cl)]_2Cr^{II}\}$ (**24**) with ellipsoids drawn at 50% probability

Table 25: Selected Bond Distances (Å) and Angles (°) for $\{[\eta^2\text{-}(DMI\text{-}AlEt_2Cl)]_2Cr^{II}\}$ (**24**)

Cr(1)-N(1)	2.130(3)	N(1a)-Cr(1)-N(1)	180.00(6)
Cr(1)-Cl(1)	2.3617(11)	N(1)-Cr(1)-Cl(1)	84.21(9)
Al(1)-N(1)	1.959(3)	C(1)-C(2)	1.345(6)
Al(1)-Cl(1)	2.3248(16)	C(2)-C(3)	1.432(6)
N(1)-C(8)	1.428(5)	C(3)-C(8)	1.407(6)
N(1)-C(1)	1.460(5)		

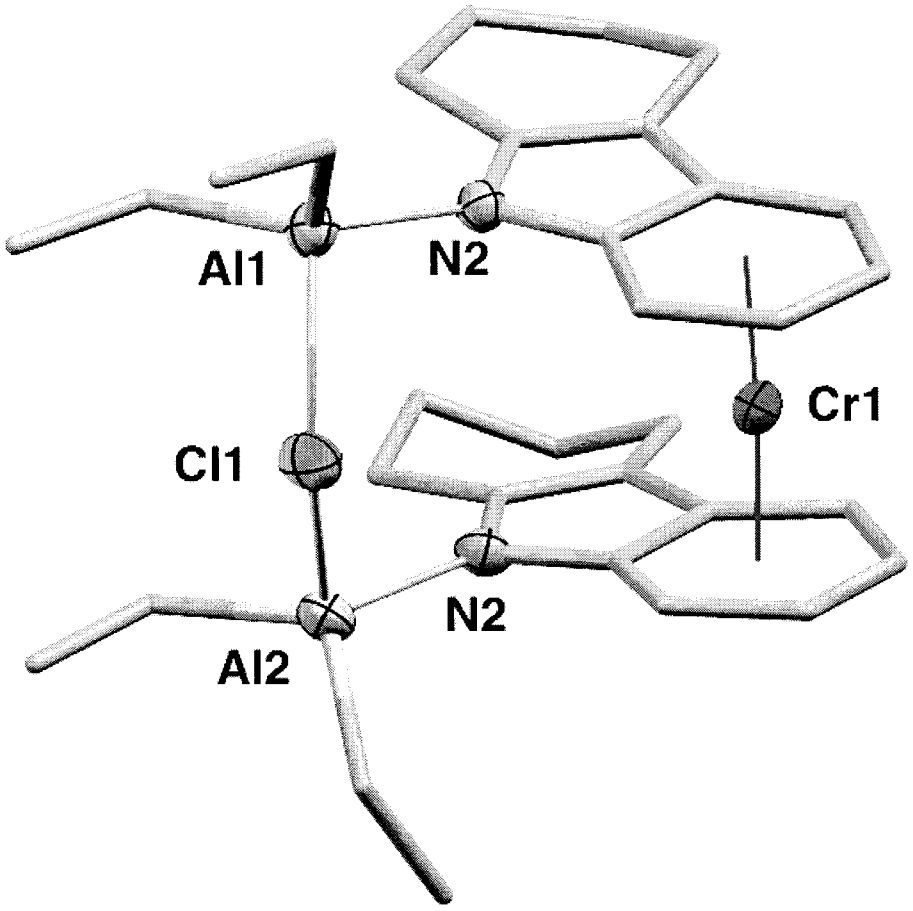

Figure 63: Partial thermal ellipsoid plot of {[(η^6-THC-$AlEt_2$)$_2$(μ-Cl)]Cr^I} (**25**) with ellipsoids drawn at 50% probability.

Table 26: Selected Bond Distances (Å) and Angles (°) for {[(η^6-THC-$AlEt_2$)$_2$(μ-Cl)]Cr^I} (**25**)

Cr1-Cnt	1.64(5)	N(2)-Al(2)-Cl(1)	101.26(14)
N(1)-C(1)	1.397(6)	Cnt.-Cr1-Cnt.	176.2(5)
N(1)-C(12)	1.397(6)	Al1-Cl1-Al2	117.55(8)
C(1)-C(6)	1.333(6)	N1-Al1-Cl1	103.56(14)
C(6)-C(7)	1.416(7)	C(7)-C(12)	1.431(6)

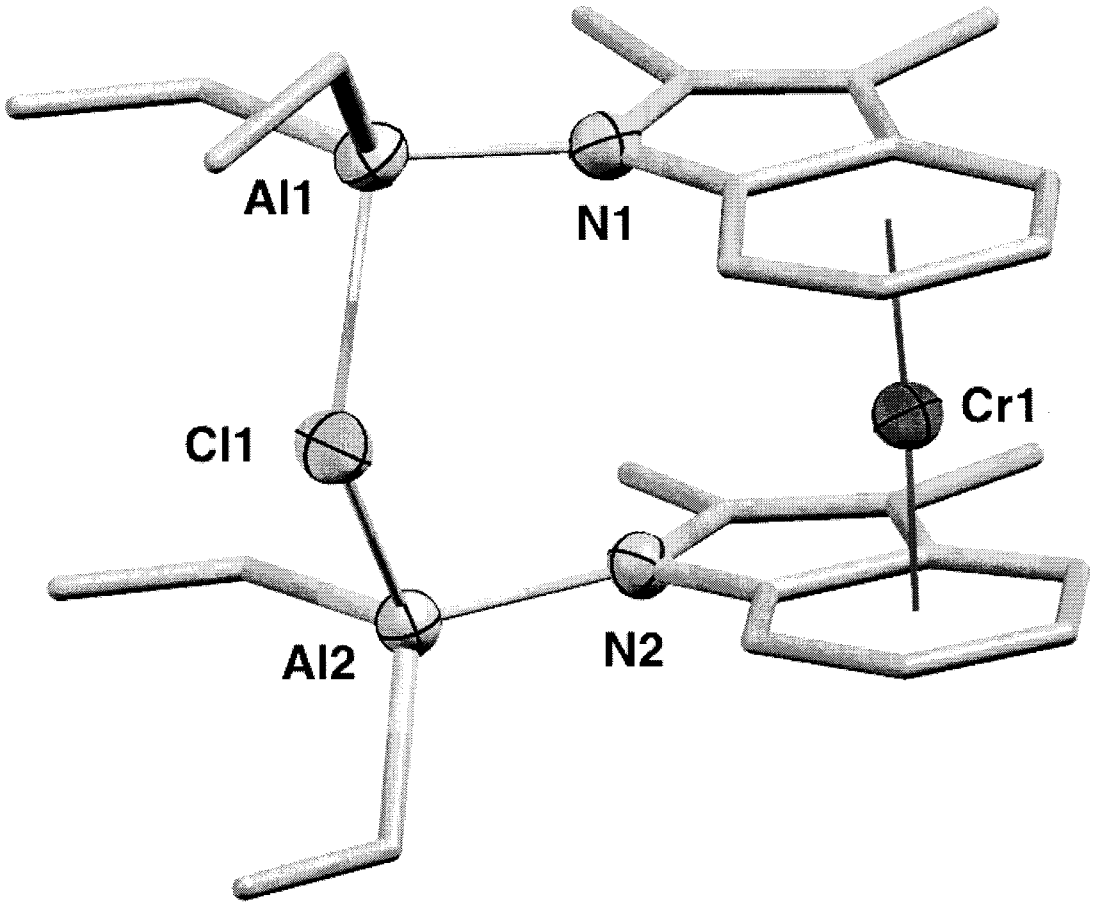

Figure 64: Partial thermal ellipsoid plot of {[(η^6-DMI-$AlEt_2$)$_2$(μ-Cl)]Cr^I} (**26**) with ellipsoids drawn at 50% probability.

Table 27: Selected Bond Distances (Å) and Angles (°) for {[(η^6-DMI-$AlEt_2$)$_2$(μ-Cl)]Cr^I} (**26**)

Cr1 Cnt	1.654	Cnt Cr Cnt	176.55
N(1)-C(8)	1.392(4)	Al(1)-Cl(1)	2.3373(15)
N(1)-C(1)	1.399(4)	Al(2)-N(2)	1.892(2)
C(1)-C(2)	1.369(5)	Al(2)-Cl(1)	2.3468(16)
C(2)-C(3)	1.435(4)	N(1)-Al(1)-Cl(1)	101.46(9)
C(3)-C(8)	1.430(4)	Al(1)-Cl(1)-Al(2)	116.71(5)

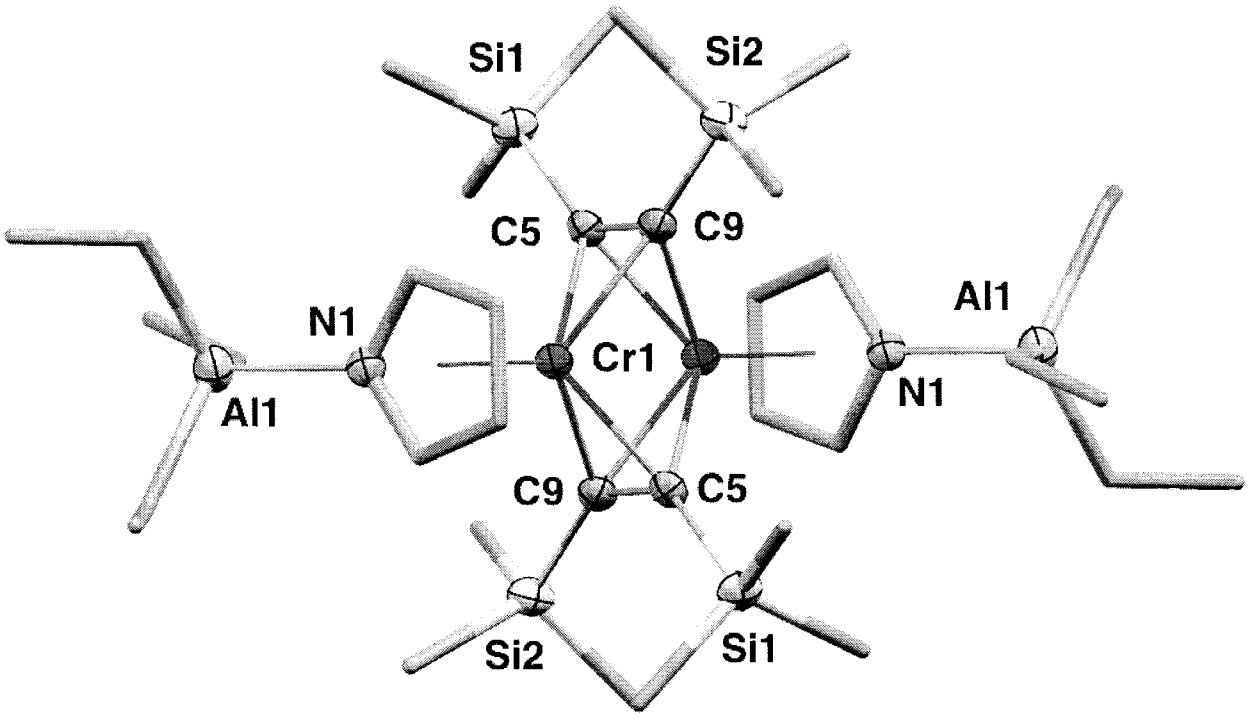

Figure 65: Partial thermal ellipsoid plot of $\{[\eta^5\text{-}(C_4H_4N\text{-}AlEt_3)Cr(\mu\text{-}C_2(SiMe_3)_2]_2\}$ (**27**) with ellipsoids drawn at 50% probability.

Table 28: Selected Bond Distances (Å) and Angles (°) for $\{[\eta^5\text{-}(C_4H_4N\text{-}AlEt_3)Cr(\mu\text{-}C_2(SiMe_3)_2]_2\}$ (**27**)

Cr(1)-Cr(1a)	2.2992(15)	C(9)-Cr(1)-C(5a)	37.89(17)
Cr(1)-C(9)	2.060(5)	C(9a)-C(5)-Si(1)	140.1(4)
Cr(1)-C(5)	2.063(5)	C(1)-C(2)	1.399(7)
C(5)-C(9a)	1.343(6)	C(2)-C(3)	1.402(7)
C(1)-N(1)	1.379(6)	C(3)-C(4)	1.396(7)
N(1)-C(4)	1.389(6)		

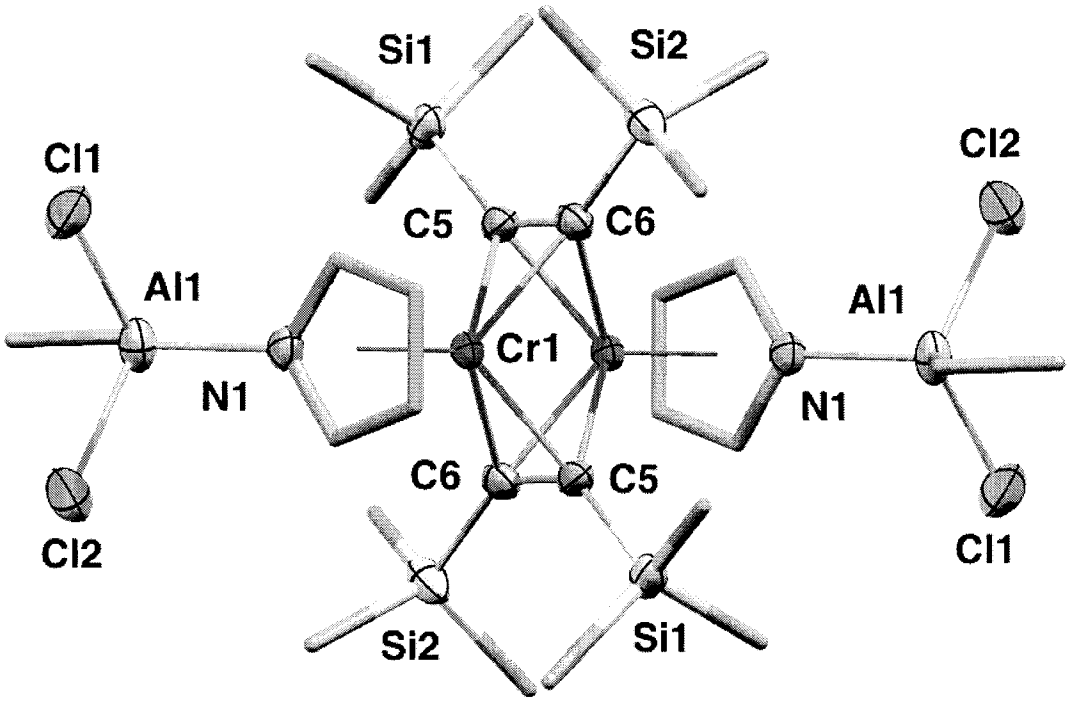

Figure 66: Partial thermal ellipsoid plot of $\{[\eta^5\text{-}(C_4H_4N\text{-}AlEt_2Cl)Cr(\mu\text{-}C_2(SiMe_3)_2]_2\}$ (**28**) with ellipsoids drawn at 50% probability.

Table 29: Selected Bond Distances (Å) and Angles (°) for $\{[\eta^5\text{-}(C_4H_4N\text{-}AlEt_2Cl)Cr(\mu\text{-}C_2(SiMe_3)_2]_2\}$ (**28**)

Cr(1)-C(5)	2.067(4)	C(1)-C(2)	1.390(6)
Cr(1)-C(6)	2.055(4)	C(2)-C(3)	1.420(7)
Cr-Cnt	1.949	C(3)-C(4)	1.377(6)
C(5)-C(6)	1.330(6)	N(1)-C(1)	1.385(5)
N(1)-C(4)	1.377(5)		

4.2.13 Catalytic Data

Table 30: Catalytic Data for Cr Pyrrole

Cat.	Cocatalyst	Solvent	Alkenes	PE	activity	C_6[b]	C_8	C_{10}
#	(eq.)		(mL)[a]	(g)	(g/mmol/h)	(mol%)	(mol%)	(mol%)
19	Et_3Al(10)/ Et_2AlCl (10)	CyMe	4.2	1.2	551	91	5	4
	AlEt (10)	CyMe	2.4	0.2	245	42	21	16
	Et_2AlCl(10)	CyMe	traces	3.5	357	-	-	-
21	Et_2AlCl (10)	CyMe	0	10.4	1061	96	3	4
	Et_3Al(10)	CyMe	4.2	0.1	428	90	5	5
22	Me_3Al(5)	PhMe	0	8.3	846	-	-	-
23	-	CyMe	0	3.4	346	-	-	-
	-	PhMe	0	3.8	387	-	-	-
	Et_3Al(10)	CyMe	1.8	1.2	265	93	3	3
24	-	CyMe	0	3.4	347	-	-	-
	Et_3Al(10)	CyMe	1.6	2.4	275	93	3	3
25	-	PhMe	traces	0.2	-	-	-	-
	-	CyMe	2.4	0.2	245	94	3	3
	Et_3Al(10)	CyMe	9.3	0.1	950	92	5	4
26	-	CyMe	2.1	0.2	214	94	3	3
	Et_3Al (10)	CyMe	7.7	0.1	785	90	5	5
27	-	CyMe	3.6	0.1	367	30	17	10
	Et_2AlCl(10)	CyMe	4.3	0.1	439	88	6	6
28	-	CyMe	0.2	0.1	20	98	traces	traces
	Et_3Al (10)	CyMe	2.8	0.1	286	92	4	5
c	Et_3Al (10)/Et_2AlCl (10)	CyMe	11.5	0.2	1170	92	4	4
d	Et_3Al(10)/Et_2AlCl (10)	CyMe	3.4	0.2	347	93	4	3
e	-	CyMe	0.5	0.1	51	98	traces	traces
e	Et_3Al (10)	CyMe	5.7	0.1	581	92	5	4

T = 115 °C, V = 20 mL, P = 40 bar, catalyst = 20 μmole, time = 30 min. [a] By integration of the NMR olefinic resonances with respect to the Me of the solvent. [b] By G.C.: Non-PE fraction, values of C_4 are not given due to volatility. [c] benchmark in-situ DMP catalyst : $Cr(EH)_3$/DMP/Et_3Al/Et_2AlCl = 1:3:10:10. [d] benchmark in-situ THC catalyst: Cr(EH)3/THC/Et_3Al/Et_2AlCl = 1:3:10:10. [e] brown material isolated from in-situ DMP catalyst. the symbol (-) means that only traces of oligomers detected.

4.3 Results

4.3.1 Synthesis of chromium pyrrolyl precursors and their reaction with AlR_3 reagents.

The reaction of $CrCl_3(THF)_3$ and $CrCl_2(THF)_2$ with a variety of alkali-pyrrolide salts was examined with the goal of generating well-defined chromium pyrrolide precursors, which are established to form trimerization catalysts when reacted with aluminum alkyl cocatalysts.[68, 61,

19, 20, 114] Thus the well-defined chromium (II) bis-DMP ethylene trimerization catalyst precursor, $\{(DMP)_2Cr^{II}(THF)_2\}$ (**19**), was synthesized by the method originally reported in the literature (Figure 67).[108] This preparation method was also explored with the related ligands 2,3,4,5-tetramethylpyrrole (TMP), 2,3,4,5-tetraphenylpyrrole (TPP), tetrahydrocarbazole (THC), and 2,3-dimethylindole (DMI). However, crystals of sufficient X-ray quality were obtained only for the previously reported **19** and the dimeric square-pyramidal chromium (II) mono-THC complex, $\{[(THC)Cr^{II}(THF)_2(\mu\text{-}Cl)]_2\}$(**21**) (Figure 67).

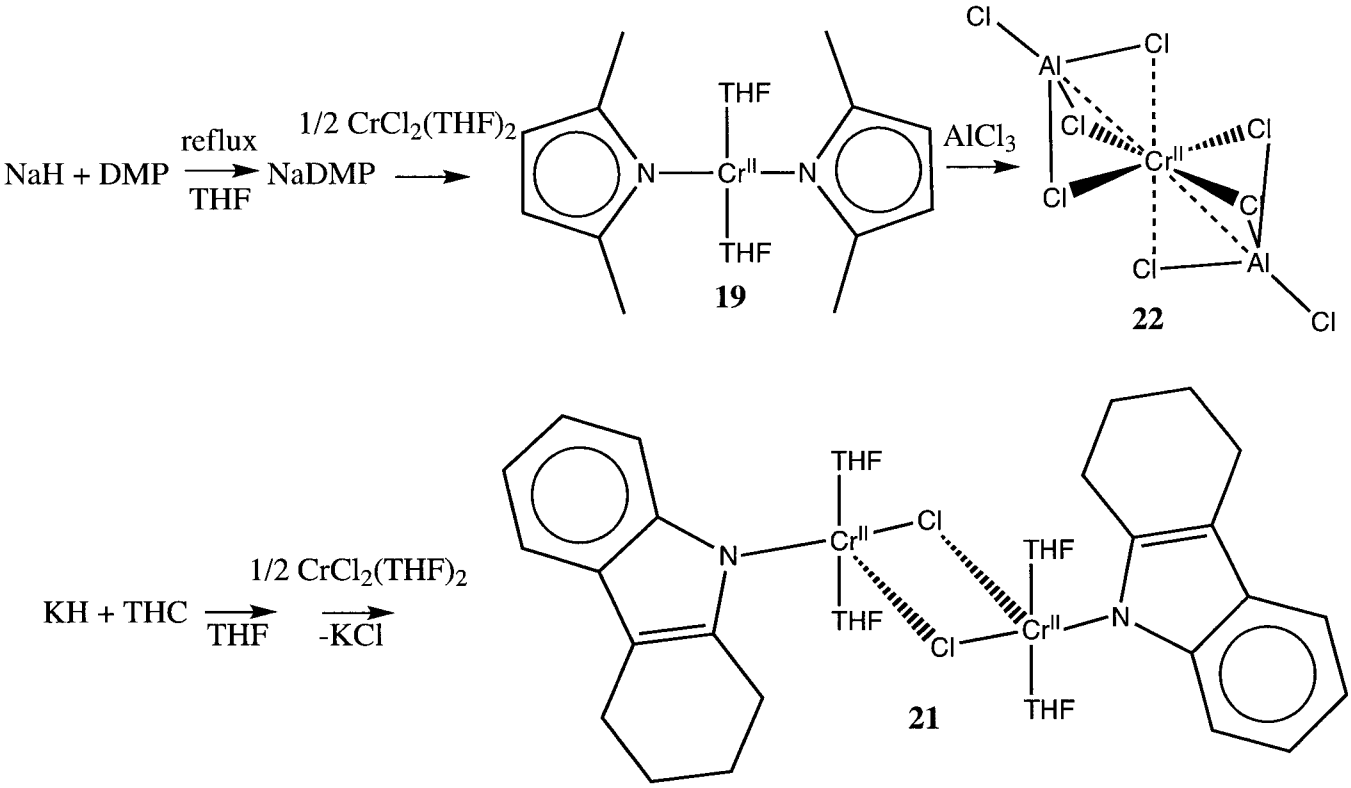

Figure 67: Synthesis of chromium pyrrolide precursors **19-21**, and reaction of **19** with $AlCl_3$ to generate **22**

The X-ray structural analyses of both monomeric bis-pyrrole complexes **19** has not been reported previously in the literature. The X-ray structure of **19** (Figure 58) reveals that the chromium (II) centre is in the standard square-planar geometry expected for a high spin d^4 (μ_{eff} = 4.86 μ_B) electronic configuration, where the four atoms attached to chromium are the two nitrogen atoms of the trans aromatic pyrrole rings and the two oxygen atoms of the trans THF rings.

The X-ray structure of the dimeric mono-THC complex **21** (Figure 59) reveals that both

chromium (II) centres (μ_{eff} = 4.74 μ_B per chromium atom) in the symmetry-generated dimeric unit are in a distorted square pyramidal environment. The equatorial positions are occupied by the indole nitrogen, the oxygen atoms of the two THF molecules, and the chloride [Cr(1)-Cl(1) = 2.412(3) Å]. The apical site is distorted, and is occupied by the chloride [Cr(1)-Cl(1a) = 2.640(3) Å] connected to the neighboring chromium (II) molecule. The dimerization of **21** in the solid state is probably due to the stronger electrophilicity of the chromium centre and the decreased steric bulk of the molecule compared to **19** and **20**. However, crystal packing forces might also be a contributing factor. Thus, in solution it might be possible that the weak bridging interactions present in the dimer **21** are weak enough to result in a dissociation to the monomeric form.

Treatment of complexes **19**, and **21** with a wide range of alkylaluminum reagents resulted in the isolation of either poorly soluble, light colored microcrystalline materials (when using alkylaluminum halides) or highly soluble dark-brown oily products (when using a trialkyl aluminum reagent), preventing the growth of suitable X-ray quality crystals. However, treatment of **19** with the fully-chlorinated $AlCl_3$ reagent afforded complete ligand extraction and generated the monomeric chromium (II) bis-tetrachloroaluminate complex, $\{Cr^{II}[(\mu\text{-}Cl)_2AlCl_2]_2\}$ (**22**) (Figure 67).

The X-ray structure of **22** (Figure 60) reveals that the chromium (II) centre (μ_{eff} = 4.92 μ_B) is in a tetragonally distorted octahedral environment. The equatorial positions are occupied by the four chlorides of the two symmetrical $AlCl_4$ ligands [Cr(1)-Cl(2) = 2.4742(19) Å, Cr(1)-Cl(1) = 2.4937(10) Å] while the apical site is also occupied by a bridging chloride to both chromium [Cr(1)-Cl(3) = 2.7234(11) Å] and a significantly stretched bond of the same chloride ligand to the aluminum centre [Al(1)-Cl(3) = 2.3075(19) Å] when compared to the other terminal and bridging Al-Cl bond lengths in the molecule [Al(1)-Cl(4) = 2.070(2) Å, Al(1)-Cl(1) = 2.154(2) Å]. This suggests that the complex is partially ionized with the negative charge mainly residing on the two apical chloride donors. While this removal of electron density from aluminum results in more Lewis acidity, it is possible that electron density is provided by chromium due to the close proximity of aluminum and the electron rich Cr (II) centre [Cr(1)-Al(1) = 2.4742(19) Å].

Finally, as a chromium (I) species is proposed to play an important role in ethylene trimerization

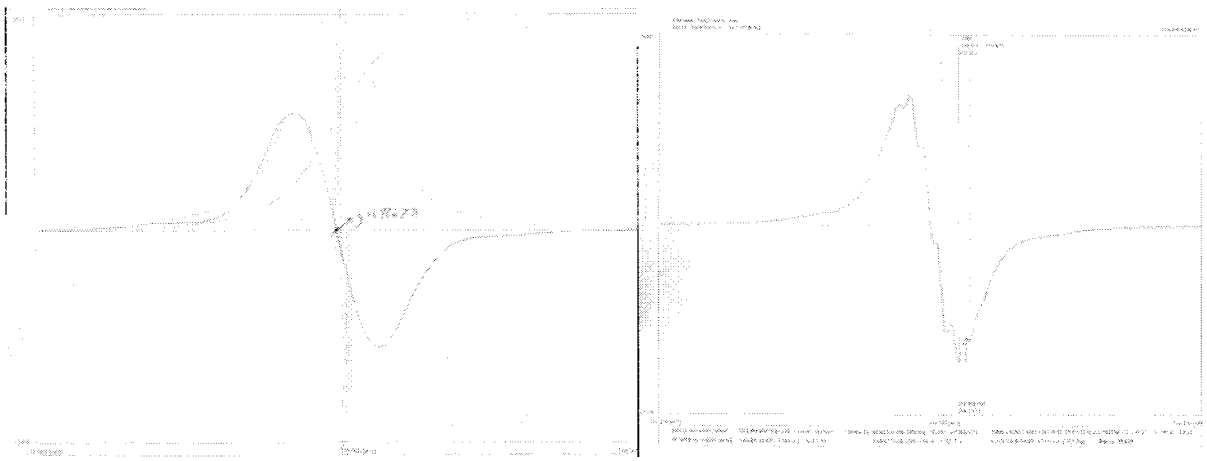

Figure 68: Comparison of powder E.P.R. spectra of the commercially used DMP-based catalyst (left, at r.t., g = 1.9863), and of complex **25** (right, at -198 C)

catalysis, the attempt to directly form a Cr(I) pyrrolide precursor by the reaction of the well-defined cationic Cr(I) bis-arene iodide precursor, $\{(\pi\text{-}C_6H_6)_2Cr^I\}$ {I}, with the lithium salt of DMP unfortunately resulted in the formation of black colored crystals of $\{(\pi\text{-}C_6H_6)_2Cr^0\}$ upon workup, attesting to the previously established kinetic-inertness of Cr bis-arene species.

4.3.2 Isolation of complexes from in-situ preparation

Based on the difficulties encountered for the isolation of well-defined complexes from the original strategy discussed above, the next strategy employed was the direct isolation of catalytic intermediates via the in-situ used catalyst preparation method. This involves a combination of the chromium precursor, pyrrole ligand, and aluminum alkyl cocatalyst together, as reported in the patent literature. The combination of $CrCl_3(THF)_3$, DMP and Et_3Al/Et_2AlCl in the ratio of 1:2:6:6 afforded a homogeneous brown microcrystalline material. Unfortunately, no X-ray quality crystals of this material could be grown, which prevented structural characterization. However, the powder E.P.R. spectrum of this homogeneous brown product was recorded and revealed a single wave resonance which is characteristic for a low-spin Cr(I) complex (Figure 68).[115, 116] Thus, based on this promising start, this method of catalyst preparation was attempted with other pyrrole ligands in the hopes of improving crystallinity for structural characterization.

Fortunately, the method of catalyst preparation in-situ with the THC or DMI ligands substituted for the DMP ligand led to the successful isolation of blue crystals, which were composed of

the monomeric square-planar chromium (II) bis-indolyls, $\{\eta^2$-THC-$AlEt_2Cl)_2Cr^{II}\}$ (**23**) and $\{(\eta^2$-THC-$AlEt_2Cl)_2Cr^{II}\}$ (**24**), respectively (Figure 69). The formulae of the ligands in **23** and **24** are listed as η^2-THC-$AlEt_2Cl$ for clarity to reflect the bidentate nature of the indolyl-aluminate ligand as a whole to chromium, but are however inconsistent with IUPAC guidelines for nomenclature of organometallic complexes. However, the yields of the Cr (II) products in these reactions were always below 45%, and were accompanied by a significant quantity of a dark red oily byproduct. The X-ray structures of **23** (Figure 61) and **24** (Figure 62) display the characteristic square-planar coordination geometry expected for a high-spin d^4 Cr(II) centre (μ_{eff} = 4.9 and 4.82 μ_B, respectively). Improved yields could be obtained when starting from the $CrCl_2(THF)_2$ precursor with the same conditions (> 80%). The coordination environment around chromium in **23** and **24** is defined by the nitrogen atoms of the indolyl ligands, which, in turn, bridge an Et_2AlCl residue. The chlorine atoms bridge between the aluminum atom and chromium atom, thus occupying the two remaining coordination sites of the square-planar chromium centre. Based on the bridging geometry of the nitrogen donors of the two indolyl rings, the electronic hybridization can be considered to be more amide-like than pyrrole-like, and to be bonding via mainly σ-sp^3 like hybrid orbitals. This is confirmed by the analysis of the heterocyclic ring bond lengths, which reveals the changes in bond lengths consistent with the loss of aromaticity when the nitrogen lone pair is not involved in the π system anymore [N(1)-C(1)= 1.436(2) Å, C(7)-C(12) = 1.353(2) Å, C(1)-C(2)= 1.399(2) Å, N(1)-C(12)= 1.436(2) Å].

The same preparation was attempted by using the chloride-free chromium (III) tris-octanoate precursor with the THC and DMI and Et_3Al/Et_2AlCl. The reaction resulted in the isolation of brown crystals of the monomeric bis-indolyl Cr(I) species $\{[(\eta^6$-THC-$AlEt_2)_2(\mu$-Cl)]$Cr^I\}$ (**25**) and $\{[(\eta^6$-DMI-$AlEt_2)_2(\mu$-Cl)]$Cr^I\}$ (**26**) (Figure 69). The isolation of homogeneous crystalline samples of **25** and **26** by this direct method was complicated by the formation of oily byproducts, possibly due to the interference of excess aluminum alkyl reagent in the preparation. Pure crystals of **25** and **26** could be obtained in much higher yields via the one-electron reduction of the Cr (II) analogs, **23** and **24**, with potassium metal.

The X-ray structures of **25** (Figure 63) and **26** (Figure 64) display a sandwich coordination

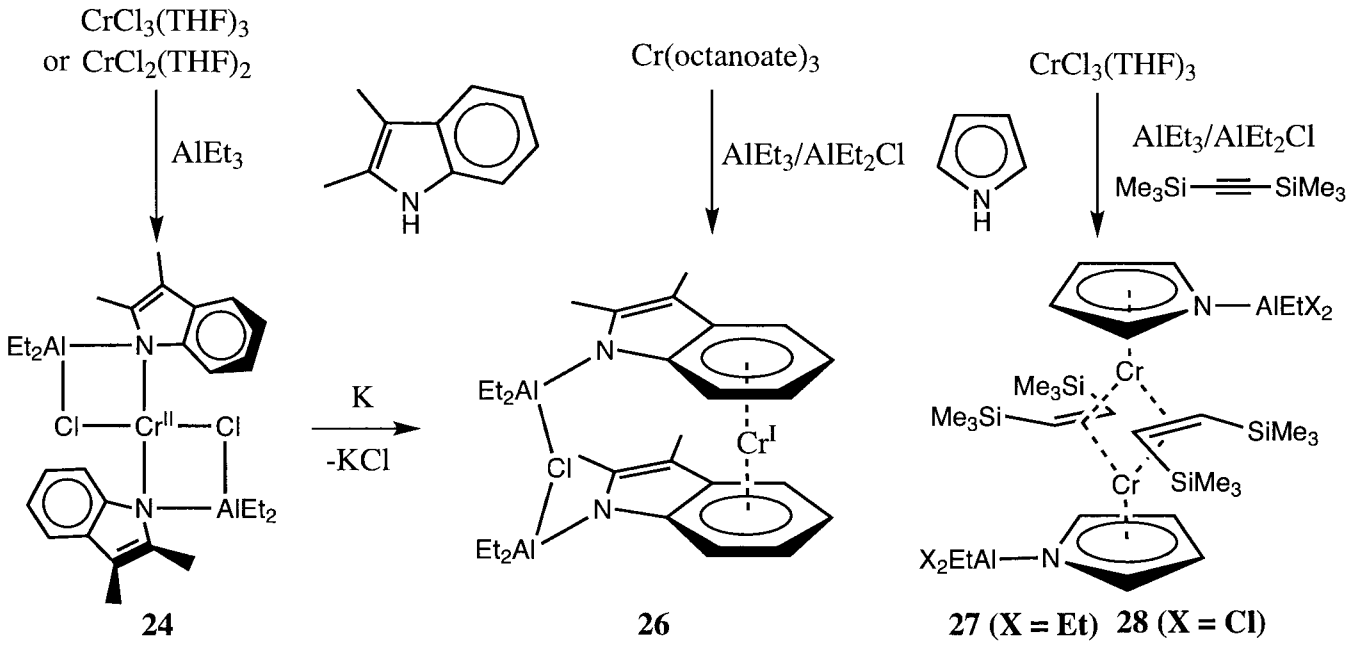

Figure 69: Synthesis of complexes **24**, **26**, **27**/**28** in this chapter (synthesis of **23** and **25** not shown, but are the same as **24** and **26** with THC instead of DMI).

geometry. The magnetism was as expected for a low-spin configuration of a d^5 chromium (I) centre in a pseudooctahedral ligand field (with a formal electron count of 17), leaving one unpaired electron on the chromium centre (1.87 and 1.90 μ_B for **25** and **26**). In the structure, each nitrogen atom of the carbazolyl anions are bonded to an Et_2Al residue. The two aluminum atoms are connected through one residual bridging chlorine atom, which is too distant from chromium to form a bonding interaction. The powder EPR spectra was also recorded for complex **25** at low temperature, which reveals a single wave pattern as expected for one unpaired electron, with hyperfine coupling to nitrogen (9 peaks).[117] Improved EPR spectra in the future work could be recorded with a diamagnetic Rh(I), Mn(I), or even potassium salt matrix. The formation under nearly identical conditions of **23**/**24** and **25**/**26**, depending on the counteranion of the chromium starting salt, clearly reiterates the mechanistically complex nature of organochromium (III) reduction pathways. The direct reduction to the monovalent state by using a non-chlorinated starting material can be readily explained, however, by assuming more extensive alkylation of the monomeric Cr(III) centre in the early stage of the reaction before dimerization can occur and bimetallic reduction/disproportionation pathways become dominant as in the [PNP] system.

As the role of the chromium (I) oxidation state in ethylene trimerization catalysis is postulated

to be the binding of two olefins, the reaction of the well-defined Cr (I) species **25** and **26** with a variety of olefins, dienes, and alkynes was attempted to isolate and characterize a Cr(I) olefin complex. While no crystals could be isolated from these reactions, the reaction of the poorly-defined microcrystalline brown material, which forms in the reaction of $CrCl_3(THF)_3$, pyrrole, and Et_3Al, with the bulky alkyne, $C_2(SiMe_3)_2$, allowed for the growth of green X-ray quality crystals of the dimeric chromium (I) alkyne complex $\{[\eta^5\text{-}(C_4H_4N\text{-}AlEt_3)Cr(\mu\text{-}C_2(SiMe_3)_2]_2\}$ (**27**) (Figure 69). Complex **27** was found to exhibit residual paramagnetism. The temperature dependent paramagnetism should be recorded first to indicate whether there is temperature dependent antiferromagnetic coupling or a paramagnetic impurity. Its solution NMR spectra contains reasonably sharp signals for all the protons and carbons in the molecule. A structurally identical chlorinated derivative of **27**, $\{[\eta^5\text{-}(C_4H_4N\text{-}AlEt_2Cl)Cr(\mu\text{-}C_2(SiMe_3)_2]_2\}$ (**28**), could be formed by the addition of $AlCl_3$ to the mixture originally containing **27**. Unfortunately **28** exhibited very poor solubility once crystallized, possibly due to the absence of ethyl groups.

The X-ray structures of **27** (Figure 65) and **28** (Figure 66) reveals that these species are dimeric, with each chromium centre π bonded to a pyrrole ring, and contain a short Cr···Cr contact (2.3 Å). The bridging interaction between the two Cr-containing residues is supported by the two bridging alkynes which are side-on bonded to both metal centres. Complexes **27**/**28** are the first examples of structurally characterized chromium alkyne complexes which do not contain phosphine or carbonyl ligands. Their formation is the result of oxidative addition of a monovalent Cr(I) pyrrolide intermediate to the alkyne molecule, affording what appears to be a trivalent species, given the elongation of the coordinated alkyne C-C bond (1.33 Å) to the ideal C=C bond length (1.3 Å) and the C-C-Si bond angle (C(9)-C(5)-Si(1) =140.1(4)°) which is closer to the ideal angle of an sp^2 hybridized carbon (120°) rather than that of an *sp* hybridized carbon (180°) for an alkyne. These structural parameters suggest that the proposed low spin Cr(I) bis-pyrrolyl intermediate that initially forms has undergone a two-electron oxidation by the alkyne. In agreement with the trivalent state, Mulliken charge distributions for the two chromium atoms were 3.14 and 2.43, respectively (obtained with DFT-B3LYP using the 6–311G + basis set and the singlet state, and on a truncated model optimized using Gaussian '03). Mulliken charges are not the de-facto way

to describe the charge of elements, and more detailed analysis must be carried out to verify the electronic state of **27**.

4.3.3 Catalytic evaluation of complexes 19-28

The well-defined chromium pyrrolide complexes **19-28** were evaluated for ethylene trimerization in either methylcyclohexane or toluene at 115 °C for 30 min (Table 30), allowing for a comparison of their catalytic performances to gain mechanistic insights into the role of the chromium oxidation state and coordination sphere on the product selectivity.

Thus the catalyst precursors which did not contain any aluminum alkyl residues, **19-22**, were combined with the standard activators used in the reported literature as discussed in the introduction. The ethylene trimerization activity and selectivity of **19-21** were found to be consistent with that reported previously for well-defined chromium pyrrolyl precursors. However, it is of interest to mention that the amount of polymer formed in these catalyst samples was roughly consistent with the ratio of Et_2AlCl cocatalyst relative to Et_3Al cocatalyst used. The exclusive use of Et_2AlCl resulted in mainly polymer formation, but some chlorinated cocatalyst was still required for higher activity and selectivity. Thus, the already established "chloride effect" was reproduced. The pyrrole-free precursor **22** was found to be a surprisingly potent polymerization catalyst upon activation, operating most likely as a heterogeneous catalyst similar to the originally reported heterogeneous Ziegler-Natta catalysts based on a mixture of $TiCl_3$ and $AlEtCl_2$.

While the poorly-defined brown species isolated from the in-situ DMP system (entry f) was found to give low but non-negligible activity for ethylene trimerization, high activity could be restored in the presence of additional Et_3Al, suggesting that this brown material, which is thought to contain low-spin Cr(I), is a stable precatalyst which can be activated in the presence of aluminum cocatalyst. This is consistent with reports of the long-term stability of the chromium-pyrrole mixture, allowing for long term storage of the pre-activated catalyst for months without significant loss in performance.[109, 110]

The well-defined complexes **23-28** were evaluated both with and without any additional activator, as aluminum alkyl is already incorporated into the structures of these complexes. Thus,

it was found that the bis-indolyl complexes **23** and **24** are single-component catalysts for ethylene polymerization, which reveals clearly that Cr(II) bis-pyrrole is a polymerization catalyst. Of additional mechanistic interest, when the Cr(II) bis-indolyls, **23**/**24**, were combined with a large excess of Et_3Al activator, some 1-hexene forms in addition to the main P.E. product. The addition of excess Et_2AlCl to **23**/**24** resulted only in increased activity for the undesired P.E.

In contrast, when the the Cr(I) sandwich complexes **25** and **26** were tested as single-component catalysts in methylcyclohexane, mainly 1-hexene was produced with some higher oligomers and a small amount of P.E. Thus complexes **25** and **26** are the first reported examples of structurally-characterized single-component ethylene trimerization catalysts. This evidence strongly suggests that the low-spin chromium (I) derivative is a trimerization catalyst, while the chromium (II) analogue is responsible for the polymer byproduct. As in the patented chromium-pyrrolide trimerization catalytic system, **25**/**26** are inactive in toluene, even at elevated temperatures.

Finally, the chromium (III) alkyne complexes **27** and **28** were found to be single-component oligomerization catalysts, suggesting that Cr(I) olefin complexes are catalytic intermediates in ethylene trimerization. However, the chloride-free catalyst **27** did not selectively produce 1-hexene, but a S.F. distribution of oligomers. The chloride-containing **28** was selective but gave poor activity possibly due to its extremely low solubility. Thus, these last two results suggests that olefin complexes can act as trimerization catalytic intermediates. Most likely their activation occurs through initial dissociation of these dimers into monomeric species which have vacant sites on the chromium centre to coordinate ethylene molecules and initiate catalytic trimerization.

4.4 Mechanistic Discussion

The introduction to this chapter providing a background to the literature on the chromium-pyrrole catalyst raised some important mechanistic questions which led to this experimental work. The analysis of these results affords insights which are a key piece to the mechanistic puzzle of ethylene trimerization. These insights are discussed in the following four categories: the effect of chromium oxidation state, effect of ligand, effect of cocatalyst, and effect of solvent. Finally some speculation related to the overall mechanism is presented.

4.4.1 Effect of chromium oxidation state

Insights into the effect of the chromium oxidation state on the catalytic selectivity are found in the analysis of the catalytic product distribution obtained from the well-defined aluminum-containing complexes **23-28**. These product distributions have led to the unambiguous conclusion that the low spin Cr(I) pyrrolide **25** and **26** are ethylene trimerization catalysts. Budzelaar has recently reported a DFT study [118] of the trimerization precursor **25** and some closely related Cr(I)-pyrrolide species, concluding that the slippage of one indole ring away from the bis-pyrrolide **25** is kinetically facile, opening up vacant sites on chromium for binding ethylene. The calculations concluded as well that a stable intermediate binding two molecules of ethylene is possible, and that the proposed oxidative coupling of the two ethylene molecules to generate a chromacyclopentane intermediate is very favorable with a low barrier. In addition, any coordinatively unsaturated intermediates are partially stabilized by the bridging chloride hemilability from the aluminum moiety, which is a mechanistic basis for the chloride effect that is observed in the catalytic experiments.

The analogous Cr(II) bis-pyrrolide complexes **23** and **24** are catalyst precursors to ethylene polymerization, probably occurring through rearrangement of the complex at high temperatures. The species so generated can insert ethylene into either a Cr-alkyl or directly to the aluminum-alkyl in a chromium-catalyzed "aufbau" type reaction, which has been previously reported for a chromium-aluminum system.[119, 120] Catalytic trimerization is always accompanied by the formation of some polymer, which cannot be avoided even with single-component trimerization precursors **25** and **26**. It can be surmised that a pathway for the formation of the bis-pyrrolyl Cr (II) polymerization catalyst from the bis-pyrrolyl Cr (I) trimerization catalyst occurs in-situ, resulting in the polymer formation observed. The pathway to the formation of the bis-pyrrolyl Cr (II) species is possibly proceeding through bimetallic intermediates from the comproportionation of Cr(III) and Cr(I) intermediates. However, as polymer formation leads to reactor fouling, highly undesirable for commercial operators, it is important to understand the mechanism of its formation.

4.4.2 Effect of ligand

The second parameter affecting the reactivity of chromium was the pyrrole ligand. The reduction to the monovalent state through the use of a nonchlorinated starting material can be readily explained by assuming a more extensive alkylation and reduction of the monomeric octanoate precursor (Figure 71). The diethyl chromium intermediate could then undergo facile elimination of ethane as depicted in Figure 70 to form a Cr(I) ethylene complex, which is a favored pathway via DFT calculations for a tantalum based trimerization catalyst.[121] In contrast the chloride precursor will dimerize more readily in the early stage of the reaction leading to either disproportionation or bimetallic reductive elimination to Cr(II). Unfortunately, at this stage the direct comparison of pyrrole ligand effects on catalytic performance is impossible due to the different nature of complexes **23-28**. However, based on the model of catalytic performance discussed above, it can be proposed that a major role of the pyrrole ligand is in the control of the formation of the active catalytic intermediates via hemilability. Thus, the further understanding of the effects of the pyrrole substituents on this hemilability, as well as on the energy of transition states and intermediates in the catalytic cycle will provide further insights into how to rationally optimize the catalyst. Based on the experimental results discussed above indicating extensive pyrrolide hemilability, the thermodynamic and kinetic stability of the unbound aluminum pyrrolides must be considered as they are possibly in equilibrium with the pyrrolide-bound chromium intermediates. One possibility is that some control of the bonding properties of pyrrole to chromium can be achieved through the variation of the concentration and nature of the aluminum cocatalyst (which also binds to pyrrole and can thus compete with chromium for free pyrrolide ligands).

4.4.3 Effect of cocatalyst and chloride

The analysis of the experimental results discussed above furnishes an underlying mechanistic basis for the established effects of the aluminum alkyl concentration and composition on the catalytic performance. The well-defined chloride-containing Cr(I) and Cr(III) pyrrolyl complexes were found to trimerize ethylene selectively, while the chloride-free complex **27** was non-selective. As predicted in the [SNS]Cr system, it is also proposed that cocatalyst hemilability is necessary for selectivity

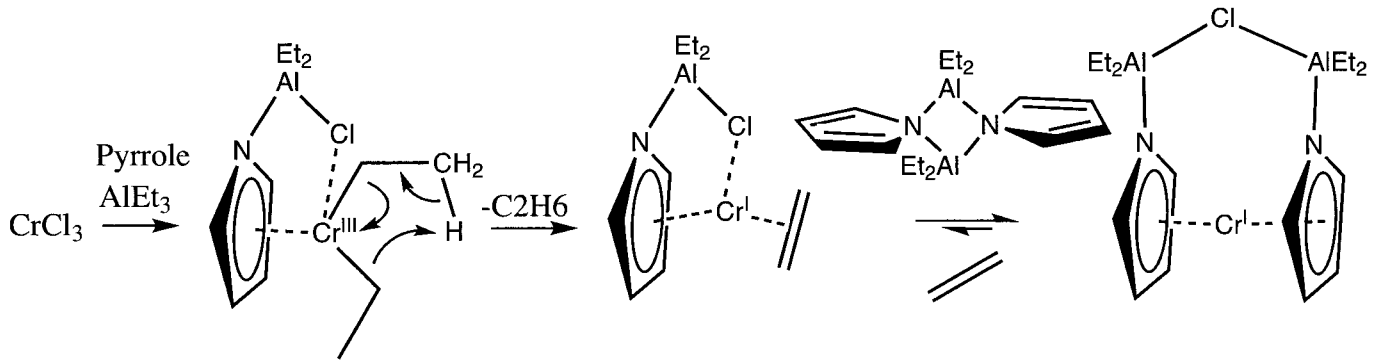

Figure 70: Proposed monomeric concerted two-electron reduction mechanism in formation of Cr(I) pyrrolide precursor.

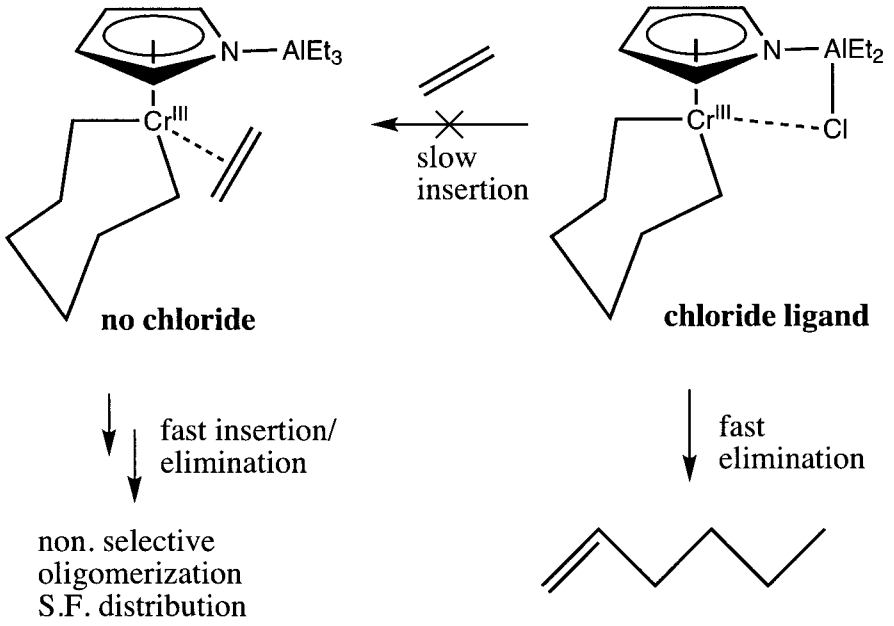

Figure 71: Non-selective vs. selective pyrrole catalyst via chloride hemilability.

due to via the aluminum-bridged chloride in close proximity to chromium which prevents rapid insertion of ethylene into metallacycle intermediates. The absence of this chloride hemilability to chromium which would lead to non-selective oligomerization as the rate of metallacycle growth will be higher than the rate of collapse due to the rapid insertion of ethylene into the coordinatively unsaturated metallacycle intermediates (Figure 71).

In addition to the effect of chloride ligand on selectivity, it was also found that additional aluminum cocatalyst was required to achieve high activity, suggesting that free trialkylaluminum coordination to the bis-pyrrolyl Cr(I) complex extracts one pyrrolide and activates the chromium centre as depicted in Figure 72. Thus the energies of the resulting species are responsible for the

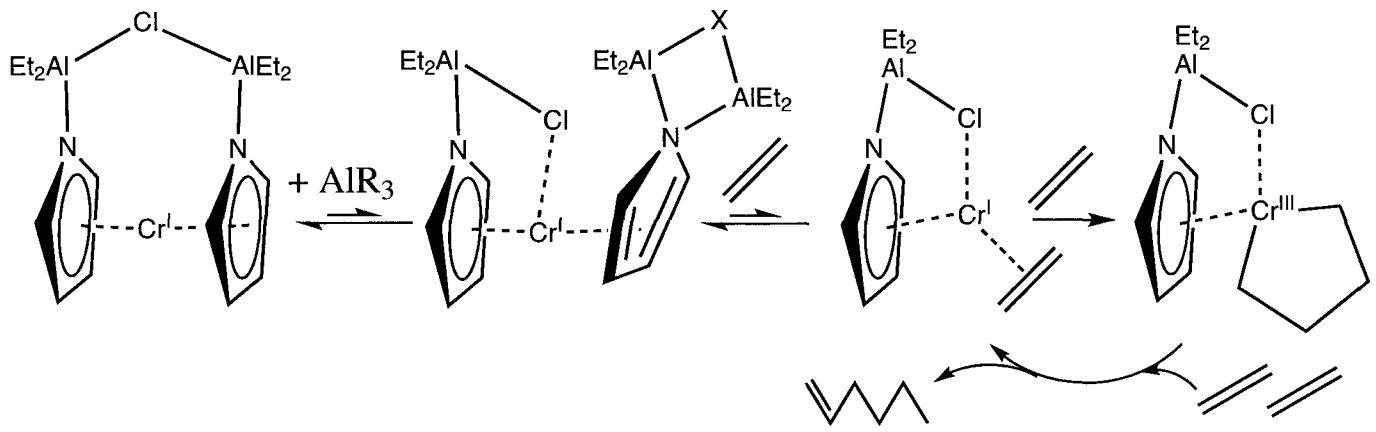

Figure 72: Proposed effect of cocatalyst

observed catalytic performance and can be rationalized in terms of these mechanistic features.

4.4.4 Effect of Solvent

The effect of the solvent is well known in catalytic performance, and some mechanistic insights into the effect of solvent on the coordination chemistry of chromium are now available to help to rationalize the observed behavior. The poisoning effect of toluene in the Phillips catalytic systems can now be understood in terms of the nature of the catalytically active species (Figure 73). Assuming that the proposed bis-pyrrolyl Cr(I) complex dissociates one pyrrole ligand to vacate the necessary coordination sites, it is conceivable that toluene could simply bind and form a kinetically inert Cr(I) bis-arene structure. The same ligand dissociation in methylcyclohexane would allow ethylene to coordinate, without the unfavorable competition of the arene solvent. Thus, the fact that Cr(I) arene complexes are highly kinetically inert means that once a bis-arene chromium (I) species forms the catalyst is effectively deactivated. A previous study by Kohn also made this conclusion, as an inactive chromocene was isolated in a different trimerization catalyst.[122]

4.4.5 Mechanistic speculation

In summary of the mechanistic effects which are proposed to underlie the established experimental parameters discussed above, the following mechanistic speculation for the chromium pyrrolyl based ethylene trimerization catalyst can be drawn (Figure 74). It summarizes the current state of the knowledge of the pyrrolide chromium catalyst. Loss of one pyrrolide ligand from a stable bis-

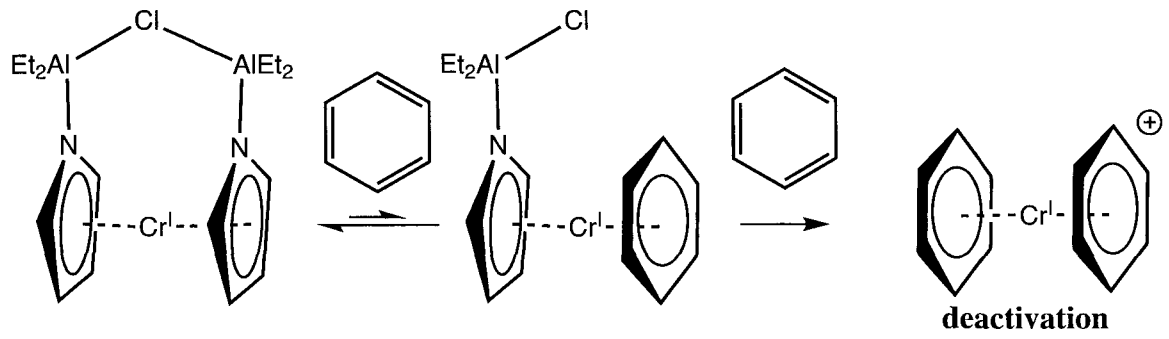

Figure 73: Proposed effect of aromatic solvent

pyrrolide species (a possible resting state for the catalyst) is expected to generate a reactive mono-pyrrolide olefin intermediate which can rapidly couple two ethylenes to form a bridging chloride-stabilized metallacyclopentane intermediate. The hemilable chloride can dissociate to generate a reactive chromacyclopentane intermediate which inserts ethylene and either collapses to either the bis-olefin intermediate or the catalytic resting state.

Thus, if this speculation proves correct, then the major mechanistic key to the ethylene trimerization process based on chromium has been found, which can lead the way to rational catalyst design and future optimization. In addition, at the centre of the scheme is the proposal that the comproportionation of Cr(III) and Cr(I) intermediates to form bimetallic Cr(II) intermediates can produce polyethylene as discussed in more detail below (Figure 75).

As polymer is invariably formed in all trimerization catalysts, it was proposed that an equilibrium exists between the proposed trimerization active mono-pyrrolide Cr(I) and Cr(III) intermediates with the polymerization-active bis-pyrrolide Cr(II) intermediates. Thus certain experimental parameters can favors either Cr(II) or Cr(I) and Cr(III), such as the ligand, aluminum alkyl, ethylene and halogen concentrations in solution. The main kinetic pathway which allows the interconversion between Cr(I)/Cr(II)/Cr(III) assumed to be the disproportionation/comproportionation pathway of bimetallic chromium (II) intermediates as discussed in previous chapters. Thus, the understanding of how the experimental parameters which control the selectivity also affect this underlying pathway and the relative equilibria of the intermediates is critical to rational trimerization catalyst design and optimization in the future. Although this proposal based on disproportionation of bimetallic Cr(II) intermediates is purely speculative, it can lead to direct experimentation and

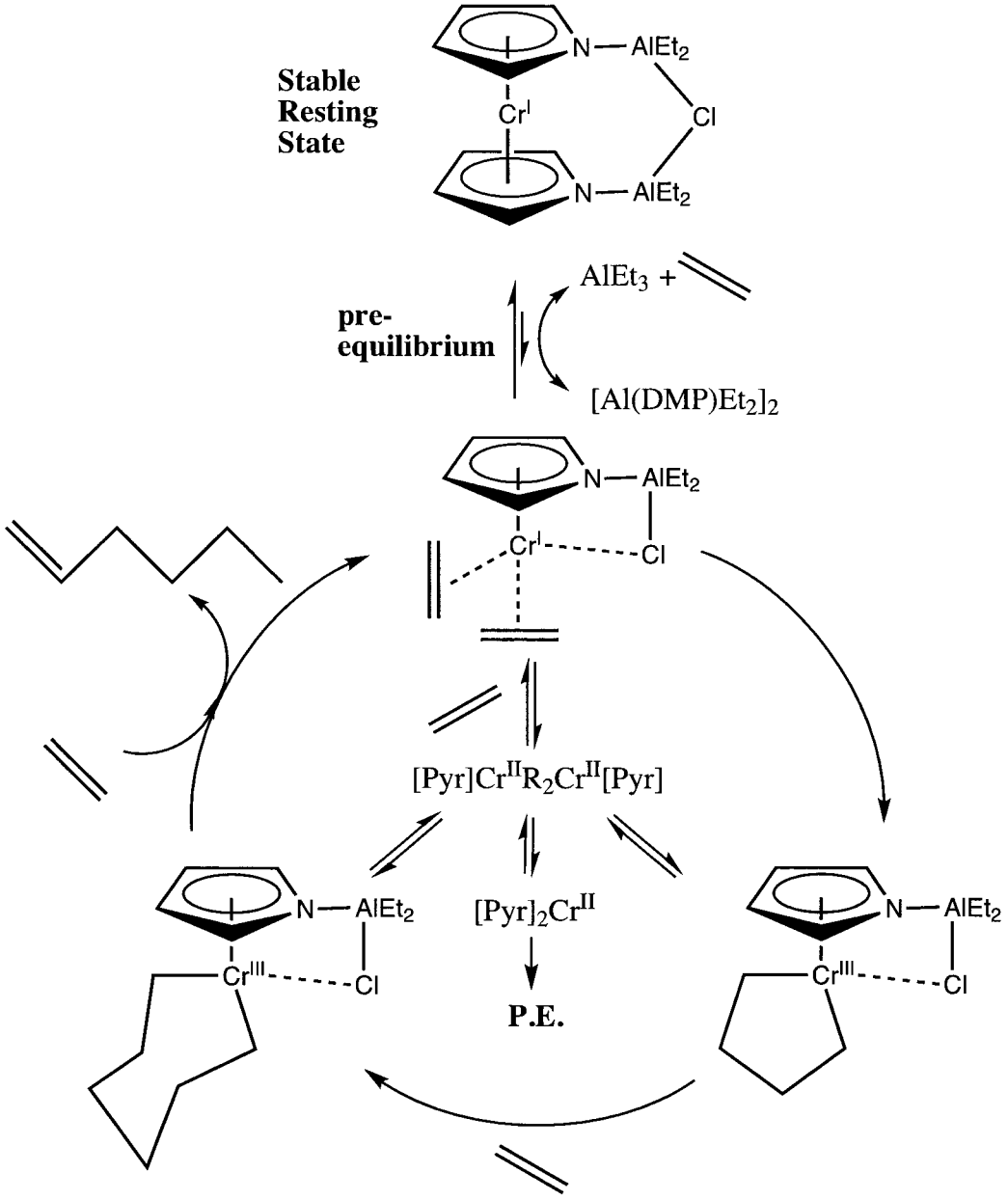

Figure 74: Proposed resting states and intermediates in pyrrole chromium catalyzed ethylene trimerization

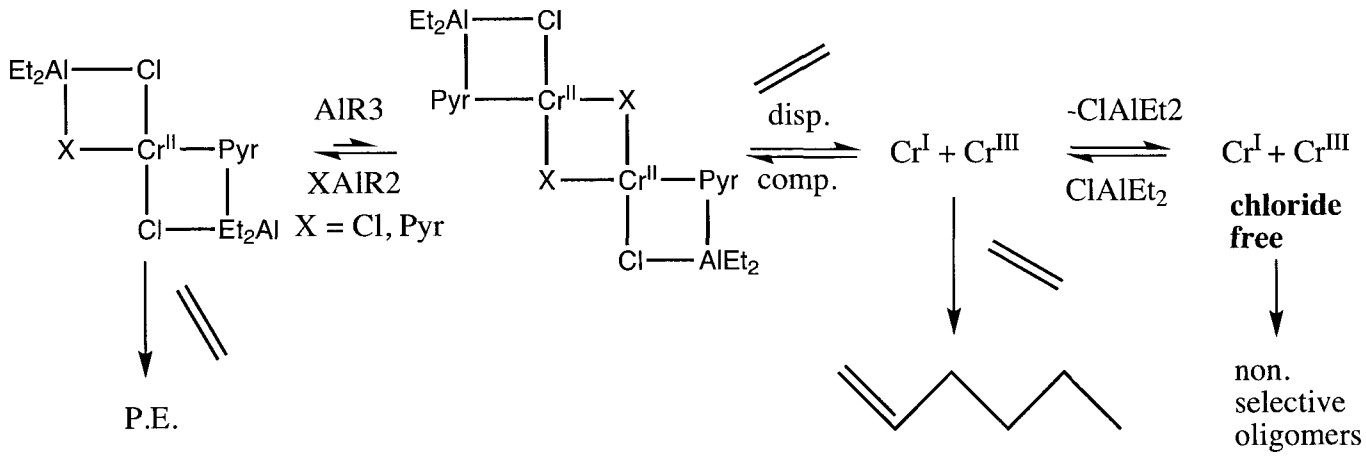

Figure 75: Proposed chloride effect on both polymer/1-hexene selectivity via linked rapid I-II-III disproportionation/comproportionation

DFT analysis. For example, it would be of interest for industry to study mixed-pyrrole systems which contain a more labile pyrrole ligand which would lead to a higher concentration of active Cr (I)/Cr (III) trimerization catalyst in solution and suppress formation of the undesirable bis-pyrrole Cr(II) polymerization catalyst (Figure 76).

4.5 Conclusions - Cr Pyrrole System

Although the first part of the chapter, dealing with anionic pyrrolide salts reacted with chromium precursors, did not result in the isolation of catalytic intermediates, they may give rise to highly reactive catalytic species when properly activated. This is being pursued by researchers in our group currently. The main objective, however, was the isolation and analysis of well-defined complexes from the catalytic mixtures. This objective has been completed by utilizint the in-situ activation procedure as developed by commercial producers. Thus based on this initial mechanistic study some interesting questions specific to the dynamics and equilibria that underlie the chromium-pyrrole trimerization catalyst have been raised, and may lead to a rational catalyst development in the future. In addition, some of the redox themes encountered in the [PNP] and [SNS] system have been implicated strongly in the pyrrole system as well, suggesting that chromium trimerization catalysts are mechanistically similar in their underlying organochromium redox chemistry.

Finally, the key unexpected discovery in this work is the isolation of well-defined single-

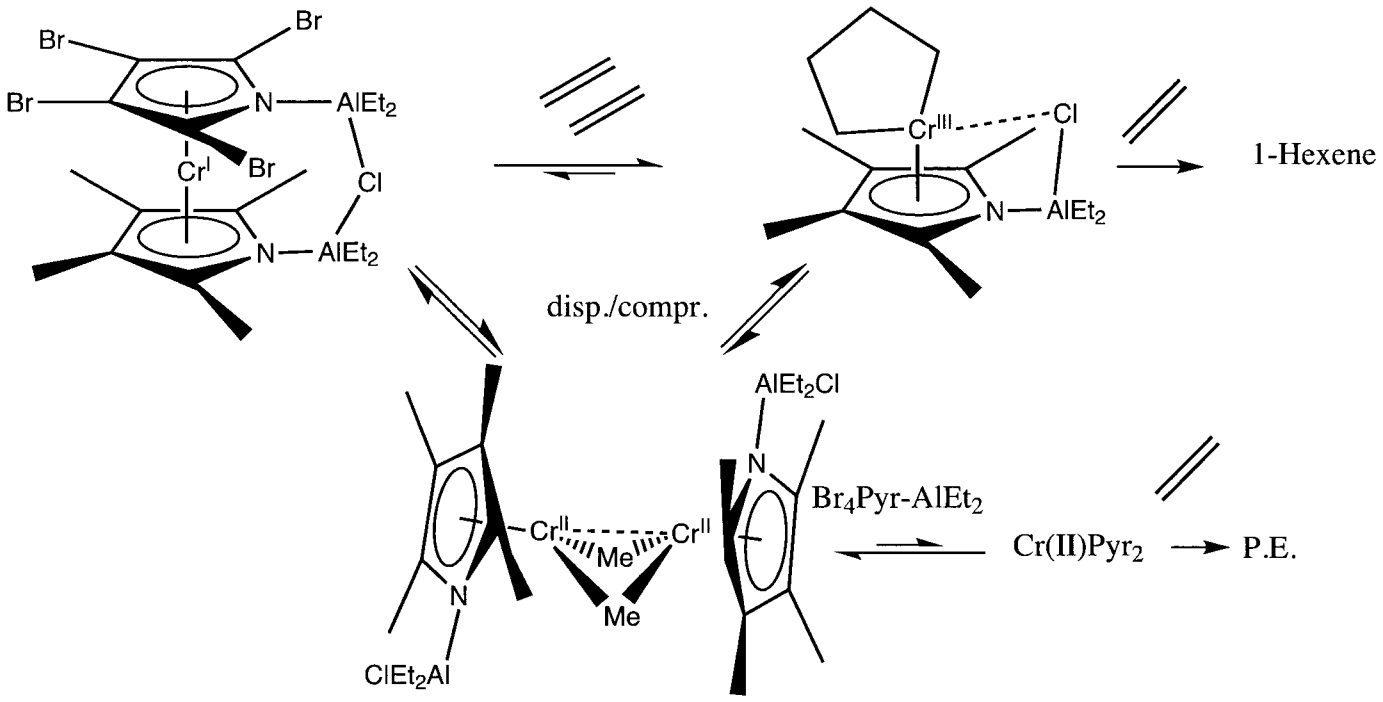

Figure 76: Proposed optimized mixed-ligand trimerization catalyst.

component polymerization and trimerization catalysts using inexpensive aluminum alkyl reagents rather than the more expensive cocatalysts like MAO or trityl borane. This is attributed to the hemilabile properties of the pyrrole donor which increases the kinetic lability of the otherwise inert species usually requiring strong MAO activation. Thus the pyrrole ligand may form the basis of a polymerization catalyst platform with other metals which will afford the cost-benefits of using small amounts of aluminum activators. An additional benefit to academic researchers is the well-defined nature of the catalytic resting states and/or precursors in the pyrrole system, which allows for the isolation and mechanistic analysis of these intermediates, which can aid further rational development. Thus, the pyrrolide ligand platform is expected to provide an ideal set of features which will bring together both industrial and academic researchers for many years to come. Wishing to further understand the underlying mechanistic pyrrole effects related to olefin polymerization, studies were initiated in the course of this thesis to isolate catalytic resting states containing the pyrrole ligand with vanadium and titanium. These studies, in addition to the study of the fundamental reactivity of pyrrole ligands with aluminum alkyls, composes part (II) of this thesis.

Conclusions from Part I: Mechanistic investigation of chromium catalyzed ethylene trimerization/tetramerization

The previous three chapters on the mechanistic study of chromium catalyzed ethylene trimerization has raised some unprecedented conclusions related to the general nature of the organochromium intermediates involved in the chemistry. These major insights are discussed in the following categories: ligand directed-cocatalyst hemilability, bimetallic redox chemistry, comparative ligand effects, possible catalytic resting states, and is concluded with a general overview of the mechanistic pathways encountered.

Ligand directed cocatalyst hemilability in ethylene trimerization

This idea comes from the observation of the unexpected coordination properties of the acidic [SNS] ligand N-H group, which was found to direct the aluminate anion via hydrogen bonding to coordinate loosely to chromium. The other example in this category is the pyrrole system which also forms a strongly directed heterobimetallic species which results in a critical hemilabile donation from the chloride attached to aluminum. These weak hemilabile interactions are proposed to play a critical role in determining the selectivity of the oligomerization catalyst by changing the relative rate of insertion of ethylene to the rate of elimination of the alpha-olefin product.

Bimetallic redox chemistry

This second point comes from the discussion of all three chapters, where bimetallic intermediates are proposed to play a large role in the observed catalytic sysem. From the [SNS] system it was found that a bimetallic Cr(II) intermediates underwent disproportionation, while in the case of the [PNP] system it was found that a bimetallic Cr(III) complex undergoes reductive C-C coupling to a bimetallic Cr(II) species. Finally, there was indirect evidence bimetallic chromium pyrrolide

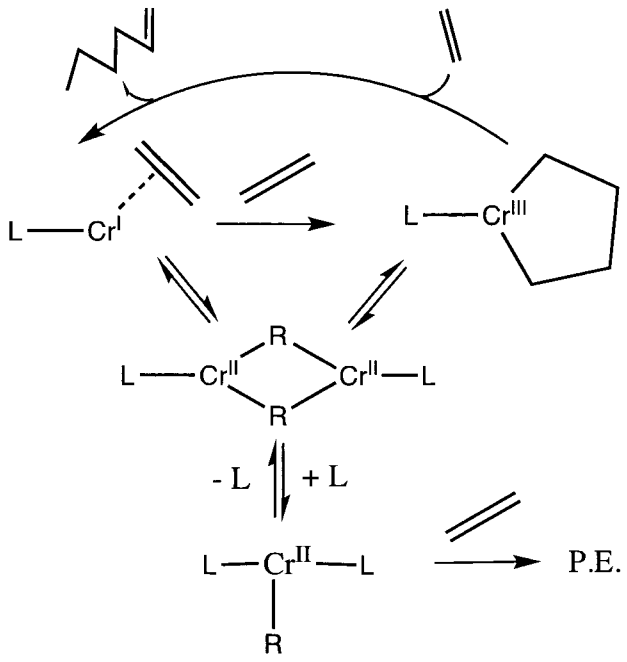

Figure 77: General summary of proposed mechanistic pathways in ethylene trimerization.

intermediates being involved in disproportionation/comproportionation from the fact that polymer is produced by Cr(II) and oligomers are produced by Cr(I) and Cr(III). Based on the similar conclusion that there is extensive bimetallic redox chemistry in the catalysis with three ligand systems, a general mechanistic scenario for the redox chemistry in chromium catalyzed ethylene trimerization is outlined in Figure 78.

Evidence for catalytic resting states

Generally in catalysis, one or more species are the main observed complex in the catalytic system. Usually these complexes are not in fact catalytic intermediates but stable pre-catalysts whicha are also called resting states. The fact that under these catalytic conditions some well-defined complexes were isolated which were obviously not catalytic intermediates suggests that these species that are stable are also the catalytic resting states. However certain parameters were not explored limiting the accuracy of these predictions based purely on a few complexes. Thus the activation of these species to form the active catalytic intermediates is expected to be the subject of intense study in the future.

Ligand effects on the underlying organochromium transformations.

From the comparison of the [SNS], [PNP], and pyrrole ligands, it was found that the catalyst resting state differed for each ligand. In the [SNS] system, the catalyst resting state was most likely a Cr(III) species, while in the [PNP] system it was most likely Cr(II), and in the pyrrole system it is most likely Cr(I). In addition to these conclusions, the [PNP] system illustrated the effect of coordinatively unsaturated chromium centres, resulting in bimetallic Cr(III) intermediates which can allow for C-C coupling.

Future catalyst development

Future catalyst development could focus on elaborating on this basic mechanistic model, and the thermodynamic equilibria of all the intermediates their relative kinetic barriers (possibly via the transition state geometry and energy via DFT calculations) to interconversion, as well as the development of more accurate models which can better match the experimental results and be used for the successful kinetic modelling and design of improved catalysts. For instance, the rational development of tetramerization catalysts in the future could rely on the effect of close tethering two chromium centres on the resulting bimetallic reactivity and catalytic selectivity, and how various types of spacing between the chromium centres could alter this selectivity. This type of catalyst development has never been proposed before, but is a logical progression based on the questions raised above in this thesis. Other trimerization catalyst development could focus on the synthesis of ligands containing hemilabile donors. In addition, electrochemistry can be conducted in the ionic solvents used in trimerization catalysis, which may shed more light on the redox chemistry of chromium in catalytic conditions.

Part II

Pyrrole as a hemilabile ligand in catalytic olefin polymerization

5 Exploration of vanadium pyrrolide complexes for ethylene polymerization catalysis

Abstract

This chapter discusses the exploration of the coordination properties of the pyrrolide ligand in vanadium-based olefin polymerization catalysis. The attempt to synthesize a well defined vanadium pyrrolide precursor by the reaction of LiDMP with $VCl_3(THF)_3$ resulted in the formation the mixed valent ionic species, $\{(THF)_3V^{II}(\mu\text{-}Cl)_3V^{II}(THF)_3\}$ $\{(\eta^1\text{-}DMP)_4V^{III}\}$ (**29**). The in-situ reaction of $VCl_3(THF)_3$ with DMP and excess Me_3Al led to the formation of the V(II) sandwich complex, $\{(\eta^5\text{-}DMP\text{-}AlMe_2Cl)_2V^{II}\}$ (**31**). The reaction of **31** with azobenzene led to its oxidation to the dimeric mono-DMP V(IV) bridging-imido methyl, $\{[(\eta^5\text{-}DMP\text{-}AlMe_2Cl)V^{IV}Me(\mu\text{-}NPh)_2]_2\}$ (**32**), which is direct confirmation of alkyl-migration from aluminum to vanadium via pyrrolide ring slippage. The treatment of **31** with $(SiMe_3)N_3$ resulted in an imido-bridged V(IV) dimer, $\{[(\eta^5\text{-}DMP\text{-}Me_2Al(\eta^1,\mu\text{-}N_3)AlMe_2(\mu^3\text{-}N)]V^{IV}Me]_2\}$ (**33**), which is the product of extensive $SiMe_3$-N bond cleavage that results in the unusual $(Me_2Al(\eta^1,\mu\text{-}N_3)AlMe_2)$ bridging unit. When the same in-situ preparation with $VCl_3(THF)_3$ and Me_3Al is carried out with the sterically hindered TMP ligand, the binuclear mono-TMP V(III) methyl dimer, $\{[(\eta^5\text{-}TMP\text{-}AlMe_2Cl\}V^{III}(\mu\text{-}Me)(\mu\text{-}Cl)]_2\}$ (**34**), is isolated. The in situ preparation method using $VCl_3(THF)_3$, DMP and the highly reducing Et_3Al cocatalyst allowed the isolation of the pentanuclear vanadium cluster, $\{[(\eta^5\text{-}DMP\text{-}AlEt_2Cl)V^{II}(\mu^3\text{-}H)]_4V(\mu^3\text{-}H)_2\}$ (**35**), containing a μ^3-hydride ligand capping each of the six triangular vanadium faces. The hydride **35** is proposed to derive via β-H elimination from a highly reactive $\{[(\eta^5\text{-}DMP\text{-}AlEt_2Cl)V^{II}Et]_n\}$ intermediate. This proposal is supported by the oxidative trapping of the intermediate V^{II}ethyl with azobenzene, allowing the isolation of the dimeric vanadium(IV) μ-imido ethyl complex, $\{[(\eta^5\text{-}DMP\text{-}AlEt_2Cl)V^{IV}Et(\mu\text{-}NPh)_2]_2\}$ (**36**). Finally, the in-situ preparation using the $^iBu_3Al$ cocatalyst resulted in the isolation of the trinuclear cluster, $\{[(\eta^5\text{-}DMP\text{-}Al^iBu_2Cl)V^{II}(\mu\text{-}Cl)]_2(\mu\eta^1\eta^5\text{-}DMP)V^{II}\}$ (**37**). The readily available complexes **31**, **32**, **34**, and **36** were evaluated in ethylene polymerization catalysis, revealing that the pyrrolide hemilability imparts unprecedented catalytic performance and selectivity to the vanadium centres.

5.1 Introduction

This chapter describes the experimental exploration of the hemilabile pyrrole ligand in olefin polymerization catalysis. The experimental methodology described in part II is derived from part I, which focused on the isolation of catalytically active species in ethylene trimerization. The introduction to this thesis and the previous chapter discussed the importance of pyrrole hemilability in catalysis. Thus the unique hemilability of pyrrole was concluded to be of potential value to polymerization catalysis with other established early metals such as vanadium and titanium, which are discussed in this and the next chapter.

Among the plethora of metals capable of performing ethylene polymerization, oligomerization, and copolymerization, vanadium has traditionally played a relatively minor role commercially. Nonetheless, the perfectly random copolymerization performed by some vanadium catalysts makes these derivatives commercially irreplaceable.[123] The major issue preventing more widespread commercialization of vanadium based polymerization catalysts is the instability of vanadium (III) alkyl bond in commercially valuable catalysts, due to rapid reduction to the kinetically inert vanadium (II) products. Commercial catalysts use oxidizing agents to reoxidize the inactive V(II) to the higher oxidation states. Thus, the mechanistic understanding of important factors to the stabilization of organovanadium (III) intermediates has been limited by the absence of well-defined catalytically active species in the literature. The pyrrole ligand was expected to be ideally suited for the isolation and study of these vanadium polymerization catalyst resting states, to gain a key mechanistic piece to the vanadium polymerization mechanistic puzzle.

Recent reports of a highly active vanadium (V) based catalyst for olefin metathesis[124] and a vanadium (I) based ethylene trimerization catalyst[68] have also renewed interest in the development catalysts based on this metal. One of the most attractive features is the great versatility of vanadium in carrying out a variety of catalytic transformations through several oxidation states. The unparalleled ability of the pyrrolide ligand to stabilize a wide range of metal oxidation states coordinative flexibility is expected to make vanadium pyrrolide systems particularly versatile. [124, 125, 68]

5.2 Experimental Procedure

All manipulations were carried out using standard Schlenk line or drybox techniques under an atmosphere of dry dinitrogen. Protio solvents were dried using an aluminum oxide solvent purification system. Deutero solvents were predried over activated 4 Å molecular sieves and were refluxed over the appropriate drying agent, distilled, and stored under dinitrogen. NMR samples were prepared under dinitrogen in 5 mm Wilmad 507-PP tubes flame sealed under dinitrogen using standard Schlenck apparatus. ^{1}H, and $^{13}C\{^{1}H\}$, NMR spectra were recorded on a Bruker Avance 300 MHz multinuclear NMR instrument. ^{1}H and ^{13}C assignments were confirmed when necessary with the use of DEPT-135, DEPT-90, and two-dimensional ^{1}H-^{1}H and ^{13}C-^{1}H NMR experiments. ^{1}H and ^{13}C spectra were referenced internally to residual protio solvent (^{1}H) or solvent (^{13}C) resonances and are reported relative to tetramethylsilane (δ) 0 ppm). Chemical shifts are quoted in δ (ppm), and coupling constants in hertz. Samples for magnetic susceptibility were preweighed inside a drybox equipped with an analytical balance and measured on a Johnson Matthey Magnetic Susceptibility balance. Elemental analysis was carried out with a Perkin-Elmer 2400 CHN analyzer. Data for X-ray crystal structure determination were obtained with a Bruker diffractometer equipped with a 1 K Smart CCD area detector.

5.2.1 $\{(THF)_3V^{II}(\mu\text{-}Cl)_3V^{II}(THF)_3\}$ $\{(\eta^1\text{-}DMP)_4V^{III}\}$ (29)

To a solution of DMP (190 mg mg, 2 mmol) in THF (10 mL) was slowly added nBuLi (0.84 mL of a 2.5 M solution in hexanes, 2.1 mmol), resulting in a pale yellow solution. To this solution was added $VCl_3(THF)_3$ (373 mg, 1 mmol) resulting in a dark green solution. The solution was taken to dryness and the residue was redissolved in THF (10 mL), filtered and then layered with hexanes (10 mL) resulting in the formation of green crystals of **29** (224 mg, 66 %). μ_{eff}= 3.41 μ_B average per vanadium centre. Elemental analysis (%) calcd for C48H80Cl3N4O6V3: C 53.93, H 7.49, N 5.24; found: C 53.88, H 7.39, N 5.08.

5.2.2 In-situ reaction of $V(acac)_3$ with DMP and Me_3Al: formation of 30.

To a solution of $V(acac)_3$ (348 mg, 1 mmol) and DMP (190 mg, 2 mmol) in toluene (10 mL) was added Me_3Al (432 mg, 6 mmol) resulting in a dark brown solution from which colorless crystals of **30** (160 mg, 45 %) deposited within minutes. Elemental analysis could not be carried out due to the highly pyrophoric nature of **30**.

5.2.3 $\{(\eta^5\text{-DMP-AlMe}_2\text{Cl})_2\text{V}^{\text{II}}\}$ (31)

A purple solution of $VCl_3(THF)_3$ (367 mg, 1 mmol) in toluene (7 mL) was combined with a freshly prepared solution of Me_3Al (432 mg, 6 mmol) and DMP (190 mg, 2 mmol) in toluene (7 mL). The color of the mixture immediately changed to black-green. The solution was stirred for a period of 10 minutes, centrifuged to eliminate a small amount of insoluble brown pyrophoric residue, and layered with an equal portion of hexanes to yield black-green plates of **31** (250 mg, 0.63 mmol, 63 %). μ_{eff}= 3.83 μ_B. Elemental analysis (%) calcd for C16H28Al2Cl2N2V: C 45.01, H 6.53, N 6.51; found: C 45.30, H 6.65, N 6.60.

5.2.4 $\{[(\eta^5\text{-DMP-AlMe}_2\text{Cl})\text{V}^{\text{IV}}\text{Me}(\mu\text{-NPh})_2]_2\}$ (32)

Method A: **31** (398 mg, 1 mmol) in chlorobenzene (15 mL) was treated with azobenzene (91 mg, 0.5 mmol). The color immediately changed to dark red. Crystals of **32** (270 mg, 88 %) separated upon slow diffusion of hexane into the chlorobenzene solution.

Method B: A solution of Me_3Al (288 mg, 4 mmol) and 2,5-dimethylpyrrole (95 mg, 1 mmol) in chlorobenzene (7 mL) was added to a purple solution of $VCl_3(THF)_3$(367 mg, 1 mmol) and azobenzene (91 mg, 0.5 mmol) in chlorobenzene (7 mL). The addition was accompanied by an immediate color change to dark red. The solution was stirred for a period of 10 minutes, centrifuged, and layered with an equal portion of hexanes to yield dark red crystals of **32** (283 mg, 92 %). Compound contains a small amount of residual paramagnetism, but solubility was too low to record the NMR spectra in any non-coordinating solvents. Elemental analysis (%) calcd for C30H44Al2Cl2N4V2: C 52.38, H 6.38, N 8.07; found: C 52.41, H 6.45, N 8.15.

5.2.5 {[(η^5-DMP-$Me_2Al(\eta^1\mu$-$N_3)AlMe_2(\mu^3$-N)]$V^{IV}Me]_2$} (33)

31 (398 mg, 1 mmol) in toluene (15 mL) was treated with $(SiMe_3)N_3$ (115 mg, 1 mmol), accompanied by gas evolution and a color change to dark blue. The solution was centrifuged and stored for one week at -35°C resulting in the formation of a small amount of blue crystals of **32** (60 mg, 17 %) accompanied by an oily red material which prevented complete characterization.

5.2.6 {[(η^5-TMP-$AlMe_2Cl$}$V^{III}(\mu$-Me)(μ-Cl)$]_2$} (34)

Me_3Al (288 mg, 4 mmol) was added to a solution of $VCl_3(THF)_3$ (367 mg, 1 mmol) and TMP (123 mg, 1 mmol) in toluene (15 mL) resulting in a green solution, which was quickly filtered and stored at -35°C for one week resulting in the growth of dark green crystals of **34** (247 mg, 73%) containing a molecule of toluene in the lattice. μ_{eff}= 2.23 μ_B per Vanadium centre. ESI-MS m/z: 590 ([M]-). Anal. Calcd (found) for C31.28H56.84Al2Cl1.72N2V2: C, 55.37 (55.38); H, 7.38 (7.31); N, 4.13 (4.13).

5.2.7 {[(η^5-DMP-$AlEt_2Cl)V^{II}(\mu^3$-H)$]_4V(\mu^3$-H$)_2$} (35)

To a purple solution of $VCl_3(THF)_3$ (367 mg, 1 mmol) in toluene (7 mL) was added dropwise over the course of 5 minutes a freshly prepared solution of DMP (95 mg, 1 mmol) and Et_3Al (504 mg, 7 mmol) in toluene (7 mL), accompanied by a gradual color change to black. The solution was stirred for a period of 1 h, stripped of solvent under vacuum till a black oil residue was left, which was redissolved in hexanes (10 mL), filtered and stored at -35°C for one month to yield a few dark black crystals of **35** (50 mg, 10%). Poor reproducibility and low yields prevented full characterization. ESI mass spectrum of **35** in toluene (M = C40H78Al4Cl4N4V5, Mr = 1119 m/z located). IR (KBr, cm-1, Nujol mull): (V-H overtones) 4381, 4336, 4251, 4168, 4090, 4055, 3946, 3798, strong signals: 3116, 3092, 2923 (nujol), weak signals (overtones): 2544, 2420, 2208, 2060, 1996, 1951, 1877, 1773, 1680, strong signals: 1408, 1499, 1455, 1384, 1355, 1277, 1244, 1055, 1006, 955, 838, 640. Compound was found to be highly paramagnetic via the Evans NMR tube method (as a large shift was observed between the capillary solvent and the solvent containing the vanadium complex).

5.2.8 {[(η^5-DMP-AlEt$_2$Cl)V^{IV}Et(μ-NPh)$_2$]$_2$} (36)

Et_3Al (456 mg, 4 mmol) was added to a solution of DMP (95 mg, 1 mmol), $VCl_3(THF)_3$(367 mg, 1 mmol) and azobenzene (91 mg, 0.5 mmol) in toluene (10 mL). The addition was accompanied by an immediate color change to dark red. The solution was stirred for a period of 10 minutes, centrifuged, and layered with an equal portion of hexanes to yield dark red crystals of **36** (242 mg, 63 %). Compound **36** is nearly diamagnetic, and was sufficiently soluble to record the ^{1}H NMR spectrum, but both the low solubility and slow decomposition to paramagnetic byproducts in solution at room temperature prevented the aquisition of a quality ^{13}C spectrum. ^{1}H NMR (300 MHz, CD_2Cl_2), δH (ppm) = 7.60 (m, 2H, NPh), 7.44 (m, 1H, NPh), 7.07 (m, 2H, NPh), 5.37 (s, 2H, PyrH), 2.44 (s, 6H, Pyr$(CH_3)_2$), 1.357 (t, J_{HH} = 3 Hz, 3H, VCH_2CH_3), 1.066 (t, J_{HH} = 5 Hz, 6H, $AlCH_2CH_3$), 0.974 (q, J_{HH} = 5 Hz, 4 H, $AlCH_2CH_3$), 0.01 (quartet of octet, J_{VH} = 10 Hz, J_{HH} = 3 Hz, 2H, VCH_2CH_3 (- strong methylene proton coupling to the spin (7/2) V nucleus is observed in the NMR spectrum)). Elemental analysis (%) calcd for C36H56Al2Cl2N4V2: C 55.99, H 7.25, N 7.25; found: C 60.00, H 7.11, N 7.31.

5.2.9 {[(η^5-DMP-Al^{i}Bu$_2$Cl)V^{II}(μ-Cl)]$_2$($\mu\eta^1\eta^5$-DMP)V^{II}} (37)

To a solution of $VCl_3(THF)_3$ (367 mg, 1 mmol) in toluene (7 mL) was added dropwise a mixture of DMP (95 mg, 1mmol) and Al^iBu_3 (1.4 g, 7 mmol) in toluene (7 mL), accompanied by an immediate color change to dark red. The solution was stirred for a period of 10 minutes, and stripped of solvent under vacuum to give a red oil which was then redissolved in hexanes (5 mL), filtered and stored at -35°C for two weeks to yield red plates of **37** (21 mg, 5 %). Due to high solubility, **37** could not be isolated in sufficient yields for full characterization and catalytic evaluation.

5.2.10 X-ray Data for vanadium pyrrolide complexes 29-37

Table 31: Crystal Data and Structure Analysis Results for Vanadium Pyrrole complexes **29-37**

Complex #	**29**	**31**	**32**	**33**
formula	C48H80Cl3	C16H28Al2	C30H44Al2	C21H43Al4
	N4O6V3	Cl2N2V	Cl2N4V2	ClN10V2
Mw	1068.33	424.20	687.43	680.90
space group	P2(1)/n	P2(1)/n	P-1	P-1
a (Å)	10.317(3)	8.227(2)	9.031(2)	9.971(2)
b (Å)	37.036(11)	18.349(5)	9.889(2)	12.963(3)
c (Å)	14.417(4)	8.263(2)	10.313(3)	14.656(3)
α	90	90	66.972(3)	114.998(3)
β	99.248(5)	119.116(4)	88.399(4)	97.344(4)
γ	90	90	89.769(4)	90.045(4)
V (Å^3)	5437(3)	1089.7(5)	847.3(4)	1699.6(6)
Z	4	2	1	2
radiation	0.71073	0.71073	0.71073	0.71073
T (K)	203(2)	208(2)	203(2)	208(2)
D_{calcd} (g cm^{-3})	1.305	1.293	1.252	1.330
μ_{calcd} (mm^{-1})	0.700	0.781	0.787	0.760
F000	2256	442	1847	708
R, Rw_2	0.0800, 0.1812	0.0486, 0.1341	0.0632, 0.1615	0.0783, 0.1587
GoF	1.015	1.051	1.060	0.952
Complex #	**34**	**35**	**36**	**37**
formula	C31.28H56.84	C43.75H86.75	C36H56Al2	C43.50H72
	Al2Cl1.72N2V2	Al4Cl4N4V5	Cl2N4V2	Al2 Cl4N4V3
Mw	677.80	1173.34	771.59	999.63
space group	P-1	P2(1)/n	P2(1)/c	P-1
a (Å)	8.792(2)	15.815(4)	8.9108(15)	12.118(3)
b (Å)	9.052(2)	24.607(7)	14.602(2)	15.035(4)
c (Å)	13.131(4)	17.212(5)	14.780(2)	15.799(4)
α	100.499(4)	90	90	98.337(4)
β	96.530(4)	113.590(5)	92.487(2)	104.303(4)
γ	112.912(3)	90	90	106.524(4)
V (Å^3)	926.6(4)	6138(3)	1921.4(5)	2601.3(11)
Z	1	4	2	2
radiation	0.71073	0.71073	0.71073	0.71073
T (K)	203(2)	200(2)	203(2)	203(2)
D_{calcd} (g cm^{-3})	1.215	1.270	1.334	1.276
μ_{calcd} (mm^{-1})	0.697	0.995	0.702	0.799
F000	360	2449	812	1048
R, Rw_{2a}	0.0430, 0.1097	0.0707, 0.1227	0.0439, 0.1036	0.0641, 0.1437
GoF	1.057	1.019	1.014	1.010

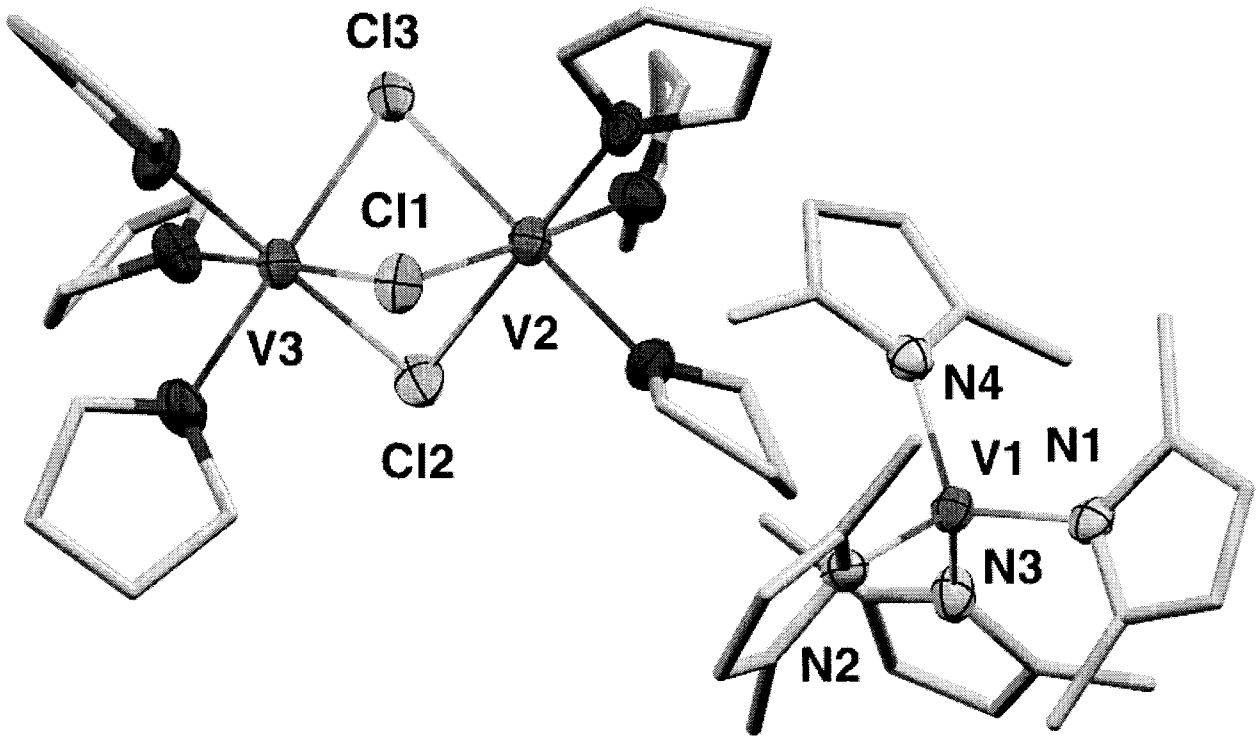

Figure 78: Partial thermal ellipsoid plot of $\{(THF)_3V^{II}(\mu\text{-}Cl)_3V^{II}(THF)_3\}$ $\{(\eta^1\text{-}DMP)_4V^{III}\}$ (**29**) with ellipsoids drawn at 50% probability.

Table 32: Selected Bond Distances (Å) and Angles (°) for $\{(THF)_3V^{II}(\mu\text{-}Cl)_3V^{II}(THF)_3\}$ $\{(\eta^1\text{-}DMP)_4V^{III}\}$ (**29**).

V(1)-N(3)	1.966(8)	N(3)-V(1)-N(1)	114.5(3)
V(1)-N(1)	1.970(7)	N(3)-V(1)-N(4)	101.2(3)
V(1)-N(4)	1.985(7)	N(1)-V(1)-N(4)	116.6(3)
V(1)-N(2)	1.991(7)	N(3)-V(1)-N(2)	113.0(3)
V(2)-Cl(3)	2.487(3)	N(1)-V(1)-N(2)	100.0(3)
V(2)-Cl(2)	2.488(3)	N(4)-V(1)-N(2)	112.2(3)
V(2)-Cl(1)	2.490(3)	Cl(3)-V(2)-Cl(2)	87.67(9)
V(3)-Cl(1)	2.462(3)	Cl(3)-V(2)-Cl(1)	86.86(9)
V(3)-Cl(2)	2.468(3)	Cl(2)-V(2)-Cl(1)	86.09(9)
V(3)-Cl(3)	2.471(3)		

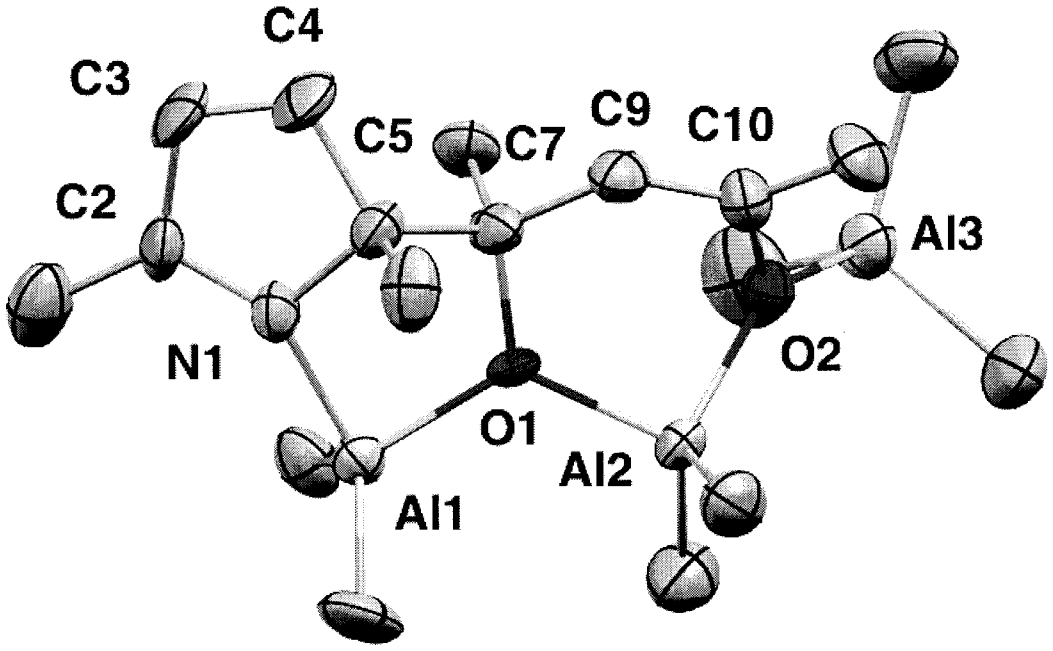

Figure 79: Partial thermal ellipsoid plot of **30** with ellipsoids drawn at 50% probability.

Table 33: Selected Bond Distances (Å) and Angles (°) for **30**.

Al(1)-N(1)	1.9494(3)	N(1)-Al(1)-O(1)	84.70
N(1)-C(2)	1.3213(4)	O(1)-Al(2)-O(2)	94.50
C(2)-C(3)	1.4615(3)	AL(2)-O(2)-AL(3)	128.28
C(3)-C(4)	1.2995(2)	AL(2)-O(1)-AL(1)	123.79
C(4)-C(5)	1.5065(4)	C(9)-C(10)	1.3499(3)
C(5)-C(7)	1.5354(4)	C(10)-O(2)	1.3882(3)
C(7)-C(9)	1.5006(3)	C(7)-O(1)	1.4654(3)

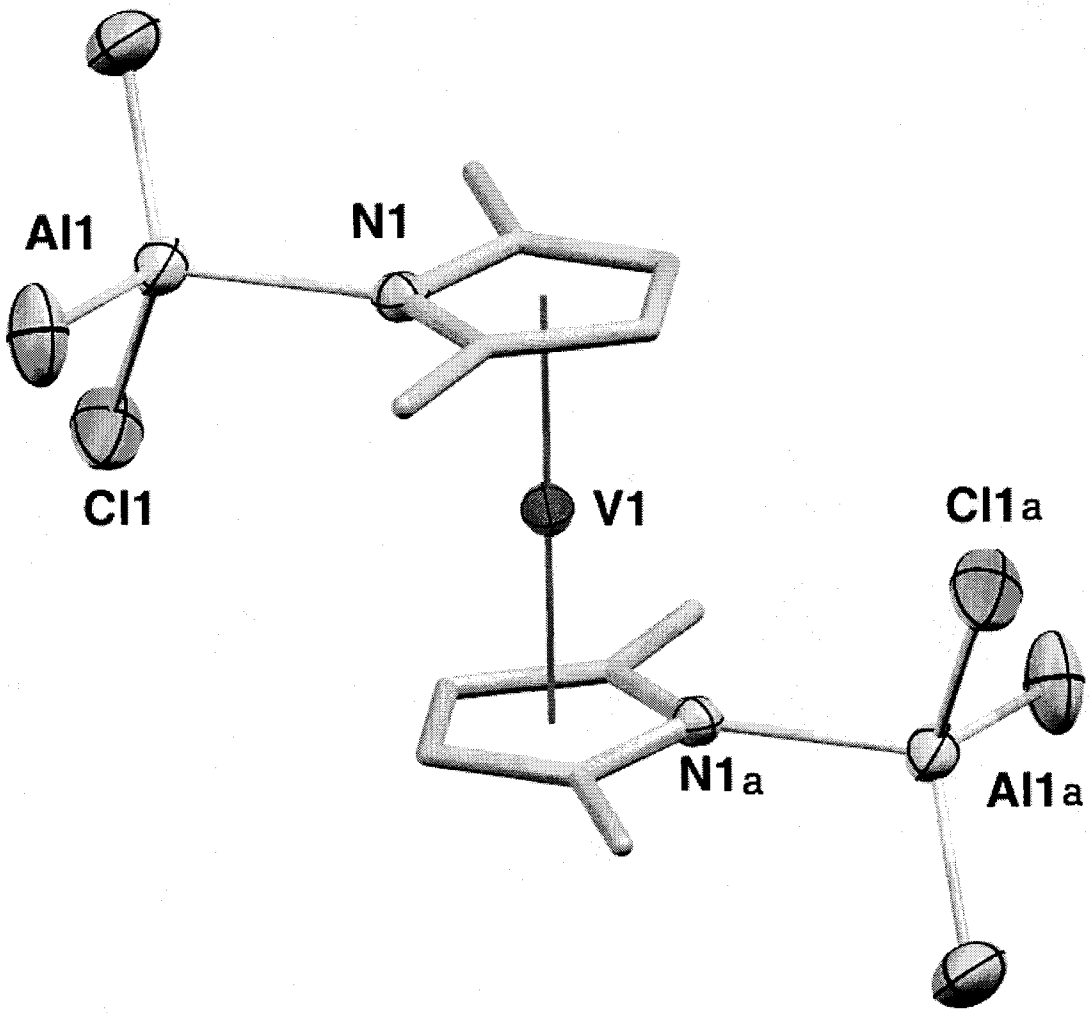

Figure 80: Partial thermal ellipsoid plot of $\{(\eta^5\text{-DMP-AlMe}_2\text{Cl})_2\text{V}^{\text{II}}\}$ (**31**) with ellipsoids drawn at 50% probability.

Table 34: Selected Bond Distances (Å) and Angles (°) for $\{(\eta^5\text{-DMP-AlMe}_2\text{Cl})_2\text{V}^{\text{II}}\}$ (**31**).

V1–N1	2.234(3)	V-Cnt-N	87.59
V-(Cnt)	1.939	Cnt-N-Al	172.31
N(1)-C(5)	1.396(4)	C(3)-C(4)	1.416(6)
N(1)-C(2)	1.409(4)	C(4)-C(5)	1.389(5)
C(1)-C(2)	1.485(5)	C(5)-C(6)	1.490(5)
C(2)-C(3)	1.387(5)		

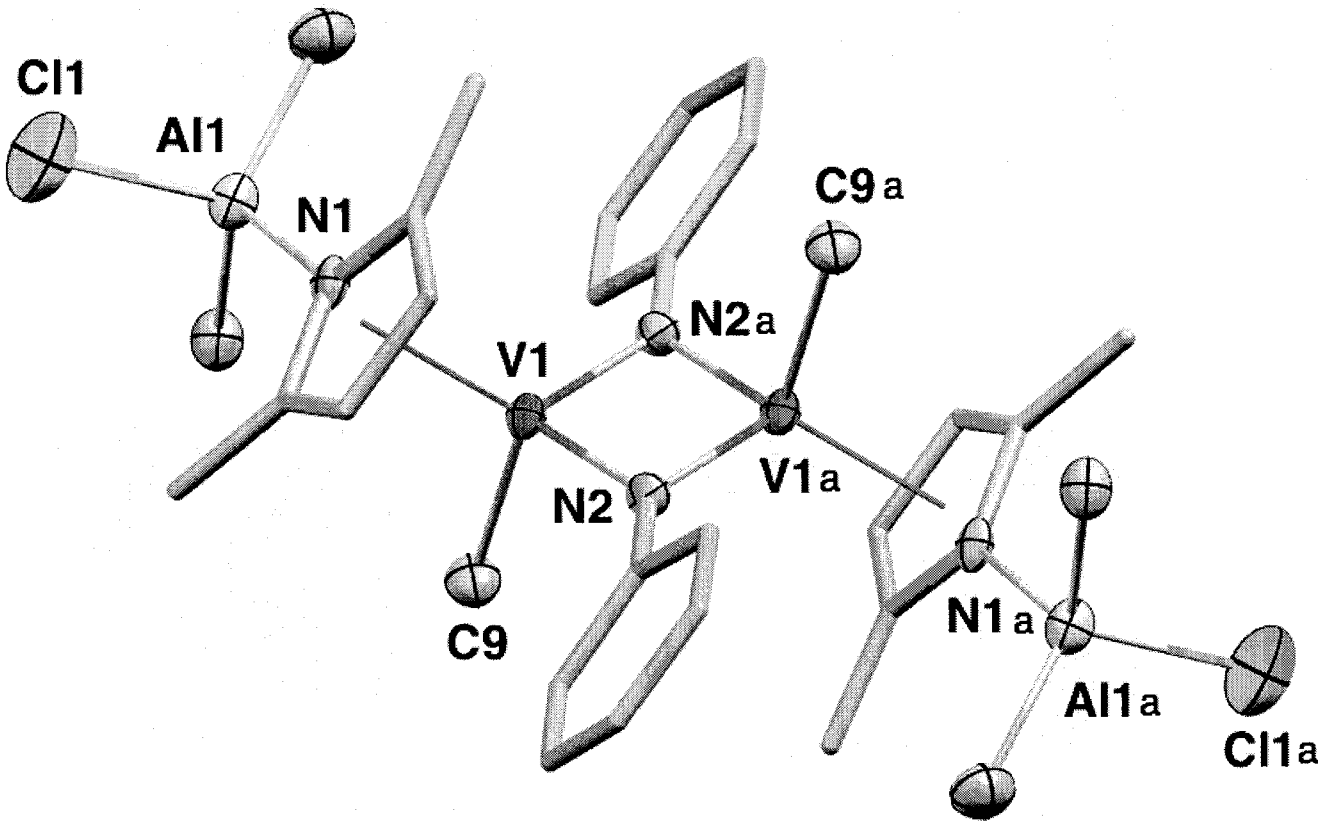

Figure 81: Partial thermal ellipsoid plot of $\{[(\eta^5\text{-DMP-AlMe}_2\text{Cl})\text{V}^{\text{IV}}\text{Me}(\mu\text{-NPh})_2]_2\}$ (**32**) with ellipsoids drawn at 50% probability.

Table 35: Selected Bond Distances (Å) and Angles (°) for $\{[(\eta^5\text{-DMP-AlMe}_2\text{Cl})\text{V}^{\text{IV}}\text{Me}(\mu\text{-NPh})_2]_2\}$ (**32**).

V1···V1a	2.511(2)	C2–C3	1.397(10)
V1–C9	2.083(7)	C3–C4	1.401(10)
V1–N2	1.861(5)	C4–C5	1.381(9)

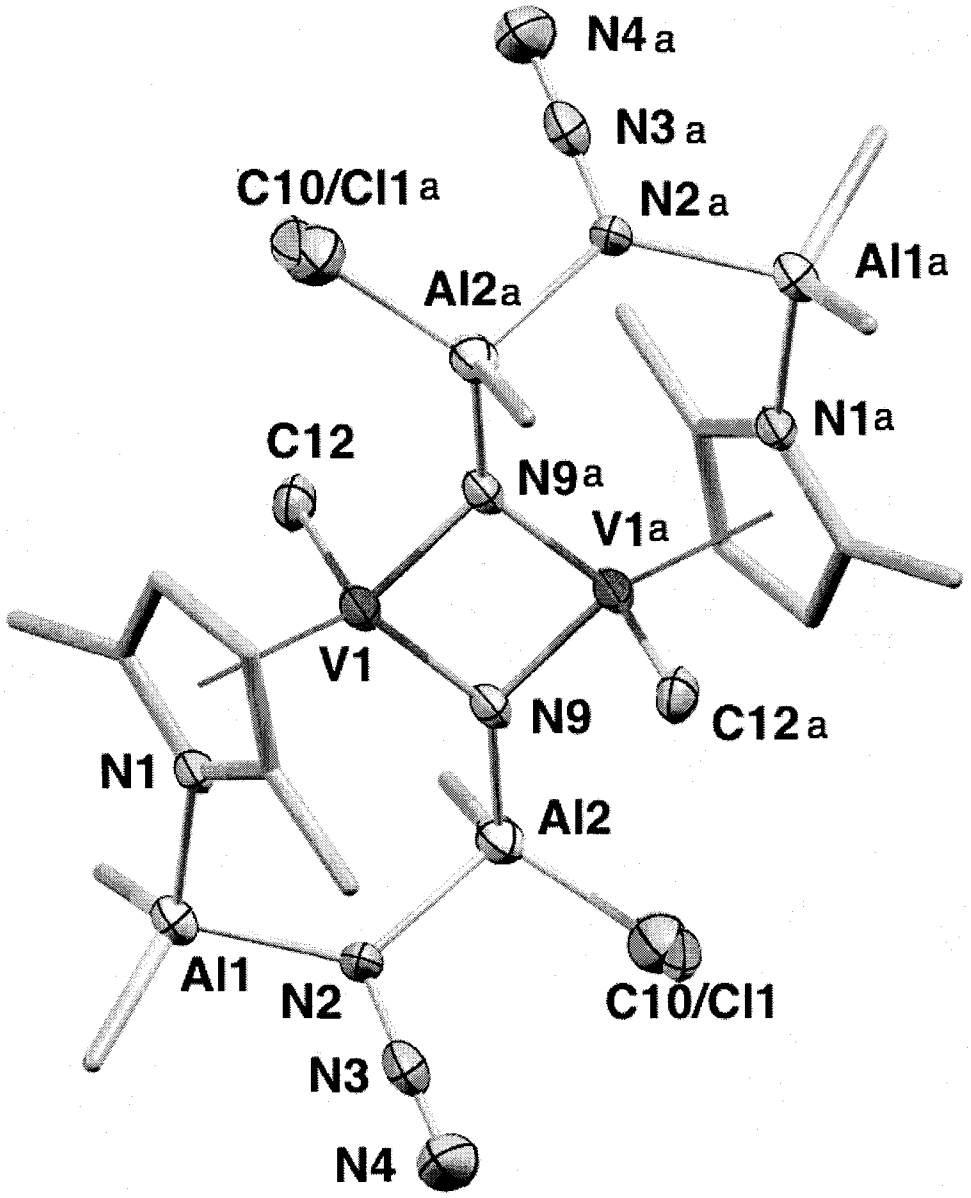

Figure 82: Partial thermal ellipsoid plot of $\{[(\eta^5\text{-DMP-Me}_2\text{Al}(\eta^1\mu\text{-N}_3)\text{AlMe}_2(\mu^3\text{-N})]\text{V}^{\text{IV}}\text{Me}]_2\}$ (**33**) with ellipsoids drawn at 50% probability.

Table 36: Selected Bond Distances (Å) and Angles (°) for $\{[(\eta^5\text{-DMP-Me}_2\text{Al}(\eta^1\mu\text{-N}_3)\text{AlMe}_2(\mu^3\text{-N})]\text{V}^{\text{IV}}\text{Me}]_2\}$ (**33**).

V(1)-N(9)	1.837(7)	N(9)-V(1)-N(9a)	92.0(3)
V(1)-N(9a)	1.850(7)	N(9)#1-V(1)-C(12)	101.3(3)
V(1)-C(12)	2.107(9)	N(9)-Al(2)-N(2)	101.4(3)
Al(2)-N(9)	1.853(7)	N(4)-N(3)-N(2)	178.2(11)
Al(2)-N(2)	1.985(8)	Al(1)-N(2)	1.959(7)
N(2)-N(3)	1.254(11)	N(3)-N(4)	1.133(11)

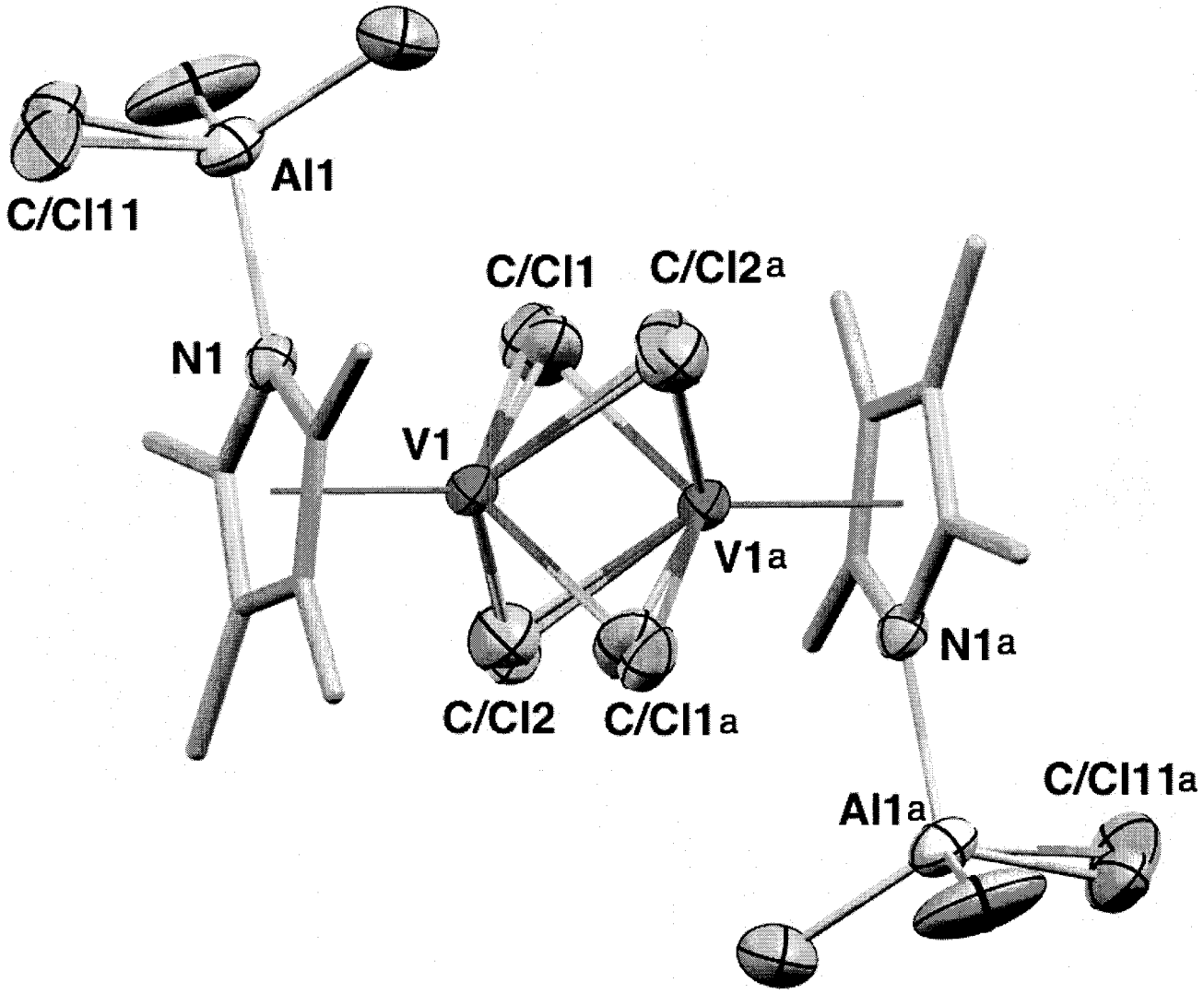

Figure 83: Partial thermal ellipsoid plot of $\{[(\eta^5\text{-TMP-AlMe}_2\text{Cl}\}\text{V}^{\text{III}}(\mu\text{-Me})(\mu\text{-Cl})]_2\}$ (**34**) with ellipsoids drawn at 50% probability.

Table 37: Selected Bond Distances (Å) and Angles (°) for $\{[(\eta^5\text{-TMP-AlMe}_2\text{Cl}\}\text{V}^{\text{III}}(\mu\text{-Me})(\mu\text{-Cl})]_2\}$ (**34**).

V(1)-C(1L)	2.17(3)	C(1)-V(1)-C(2a)	78.5(11)
V(1)-Cl(2)	2.355(15)	C(2a)-V(1)-C(1a)	72.7(11)
V(1)-Cl(1)#1	2.396(16)	C(1)-V(1)-Cl(2a)	76.6(10)
V(1)-N(1)	2.266(2)		

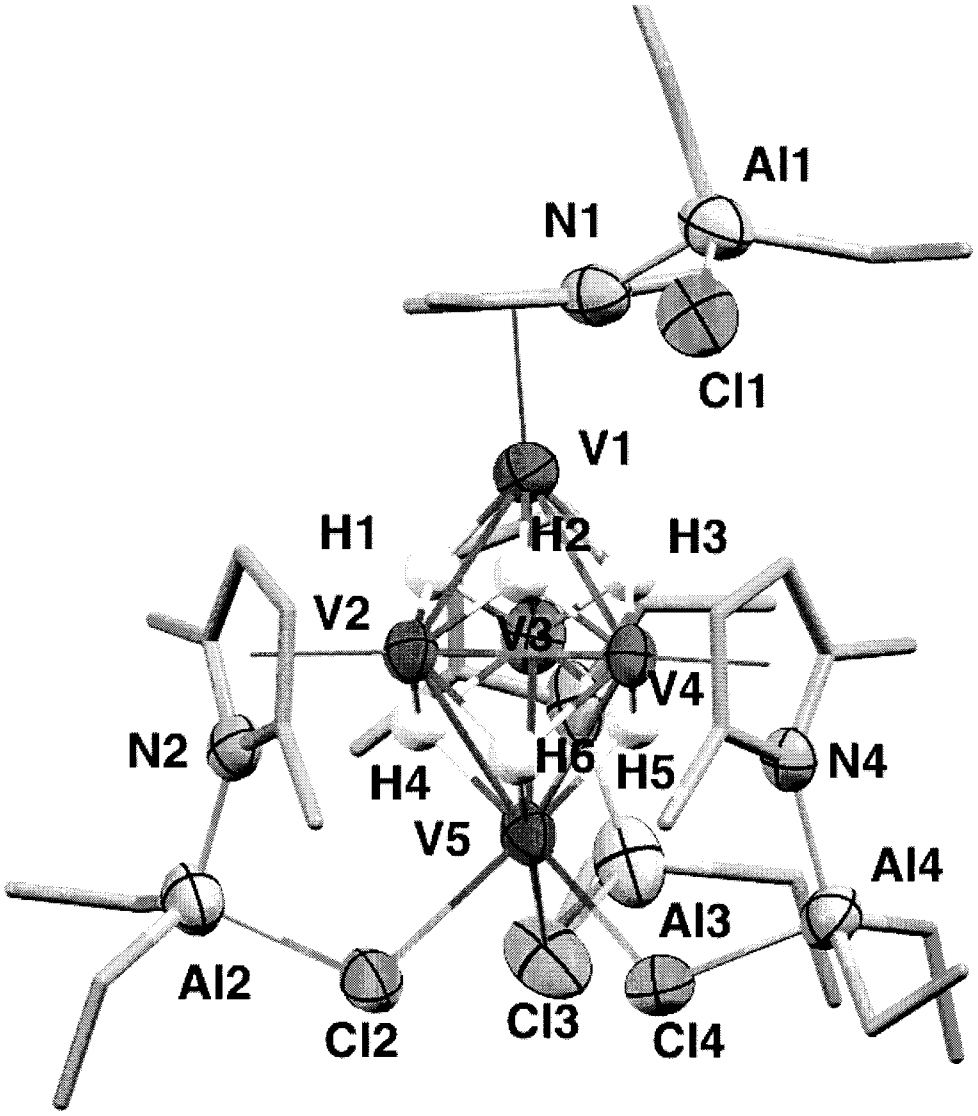

Figure 84: Partial thermal ellipsoid plot of $\{[(\eta^5\text{-DMP-AlEt}_2\text{Cl})\text{V}^{\text{II}}(\mu^3\text{-H})]_4\text{V}(\mu^3\text{-H})_2\}$ (**35**) with ellipsoids drawn at 50% probability.

Table 38: Selected Bond Distances (Å) and Angles (°) for $\{[(\eta^5\text{-DMP-AlEt}_2\text{Cl})\text{V}^{\text{II}}(\mu^3\text{-H})]_4\text{V}(\mu^3\text{-H})_2\}$ (**35**).

V(1)-V(2)	2.568(2)	V(2)-V(5)	2.752(2)
V(1)-V(3)	2.580(2)	V(2)-V(3)	2.888(2)
V(1)-V(4)	2.595(2)	V(3)-V(5)	2.643(3)
V(2)-V(4)	2.519(2)	V(3)-V(4)	2.900(2)

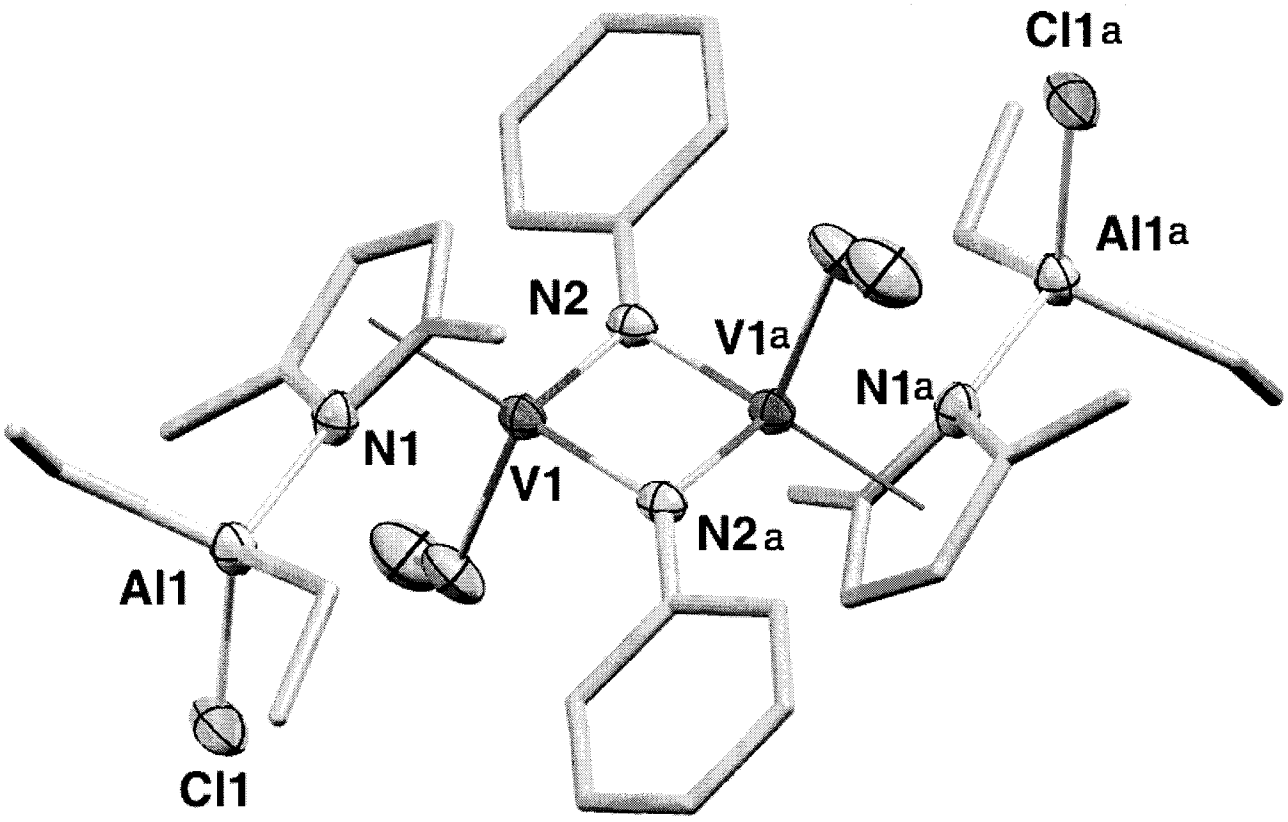

Figure 85: Partial thermal ellipsoid plot of $\{[(\eta^5\text{-DMP-AlEt}_2\text{Cl})\text{V}^{\text{IV}}\text{Et}(\mu\text{-NPh})_2]_2\}$ (**36**) with ellipsoids drawn at 50% probability.

Table 39: Selected Bond Distances (Å) and Angles (°) for $\{[(\eta^5\text{-DMP-AlEt}_2\text{Cl})\text{V}^{\text{IV}}\text{Et}(\mu\text{-NPh})_2]_2\}$ (**36**).

V(1)-N(2)	1.866(3)	C(3)-C(4)	1.399(6)
V(1)-C(7)	2.097(4)	C(4)-C(5)	1.382(6)
N(1)-C(2)	1.399(5)	N(1)-C(5)	1.412(5)
C(2)-C(3)	1.371(6)	N(2a)-V(1)-N(2)	94.63(13)
V(1)-V(1a)	2.5162(13	N(2)-V(1)-C(7)	102.94(16)
		V(1a)-N(2)-V(1)	85.37(13)

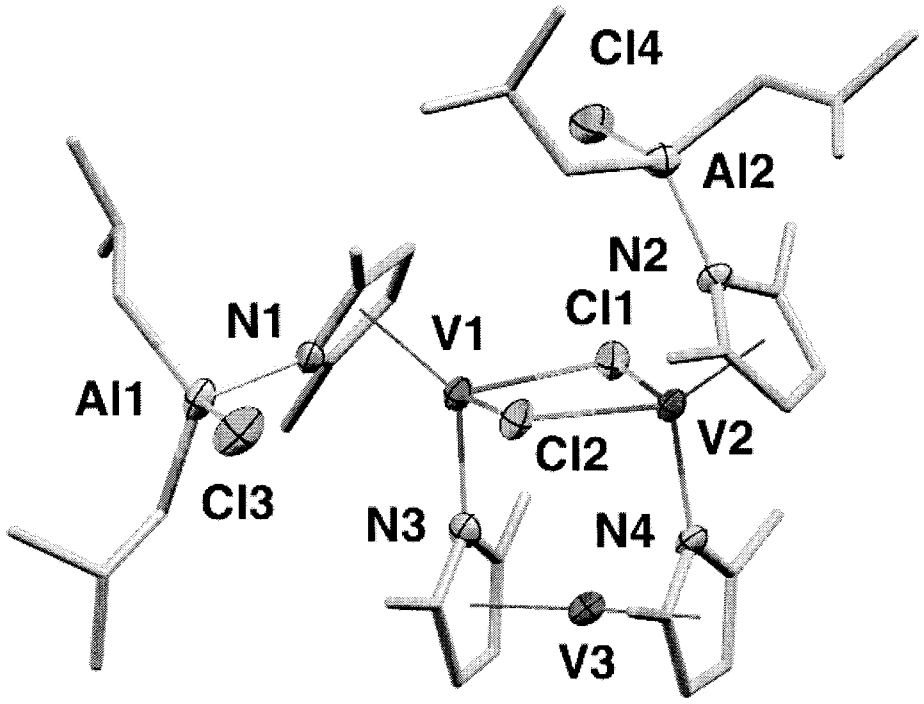

Figure 86: Partial thermal ellipsoid plot of $\{[(\eta^5\text{-DMP-Al}^i\text{Bu}_2\text{Cl})\text{V}^{\text{II}}(\mu\text{-Cl})]_2(\mu\eta^1\eta^5\text{-DMP})\text{V}^{\text{II}}\}$ (**37**) with ellipsoids drawn at 50% probability.

Table 40: Selected Bond Distances (Å) and Angles (°) for $\{[(\eta^5\text{-DMP-Al}^i\text{Bu}_2\text{Cl})\text{V}^{\text{II}}(\mu\text{-Cl})]_2(\mu\eta^1\eta^5\text{-DMP})\text{V}^{\text{II}}\}$ (**37**).

V(1)-N(3)	2.170(7)	N(3)-V(1)-Cl(1)	94.24(19)
V(1)-Cl(1)	2.450(2)	N(3)-V(1)-Cl(2)	96.84(19)
V(1)-Cl(2)	2.456(2)	N(4)-V(2)-Cl(2)	97.21(19)
V(2)-N(4)	2.154(7)	Cl(1)-V(2)-Cl(2)	86.72(8)
V(2)-Cl(1)	2.431(2)		
V(2)-Cl(2)	2.445(3)		

5.2.11 Catalytic Data

Table 41: Catalytic Data for V Pyrrole complexes **31-37**

Cat.	MAO	P	T	PE	activity	Tm_{1st}	Tm_{2nd}	Mw	PDI
#	(eq.)	bar	°C	(g)	(g/mol/h)	°C	°C	g/mol	Mw/Mn
31	0	35	25	0.4	13 000	144.0	136.7	1 546 000	3.3
	0	35	50	6.0	200 000	143.0	134.9	1 689 500	1.6
	0	35	75	12.5	417 000	141.2	137.1	1 160 500	2.0
	0	35	100	5.1	170 000	144.9	135.6	1 135 500	2.1
	0	17	75	0.5	17 000	146.1	137.4	1 494 000	2.2
	1000	35	100	1.9	63 000	132.8	130.8	79 660	8.4
32	0	35	75	7.6	253 000	146.1	137.4	1 075 500	1.3
34	0	35	100	3.6	120 000	-	-	-	-
	500	35	120	31.2	1 040 000	-	-	-	-
36	0	35	80	0.1	3 000	-	-	-	-
	500	35	80	1.6	55 000	-	-	-	-

V = 150 mL, catalyst = 30 μmole, time = 1 h. (-) = measurement not available

5.3 Results

5.3.1 Attempted synthesis of well-defined vanadium-pyrrolide precursors.

To answer some of the mechanistic questions raised in the introduction, the synthesis of well-defined vanadium pyrrolide precursors was first attempted. Treatment of $VCl_3(THF)_3$ with LiDMP resulted in the isolation of the mixed valent ionic species, $\{(THF)_3V^{II}(\mu\text{-}Cl)_3V^{II}(THF)_3\}$ $\{(\eta^1\text{-}DMP)_4V^{III}\}$ (**29**) (Figure 87 and 78). The crystal structure of **29** (Figure 79) reveals a face-sharing bioctahedral vanadium (II) cationic dimer, counterbalanced by an anionic tetrapyrrolide vanadium (III) metallate. The kinetically inert cationic fragment makes **29** obviously an unsuitable vanadium pyrrolide precursor for catalysis. Next, the in situ method, which was successfully used as described in the previous chapter, was attempted by treating the $V(acac)_3$ polymerization precatalyst with DMP and Me_3Al. Unfortunately, the reaction resulted in a curious oxidative coupling of acac and DMP (Complex **30**, Figure 87 and 79).

5.3.2 In-situ vanadium-pyrrolide catalyst preparation.

As an alternative to the strategy described above, the in-situ preparation, as discussed in the previous chapter, was attempted with a mixture of $VCl_3(THF)_3$, DMP, and excess Me_3Al. The

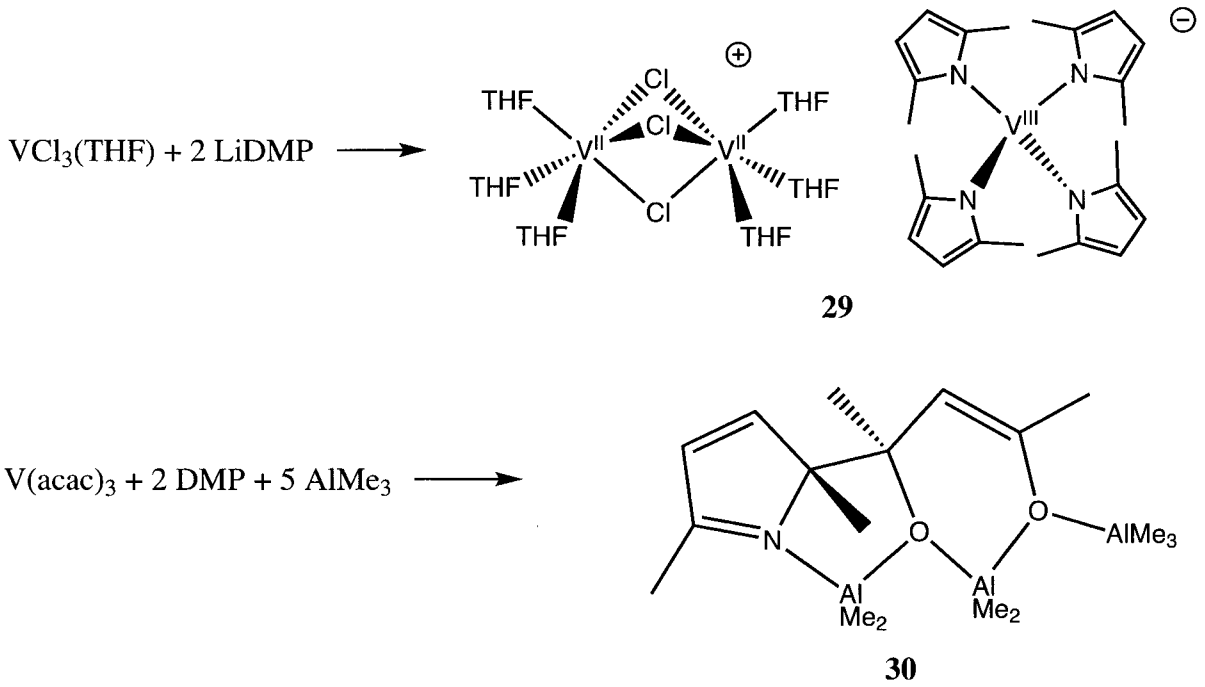

Figure 87: Attempted synthesis of well-defined vanadium pyrrolide precursors

reaction afforded the divalent bis-pyrrole V(II) sandwich complex, $\{(\eta^5\text{-DMP-AlMe}_2\text{Cl})_2\text{V}^{\text{II}}\}$ (**31**) (Figure 88).

The crystal structure of **31** (Figure 80) shows a vanadocene-type arrangement with the two parallel pyrrole rings symmetrically π-bonded to the d^3 (μ_{eff}= 3.79 μ_B) V(II) centre. As expected, each pyrrolyl nitrogen atom coordinates to one coplanar Me_2AlCl residue. The ring C-C bond lengths show only a very minor extent of double-bond localization, thus suggesting an aromatic Cp-like donation to the vanadium centre. The complex is surprisingly thermally robust and does not decompose upon heating in toluene solution at 100 °C for 12 h. During the formation of **31**, Me_3Al has both deprotonated the pyrrole and reduced vanadium to the divalent state. Given the poor stability of trivalent organovanadium,[126, 127, 128, 129, 123] this reduction is hardly surprising. Incidentally, the coordination of the pyrrolide ring may be formally described in terms of a zwitterionic structure, which would imply that the vanadium atom is acquiring some extent of a formal positive charge.

To probe the pyrrole hemilability, complex **31** was reacted with the oxidizing azobenzene reagent. The reaction resulted in the formation of the binuclear V(IV) imido complex, $\{[(\eta^5\text{-DMP-AlMe}_2\text{Cl})\text{V}^{\text{IV}}\text{Me}(\mu\text{-NPh})_2]_2\}$ (**32**) (Figure 88). The complex is a symmetrical dimer (Figure

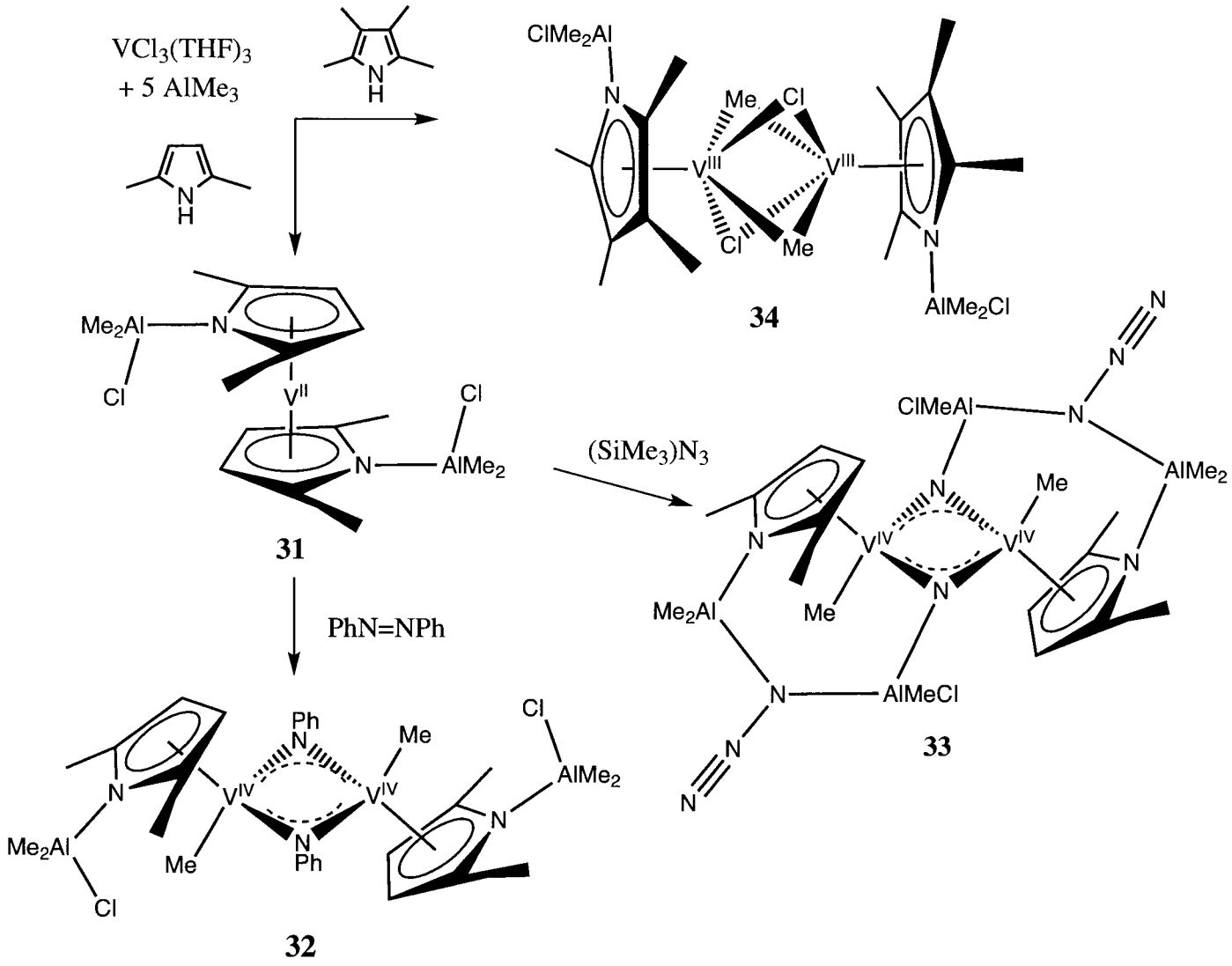

Figure 88: Isolation and reaction of products of $VCl_3(THF)_3$ with Me_3Al and DMP or TMP to generate **31** and **32** respectively. The reaction of **31** with azobenzene and $(SiMe_3)N_3$ results in **32** and **33** respectively.

81) formed by two identical (η^5-DMP-$AlMe_2Cl$)$V^{IV}Me$ residues linked by two bridging PhN imido groups. The short V-V contact [V-V = 2.511(2) Å] is in the range of what might be normally regarded as a V-V single bond. Nonetheless, the complex displays a small residual paramagnetism that indicates the presence of antiferromagnetic coupling. The slight paramagnetism, together with the very poor solubility in any solvent with which the complex does not react, prevented obtaining of meaningful data from NMR spectroscopy. Formation of **32** is easily rationalized in terms of overall dissociation of the DMP-$AlMe_2Cl$ unit and formation of a (η^5-DMP-$AlMe_2Cl$)$V^{II}Me$ residue. A four-electron oxidative attack at the azobenzene molecule by two of these intermediates results in the N=N double-bond cleavage and formation of the imido group. The presence of the V-Me bond in **32** demonstrates that alkyl migration from Al to V is indeed possible with the dissociation of a neutral DMP($AlMe_2$) unit. The treatment of **31** with ($SiMe_3$)N_3, resulted in a similar imido-bridged V(IV) dimer, {[(η^5-DMP-Me_2Al($\eta^1\mu$-N_3)$AlMe_2$(μ^3-N)]$V^{IV}Me$]$_2$} (**33**), which is the product of azide rearrangement affording the unusual (Me_2Al(η^1,μ-N_3)$AlMe_2$) bridging unit (Figure 88). The crystal structure of **33** (Figure 82) reveals a very similar coordination environment around vanadium as in **32**. In addition, the $\eta^1\mu$-N_3 unit displays bond lengths consistent with charge depletion in the system by the two strongly Lewis acidic aluminum atoms attached to it [N(2)-N(3) = 1.254(11) Å, N(3)-N(4) = 1.133(11) Å].

The effect of the pyrrolide ring substituents on the metal oxidation state, as discussed in the previous chapter, is also observed in the case of vanadium. When the in-situ preparation using $VCl_3(THF)_3$ and Me_3Al was carried out with the sterically-hindered TMP ligand, the unusual binuclear mono-pyrrolide V(III) methyl dimer, {[(η^5-TMP-$AlMe_2Cl$}V^{III}(μ-Me)(μ-Cl)]$_2$} (**34**), which contains four bridging atoms between the two vanadium centres was obtained (Figure 88). The crystal structure of **34** reveals Me/Cl disorder over several positions (Figure 83).

As the alkyl group substitution on the aluminum cocatalyst is established to strongly affect catalytic performance, the effect of the more reducing Et_3Al cocatalyst was probed again, using in situ preparations. The reaction gave the pentanuclear V(II) hydride cluster, {[(η^5-DMP-$AlEt_2Cl$)V^{II}(μ^3-H)]$_4$V(μ^3-H)$_2$} (**35**) (Figure 89). The crystal structure of **35** (Figure 84) reveals that a μ^3-hydride ligand caps each of the six triangular vanadium faces. The difficulty in the

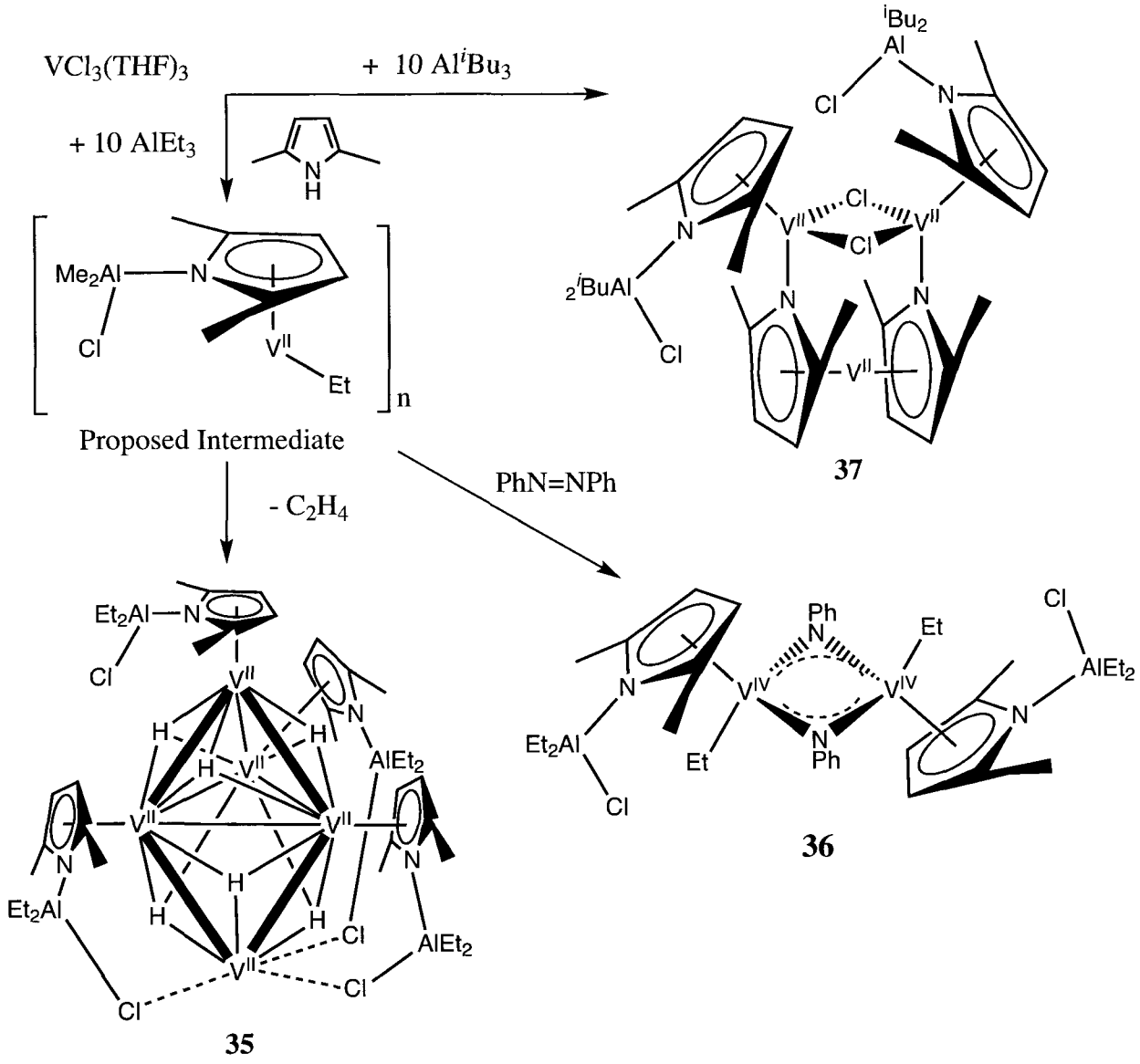

Figure 89: Reaction of $VCl_3(THF)_3$ and DMP with Et_3Al and Al^iBu_3

preparation of significant quantities of this material frustrated repeated attempts to complete its characterization. However, this species may reveal a possible catalyst deactivation pathway.

The hydride ligands of **35** are proposed to derive from β-H elimination from an initially formed and highly reactive (DMP-$V^{II}Et)_n$ polymetallic intermediate. The addition of the azobenzene trapping agent to the in-situ mixture allows the isolation of the dimeric vanadium(IV) μ-imido ethyl complex, $\{[(\eta^5\text{-DMP-AlEt}_2\text{Cl})V^{IV}\text{Et}(\mu\text{-NPh})_2]_2\}$ (**36**), containing a similar structure to **32** (Figure 89). Finally, similar reaction carried out with $^iBu_3Al$ afforded the trinuclear cluster, $\{[(\eta^5\text{-DMP-Al}^i\text{Bu}_2\text{Cl})V^{II}(\mu\text{-Cl})]_2(\mu\text{-}\eta^1\eta^5\text{-DMP})V^{II}\}$ (**37**) (Figure 89).

5.3.3 Ethylene polymerization catalysis by vanadium pyrrolide complexes.

The readily available complexes described above (**31**, **32**, **34**, and **36**) were evaluated as ethylene polymerization catalysts.

In spite of the divalent state and its thermal robustness, complex **31** is a highly active single-component, single-site catalyst. This behavior is highly unusual in this category of catalysts since **31** does not have a preformed V-R bond. Exposure of a toluene solution of 31 to ethylene under pressure and at moderately high temperature started the polymerization reaction, which produced PE with very high molecular weight, high linearity, and with polydispersity characteristic of a single-site catalyst (Table 41). Moderate heating is necessary to start the polymerization reaction, thus indicating that a molecular reorganization of **31** must occur in order to fulfill the polymerization prerequisites. Lower pressure also seems to have a detrimental effect on the activity. The polymers produced also contained a melting point in the first heating curve above 141 °C, which is a primary characteristic of linear UHMW-PE. The melting points in the second heating curve are as expected for linear polyethylene. Instead, polymerization reactions carried out in the presence of methylalumoxane (MAO) as activator show both a decrease in catalytic activity and formation of broadly dispersed polymers with lower molecular weight.

Accordingly, complexes **32** and **34** are also single-component catalysts that start polymerization with no need for further activation. Likely, a simple dimer–monomer dissociation equilibrium may generate the required empty coordination site for ethylene insertion. The catalytic activity is somewhat lower than for **31** under the best polymerization conditions, but the polymer properties appears to be similar, with improved polydispersity. Finally, the addition of MAO results in very high activity for **34** , confirming that a cationic V (III) catalyst is highly active. These results are discussed in more detail in the next section.

5.4 Discussion

The isolation of the V(III) dimer **34** suggests the intermediacy of a similar V(III) species in the case of the formation of **31**. In fact a microcrystalline brown solid forms as a byproduct in the synthesis of the divalent **31**, which is most likely a trivalent intermediate (Figure 90). Possibly the

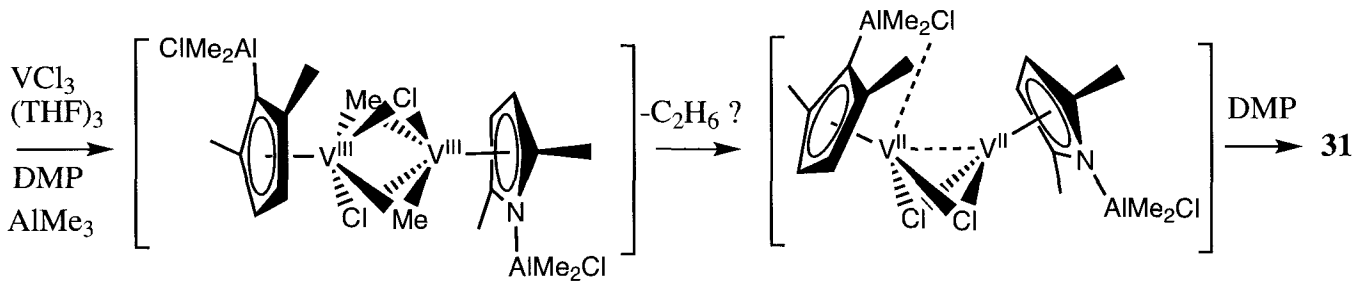

Figure 90: Proposed mechanism for formation of **31** via V (III) dimer intermediate similar to **34**.

lower steric hindrance of the DMP ligand relative to the TMP ligand allows for the formation of even higher order vanadium clusters, which are highly reactive.

As in the pyrrolide-based chromium catalysts discussed in the previous chapter, pre-equilibration is thought to play a large role in the catalysis by these vanadium species. It is likely that the pyrrole hemilability contributes both to catalyst stabilization as well as activation, which is especially obvious in the case of **31**.

Some mechanistic proposals for these possible activation pathways are depicted in Figures 91 and 92, and are awaiting further DFT and experimental investigations. Of particular interest is the link with the polymerization mechanism in view of the valuable ultra-high Mw polyethylenes produced. Thus the mechanistic study of these well-defined species may yield the key to the design of catalysts for the production of valuable ultra high Mw polymers.

5.5 Conclusions

In conclusion, probing the effect of the pyrrolide ligand on vanadium resulted in the isolation of several single-site, single-component polymerization catalysts with the formal oxidation states of vanadium of II, III, and IV. Thus the pyrrolide hemilability allows for the activation of both the normally kinetically inert V(II), as well as higher valent species which are established to be excellent catalysts for olefin copolymerizaton, such as in LLDPE production. While the exact pre-equilibriation involved in the thermal activation of these species is unknown, future studies including DFT of the dynamics of these well-defined catalyst resting states may shed light on the polymerization mechanism. In addition, future work could also focus on the further reduction of **31** to a V (I) analog that may yield a highly active ethylene trimerization catalyst, as the vanadium (I)

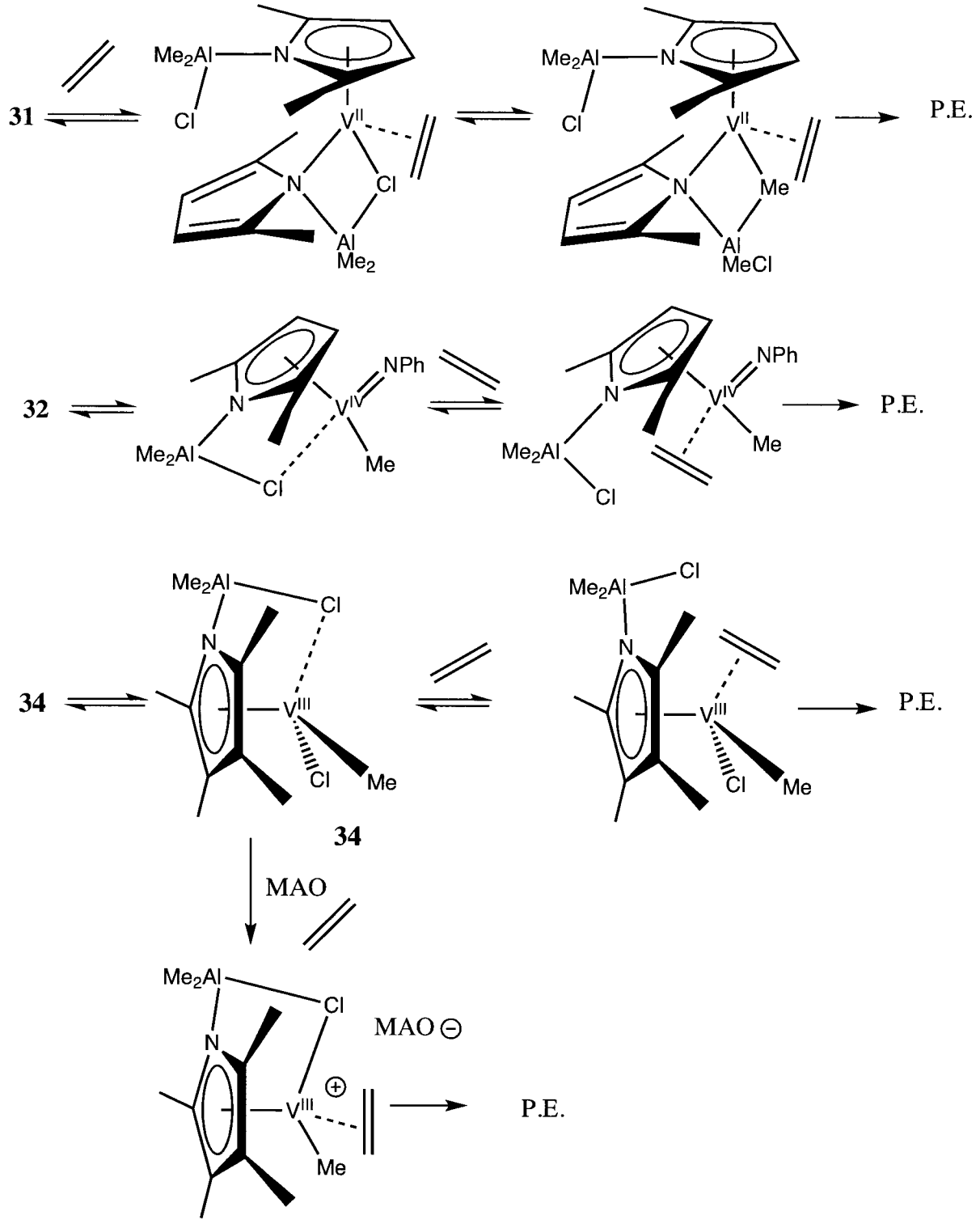

Figure 91: Proposed ethylene polymerization mechanisms by 31, 32, and 34 (with and without MAO).

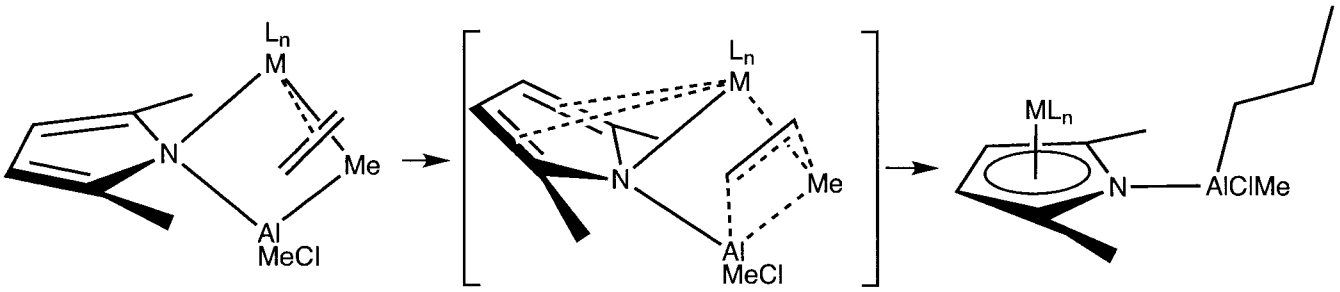

Figure 92: Proposed "aufbau"-like polymerization mechanism by metal-pyrrolide polymerization catalysts.

centre is expected to be more kinetically labile than the Cr (I) centre (Figure 93). Conversely, the generation of a V (V) alkylidene with the pyrrole ligand may yield highly active olefin metathesis catalysts, in analogy to Schrock's molybdenum and tungsten pyrrolide alkylidene catalysts, where the pyrrole hemilability was found to enhance tremendously the catalytic performance.[58]

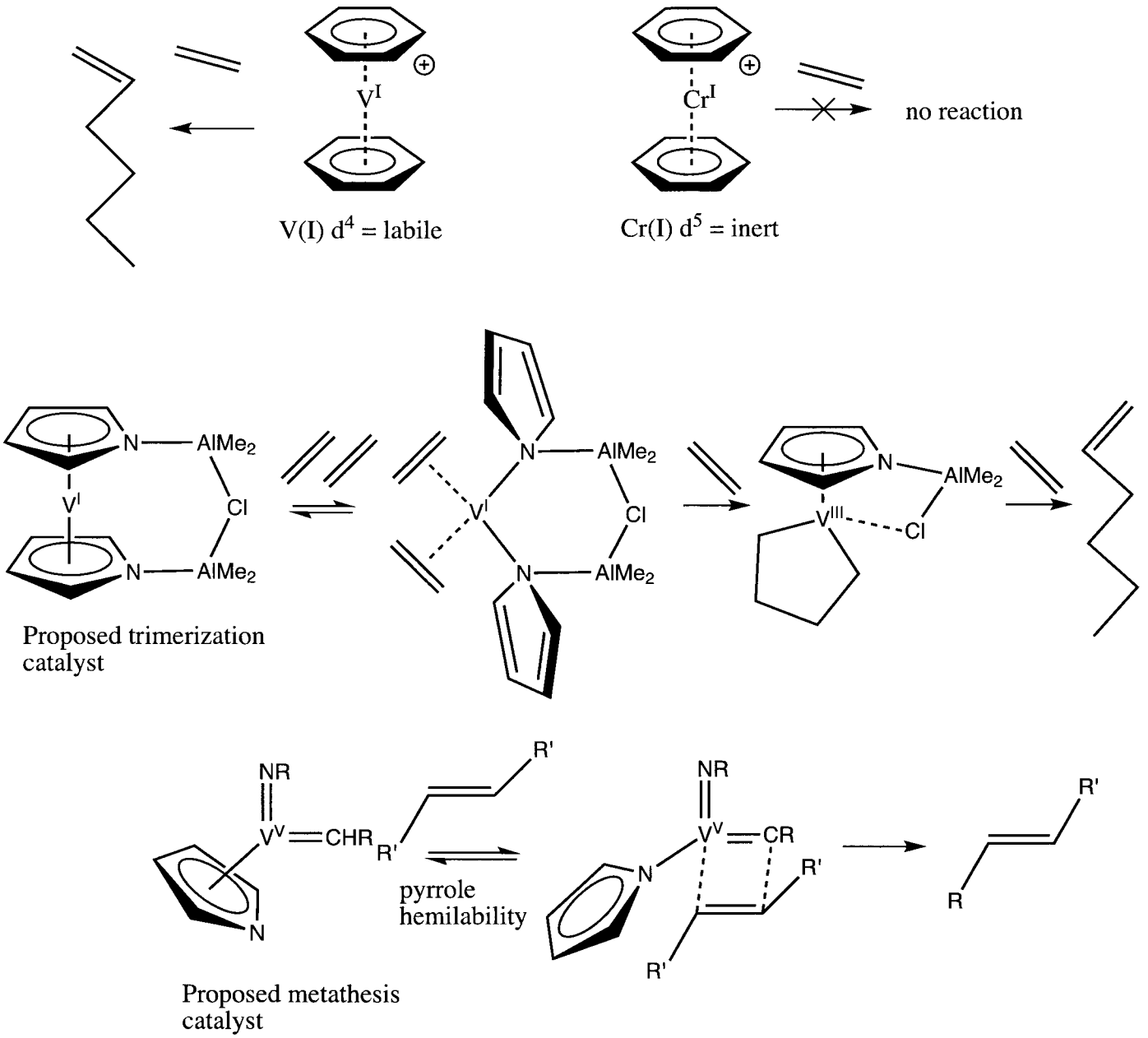

Figure 93: Proposed V (I) and V (V) pyrrolide catalyst opportunities for trimerization and metathesis, respectively

6 Exploration of titanium pyrrolide complexes for ethylene polymerization catalysis

Abstract

This chapter discusses the exploration of titanium pyrrolide complexes for ethylene polymerization. The in-situ reaction of $TiCl_4$, DMP, and Me_3Al resulted in the clean formation of either the bis-DMP sandwich complex, $\{(\eta^5\text{-DMP-AlMe}_2\text{Cl})_2\text{Ti}^{IV}\text{Me}_2\}$ (**38**), or electron-deficient mono-DMP complex $\{(\eta^5\text{-DMP-AlMeCl}_2)\text{Ti}^{IV}\text{Cl}_2\text{Me}\}$ (**39**), depending on the ratio of pyrrole to titanium used. Bis-DMP complex **38** is completely inactive for ethylene polymerization when reacted with either MAO or Ph_3C $B(C_6F_5)_4$, but the mono-DMP complex **39** is highly active, suggesting the monopyrrole titanium configuration is ideal for olefin polymerization. The effect of modifying the pyrrole ligand substituents on the resulting structural parameters and activity was evaluated with the following series of mono-pyrrole complexes: $\{(\eta^5\text{-TMP-AlCl}_2\text{Me})\text{Ti}^{IV}\text{Cl}_2\text{Me}\}$ (**40**), $\{(\eta^5\text{-DMI-AlCl}_2\text{Me})\text{Ti}^{IV}\text{Cl}_2\text{Me}\}$ (**41**), $\{(\eta^5\text{-THC-AlMeCl}_2)\text{Ti}^{IV}\text{Cl}_2\text{Me}\}$ (**42**), and $\{(\eta^5\text{-TPP})\text{Ti}^{IV}\text{Cl}_3\}$ (**43**). The solution NMR analysis of **39-42** reveal not a single complex but a mixture of several isomers. The reaction of pyrrole, $TiCl_4$ and Me_3Al resulted in a reduced ansa-pyrrolide based dicationic titanium (III) dimer $\{[\text{Ti}^{III}(\mu\text{-Cl})(\mu\text{-AlMe}_2(\eta^5\text{-Pyr})_2]_2\}$ $\{Me_2AlCl_2\}_2$ (**44**), which is also active for polymerization, suggesting that Ti (III) mono-pyrrolide complexes are the highly active catalyst species, with a geometry similar to the highly active "constrained geometry" catalyst family.

6.1 Introduction

The previous two chapters described the coordination chemistry and ethylene trimerization and polymerization catalysis by well-defined pyrrolide complexes of chromium and vanadium. In these previous studies it was concluded that the polymerization catalyst was formed by alkyl migration from aluminum to the transition metal centre. A related process in olefin polymerization is defined as polymer chain transfer between the transition metal and aluminum cocatalyst. This chapter extends this study to titanium. The goal was to further understand the mechanistic implications of pyrrolide hemilability to chain transfer between the aluminum alkyl and transition metal centres,

and how it may affect the properties of the polymer produced. As mentioned in the introduction, titanium based catalysts make up the majority of commercially used systems due to inherently high activity and low cost, and their use is preferred both in the commercial production of very high Mw PE and LLDPE. Thus the use of pyrrolide titanium derivatives might open interesting perspectives.

As briefly discussed in the introduction to this thesis, extensive theoretical and experimental studies to understand the mechanism of olefin polymerization catalysis have established that the dual roles for the commonly used aluminum alkyl based activators such as Me_3Al, Et_2AlCl and MAO (which is composed of a mixture of $[AlMe(O)]_n$ and 15% Me_3Al) are both cationization and alkylation of the transition-metal precatalyst. The resulting metal catalyst is electrophillic enough to coordinate olefins and insert them into a growing polymer chain. Mechanistic studies of such systems have shown that generally the most stable catalyst resting state is the catalytically inactive cationic heterobimetallic species of the type $[LnM(\mu\text{-}R)_2AlR_2]$.[130, 131] The kinetics of the disassociation of the trialkylaluminum from this heterobimetallic catalytically inactive resting state to generate the active polymerization catalyst is important to understand mechanistically. In general, an increased steric bulk of the transition metal ligands results in faster rates of chain transfer possibly due to increased steric repulsion with the aluminum adduct. By comparing the rate of chain transfer of two sterically similar metallocenes, the electron deficient metallocene provide faster rates of dissociation of aluminum from the transition metal centre.[132, 133]

Increasing the rate of olefin polymerization is very desirable from an economic standpoint, and mechanistic insight into the dynamics of such heterobimetallic resting states are thus very valuable as they could provide rational strategies to design improved olefin polymerization catalysts. Some strategies which have developed involve removing excess Me_3Al from MAO under vaccum, or addition of alcohols to protonate the free Me_3Al. These methods obviously work by preventing the formation of stable heterobimetallic adducts by removing free alkyl aluminum, but they have the disadvantage of also preventing chain transfer to aluminum which is desirable in certain applications as described below. As there are relatively few established examples of highly active aluminum-alkyl activated olefin polymerization catalysts displaying rapid rates of chain transfer between the

transition metal and aluminum alkyl cocatalyst, researchers have explored alternative main-group alkyls as improved chain-transfer agents. Magnesium and zinc alkyls are now used extensively as chain transfer agents due to their enhanced lability, resulting in rapid chain transfer rates without the severe catalyst deactivation observed in the aluminum systems. In a recent classification of the relative chain transfer rates with zinc alkyls in a broad range of catalysts, it was found that sterically unencumbered catalysts remain inactive upon addition of zinc alkyls possibly due to the formation of stable heterobimetallic complexes.[134] Increasing the steric bulk of the ligands resulted in much higher rates of chain transfer and propagation, probably due to increased steric repulsion between the ligand and zinc alkyl adduct which labilizes the interaction. In these heterobimetallic catalytic systems it was established that the molecular weight of the polymer product depends completely on the relative rates of the propagation, chain transfer to zinc, and chain termination steps. The higher rate of chain transfer for zinc compared to aluminum was found to be due to the lower bonding energy of the zinc heterobimetallic, approximately 7 kcal/mol less stable than the analogous aluminum adduct.

Very recently, the relevance of rapid chain transfer for the commercial viability of a process was demonstrated with the design of a catalyst for the production of olefin block copolymers.[135, 136] These discoveries have re-invigorated mechanistic investigations aimed at improving the rates of chain transfer, which controls both the sequence and length of the copolymer blocks. These are the factors controlling the properties and rheology of the copolymer. Rational control of intramolecular alkyl exchange between the transition metal and main group alkyl is one obvious feature which is needed for rationally controlling this rate of chain transfer for each catalytic site separately. One avenue of research which has not been considered is the influence of bridging ligands on heterobimetallic chain transfer dynamics. Ligands bridging aluminum to the transition metal could provide the desired level of control of enhanced chain transfer dynamics over traditional alkyl-bridged heterobimetallics. There are many of these non-classical heterobimetallics deposited in the Cambridge structural database, which may contain enhanced rates of chain transfer to aluminum (Figure 94).

It was concluded in the last two chapters that chain transfer is occuring between the aluminum

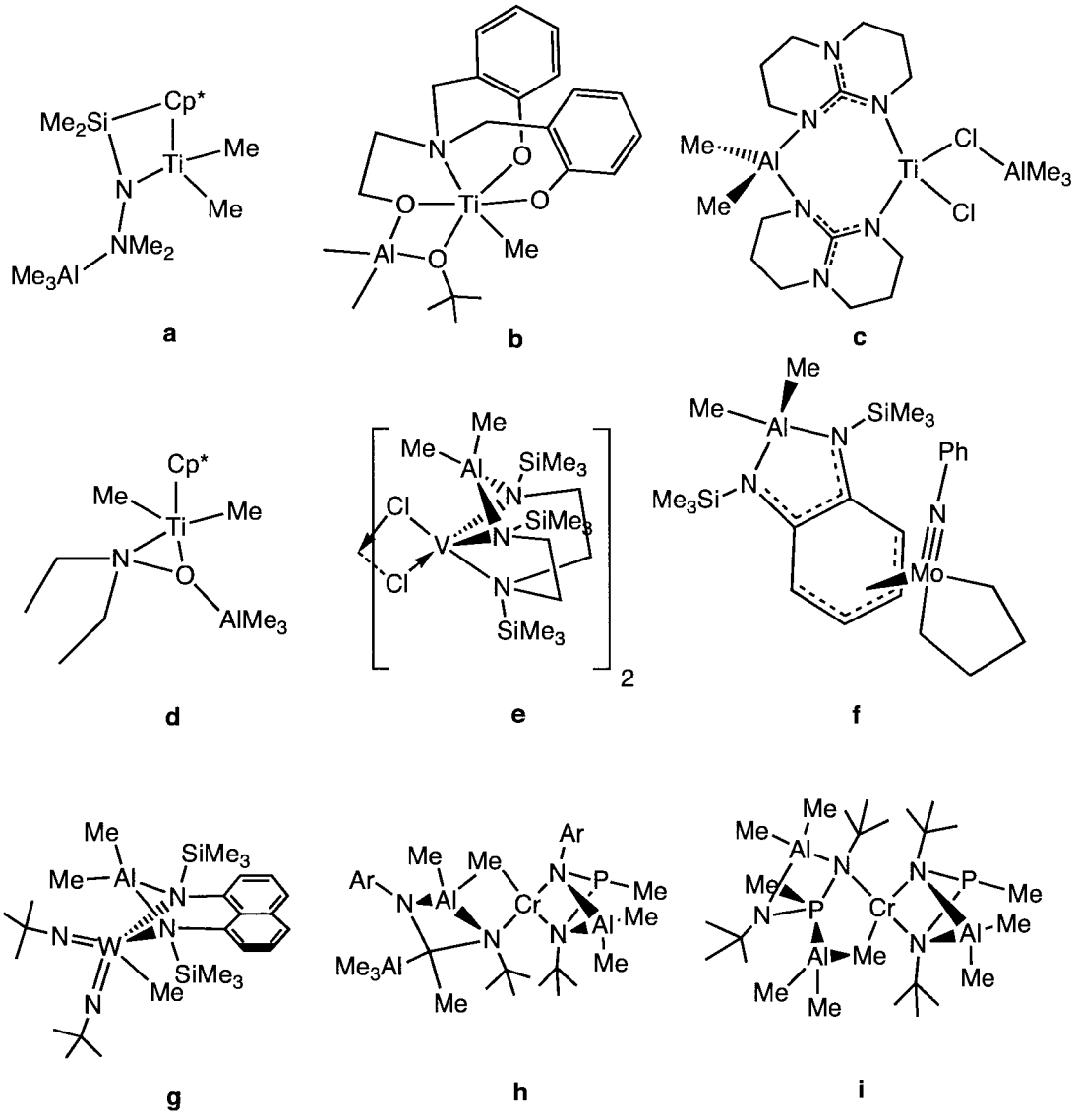

Figure 94: Structurally characterized examples of non-traditional heterobimetallic species

and transition metal centres via the pyrrolide hemilability. Thus the development of diamagnetic hetero-bimetallic Ti (IV) pyrrolide systems would be expected to furnish a means to understand better the mechanistic aspects of this process.

6.2 Experimental

All manipulations were carried out using standard Schlenk line or drybox techniques under an atmosphere of dry dinitrogen. Protio solvents were dried using an aluminum oxide solvent purification system. Deutero solvents were predried over activated 4 Å molecular sieves and were refluxed over the appropriate drying agent, distilled, and stored under dinitrogen. NMR samples were prepared under dinitrogen in 5 mm Wilmad 507-PP tubes flame sealed under dinitrogen using standard Schlenck apparatus. ^{1}H, and $^{13}C\{^{1}H\}$, NMR spectra were recorded on a Bruker Avance 300 MHz multinuclear NMR instrument. ^{1}H and ^{13}C assignments were confirmed when necessary with the use of DEPT-135, DEPT-90, and two-dimensional ^{1}H-^{1}H and ^{13}C-^{1}H NMR experiments. ^{1}H and ^{13}C spectra were referenced internally to residual protio solvent (^{1}H) or solvent (^{13}C) resonances and are reported relative to tetramethylsilane (δ) 0 ppm). Chemical shifts are quoted in δ (ppm), and coupling constants in hertz. Samples for magnetic susceptibility were preweighed inside a drybox equipped with an analytical balance and measured on a Johnson Matthey Magnetic Susceptibility balance. Elemental analysis was carried out with a Perkin-Elmer 2400 CHN analyzer. Data for X-ray crystal structure determination were obtained with a Bruker diffractometer equipped with a 1 K Smart CCD area detector. TMA (Strem), MAO (Chemtura), and 1 M $TiCl_4$ in toluene (Aldrich) were used as received. Triphenylcarbenium tetrakis(pentafluorophenyl)borate (Strem) was reprecipitated from a dichloromethane/pentane mixture. 2,5-dimethylpyrrole and 2,3,4,5-tetramethylpyrrole were also conveniently prepared on a large scale from the inexpensive diketone precursors via the high-pressure Paal-Knorr condensation with excess concentrated ammonia solution in a high pressure autoclave at 100 °C for several hours (0.2 - 1.0 Kg scale). 2,3,4,5-tetraphenylpyrrole was synthesized according to a previously reported literature method which was readily scaled up to 200 grams without loss of yield or purity.[137]

6.2.1 {(η^5-DMP-$AlMe_2Cl)_2TiMe_2$} (38)

$TiCl_4$(1 mL of a 1 M solution in toluene, 1 mmol) was rapidly added to a freshly prepared solution of 2,5-dimethylpyrrole (190 mg, 2 mmol) and Me_3Al (288 mg, 4 mmol) in toluene (10 mL), with stirring for an additional five minutes resulting in a yellow solution, which was then layered with hexanes (10 mL) and stored in the dark at -35 °C for 1 week to yield yellow, light sensitive crystals of **38** suitable for X-ray diffraction. The mother liquor was carefully decanted away, and the crystals were dried in vacuo. Yield: 340 mg, 76 %. ^{1}H NMR (C_6D_6, 300 MHz, 293 K): δ = 6.04 (s, 4H; Pyr CH), 2.53 (s, 12H; Pyr CH_3), 0.61 (s, 6 H; $TiCH_3$), -0.61 (s, 12H; $AlCH_3$). $^{13}C\{^1H\}$ NMR: 148.8 (s, PyrC2,5) 116.6 (s, PyrC3,4), 70.8 (s, $TiCH_3$), 18.3 (s, $PyrCH_3$), -4.0 (s, $AlCH_3$). Anal. Calcd. (found) for C18H34Al2Cl2N2Ti: C, 47.89 (47.38); H, 7.53 (7.31); N, 6.20 (6.14).

6.2.2 {(η^5-DMP-$AlMeCl_2$)$TiCl_2Me$} (39)

$TiCl_4$(1 mL of a 1 M solution in toluene, 1 mmol) was rapidly added to a freshly prepared solution of 2,5-dimethylpyrrole (95 mg, 1 mmol) and Me_3Al (72 mg, 1 mmol) in toluene (10 mL), with stirring for additional five minutes resulting in a yellow solution, which was then layered with hexanes and stored in the dark at -35 °C for 1 week to yield yellow, light sensitive crystals of **39** suitable for X-ray diffraction as a toluene solvate. The mother liquor was carefully decanted away, and the crystals were dried in vacuo. Yield: 277 mg (84 %). ^{1}H NMR (C_6D_6, 300 MHz, 293 K) of observed mixture of three isomers a:b:c = 84:13:2 via ^{1}H integration: δ = 6.88, 6.72, 6.59 (s, PyrCH a, b, c, 3H), 2.92, 2.81, 2.79 (s, $PyrCH_3$ a, c, b, 6H), 2.55, 2.50, 2.38 (s, $TiCH_3$ c, a, b), -0.21, -0.26, -0.48 (s, $AlCl_2CH_3$ a, c, b, 3H). $^{13}C\{^1H\}$ NMR: 151.3 (s, Pyr C3,4), 121.5 (s, Pyr C2,5), 102.8, 97.3, 92.5 (s, $TiCH_3$ a, b, c), 34.6, 31.7 (s, Pyr CH_3 a, b), -4.0 (br, $AlCH_3$). Elemental analysis (after removal of the interstitial toluene under dynamic vacuum for 1 hour) Calcd. (found) for C7H14AlCl4NTi: C, 25.55 (24.38); H, 4.29 (4.15); N, 4.26 (4.13).

6.2.3 {(η^5-TMP-$AlCl_2Me$)$TiCl_2Me$} (40).

$TiCl_4$(1 mL of a 1 M solution in toluene, 1 mmol) was rapidly added to a freshly prepared solution of 2,3,4,5-tetramethylpyrrole (123 mg, 1 mmol) and Me_3Al (72 mg, 1 mmol) in toluene (10 mL),

with stirring for an additional five minutes resulting in a yellow solution, which was layered with hexanes (10 mL) and stored in the dark at -35 °C for 1 week to yield yellow, light sensitive crystals of **40** suitable for X-ray diffraction as a toluene solvate. The mother liquor was carefully decanted away, and the crystals were dried in vacuo. Yield: 283 mg (76 %). ^{1}H NMR (C_6D_6, 300 MHz, 293 K) observed mixture of three isomers a:b:c = 65:25:10 via ^{1}H integration: δ = 2.40, 2.15, 2.05 (m, Pyr3,4CH_3 a, c, b, 6H), 1.97, 1.61 (s, TiCH_3 a, c), 1.29 (s, Pyr2,5CH_3 a), 1.26 (s, TiCH_3 b, [a + b + c] = 3H), 1.14, 0.92 (m, Pyr2,5CH_3 c, b, [a + b + c] = 6H), 0.60 (s, AlCH_3, a), -0.08 (s, AlCH_3 c), -1.23 (s, AlCH_3 b, [a + b + c] = 3H). ^{13}C{1H} NMR: 135.5 (s, PyrC3,4), 131.2 (s, PyrC2,5), 96.2, 84.5, 74.1 (s, TiCH_3 a, c, b), 32.1, 33.3, 31.5 (s, Pyr3,4CH_3 a, b, c), 23.2, 15.7, 11.1 (s, Pyr2,5CH_3 a, b, c), -3.5 (br, AlCH_3). Elemental analysis (after removal of the interstitial toluene under dynamic vacuum for 1 hour) Calcd. (found) for C10H18AlCl4NTi: C, 32.54 (32.57); H, 4.92 (4.85); N, 3.80 (3.73).

6.2.4 {(η^5-DMI-AlCl_2Me)TiCl_2Me} (41)

$TiCl_4$(1 mL of a 1 M solution in toluene, 1 mmol) was added to a solution of 2,3-dimethylindole (145 mg, 1 mmol) and Me_3Al (72 mg, 1 mmol) in toluene (10 mL), with stirring for an additional five minutes resulting in a yellow solution, which was then layered with hexanes and stored in the dark at -35 °C for 1 week to yield yellow, light sensitive crystals of **41** suitable for X-ray diffraction as a toluene solvate. The mother liquor was carefully decanted away, and the crystals were dried in vacuo. Yield: 308 mg (79 %). ^{1}H NMR (C_6D_6, 300 MHz, 293 K) observed mixture of three isomers a:b:c = 64:24:12 via ^{1}H integration: δ = 8.79, 8.68, 8.50, 8.47 (d, $3J_{HH}$ = 7 Hz, IndCH a, b, b, c, 1H), 7.00 (t, $3J_{HH}$ = 7 Hz, IndCH, 1H), 6.95 (t, $3J_{HH}$ = 10 Hz, IndCH, 1H), 6.81 (d, $3J_{HH}$ =10 Hz, IndCH, 1H), 2.32, 2.25, 2.23 (s, Ind7CH_3 a, b, c, 3H), 1.71, 1.65, 1.58 (s, TiCH_3 a, b, c), 1.48, 1.43, 1.35 (s, Ind8CH_3 a, b, c, 3H), 0.32, 0.26, 0.18, 0.12 (s, AlCH_3, a, b, b, c, 3H). ^{13}C{1H} NMR: 147.5 (s, Ind), 136.3 (s, Ind), 135.0 (s, Ind), 132.3 (s, Ind), 131.8 (s, Ind), 123.6 (s, Ind), 123.0 (s, Ind), 104.3, 101.7, 92.7, 88.8 (s, TiCH_3 a, b, b, c), 53.4, 32.7, 27.6, 14.5 (s, IndCH_3), -3.5 (br, AlCH_3). Elemental analysis (after removal of the interstitial toluene under dynamic vacuum for 1 hour) Calcd. (found) for C12H16AlCl4NTi: C, 36.85 (67.38); H, 4.13 (7.31); N, 3.58 (2.14).

6.2.5 {(η^5-THC-AlMeCl$_2$)TiCl$_2$Me} (42)

$TiCl_4$(1 mL of a 1 M solution in toluene, 1 mmol) was added to a solution of 3,4,5,6-tetrahydrocarbazole (160 mg, 1 mmol) and Me_3Al (72 mg, 1 mmol) in toluene (10 mL), with stirring for an additional five minutes resulting in a yellow solution, which was layered with hexanes and stored in the dark at -35 °C for 1 week to yield pale-yellow light sensitive crystals of **42** suitable for X-ray diffraction. The mother liquor was carefully decanted away, and the crystals were dried in vacuo. Yield: 337 mg, (81 %). ^{1}H NMR (C_6D_6, 300 MHz, 293 K) equilibrium of three isomers a:b:c = 60:25:15 via ^{1}H integration at: δ 8.91, 8.83, 8.71, 8.65 8.51 (d, $3J_{HH}$ = 6 Hz, IndCH a, b, c, 1H), 7.07 (t, $3J_{HH}$ = 11 Hz, IndCH, 1H), 6.88 (t, $3J_{HH}$ = 6 Hz, IndCH, 1H), 6.80 (d, $3J_{HH}$ = 11 Hz, IndCH, 1H), 2.85 (m, CH_2 c, 2H), 2.45 (m, CH_2 b, 2H), 2.09 (m, CH_2 a, 2H,), 1.65, 1.56, 1.49 (s, $TiCH_3$, b, a, c, 3H), 1.31 (m, CH_2, 2H), 1.18 (m, CH_2, 2H), 0.324, 0.254, 0.230, 0.127 (s, $AlCH_3$ a, b, b, c, 3H). ^{13}C{1H} NMR: 148.7 (s, IndCCH$_2$) 144.8 (s, IndCCH), 138.6 (s, IndCCH), 132.5 (s, IndCH), 131.3 (s, IndCH), 129.7(s, IndCH), 129.6(s, IndCH), 126.6(s, IndC), 126.3 (s, IndCH), 124.2 (s, IndCH), 102.7 (s, $TiCH_3$ a), 91.2 (s, $TiCH_3$ b), 87.9 (s, $TiCH_3$ c), 51.6 (IndCH$_2$), 32.1 (IndCH$_2$), 18.4 (IndCH$_2$CH$_2$), 15.7 (IndCH$_2$CH$_2$), 13.7 (IndCH$_2$CH$_2$), -3.2 (br s, $AlCH_3$). Anal. Calcd. (found) for C14H21AlCl4NTi: C, 40.02 (39.89); H 5.04 (5.13); N 3.34 (3.28).

6.2.6 {(η^5-TPP)TiCl$_3$} (43)

To a solution of 2,3,4,5-tetraphenylpyrrole (371 mg) in toluene (15 mL) was slowly added a solution of n-butyllithium (0.400 mL of a 2.5 M solution in hexanes) with stirring for 5 minutes, forming a white suspension. To this suspension was added a solution of $TiCl_4$ (1 mL of a 1M solution in Toluene) with stirring for 1 hour, resulting in a dark red solution containing a white LiCl suspension, which was subsequently filtered, layered with hexanes and stored at -35°C for one week to yield dark red crystals of **44**. The mother liquor was carefully decanted away, and the crystals were dried in vacuo. Yield: 370 mg, (72 %). ^{1}H NMR (C_6D_6, 300 MHz, 293 K): δ = 7.76 (m, 4H, CH), 7.55 (m, 16H, CH), 7.41 (m, 4H, CH). ^{13}C{1H} NMR: δ = 138.1 (s, PyrC), 129.2 (s, CH), 128.6 (s, CH), 127.5 (s, CH) 121.3 (s, C), 114.8 (s, C). Anal. Calcd (found) for C28H20AlCl3NTi: C, 60.94 (61.38); H, 3.66 (3.31); N, 2.54 (2.34).

6.2.7 {[Ti(μ-Cl)(μ-AlMe$_2$(η^5-Pyr)$_2$]$_2$} {Me$_2$AlCl$_2$}$_2$ (44)

$TiCl_4$(1 mL of a 1 M solution in toluene, 1 mmol) was added to a solution of pyrrole (134 mg, 2 mmol) and Me_3Al (144 mg, 2 mmol) in toluene (10 mL), with stirring for an additional five minutes, resulting in a red solution from which green crystals of **45** slowly deposited while standing over the course of 24 h. The mother liquor was carefully decanted away, and the crystals were dried in vacuo. Yield: 221 mg (53 %). Due to poor solubility, a quality solution NMR could not be obtained of otherwise diamagnetic 4. Anal. Calcd (found) for C24H40Al4Cl6N4Ti2: C, 35.97 (36.38); H, 5.04 (4.68); N, 7.00 (6.71). Polymerization results. Samples were tested in a 300 mL high pressure Büchi reactor containing a heating/cooling jacket and a glass insert.

6.2.8 X-ray Data

Table 42: Crystal Data and Structure Analysis Results for Titanium Pyrrole

Complex #	**38**	**39**	**40**	**41**
formula	C18H34Al2 Cl2N2Ti	C8 H14 Al1 Cl4 N1 Ti1	C13.50H22 AlCl4NTi	C15.50H20 AlCl4NTi
Mw	451.23	233.23	415.00	437.01
space group	Pbca	P-2(1)/c	P-1	P-1
a (Å)	13.891(8)	7.8309(10)	9.030(8)	8.7665(12)
b (Å)	15.071(8)	12.8390(16)	9.165(7)	9.7285(14)
c (Å)	23.388(12)	18.004(2)	13.978(11)	13.2278(19)
α	90	90	102.87(2)	75.600(2)
β	90	97.557(2)	99.42(2)	79.771(2)
γ	90	90	111.624(15)	67.390(2)
V (Å3)	4896(5)	1794.4(4)	1009.1(15)	1004.5(2)
radiation	0.71073	0.71073	0.71073	0.71073
T (K)	208(2)	208(2)	208(2)	208(2)
Dcalcd (g cm-3)	1.224	1.239	1.366	1.445
μcalcd (mm-1)	0.644	0.980	0.989	0.998
F000	1904	664	426	446
R, Rw2	0.0689, 0.1384	0.1038, 0.1395	0.0508, 0.1468	0.0425, 0.1236
GoF	1.075	1.096	1.044	1.092
Complex #	**42**	**43**	**44**	
formula	C15H21Al Cl3NTi	C28H20 Cl3NTi	C31H47Al4 Cl6N4Ti2	
Mw	396.56	524.70	897.24	
space group	P2(1)/n	P2(1)/n	P-1	
a (Å)	10.865(2)	11.179(9)	10.115(4)	
b (Å)	12.315(2)	17.464(9)	10.634(4)	
c (Å)	13.627(3)	12.384(9)	11.237(4)	
α	90	90	94.341(5)	
β	93.293(2)	111.49(2)	106.071(5)	
γ	90	90	111.807(5)	
V (Å3)	1820.4(6)	2250(3)	1056.5(7)	
radiation	0.71073	0.71073	0.71073	
T (K)	208(2)	208(2)	208(2)	
Dcalcd (g cm-3)	1.447	1.549	1.410	
μcalcd (mm-1)	0.951	0.755	0.880	
F000	816	1072	462	
R, Rw2a	0.0621, 0.1660	0.0620, 0.1559	0.0503, 0.1247	
GoF	1.072	1.033	1.057	

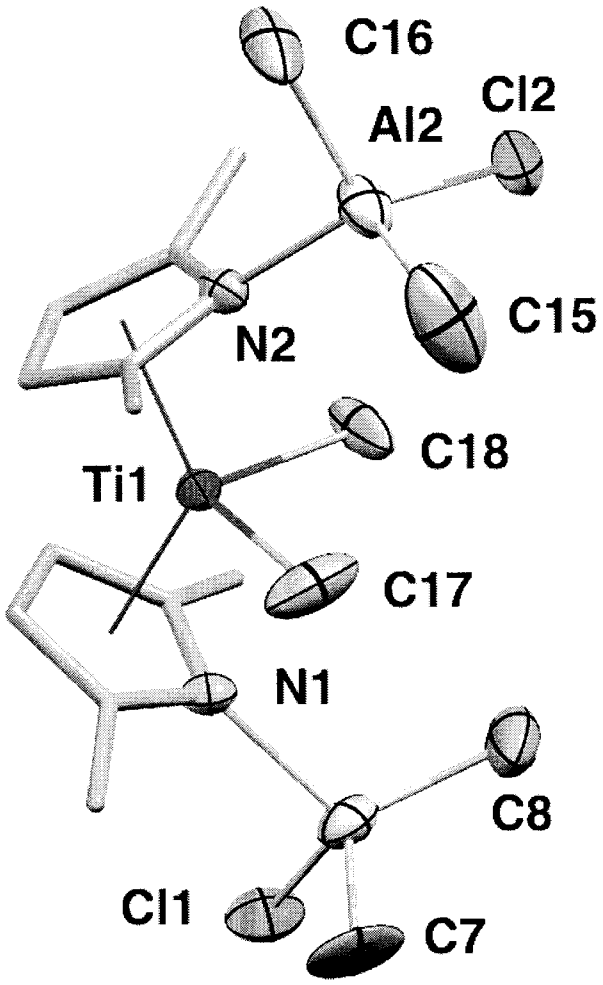

Figure 95: Partial thermal ellipsoid plot of $\{(\eta^5\text{-DMP-AlMe}_2\text{Cl})_2\text{TiMe}_2\}$ (**38**) with ellipsoids drawn at 50% probability.

Table 43: Selected Bond Distances (Å) and Angles (°) for $\{(\eta^5\text{-DMP-AlMe}_2\text{Cl})_2\text{TiMe}_2\}$ (**38**).

Ti-Cnt(1)	2.116	N(1)-C(2)	1.388(5)
Ti-Cnt(2)	2.136	C(2)-C(3)	1.387(7)
Ti-C(18)	2.102(5)	C(3)-C(4)	1.363(7)
Ti-C(17)	2.133(5)	C(4)-C(5)	1.370(7)
Al(1)-N(1)	1.993(4)	Cnt(1)-Ti-Cnt(2)	131.26
N(1)-C(5)	1.385(6)	N(1)-Cnt(1)-Ti	91.45
		N(2)-Cnt(2)-Ti	92.79

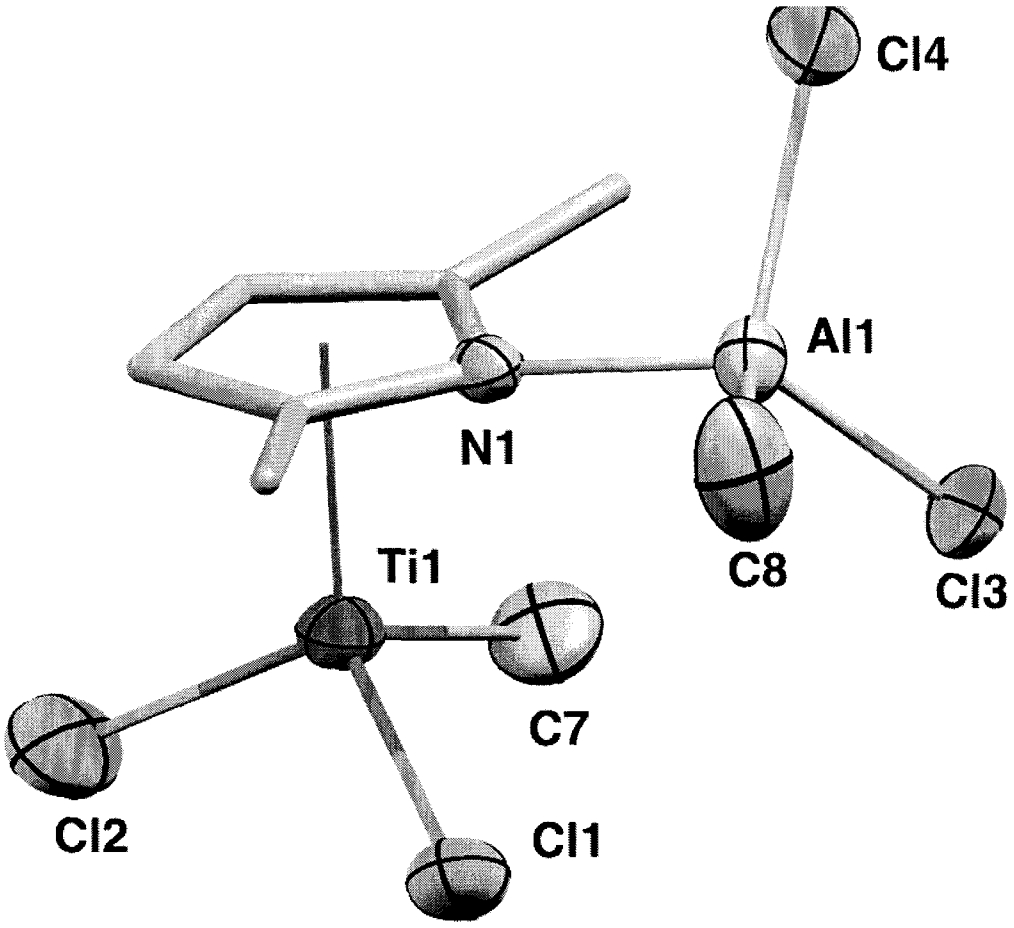

Figure 96: Partial thermal ellipsoid plot of $\{(\eta^5\text{-DMP-AlMeCl}_2)\text{TiCl}_2\text{Me}\}$ (**39**) with ellipsoids drawn at 50% probability.

Table 44: Selected Bond Distances (Å) and Angles (°) for $\{(\eta^5\text{-DMP-AlMeCl}_2)\text{TiCl}_2\text{Me}\}$ (**39**).

Ti-Cnt	2.049	C(3)-C(4)	1.397
Ti-C(11)	2.049	C(4)-C(5)	1.379
Ti-Cl(1)	2.213	C(5)-N	1.395
Ti-Cl(2)	2.204	Ti-Cnt-N	89.71
N-C(2)	1.392	Al-N-Cnt	169.92
C(2)-C(3)	1.394		

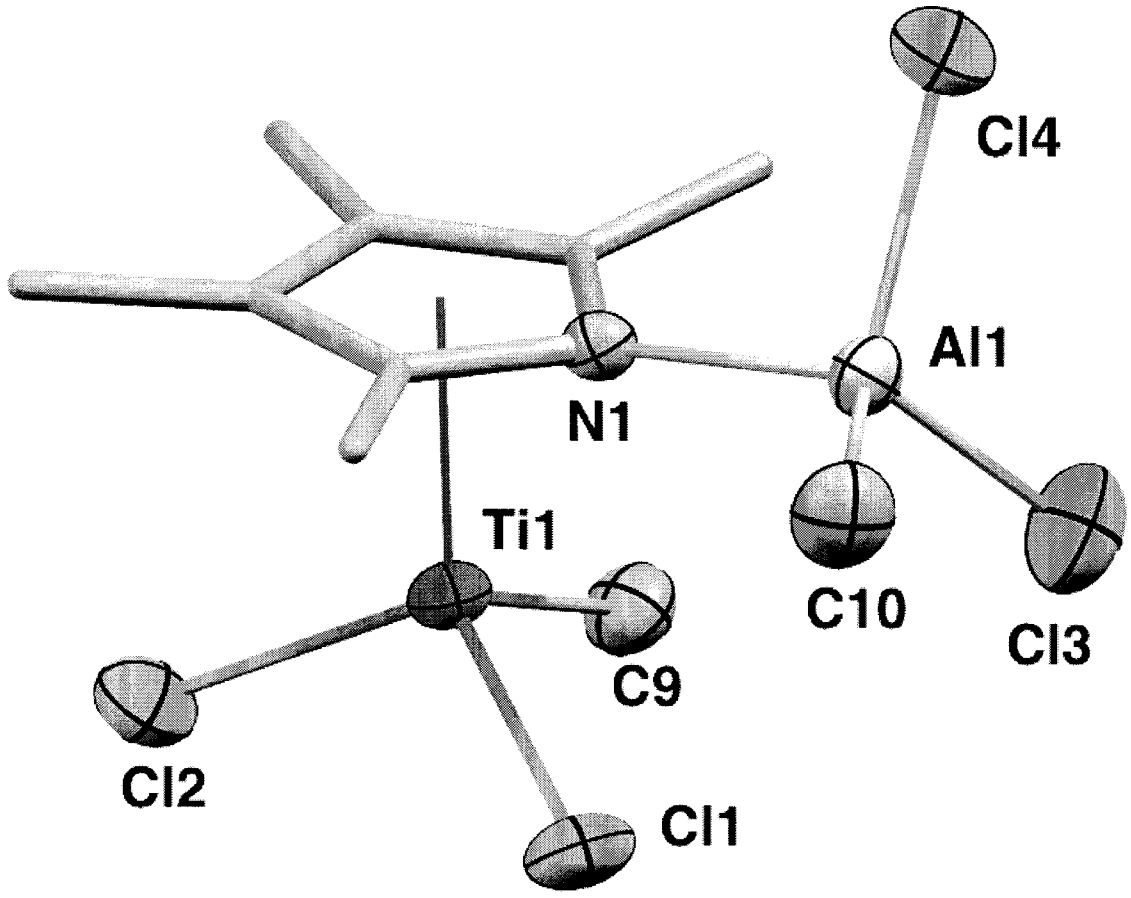

Figure 97: Partial thermal ellipsoid plot of (η^5-TMP-$AlCl_2Me$)$TiCl_2Me$} (**40**) with ellipsoids drawn at 50% probability.

Table 45: Selected Bond Distances (Å) and Angles (°) for (η^5-TMP-$AlCl_2Me$)$TiCl_2Me$} (**40**).

Ti-Cnt	2.067	C(2)-C(3)	1.429(5)
Ti-C(9)	2.092(4)	C(3)-C(4)	1.400(5)
Ti-Cl(1)	2.2281(17)	N(1)-C(4)	1.408(4)
Ti-Cl(2)	2.2295(19)	Ti-Cnt-N	84.08
C(1)-C(2)	1.408(5)	ALl-N-Cnt	170.47
N(1)-C(1)	1.410(4)		

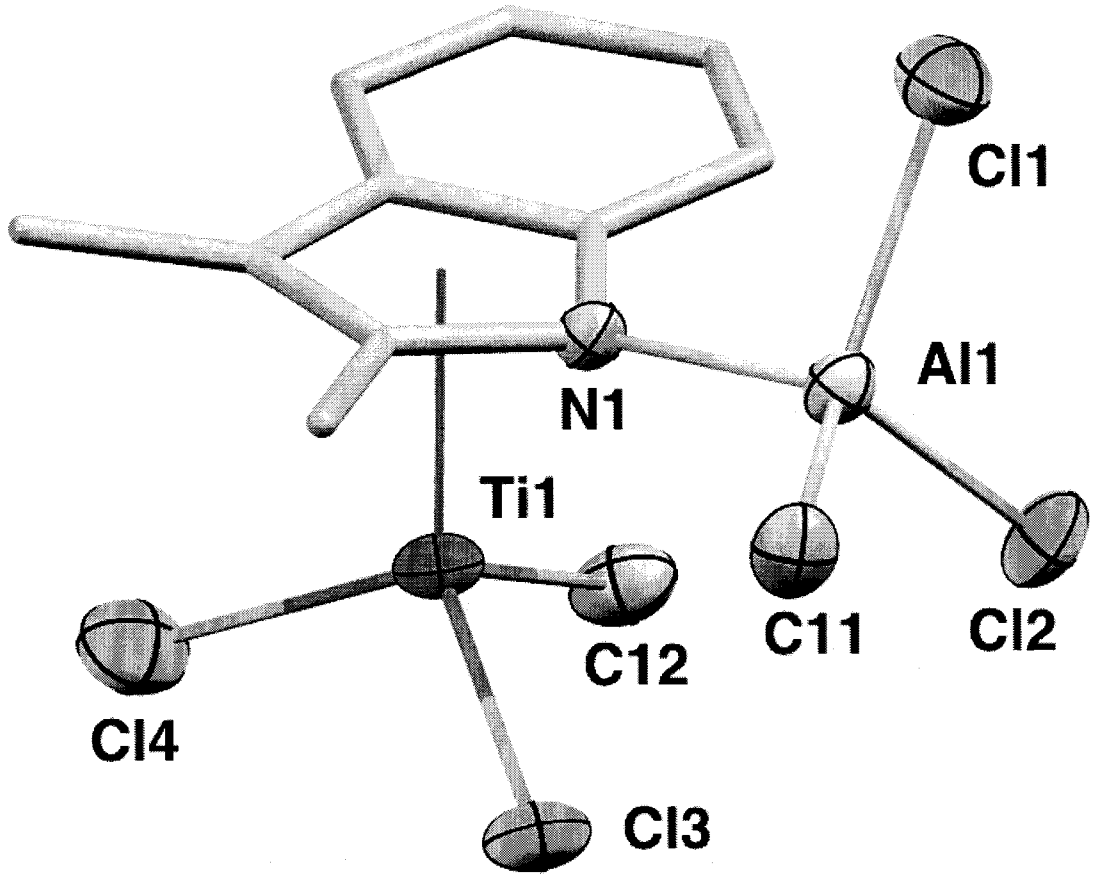

Figure 98: Partial thermal ellipsoid plot of {(η^5-DMI-$AlCl_2Me$)$TiCl_2Me$} (**41**) with ellipsoids drawn at 50% probability.

Table 46: Selected Bond Distances (Å) and Angles (°) for {(η^5-DMI-$AlCl_2Me$)$TiCl_2Me$} (**41**).

Ti-Cnt	2.084	N(1)-C(8)	1.404(4)
Ti-C(12)	2.067(4)	N(1)-C(1)	1.408(4)
Ti-Cl(3)	2.2065(11)	C(1)-C(6)	1.417(5)
Ti-Cl(4)	2.2291(13)	C(7)-C(8)	1.395(5)
Al(1)-N(1)	1.982(3)	C(6)-C(7)	1.433(5)
		Ti-Cnt-N	82.54

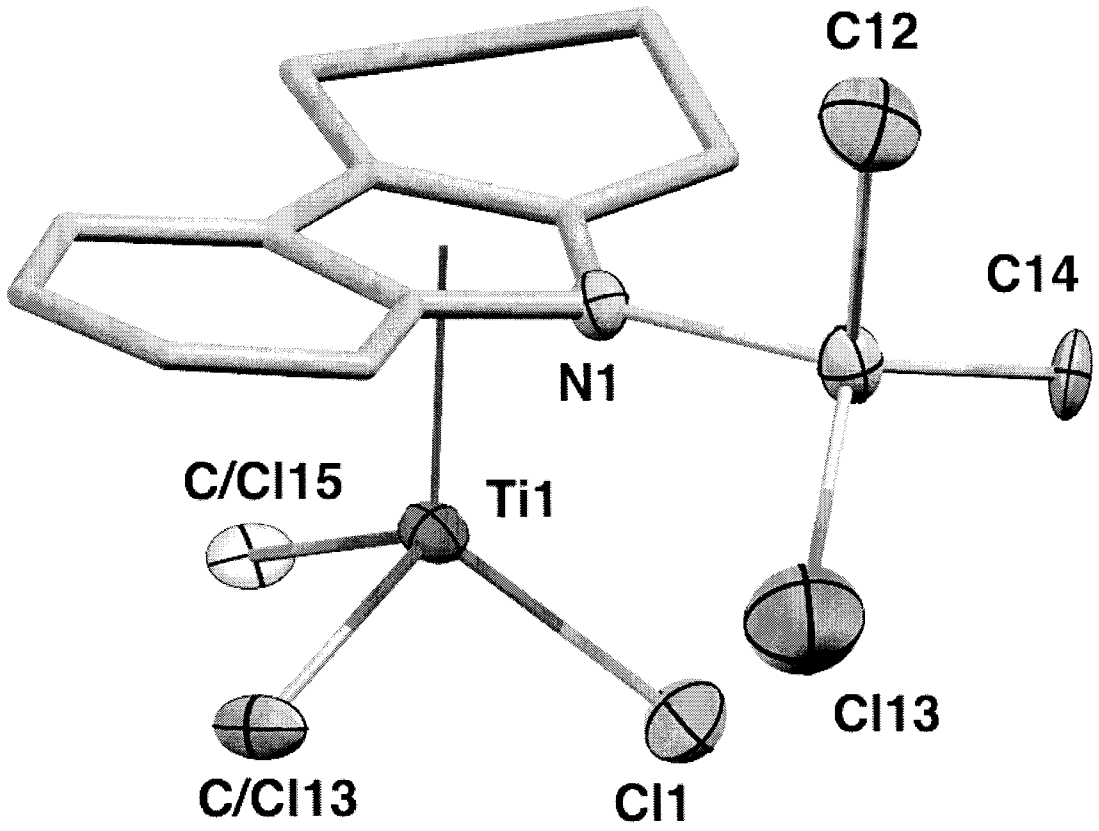

Figure 99: Partial thermal ellipsoid plot of {(η^5-THC-$AlMeCl_2$)$TiCl_2Me$} (**42**) with ellipsoids drawn at 50% probability.

Table 47: Selected Bond Distances (Å) and Angles (°) for {(η^5-THC-$AlMeCl_2$)$TiCl_2Me$} (**42**).

Ti-Cnt	2.088	N(1)-C(1)	1.413(5)
Ti-C/Cl(13)	2.139(4)	C(1)-C(6)	1.403(6)
Ti-C/Cl(15)	2.138(4)	C(6)-C(7)	1.446(6)
TI-Cl(1)	2.2100(16)	C(7)-C(12)	1.387(6)
C(6)-C(7)	1.446(6)	Ti-Cnt-N	81.51
C(7)-C(12)	1.387(6)	AL-N-Cnt	171.16
N(1)-C(12)	1.399(5)		

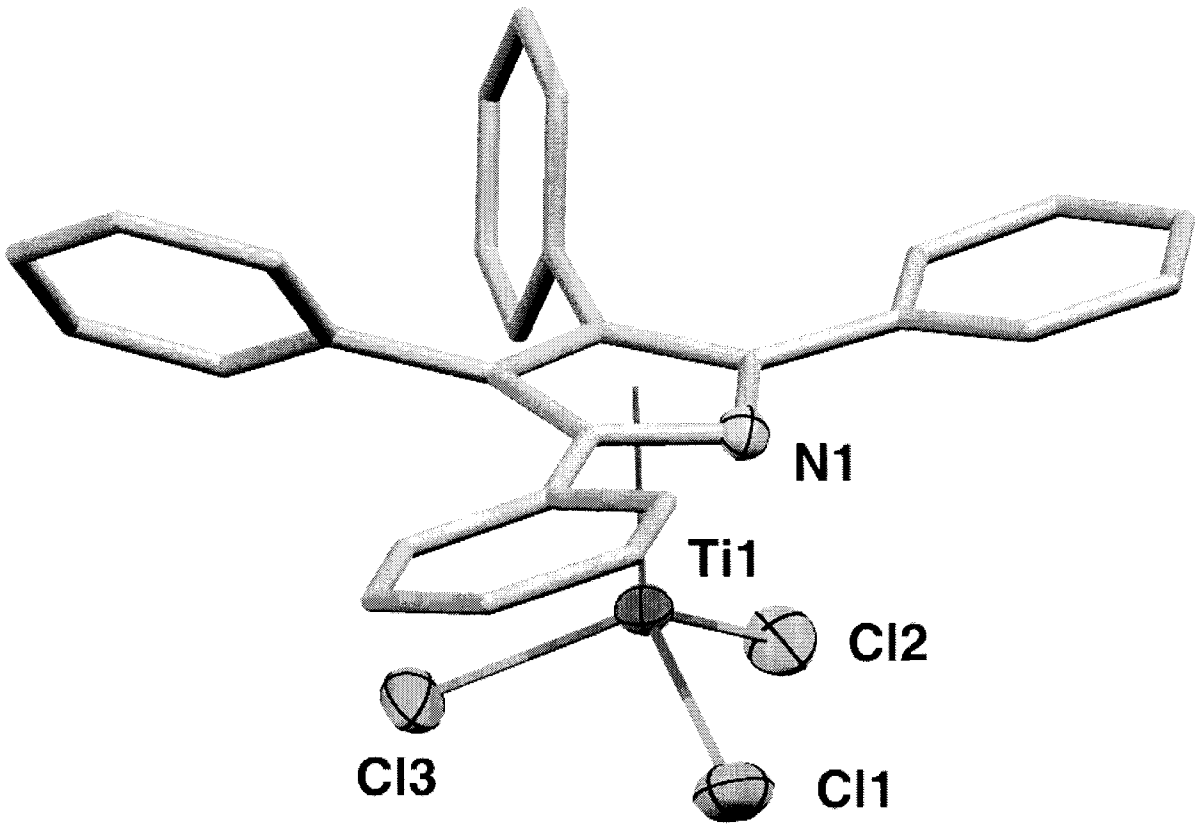

Figure 100: Partial thermal ellipsoid plot of $\{(\eta^5\text{-TPP})TiCl_3\}$ (**43**) with ellipsoids drawn at 50% probability.

Table 48: Selected Bond Distances (Å) and Angles (°) for $\{(\eta^5\text{-TPP})TiCl_3\}$ (**43**)

Ti-Cnt	2.01	C(2)-C(3)	1.399(7)
Ti-Cl(1)	2.167(2)	C(3)-C(4)	1.394(7)
Ti-Cl(2)	2.152(2)	Ti-Cnt-N	79.42
Ti-Cl(3)	2.179(2)	Phenyl Ring Torsion Angles:	
N(1)-C(4)	1.354(6)	C(4)-C(3)-C(17)-C(18)	95.59
N(1)-C(1)	1.360(6)	C(3)-C(2)-C(11)-C(16)	52.85
C(1)-C(2)	1.393(7)	N(1)-C(1)-C(5)-C(6)	21.63
		N(1)-C(4)-C(23)-C(28)	-8.56

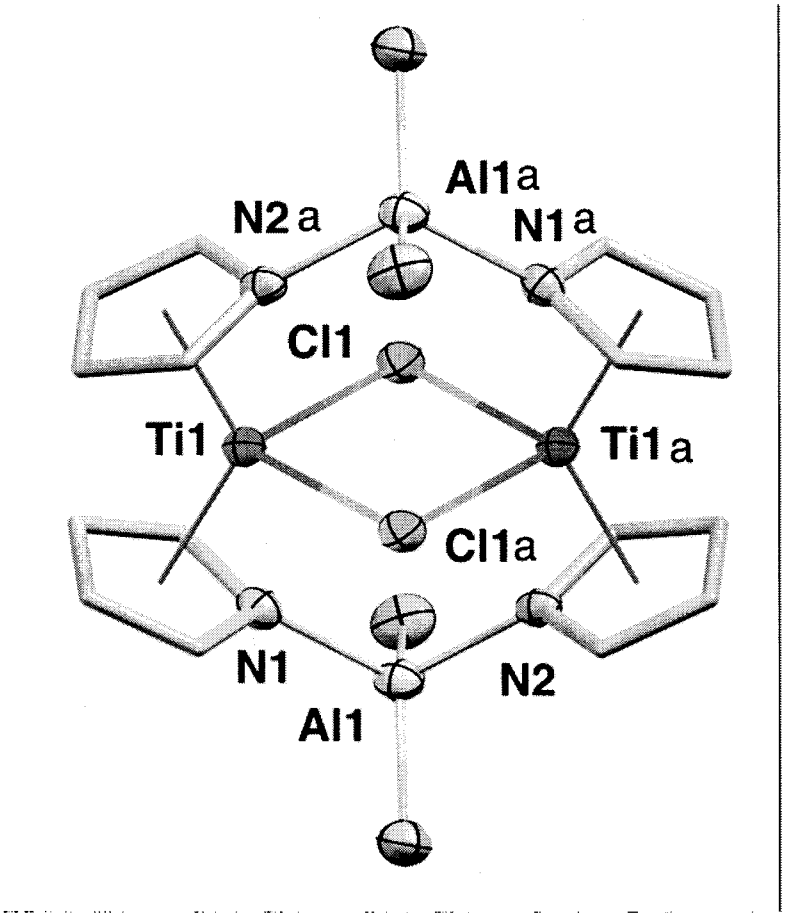

Figure 101: Partial thermal ellipsoid plot of $\{[Ti(\mu\text{-}Cl)(\mu\text{-}AlMe_2(\eta^5\text{-}Pyr)_2]_2\}$ $\{Me_2AlCl_2\}_2$ (**44**) with ellipsoids drawn at 50% probability.

Table 49: Selected Bond Distances (Å) and Angles (°) for $\{[Ti(\mu\text{-}Cl)(\mu\text{-}AlMe_2(\eta^5\text{-}Pyr)_2]_2\}$ $\{Me_2AlCl_2\}_2$ (**44**)

Ti-Cnt	2.064	C(1)-C(2)	1.38(3)
TI-Cnt(2)	2.059	C(2)-C(3)	1.42(3)
Ti-Cl	2.447(5)	C(3)-C(4)	1.37(3)
Ti-Ti	3.534(7)	Cl-Ti-Cl	87.86(16)
N(1)-C(1)	1.39(2)	Cnt-N-Al	165.05
N(1)-C(4)	1.39(2)	N1-Cnt-Ti	83.73
		Ti-Cnt-N2	84.25

6.2.9 Catalytic data

For single-component catalytic runs: the reactor was dried overnight in a 120 °C oven and then under vacuum at 130 °C for 1 hour. A pre-weighed amount of catalyst was dissolved in 100 mL of toluene under N_2 and injected into the preheated reactor. Solutions were heated using

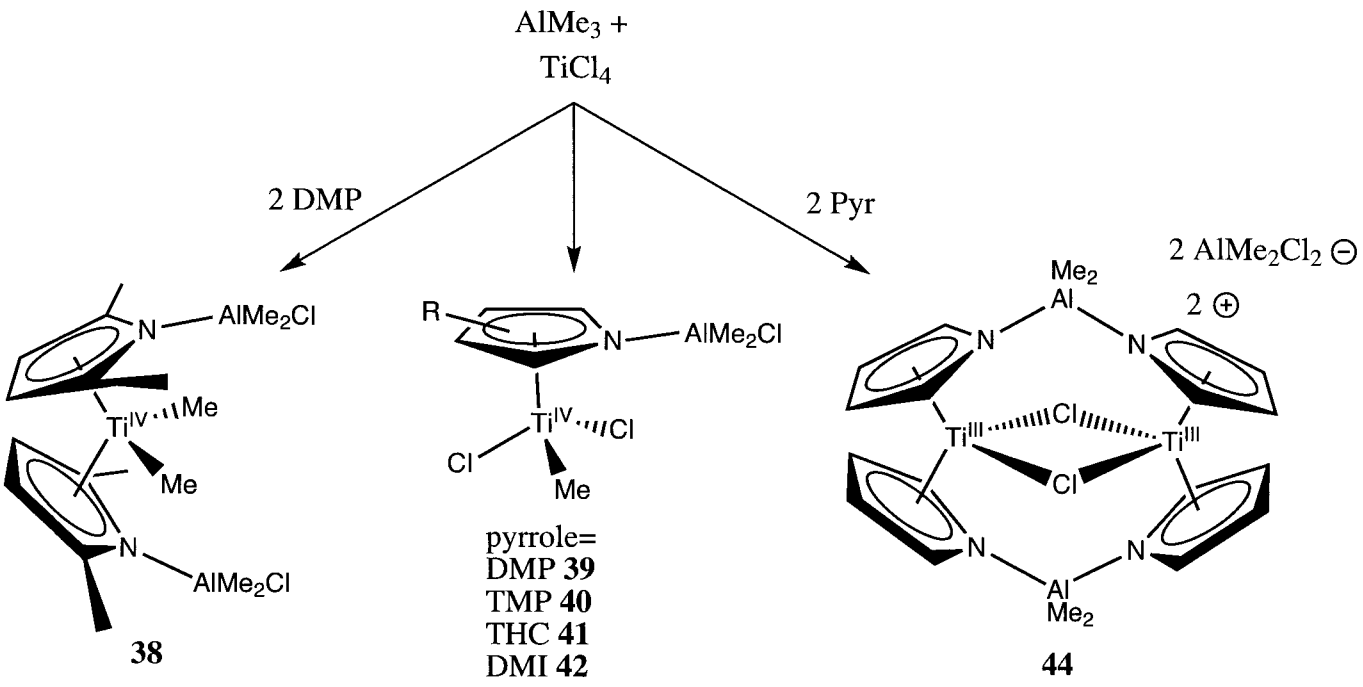

Figure 102: In-situ reaction of $TiCl_4$ with a variety of pyrrole ligands and Me_3Al

a thermostatic bath and charged with ethylene, maintaining the pressure throughout the run. Polymerizations were quenched by addition of EtOH and HCl. The resulting polymer was isolated by filtration, sonicated with an acidified ethanol solution, rinsed and thoroughly dried prior to characterization.

Table 50: Catalytic Data for Ti Pyrrole complexes **38-44**

Cat.	Cocatalyst	PE	activity	Tm_{1st}	Tm_{2nd}
#	(eq.)	(g)	(g/mol/h)	°C	°C
38	MAO (1000)	traces	0	n.a.	n.a.
38	Ph3C+ B(C6F5)3-	traces	0	n.a.	n.a.
39	Ph3C+ B(C6F5)3-	26.3	2 630 000	136	123
39	MAO (1000)	21.5	2 150 000	n.a.	n.a.
40	Ph3C+ B(C6F5)3-	14.1	1 410 000	136	123
41	Ph3C+ B(C6F5)3-	9.4	940 000	137	124
42	Ph3C+ B(C6F5)3-	11.7	1 170 000	137	124
43	Ph3C+ B(C6F5)3-	22.9	2 290 000	132	118
44	Ph3C+ B(C6F5)3-	4.0	400	n.a.	n.a.

V = 100 mL, catalyst = 10 μmole, time = 30 min. T = 60 °C.

6.3 Results and Discussion

The in-situ addition of $TiCl_4$ at 22 °C to a freshly prepared solution of Me_3Al and DMP in toluene in the ratio of Ti:Al:Pyr = 1:4:2 results in the formation of $\{(\eta^5\text{-DMP-AlMe}_2\text{Cl})_2\text{TiMe}_2\}$ (**38**) in high yield and purity within minutes (as observed via in-situ NMR) (Figure 103). The reaction is accompanied by methane gas evolution during the first minute, and large yellow plates of pure **38** form in high yield (>80%) upon suitable work-up. Despite being sufficiently thermally robust to allow storage for many months at room temperature in the solid state, complex **38** is light sensitive, turning dark brown within minutes when exposed to light in both solid state and solution of non-coordinating solvents. A suitable single crystal of **38** was analyzed by X-ray diffractometry (Figure 96), which revealed the typical sandwich structure of a bent metallocene complex. Geometric parameters are comparable with those of other bis-Cp, bis-η^5-pyrrole, and mixed Cp-η^5-pyrrole titanium complexes.[138, 45, 139, 54, 140] There still remains some measurable strain between the bulky Me_2AlCl groups of **38** resulting in slightly non-ideal titanium-centroid-nitrogen bond angles of 91.5° and 92.7°.

The ^1H and ^{13}C NMR of **38** is in agreement with the X-ray structural characterization, with one singlet observed for the two methyl groups bonded to titanium, and one singlet for the four methyl groups bonded to aluminum, suggesting that **38** is a stable structure in solution. The symmetry evident in the NMR is consistent with a C_{2v} symmetrical structure on the time scale of the experiment, which suggests that rapid rotation of the $AlMe_2Cl$ group around the N-Al axis is occuring, rendering the two methyl groups equivalent. The hydrogen atoms on the two pyrrole rings are equivalent on the NMR timescale as well.

The reaction of **38** with either MAO (1000 eq.) or $\{Ph_3C\}$ $\{B(C_6F_5)_4\}$ (1 or 2 eq.) resulted in no color change. The resulting products were exposed to ethylene but only small traces of polymer (< 100 mg) were formed under a variety of temperatures and pressures (Table 50). The poor activity of **38** was surprising based on the high performance of pyrrolide complexes as discussed in previous chapters. One possible explanation for the poor activity of **38** is that no vacant sites are generated at the titanium centre because the aluminum chloride residues on the two pyrrolide rings can chelate strongly to the metal centre. In this event, it would be expected that mono-pyrrolide

titanium complexes would be more active catalysts.

To evaluate this hypothesis, the one-pot synthetic method was adapted to generate cleanly the monopyrrolide {(η^5-DMP-$AlMeCl_2$)$TiCl_2Me$} (**39**) in high yield (84 %) by combining rapidly DMP, Me_3Al, and $TiCl_4$ in a 1:1:1 stoichiometric ratio (Figure 102). As hoped, monopyrrolide **39** is highly active for ethylene polymerization (Table 51). Thus the synthesis of other monopyrrolide derivatives was pursued to evaluate the effect of pyrrolide ligand substitution on the catalytic performance.

Fortunately, this was a straightforward task, as the same synthetic route used for **39** worked just as well for the isolation of [(η^5-TMP-$AlCl_2Me$)$TiCl_2Me$} (**40**), {(η^5-DMI-$AlCl_2Me$)$TiCl_2Me$} (**41**) and {(η^5-THC-$AlMeCl_2$)$TiCl_2Me$} (**42**) (Figure 102).

One major limitation of this synthetic method was that the more desirable sterically-hindered pyrrole TPP is too basic to be deprotonated with the $Me_3Al/TiCl_4$ mixture, resulting in a rapid decomposition to insoluble black powders. This limitation is easily overcome by using a more common multi-step synthetic protocol, which first involves lithiation of the perphenylpyrrole with n-BuLi. Subsequent complexation of the LiTPP with $TiCl_4$ generates a deep red solution of {(η^5-TPP)$TiCl_3$} (**43**), which after separation from the insoluble LiCl byproduct can be crystallized in good yield (72 %). The monopyrrolide complexes **39-42** were thermally stable but light sensitive, turning dark brown within minutes of exposure to visible light.

The crystalline samples of **39-43** were analyzed by X-ray diffraction. The resulting structures for **39-43** (Figures 96-100) were typical of the commonly encountered half-sandwich piano-stool type geometry in coordination chemistry. The structure of **42** is unique in that it has 50:50 Me/Cl disorder over (C/Cl(13)) and (C/Cl(15)). There are also substantial geometric differences between **39-43**, which are proposed to depend on the pyrrolide ring substitution in accordance with typical stereoelectronic effects as discussed below in more detail. The pyrrole-titanium ring slip angle (defined as the titanium-centroid-nitrogen angle) slightly from the near ideal in **39** (89.71°), to the most distorted in **42** (**39** = 89.71°, >**40** = 84.08°, >**41** = 82.54°, >**42** = 81.51°). Fortunately, the effect of electronic and steric factors of the pyrrole ring substituents can be deconvoluted. For instance, the electronic effect of the pyrrole ring substituents on the coordination geometry can

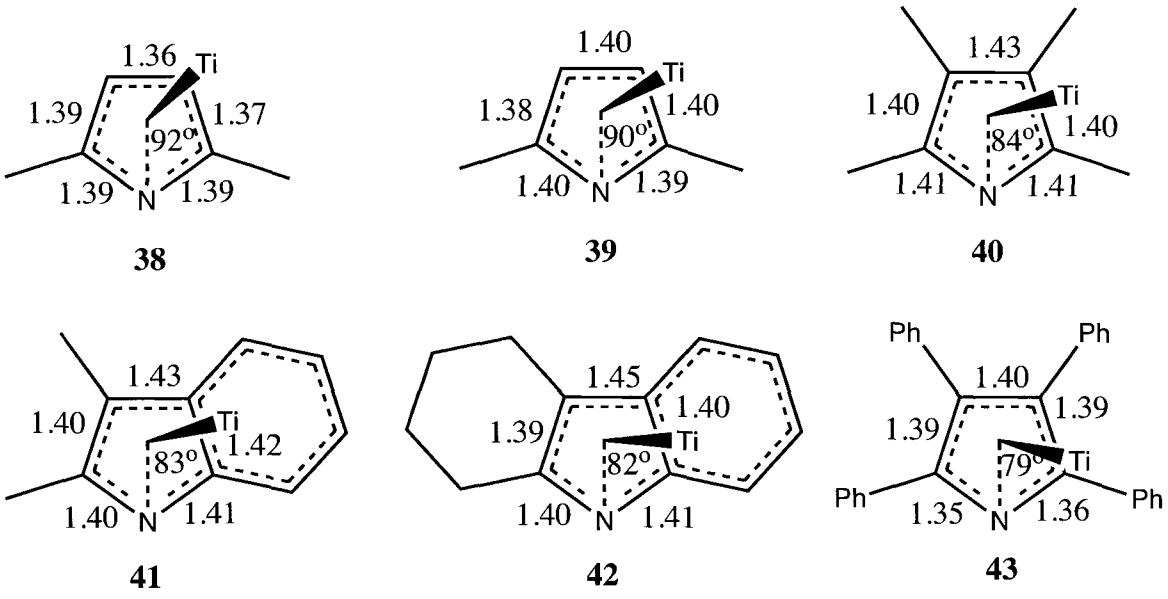

Figure 103: Comparison of pyrrolide structural parameters in **38-43**

be derived by comparing the pyrrolide complexes **39** and **40** with the indolide complexes **41** and **42**. A larger ring slip angle is observed for the fused indolide complexes by a few degrees, possibly due to the localization of negative charge on the nitrogen atom in the less aromatic indole ring (due to the fused phenyl ring). Finally, the steric effect of the ring substituents can be understood by comparing only the electronically similar pyrroles **39** to **40** and the indoles **41** to **42**, which reveals that the increasing steric bulk of the pyrrole ligand leads to a larger ring slip angle. This is probably due to steric interactions between the pyrrole ligand substituents and the other ligands bound to the titanium centre. Finally, more direct information related to the extent of aromaticity of the pyrrolide ring can be obtained directly from the bond lengths of the pyrrole ring consituents (Figure 103).

It is readily observed that the indole rings contain a more heterogeneous distribution of electron density consistent with a loss of aromaticity, as the bond lengths of the ring atoms vary much more than the pyrrole rings. By comparison, the Cr (II) indolyl complexes **23**/**24** discussed in chapter 4 show a much greater extent of ring slippage and the ring bond lengths also show greatly diminished aromaticity with increased ring slippage, thus confirming experimentally that ring slippage and a loss of aromaticity proceed in parallel. This loss of the energetically favorable resonance energy may serve as a kinetic barrier to ring slippage during catalysis, although more experimental and

computational work must be done to confirm this point.

Perphenylpyrrolide containing complex **43**, which does not retain an aluminum alkyl residue, is also unique in that the phenyl rings in the 2- and 5- ring positions are nearly co-planar with the central pyrrolide ring. This is possibly due to energetically favorable electron delocalization across all three rings for additional stabilization (the torsion angles between the central ring and the phenyl rings in the 2 and 5 positions are 21.6° and 8.6° respectively). This proposal is supported by the analysis of the bond lengths of the nitrogen atom of the TPP ring in **43** to the neighboring carbons, which are significantly shorter than in the other pyrrolide complexes discussed above, which is consistent with increased π electronic density at these bonds. The large π electron density near nitrogen in complex **43** and the increased steric impact of the phenyl groups in the 3 and 4 positions contributes to a large ring slip angle (Ti-Cnt-N = 79.42°).

The solution NMR spectra of **39-42** were recorded as part of their full characterization. As in complex **38**, the titanium methyl ^{1}H and ^{13}C signals were located with the aid of two-dimentional HMQC experiments, where generally their ^{13}C signals were characteristically in the region 60-100 ppm, and their ^{1}H signals were between 1 and 2 ppm. The ring carbons of the pyrrole and indole were between 110 and 130 ppm (^{13}C), and the alkyl substituents on the pyrrole rings were located between 50 and 10 ppm (^{13}C). The aluminum methyls came around 0 ppm in both the ^{13}C and ^{1}H spectra, but were usually very broad multiplets in the ^{13}C spectra due to the strong splitting by the quadrupolar spin 5/2 aluminum nucleus. The NMR spectra of **39-42** were, however, unusually complex and difficult to interpret, with several different isomers observable in solution. Chemical exchange is also confirmed in the NMR spectra, where EXSY experiments revealed cross peaks for certain sets of isomers, but again it was quite convoluted and very difficult to interpret. Future studies are aimed at understanding and modelling the difficult to interpret NMR spectra of **39-42**, with the hopes that further mechanistic insights into the hemilability of pyrrole can be gained. For example, the ^{1}H and EXSY NMR spectra (exchange only cross peaks)for complex **42** is presented (Figure 104).

The ethylene polymerization performance by the mono-pyrrole complexes **39-43** with one equivalent of trityl borate activator was evaluated (table 51). The most active catalysts were **39** and **43**,

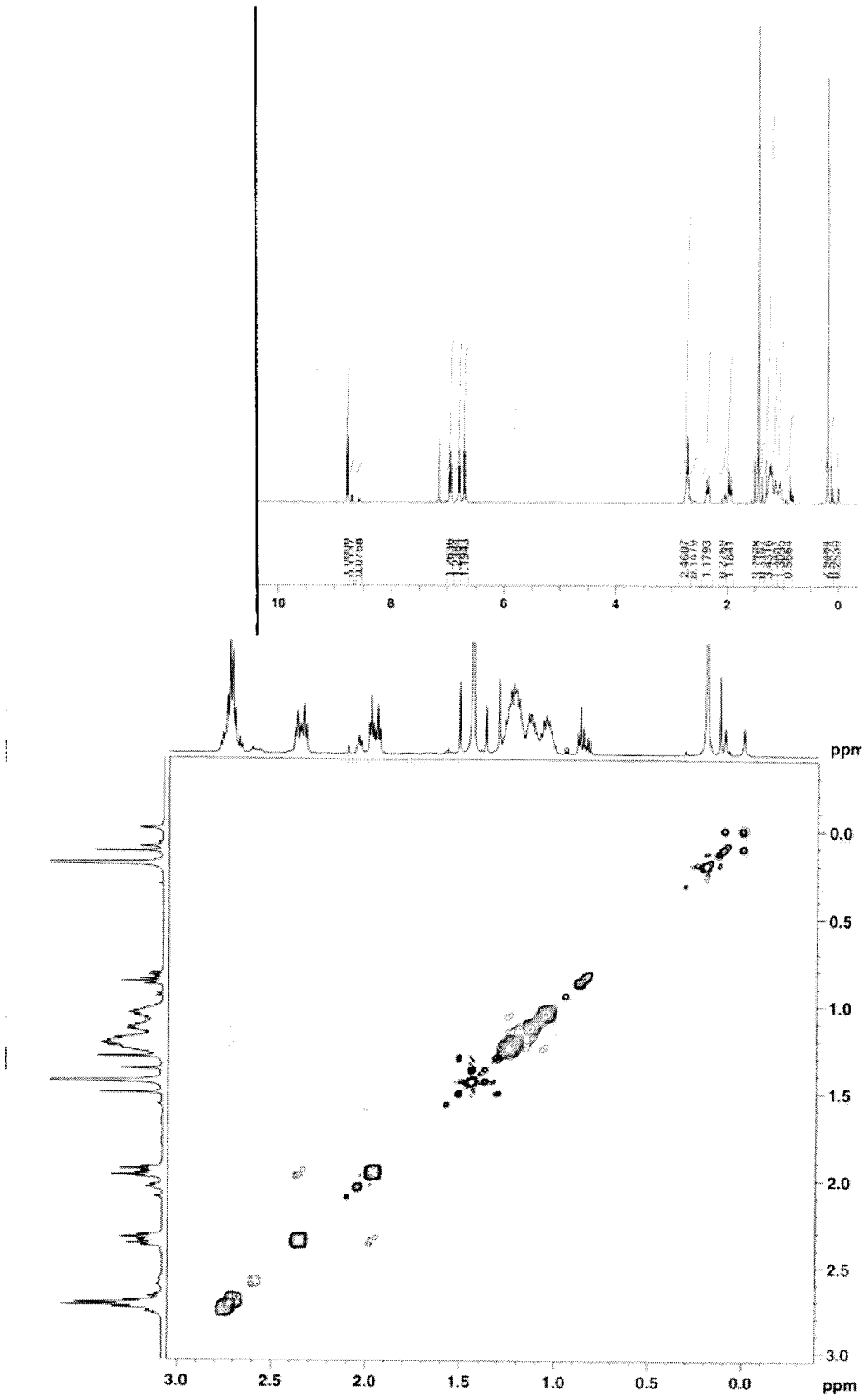

Figure 104: Top ^{1}H NMR and bottom EXSY for **42**

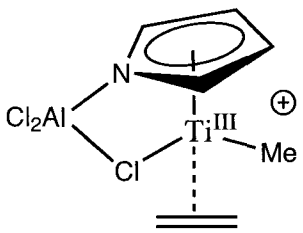

Figure 105: Proposed active catalyst for the titanium pyrrolide system containing a "constrained geometry".

and the least active was **42**, but by only a relatively small factor. This positive result confirms that the pyrrolide ligand can support highly active catalysts for titanium, vanadium, and chromium which makes it a very versatile ligand platform in olefin polymerization.

Finally, when unsubstituted pyrrole is used as a ligand, the dimeric dicationic Ti(III) complex, $\{[Ti(\mu\text{-}Cl)(\mu\text{-}AlMe_2(\eta^5\text{-}Pyr)_2]_2\}$ $\{Me_2AlCl_2\}_2$ (**44**), was isolated in moderate yield (Figure 103). This diamagnetic antiferromagnetically coupled dimeric complex displayed a somewhat lower activity than the Ti(IV) monopyrroles **39-43**, but higher than the bis pyrrolyl Ti(IV) precursor **38**. However, this fact opens the mechanistic possibility that the oxidation state of the active catalyst for **39-43** are Ti(III) as well, suggesting that they bear a resemblance to the commercially important "constrained geometry" class of titanium catalysts (Figure 105).

6.4 Conclusions

In conclusion, this chapter discussed the investigation of pyrrolide complexes with titanium for ethylene polymerization. The exact composition and oxidation state of the titanium centre was found to play a large role in the catalytic behavior. It is concluded that, most likely, the Ti(III) mono-pyrrolyl species is the active catalyst for this system, although there is no direct experimental evidence for this. Future efforts could focus on understanding these unusual NMR spectra to gain mechanistic insights into the dynamic behavior of metal pyrrolide complexes.

Conclusion of Part II: Exploration of the pyrrole ligand for olefin polymerization.

In summary, the study of the complexes of pyrrole with chromium, vanadium, and titanium has revealed mechanistic insights into the unique properties of this ligand system. Thus the pyrrole ligand can be considered an excellent ligand platform for olefin polymerization with early metal catalysts, among other catalytic applications. These properties are due to the hemilability and diverse coordination modes of pyrrole, which was alluded to in the introdution of this thesis. The recent emergence of the chain-shuttling process for block copolymer production makes the further development of the pyrrole ligand in olefin polymerization a highly topical issue, as the hemilability of pyrrole could be an important tool to control the rate of chain shuttling between the transition metal and aluminum alkyl centres.

7 Conclusions and recommendations for future work

7.1 Conclusions

The studies described in this thesis have provided many valuable mechanistic insights into both chromium-based ethylene trimerization/tetramerization catalysis and the dynamics of pyrrole-based ligands in catalysis. These insights in turn reveal new mechanistic puzzles and experimental methods for future researchers in this field to build on. In addition, many well-defined single-component catalyst systems have been developed which can be readily modelled computationally for further insights into their dynamics and rational development. A few specific key results include: 1) the discovery of ligand-directed cocatalyst hemilability, 2) the divergent bimetallic reactivity of organochromium intermediates related to ethylene tetramerization, 3) well-defined single-component catalysts for ethylene trimerization, and 4) the beneficial effect of pyrrole ring slippage for the convenient generation of catalytically active species. These discoveries are fertile grounds for further development with good prospects for commercially valuable catalytic applications and mechanistically important insights of fundamental nature, which can enhance collaboration between academic and industrial researchers.

7.2 Recommendations for future work.

As it was discovered that the pyrrole ligand is versatile enough to give rise to metal catalysts for both ethylene trimerization and polymerization via a convenient and inexpensive in-situ protocol, it would be highly economical to use this methodology for the commercial production of LLDPE in a single reactor. This project would both require to understand the underlying organometallic chemistry in addition to the process issues related to a tandem catalyst. However the potentially large cost-savings of such a process in terms of both the simplicity of building and maintaining much fewer mechanical components and a very inexpensive and convenient catalyst preparation cannot be ignored.

Secondly, the mechanistic study of the [PNP] chromium tetramerization system raised the possibility that bimetallic intermediates play a large role in the observed 1-octene selectivity, and

future efforts to design improved tetramerization catalysts could focus on the efficient synthesis of bridging ligands to control the chromium-chromium interaction.

Finally, future ligand design for olefin polymerization could focus on providing coordination sites for low-valent transition metal centres and aluminum alkyl cocatalysts, which may generate highly reactive zwitterionic species. Such systems are expected to play a large role in the future development of olefin polymerization catalysis, as they are well-defined and should provide a lower overall cost of development and implementation compared to more traditional systems.

References

[1] Jabri, A.; Crewdson, P.; Gambarotta, S.; Korobkov, I.; Duchateau, R. *Organometallics* **2006**, *25*, 715–718.

[2] Jabri, A.; Temple, C.; Crewdson, P.; Gambarotta, S.; Korobkov, I.; Duchateau, R. *J. Am. Chem. Soc.* **2006**, *128*, 9238–9247.

[3] Temple, C.; Jabri, A.; Crewdson, P.; Gambarotta, S.; Korobkov, I.; Duchateau, R. *Angew. Chem. Int. Ed. Engl.* **2006 Oct 27**, *45*, 7050–7053.

[4] Jabri, A.; Korobkov, I.; Garnbarotta, S.; Duchateau, R. *Angew. Chem. Int. Ed. Engl.* **2007**, *46*, 6119–6122.

[5] Jabri, A.; Mason, C. B.; Sim, Y.; Gambarotta, S.; Burchell, T. J.; Duchateau, R. *Angew. Chem. Int. Ed. Engl.* **2008**, *47*, 9717–9721.

[6] Jabri, A.; Gambarotta, S.; Duchateau, R. *Chemical and Engineering News* **2008**, *86*, 56.

[7] Severn, J.; Chadwick, J.; Duchateau, R.; Friederichs, N. *Chem. Rev.* **2005**, *105*, 4073–4147.

[8] Onsager, O.; Wang, H.; Blindhei, U. *Helv. Chim. Acta* **1969**, *52*, 215.

[9] Ziegler, K.; Holzkamp, E.; Breil, H.; Martin, H. *Angew. Chem. Int. Ed. Engl.* **1955**, *67*, 541–547.

[10] Natta, G. *J. Inorg. and Nuc. Chem.* **1958**, *8*, 589–611.

[11] Wilkinson, G.; Birmingham, J. *J. Am. Chem. Soc.* **1954**, *76*, 4281–4284.

[12] Breslow, D.; Newburg, N. *J. Am. Chem. Soc.* **1959**, *81*, 81–86.

[13] Breslow, D.; Newburg, N. *J. Am. Chem. Soc.* **1957**, *79*, 5072–5073.

[14] Long, W.; Breslow, D. *J. Am. Chem. Soc.* **1960**, *82*, 1953–1957.

[15] Natta, G.; Pino, P.; Mazzanti, G.; Giannini, U. *J. Am. Chem. Soc.* **1957**, *79*, 2975–2976.

[16] Zefirova, A.; Tikhomirova, N.; Shilov, A. *Doklady Akademii Nauk SSSR* **1960**, *132*, 1082–1085.

[17] Cossee, P. *J. Catal.* **1964**, *3*, 80–88.

[18] Arlman, E.; Cossee, P. *J. Catal.* **1964**, *3*, 99–104.

[19] Manyik, R.; Walker, W.; Wilson, T. *US 3300458* **1967**.

[20] Manyik, R.; Walker, W.; Wilson, T. *J. Catal.* **1977**, *47*, 197–209.

[21] Long, W.; Breslow, D. *Annalen der Chemie-Justus Liebig* **1975**, 463–469.

[22] Andresen, A.; Cordes, H.; Herwig, J.; Kaminsky, W.; Merck, A.; Mottweiler, R.; Pein, J.; Sinn, H.; Vollmer, H. *Angew. Chem. Int. Ed. Engl.* **1976**, *15*, 630–632.

[23] Chen, E.; Marks, T. *Chem. Rev.* **2000**, *100*, 1391–1434.

[24] Eisch, J.; Piotrowski, A.; Brownstein, S.; Gabe, E.; Lee, F. *J. Am. Chem. Soc.* **1985**, *107*, 7219–7221.

[25] Jordan, R.; Bajgur, C.; Willett, R.; Scott, B. *J. Am. Chem. Soc.* **1986**, *108*, 7410–7411.

[26] Braunschweig, H.; Breitling, F. M. *Coord. Chem. Rev.* **2006**, *250*, 2691–2720.

[27] Britovsek, G.; Gibson, V.; Kimberley, B.; Maddox, P.; McTavish, S.; Solan, G.; White, A.; Williams, D. *Chem. Comm.* **1998**, 849–850.

[28] Reagan, W. K. *EP0417477* **1991**.

[29] Kohn, R.; Haufe, M.; Kociok-Kohn, G.; Grimm, S.; Wasserscheid, P.; Keim, W. *Angew. Chem. Int. Ed. Engl.* **2000**, *39*, 4337.

[30] McGuinness, D.; Wasserscheid, P.; Keim, W.; Morgan, D.; Dixon, J.; Bollmann, A.; Maumela, H.; Hess, F.; Englert, U. *J. Am. Chem. Soc.* **2003**, *125*, 5272–5273.

[31] McGuinness, D.; Wasserscheid, P.; Morgan, D.; Dixon, J. *Organometallics* **2005**, *24*, 552–556.

[32] Agapie, T.; Day, M. W.; Henling, L. M.; Labinger, J. A.; Bercaw, J. E. *Organometallics* **2006**, *25*, 2733–2742.

[33] Tkach, V. S.; Suslov, D. S.; Myagmarsuren, G.; Shmidt, F. K. *Russ. J. of App. Chem.* **2007**, *80*, 1419–1423.

[34] Zhang, J.; Braunstein, P.; Hor, T. S. A. *Organometallics* **2008**, *27*, 4277–4279.

[35] Deckers, P.; Hessen, B.; Teuben, J. *Angew. Chem. Int. Ed. Engl.* **2001**, *40*, 2516.

[36] Murtuza, S.; Harkins, S.; Long, G.; Sen, A. *J. Am. Chem. Soc.* **2000**, *122*, 1867–1872.

[37] Andes, C.; Harkins, S.; Murtuza, S.; Oyler, K.; Sen, A. *J. Am. Chem. Soc.* **2001**, *123*, 7423–7424.

[38] Hagen, H.; Kretschmer, W.; van Buren, F.; Hessen, B.; van Oeffelen, D. *J. Molec. Cat. A* **2006**, *248*, 237–247.

[39] Emrich, R.; Heinemann, O.; Jolly, P.; Kruger, C.; Verhovnik, G. *Organometallics* **1997**, *16*, 1511–1513.

[40] Agapie, T.; Labinger, J. A.; Bercaw, J. E. *J Am Chem Soc* **2007**, *129*, 14281–14295.

[41] Agapie, T.; Schofer, S.; Labinger, J.; Bercaw, J. *J. Am. Chem. Soc.* **2004**, *126*, 1304–1305.

[42] Dohring, A.; Jensen, V.; Jolly, P.; Thiel, W.; Weber, J. *Macromolecular Symposia* **2001**, *173*, 117–121.

[43] Tobisch, S.; Ziegler, T. *Organometallics* **2003**, *22*, 5392–5405.

[44] van Rensburg, W.; Grove, C.; Steynberg, J.; Stark, K.; Huyser, J.; Steynberg, P. *Organometallics* **2004**, *23*, 1207–1222.

[45] Tobisch, S.; Ziegler, T. *J. Am. Chem. Soc.* **2004**, *126*, 9059–9071.

[46] Tobisch, S.; Ziegler, T. *Organometallics* **2004**, *23*, 4077–4088.

[47] Tobisch, S.; Ziegler, T. *Organometallics* **2005**, *24*, 256–265.

[48] van Rensburg, W. J.; van den Berg, J.-A.; Steynberg, P. J. *Organometallics* **2007**, *26*, 1000–1013.

[49] Bollmann, A.; Blann, K.; Dixon, J.; Hess, F.; Killian, E.; Maumela, H.; McGuinness, D.; Morgan, D.; Neveling, A.; Otto, S.; Overett, M.; Slawin, A.; Wasserscheid, P.; Kuhlmann, S. *J. Am. Chem. Soc.* **2004**, *126*, 14712–14713.

[50] McGuinness, D. S.; Suttil, J. A.; Gardiner, M. G.; Davies, N. W. *Organometallics* **2008**, *27*, 4238–4247.

[51] Tomov, A.; Chirinos, J.; Jones, D.; Long, R.; Gibson, V. *J. Am. Chem. Soc.* **2005**, *127*, 10166–10167.

[52] Hao, S.; Song, J.; Berno, P.; Gambarotta, S. *Organometallics* **1994**, *13*, 1326–1335.

[53] Matsui, S.; Yoshida, Y.; Takagi, Y.; Spaniol, T.; Okuda, J. *J. Organomet. Chem.* **2004**, *689*, 1155–1164.

[54] Buil, M. L.; Esteruelas, M. A.; Lopez, A. M.; Mateo, A. C. *Organometallics* **2006**, *25*, 4079–4089.

[55] Mazet, C.; Gade, L. *Organometallics* **2001**, *20*, 4144–4146.

[56] Altman, R. A.; Anderson, K. W.; Buchwald, S. L. *J. Org. Chem.* **2008**, *73*, 5167–5169.

[57] Banfi, S.; Manfredi, A.; Montanari, F.; Pozzi, G.; Quici, S. *J. Molec. Cat. A* **1996**, *113*, 77–86.

[58] Hock, A. S.; Schrock, R. R.; Hoveyda, A. H. *J. Am. Chem. Soc.* **2006**, *128*, 16373–16375.

[59] Drouin, S.; Foucault, H.; Yap, G.; Fogg, D. *Can. J. Chem.* **2005**, *83*, 748–754.

[60] Otten, E.; Meetsma, A.; Hessen, B. *J. Am. Chem. Soc.* **2007**, *129*, 10100.

[61] Briggs, J. *Chem. Comm.* **1989**, 674–675.

[62] Schofer, S.; Day, M.; Henling, L.; Labinger, J.; Bercaw, J. *Organometallics* **2006**, *25*, 2743–2749.

[63] McGuinness, D. S.; Brown, D. B.; Tooze, R. P.; Hess, F. M.; Dixon, J. T.; Slawin, A. M. Z. *Organometallics* **2006**, *25*, 3605–3610.

[64] Uhlig, E. *Organometallics* **1993**, *12*, 4751–4756.

[65] Richeson, D.; Hsu, S.; Fredd, N.; Vanduyne, G.; Theopold, K. *J. Am. Chem. Soc.* **1986**, *108*, 8273–8274.

[66] Non, S.; Sendlinger, S.; Janiak, C.; Theopold, K. *J. Am. Chem. Soc.* **1989**, *111*, 9127–9129.

[67] Thomas, B.; Theopold, K. *J. Am. Chem. Soc.* **1988**, *110*, 5902–5903.

[68] Dixon, J.; Green, M.; Hess, F.; Morgan, D. *J. Orgmet. Chem.* **2004**, *689*, 3641–3668.

[69] Barrera, J.; Wilcox, D. *Inorg. Chem.* **1992**, *31*, 1745–1752.

[70] Bhandari, G.; Reingold, A.; Theopold, K. *Chem. Eur. J.* **1995**, *1*, 199–203.

[71] Espenson, J. *Inorg. Chem.* **1965**, *4*, 1533–&.

[72] Elowe, P. R.; McCann, C.; Pringle, P. G.; Spitzmesser, S. K.; Bercaw, J. E. *Organometallics* **2006**, *25*, 5255–5260.

[73] Jiang, T.; Ning, Y.; Zhang, B.; Li, J.; Wang, G.; Yi, J.; Huang, Q. *J. Molec. Cat. A* **2006**, *259*, 161–165.

[74] Kuhlmann, S.; Blann, K.; Bollmann, A.; Dixon, J. T.; Killian, E.; Maumela, M. C.; Maumela, H.; Morgan, D. H.; Pretorius, M.; Taccardi, N.; Wasserscheid, P. *J. Catal.* **2007**, *245*, 279–284.

[75] Weng, Z.; Teo, S.; Hor, T. S. A. *Dalton Trans.* **2007**, 3493–3498.

[76] Jiang, T.; Zhang, S.; Jiang, X.; Yang, C.; Niu, B.; Ning, Y. *J. Molec. Cat. A* **2008**, *279*, 90–93.

[77] van Leeuwen, P. W. *Kulwer Academic Publishers "Homogeneous Catalysis: Understanding the Art* **2004**, 401.

[78] Jiang, T.; Liu, X.; Ning, Y.; Chen, H.; Luo, M.; Wang, L.; Huang, Z. *Cat. Comm.* **2007**, *8*, 1145–1148.

[79] Rucklidge, A. J.; McGuinness, D. S.; Tooze, R. P.; Slawin, A. M. Z.; Pelletier, J. D. A.; Hanton, M. J.; Webb, P. B. *Organometallics* **2007**, *26*, 2782–2787.

[80] McGuinness, D. S.; Rucklidge, A. J.; Tooze, R. P.; Slawin, A. M. Z. *Organometallics* **2007**, *26*, 2561–2569.

[81] McGuinness, D. S.; Overett, M.; Tooze, R. P.; Blann, K.; Dixon, J. T.; Slawin, A. M. Z. *Organometallics* **2007**, *26*, 1108–1111.

[82] Chen, H.; Liu, X.; Hu, W.; Ning, Y.; Jiang, T. *J. Molec. Cat. A* **2007**, *270*, 273–277.

[83] Alobaidi, F.; Ye, Z.; Zhu, S. *J. Poly. Sci. A* **2004**, *42*, 4327–4336.

[84] de Wet-Roos, D.; Dixon, J. *Macromolecules* **2004**, *37*, 9314–9320.

[85] Walsh, R.; Morgan, D.; Bollmann, A.; Dixon, J. *Appl. Cat. A* **2006**, *306*, 184–191.

[86] Kuhlmann, S.; Dixon, J. T.; Haumann, M.; Morgan, D. H.; Ofili, J.; Spuhl, O.; Taccardi, N.; Wasserscheid, P. *Adv. Syn. Cat.* **2006**, *348*, 1200–1206.

[87] Vanka, K.; Xu, Z.; Ziegler, T. *Organometallics* **2004**, *23*, 2900–2910.

[88] Blok, A.; Budzelaar, P.; Gal, A. *Organometallics* **2003**, *22*, 2564–2570.

[89] Monillas, W. H.; Yap, G. P. A.; Theopold, K. H. *Angew. Chem. Int. Ed. Engl.* **2007**, *46*, 6692–6694.

[90] Kohn, R. D. *Angew. Chem. Int. Ed. Engl.* **2008**, *47*, 245–247.

[91] Benard, M.; Rohmer, M.-M.; Lopez, X.; Theopold, K. H. *Angew. Chem. Int. Ed. Engl.* **2008**, *47*, 5597–5599.

[92] Angermund, K.; Dohring, A.; Jolly, P.; Kruger, C.; Romao, C. *Organometallics* **1986**, *5*, 1268–1269.

[93] Iczek, F.; Jolly, P.; Kruger, C. *J. Orgmet. Chem.* **1990**, *382*, C11–C13.

[94] Jolly, P.; Zakrzewski, U. *Polyhedron* **1991**, *10*, 1427–1431.

[95] Jolly, P.; Kruger, C.; Zakrzewski, U., U *J. Orgmet. Chem.* **1991**, *412*, 371–380.

[96] Betz, P.; Jolly, P.; Kruger, C.; Zakrzewski, U. *Organometallics* **1991**, *10*, 3520–3525.

[97] Betz, P.; Dohring, A.; Emrich, R.; Goddard, R.; Jolly, P.; Kruger, C.; Romao, C. *Polyhedron* **1993**, *12*, 2651–2662.

[98] Angermund, K.; Betz, P.; Dohring, A.; Jolly, P.; Kruger, C.; Schonfelder, K. *Polyhedron* **1993**, *12*, 2663–2669.

[99] Dohring, A.; Emrich, R.; Goddard, R.; Jolly, P.; Kruger, C. *Polyhedron* **1993**, *12*, 2671–2680.

[100] Jolly, P. *Acc. Chem. Res.* **1996**, *29*, 544–551.

[101] Heinemann, O.; Jolly, P.; Kruger, C.; Verhovnik, G. *Organometallics* **1996**, *15*, 5462–5463.

[102] Heigl, O.; Herdtweck, E.; Grasser, S.; Kohler, F.; Strauss, W.; Zeh, H. *Organometallics* **2002**, *21*, 3572–3579.

[103] Brueckner, A.; Jabor, K. J.; McConnell, A. E. C.; Webb, P. B. *Organometallics* **2008**, *27*, 3849–3856.

[104] Kreisel, K. A.; Yap, G. P. A.; Theopold, K. H. *Organometallics* **2006**, *25*, 4670–4679.

[105] Kreisel, K. A.; Yap, G. P. A.; Theopold, K. H. *Chem. Comm.* **2007**, 1510–1511.

[106] MacAdams, L.; Buffone, G.; Incarvito, C.; Golen, J.; Rheingold, A.; Theopold, K. *Chem. Comm.* **2003**, 1164–1165.

[107] Broussard, M.; Juma, B.; Train, S.; Peng, W.; Laneman, S.; Stanley, G. *Science* **1993**, *260*, 1784–1788.

[108] Edema, J.; Gambarotta, S.; Meetsma, A.; Vonbolhuis, F.; Spek, A.; Smeets, W. *Inorg. Chem.* **1990**, *29*, 2147–2153.

[109] Yang, Y.; Kim, H.; Lee, J.; Paik, H.; Jang, H. *Appl. Cat. A* **2000**, *193*, 29–38.

[110] Luo, H.; Li, D.; Li, S. *J. Molec. Cat. A* **2004**, *221*, 9–17.

[111] Semmelhack, M.; Chlenov, A.; Ho, D. *J. Am. Chem. Soc.* **2005**, *127*, 7759–7773.

[112] Ni, C.; Ellis, B. D.; Fettinger, J. C.; Long, G. J.; Power, P. P. *Chem. Comm.* **2008**, 1014–1016.

[113] Wolf, R.; Ni, C.; Nguyen, T.; Brynda, M.; Long, G. J.; Sutton, A. D.; Fischer, R. C.; Fettinger, J. C.; Hellman, M.; Pu, L.; Power, P. P. *Inorg. Chem.* **2007**, *46*, 11277–11290.

[114] R, B. J. *Patent: Olefin trimerisation using chromium catalyst US4668838-A US839638.*

[115] Calucci, L.; Englert, U.; Grigiotti, E.; Laschi, F.; Pampaloni, G.; Pinzino, C.; Volpe, M.; Zanello, P. *J. Orgmet. Chem.* **2006**, *691*, 829–836.

[116] Benetollo, F.; Grigiotti, E.; Laschi, F.; Pampaloni, G.; Volpe, M.; Zanello, P. *J. Solid State Electrochem.* **2005**, *9*, 732–737.

[117] Elschenbroich, C.; Mockel, R.; Zenneck, U.; Clack, D. *P.C.C.P.* **1979**, *83*, 1008–1018.

[118] Budzelaar, P. H. M. *Can. J. Chem.* **2009**, *87*, 832–837.

[119] Mani, G.; Gabbai, F. *Angew. Chem. Int. Ed. Engl.* **2004**, *43*, 2263–2266.

[120] Ganesan, M.; Gabbai, F. *Organometallics* **2004**, *23*, 4608–4613.

[121] Yu, Z.-Y.; Houk, K. *Angew. Chem. Int. Ed. Engl.* **2003**, *42*, 808–811.

[122] Kohn, R.; Smith, D.; Mahon, M.; Prinz, M.; Mihan, S.; Kociok-Kohn, G. *J. Organomet. Chem.* **2003**, *683*, 200–208.

[123] Gambarotta, S. *Coord. Chem. Rev.* **2003**, *237*, 229–243.

[124] Nomura, K.; Sagara, A.; Imanishi, Y. *Macromolecules* **2002**, *35*, 1583–1590.

[125] Yamada, J.; Fujiki, M.; Nomura, K. *Organometallics* **2005**, *24*, 2248–2250.

[126] Ma, Y.; Reardon, D.; Gambarotta, S.; Yap, G. *Organometallics* **1999**, *18*, 2773–2781.

[127] Reardon, D.; Conan, F.; Gambarotta, S.; Yap, G.; Wang, Q. *J. Am. Chem. Soc.* **1999**, *121*, 9318–9325.

[128] Ma, Y.; Reardon, D.; Gambarotta, S.; Yap, G.; Zahalka, H.; Lemay, C. *Organometallics* **2000**, *19*, 718.

[129] Aharonian, G.; Feghali, K.; Gambarotta, S.; Yap, G. *Organometallics* **2001**, *20*, 2616–2622.

[130] Coates, G.; Hustad, P.; Reinartz, S. *Angew. Chem. Int. Ed. Engl.* **2002**, *41*, 2236–2257.

[131] Brintzinger, H.; Fischer, D.; Mulhaupt, R.; Rieger, B.; Waymouth, R. *Angew. Chem. Int. Ed. Engl.* **1995**, *34*, 1143–1170.

[132] Gibson, V.; Spitzmesser, S. *Chem. Rev.* **2003**, *103*, 283–315.

[133] Domski, G. J.; Rose, J. M.; Coates, G. W.; Bolig, A. D.; Brookhart, M. *Prog. Poly. Sci.* **2007**, *32*, 30–92.

[134] van Meurs, M.; Britovsek, G.; Gibson, V.; Cohen, S. *J. Am. Chem. Soc.* **2005**, *127*, 9913–9923.

[135] Sita, L. R. *Angew. Chem. Int. Ed. Engl.* **2009**, *48*, 2464–2472.

[136] Arriola, D.; Carnahan, E.; Hustad, P.; Kuhlman, R.; Wenzel, T. *Science* **2006**, *312*, 714–719.

[137] MacLean, P. D.; Chapman, E. E.; Dobrowolski, S. L.; Thompson, A.; Barclay, L. *J. Organic Chem.* **2008**, *73*, 6623–6635.

[138] Pellecchia, C.; Pappalardo, D.; Oliva, L.; Mazzeo, M.; Gruter, G. *Macromolecules* **2000**, *33*, 2807–2814.

[139] Wu, T.; Qian, Y.; Huang, J. *J. Molec. Cat. A* **2004**, *214*, 227–229.

[140] You, Y.; Girolami, G. S. *Organometallics* **2008**, *27*, 3172–3180.